



If you have discovered material in AURA which is unlawful e.g. breaches copyright, (either yours or that of a third party) or any other law, including but not limited to those relating to patent, trademark, confidentiality, data protection, obscenity, defamation, libel, then please read our [Takedown Policy](#) and [contact the service](#) immediately

PHOSPHORUS BEARING MINERALS IN  
IRON ORES AND THEIR POSSIBLE  
BENEFICIATION

by

El-Sayed Ibrahim Elgayar (B.Sc., M.Sc.)

A thesis submitted in application for  
the degree of  
Doctor of Philosophy

The University of Aston in Birmingham

February 1980

SUMMARY

Modern electron optical techniques together with X-ray and mineralogical examination have been used to study the occurrence and form of phosphorus bearing minerals in iron ores.

Three ores have been studied - Bahariya and Aswan from Egypt and Frodingham ironstone from U.K. The iron in the Bahariya iron ore is mainly as hematite and goethite. The gangue minerals are halite, gypsum, barytes, quartz and calcite. Iron content is between 49.8 to 63.2% and phosphorus 0.14 to 0.34%. The phosphorus occurs as very fine particles of apatite which are distributed throughout the ore. Removal of the phosphorus would require very fine grinding followed by acid leaching. Aswan iron ore is an oolitic iron ore; the iron content between 41-57% and phosphorus content 0.1 to 2.9%. It is mainly hematitic with variable quantities of quartz, apatite and small amount of clay minerals. In the oolitic iron ore beds, apatite occurs in the hematite matrix; filling in the pores of the oolitic surfaces, or as matrix cementing the oololiths with the hematite grains. In sandstone claybeds the distribution of the apatite is mainly in the matrix. It is suggested that the liberation size for the apatite would be -80  $\mu\text{m}$  and flotation concentration could be applied for the removal of apatite from Aswan ore.

Frodingham ironstone occurs in the lower Jurassic bed of the South Humber side area. The average iron content is 25% and the phosphorus is 0.32%. Seven mineral phases were identified by X-ray; calcite, quartz, chamosite, hematite, siderite, apatite, and chlorite. Apatite occurs as very fine grains in the hematite and chamosite oololiths; as matrix of fine grains intergrown with chamosite and calcite grains; and as anhedral and subrounded grains in the oololiths (8-28  $\mu\text{m}$ ).

It is suggested that two processes are possible for the dephosphorisation; the Flox process or a reduction roast followed by fine grinding, magnetic separation, and acid leaching.

KEY WORDS - IRON ORE, PHOSPHORUS, MINERALOGY, ELECTRON-PROBE ANALYSIS, DEPHOSPHORISATION

## CONTENTS

	<u>Page</u>
Summary	(i)
List of Tables	(ii)
List of Figures	(iii)

### CHAPTER 1

1.	Introduction	1
----	--------------	---

### CHAPTER 2

	LITERATURE SURVEY (IRONORES)	8
2.	World Iron Ore Resources	8
2.1	Classification of iron ore deposits by type	12
2.1.1	Lake Superior type	12
2.1.2	Minette type	13
2.1.3	Bilbao type	14
2.1.4	Kiruna type	15

### CHAPTER 3

#### LITERATURE SURVEY (MARINE PHOSPHORITE)

3.1	The Origin of Marine Phosphorite	16
3.1.1	Biolithis hypothesis	16
3.1.2	Chemical hypothesis	16
3.1.3	Volcanic - Sedimentary	17
3.2	The origin of phosphates in iron ores	17

### CHAPTER 4

#### IRON ORE IN EGYPT

4.0	Introduction	21
4.1	Bahariya iron ore	25
4.1.1	Nasser Area	25
4.1.2	Gebel Ghorabi Area	26
4.1.3	El-Harra Area	26
4.1.4	El-Gedida Area	27



	<u>Page</u>	
4.1.4.1	Topography of El-Gedida iron ore deposits	27
4.1.4.2	Geology	28
4.1.4.3	Classification of El-Gedida iron ores	35
4.1.4.4	Mineralogy of El-Gedida iron ores	35
4.1.4.4.1	Hard massive ore	35
4.1.4.4.2	Banded cavernous ore	36
4.1.4.4.3	Friable ore	37
4.1.4.4.4	Black manganiferrous ore	37
4.1.4.4.5	Oolitic pisolitic ore	37
4.1.4.4.6	Ferruginous sandstone	38
4.1.4.5.1	The contact of the iron ore deposit with the underlying Bahariya formation	38
4.1.4.5.2	The contact of the iron ore deposit with the overlying Radwan formation	39
4.1.4.5.3	The contact of iron ore deposit with the surrounding Eocene deposits	40
4.1.4.6	Discussion of the origin of the iron ore	40
4.2	Experimental work	44
4.2.1	Lithology	45
4.2.2	Geochemical variation in a vertical section of El-Gedida iron ore deposit	45
4.2.3	Results of Microscopic examination of Bahariya ore	49
4.2.4	X-ray mineralogy	50
4.2.5	Scanning Electron Microscopy	53
4.2.6	Summary of results	55

	<u>Page</u>	
4.3	Aswan iron ore	57
4.3.1	Topography	57
4.3.2	The Nubian sandstone series	57
4.3.3	Geological classification of iron ore deposits in the district	60
4.3.3.1	The Ferruginous sandstone	60
4.3.3.2	The Ferruginous concretions	61
4.3.3.3	The oolitic iron ore	62
4.3.4	Experimental work	64
4.3.4.1	Lithology	68
4.3.4.2	Geochemical variation sections of Aswan iron ore deposits	68
4.3.4.3	Results of X-ray diffraction	72
4.3.4.4	Petrography	75
4.3.4.5	Scanning Electron Microscopy	75
4.3.4.6	Summary of results	99

## CHAPTER 5

### FRODINGHAM IRONSTONE

5.0	Introduction	101
5.1	Stratigraphy	106
5.2	Lithology	106
5.3	Mineralogy	111
5.4	Mineralogical classification of ironstone	113
5.5.0	Experimental work	115
5.5.1	Materials	115
5.5.2	Core logs	115
5.5.3	The chemistry of ironstone	144
5.5.3.1	Vertical chemical variation within the ironstone	144

	<u>Page</u>	
5.5.4	Results of X-ray diffraction	147
	Mineralogical analyses	
5.5.5	Scanning Electron Microscopy	150
5.5.6	Microprobe examination	158
5.5.7	Summary of results	171
<u>CHAPTER 6</u>		
6.0	Dephosphorisation of iron ores	173
6.1	Chemical processing	173
6.1.1	Nitric acid	173
6.1.2	Sodium carbonate	173
6.1.3	Flox process	174
6.2	Roasting and leaching with dilute acid or alkali	174
6.3	Flotation	176
6.4	Beneficiation of phosphoric iron ore by oil phase agglomeration methods	177
<u>CHAPTER 7</u>		
7.0	Possible application of dephosphorisation techniques to Bahariya, Aswan and Frodingham ores	178
7.1	Bahariya ore	178
7.2	Aswan iron ore	179
7.3	Frodingham ironstone	183
<u>CHAPTER 8</u>		
8.0	Conclusions	190
8.1	Bahariya ore	190
8.2	Aswan iron ore	190
8.3	Frodingham ironstone	192

CHAPTER 9

9.0	Suggestion for further work	193
9.1	Economics	193
10	Acknowledgements	194
11	References	195
12	<b>Appendix</b>	<b>202</b>

LIST OF TABLES

		<u>Page</u>
1.1	Worldwide Steelmaking practice forecast	6
1.2	Estimated worldwide demands for pre-reduced iron ore	6
2.1	Iron ore resources of the world	9
4.1	Lithology, chemical analysis, X-ray studies and Scanning Electron Microscope studies for Bahariya iron ore	46
4.2	Lithology, chemical analysis, petrography, X-ray studies, Scanning Electron Microscope and Electron Microprobe analysis	65
4.3	Lithology, chemical analysis and X-ray studies for Aswan iron ore, Core 2	67
5.1	The Mineralogical constitution of unweathered Frodingham ironstone	112
5.2	Chemical analysis, X-ray, Scanning Electron Microscope studies and Electron Microprobe analysis for Frodingham ironstone, Core Y 112	116
5.3	Chemical analysis, petrography, Scanning Electron Microscope studies and Electron Microprobe analysis for Frodingham ironstone Core Y 113	119

	<u>Page</u>
5.4 The most important points for Davies and Dixie's classification of Frodingham ironstone and the present classification	143
7.1 The size distribution of quartz, apatite and clay mineral grains in the oolith and in the matrix	182
A.1 Phosphate Minerals	202
A.2 Mineral Names and D Spacing	203

LIST OF FIGURES

	<u>Page</u>
1.1 Production of iron ore (1855-1980)	2
3.1 Schematic section of iron ore facies and physico-chemical condition	19
4.1 Map of Egypt	22
4.2a Iron deposits of El-Gedida area Bahariya Oasis, Western Desert, Egypt	29
4.2b Geological map of El-Gedida iron ore deposits area	30
4.3 Comparison between the phosphorus content of iron ore in different locations	43
4.4 Distribution of iron and phosphorus in Bahariya iron ore (Core 1)	48
4.5 Typical X-ray diffractogram of Bahariya iron ore (Sample No. B5)	51
4.6 Typical X-ray diffractogram of Bahariya iron ore (Sample No. B14)	52
4.7 Scanning electron micrograph of Bahariya iron ore sample No. 8, and X-ray distribution maps of Fe, Si, Al, P, Ca, S and Cl.	54
4.8 Geological map showing desert east of Aswan	59
4.9 Distribution of iron and phosphorus content in Aswan iron ore (core 1)	69

	<u>Page</u>
4.10 Distribution of iron and phosphorus content in Aswan iron ore deposits (Core 2)	71
4.11 Typical X-ray diffractogram of Aswan iron ore samples (Sample No. AS 7)	73
4.12 Typical X-ray diffractogram of one of Aswan iron ore samples (Sample No. As 12)	74
4.13 Scanning electron micrograph of oolitic iron ore sample No. As 10 and X-ray distribution maps of Fe, Si, Al, P and Ca	77
4.14 Scanning electron micrograph of oolitic iron ore sample No. As 9, and X-ray distribution maps of Fe, Si, Al, P and Ca	79
4.15 Scanning electron micrograph of Ferruginous sand clay sample No. As 12-2 and X-ray distribution maps of Fe, Si, Al, P and Ca	82
4.16 Scanning electron micrograph of Ferruginous sand clay sample No. As 12, and X-ray distribution maps for Fe, Si, Al, P and Ca.	84
4.17 Scanning electron micrograph for oolitic iron ore sample No. As 25 and X-ray distribution maps for Fe, Si, Al, P and Ca	86



	<u>Page</u>
4.18 Scanning electron micrograph for oolitic iron ore sample No. As 6 and the X-ray distribution maps of Fe, Si, Al, P and Ca	89
4.19 Scanning electron micrograph for oolitic iron ore sample No. As 9-2 and X-ray distribution maps of Fe, Si, Al, P and Ca	92
4.20 Scanning electron micrograph for oolitic iron ore with sand sample No. As 11 and X-ray distribution maps of Fe, Si, Al, P and Ca	95
4.21 Scanning electron micrograph for oolitic iron ore sample No. As 20 and X-ray distribution maps for Fe, Si, Al, P and Ca	98
5.1 The proportion of imported ore in U.K.	102
5.2 Average consumption of British home iron ore in 5-yearly periods	103
5.3a The Frodingham ironstone	107
5.3b Inset showing location of cores	107
5.4 The Geological map of the Frodingham ironstone	108
5.5 The Geology of the Scunthorpe area	109
5.6 Typical reference photograph of split core Y 112 (Frodingham ironstone)	122

	<u>Page</u>
5.7 Typical reference photograph of split core Y 113 (Frodingham ironstone)	123
5.8 Lithology of Frodingham core Y 112	124
5.9 Lithology of Frodingham core Y 113	132
5.10 Distribution of iron and phosphorus in Frodingham ironstone core Y 112	145
5.11 Distribution of iron and phosphorus in Frodingham ironstone core Y 113	146
5.12 Typical X-ray diffractogram of Frodingham ironstone (Sample No. A8)	149
5.13 Scanning electron micrograph of Frodingham ironstone, Sample No. B100-2 and X-ray distribution maps of Fe, Si, Al, P and Ca	151
5.14 Scanning electron micrograph of Frodingham ironstone Sample No. B55 and X-ray distribution maps of Fe, Si, Al, P, Ca and S	154
5.15 Scanning electron micrograph of Frodingham ironstone, Sample No. A85 and X-ray distribution maps of Fe, Si, Al, P and Ca	156
5.16 Microprobe electron micrographs of Frodingham ironstone, Sample No. B100-1	160

	<u>Page</u>
5.17 Microprobe electron micrographs of Frodingham ironstone, Sample No. B9	163
5.18 Microprobe electron micrographs of Frodingham ironstone, Sample No. B49, Magnification x100	167
5.19 Microprobe electron micrographs of Frodingham ironstone, Sample No. B49, Magnification x250	169
7.1 Superimposed iron and phosphorus electron microprobe line diagrams for the same oolith	186

## 1 - INTRODUCTION

A century ago iron ore production was only 2 percent of what it is at present (1). This grew at a constant rate up to 1900; then slowed down in the period 1900-1940 but has been expanding rapidly since, as is shown in Figure 1.1. The latest estimation of world iron ore reserves is  $500 \times 10^9$  tonnes and therefore even at present day usage there is approximately 500 years of iron ore availability (1).

Perhaps more important than the increasing consumption of the world's iron ore reserves is the change over from the use of lower grade ore of the U.K., and France-Belgium-Luxembourg-Saar (Minette type) to the higher grade ores of the present day discoveries in Australia, Brazil, Canada and Venezuela. Thus, the former countries have changed from being self sufficient iron ore producers (and even exporters) to large importers. Similarly, the United States has become a major importer although there are large deposits in that country of relatively high grade but more difficult to smelt ores (the Taconites of Mesabi). Further, Japan has become one of the top three iron and steel producers of the world despite having no significant home ore production. The chief reason for the switch from lower grade iron ore (<30% Fe) to the 55+% Fe contents is the need to produce the lowest cost products.

Always steelmakers are striving to get maximum production from each production unit to offset the high labour cost and inadequate depreciation allowances. This need to maximise the output from each production unit has resulted in the

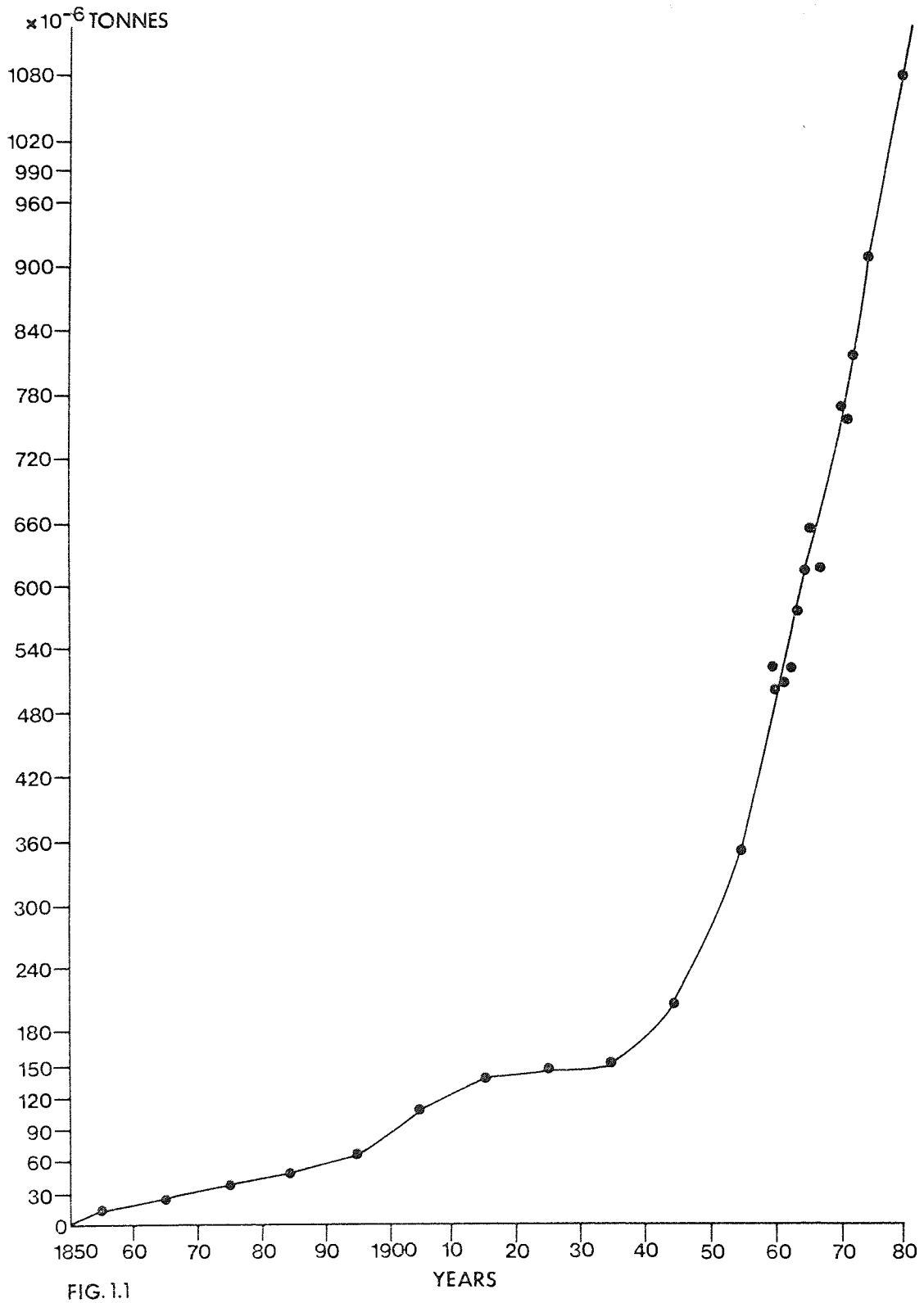


FIG. 1.1

PRODUCTION OF IRON ORE,  
(1855 — 1980)

growth of oxygen steel making processes. Molten iron is converted to steel by direct oxidation of impurities with gaseous oxygen. This is putting further emphasis on the blast furnaces to increase output in order to satisfy the prodigious appetite of these oxygen steelmaking plants for hot metal.

The demands on blast furnace performance have resulted in a number of important innovations in its operation. Such refinements as increased use of prepared burdens, high-top pressure, blast-moisture control, and injection of hydrocarbon fuels into the tuyere zone are all directed towards improving and increasing the output of existing blast furnaces and at the same time aiming to decrease costs. The most important of these innovations is the use of a prepared iron ore burden which, inevitably, contains impurities, e.g. silica, alumina, lime, magnesia and others which are usually at a lower content but very harmful, e.g. phosphorus, copper, zinc, lead, arsenic, sulphur, chloride, etc. These elements influence greatly the practical value of a deposit and can even make it useless under the present state of technology and economics.

Of these impurities, phosphorus has been a decisive factor in determining the appropriate process for the steel refining of the hot metal from the blast furnace. Unfortunately, almost all the phosphorus of the charge materials is absorbed into the molten iron. It may be recalled that when the Bessemer process was developed using converters with acid

lining in 1856, it was possible to use only ores with a very low phosphorus content, generally under 0.03% due to the inability of the acid slags to absorb phosphate minerals. This limited the use of the Bessemer process in numerous countries, chief among these were the U.K. (Midland ores contained high P) and Sweden (Kiruna iron ores contained up to 2% P).

The Thomas or Basic Bessemer process using a converter with a basic lining made it possible to handle hot metal with a high phosphorus ( $\leq 1.8\%$  P) and enabled the use of ores containing a high percentage of phosphorus to be charged to the blast furnace. However, there were also many ores in the world with an intermediate phosphorus content, which were suitable neither for the Bessemer nor the Thomas process, and the only process which was suitable was the basic Siemens-Martin process (Open-Hearth).

This process treated hot metal of any phosphorus content mixed with scrap in a very wide proportion, and was the most flexible method available to the iron and steel industry at that time for the intermediate phosphorus containing ores.

The developments in steelmaking during the last 30 years which have included the top and bottom oxygen blown converters (BO F and OBM or Q-BOP) have again imposed limitations on the amount of phosphorus that is permitted in the hot metal to facilitate high production and

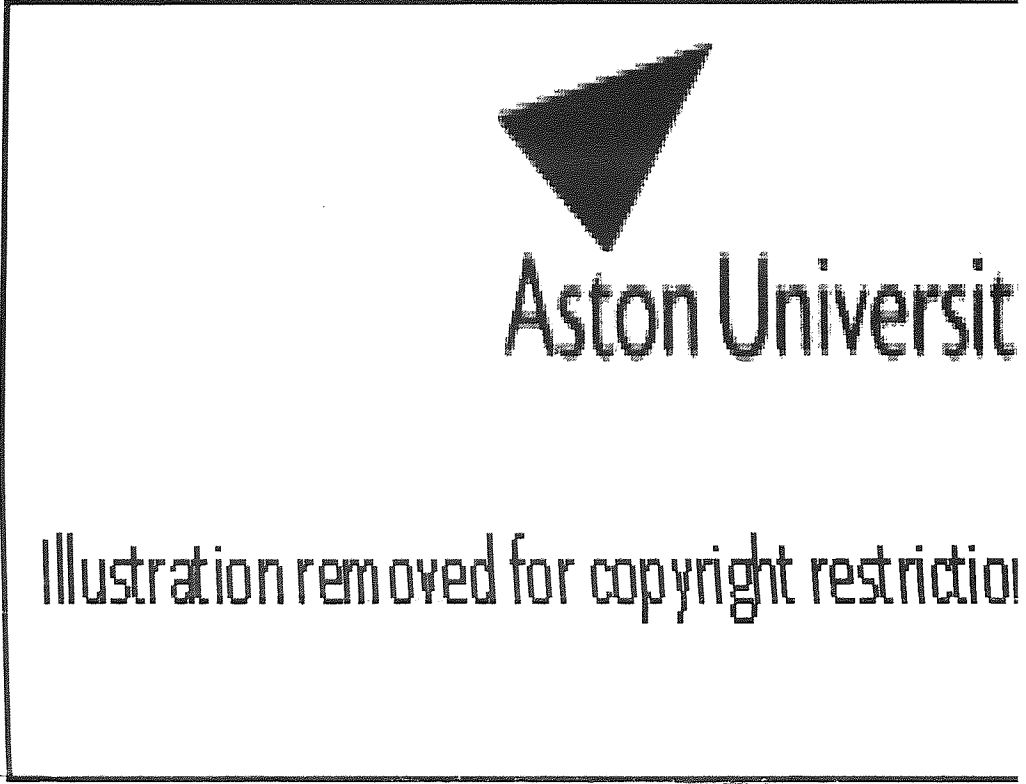
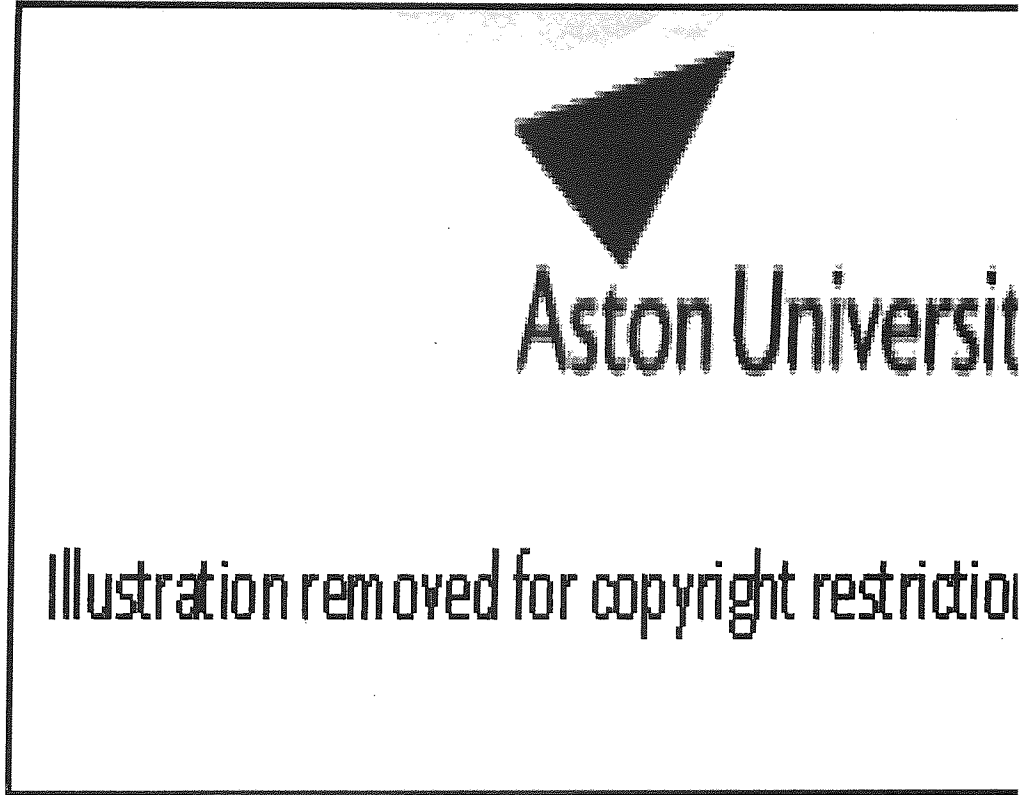
economic working. This has re-opened the possible limitation of phosphorus content in the blast furnace charge. If the process metallurgist requires a hot metal to contain less than 0.3% P then the blast furnace charge must contain the appropriate phosphorus content in relation to the iron content. For instance, ores with 50% Fe must not exceed 0.15% phosphorus, and if the iron content is 65%, the phosphorus content in the ores could reach 0.2% without exceeding 0.3% in the hot metal.

From Table 1.1 <sup>(2)</sup> it is clear that oxygen steelmaking will be predominant in many countries and the proportion will reach 65% of the steel produced in 1985. Thus, it would appear that there will be increasing pressure from the iron and steelmakers of the world to require the ore manufacturers to provide materials of as low a phosphorus content as possible which may require beneficiation to be practised on an ever increasing scale.

Another approach to iron and steelmaking has been the growth of direct reduction processes within the past twenty years and is more applicable to developing countries of the third world. These processes aim to produce iron units from ore without the use of metallurgical coke which is a fast decreasing commodity although it may be replaced by formed-coke in the future. In the same paper Miller (loc cit) forecast an eightfold increase in the production of direct-reduced iron product (Table 1.2). However, it must be said that the quality of the iron oxide feed



TABLE 1.1 WORLDWIDE STEELMAKING PRACTICE FORECASTS (Miller (2))



directly effects the quality of reduced product and also controls the overall economics of the reduction and steelmaking process. It is suggested that the phosphorus in the oxide raw material must be between 0.01 to 0.05% and thus, no alleviation of the phosphorus problem for the ore producer is apparent.

Therefore, it is important at the present time to examine the origin of phosphorus in some of the world's iron ore deposits and suggest possible beneficiation methods to remove this unwanted element.

2. World Iron Ore Resources

Iron is one of the most abundant and widely distributed elements in the earth's crust, constituting approximately 5% of the total. Its occurrence in acceptable quantities for economic extraction is extensive in very many parts of the world.

As for all ores, the principal difficulty lies in the definition of the economic and technical viability of a deposit. Not only does the iron content of the rocks determine the value but also the associated gangue minerals and, in particular, the 'tramp' elements, e.g. phosphorus and sulphur. With present and possible future techniques of mining and beneficiation ore reserves are difficult to estimate but Table 2.1 gives a guide to total world resources <sup>(1)</sup>. As mentioned earlier, the iron ores are very widespread and in many cases at high iron contents, representing very many years of useful reserves. The following notes are in amplification of the data in table 2.1:

(a) The ore resources of Europe, N. America and Russia contain many of the lower grade deposits (e.g. Taconites, Minette type) which do not appear in most of the other regions. These latter are generally higher grade ores or ill defined low grade material.

(b) The current total for world resources, although very large, must be considered a conservative

TABLE 2.1 IRON ORE RESOURCES OF THE WORLD

Region	In millions of metric tonnes					
	Resources		Potential ore		Total resources	
	Quantity	%	Quantity	%	Quantity	%
Africa	6,800	3	24,500	5	31,300	4
Middle East, Asia and the Far East	17,300	7	54,200	10	71,500	9
Australia, New Zealand and New Caledonia	16,800	7	Vast		16,800	plus 2
Canada and West Indies	36,300	14	89,400	17	125,700	16
Europe	21,300	8	12,800	2	34,100	4
South America	34,100	14	58,400	11	92,500	12
USSR	110,500	44	193,800	36	304,300	39
United States of America, Puerto Rico, Mexico and Central America	8,200	3	98,100	19	106,300	14
TOTAL	251,300	100	531,200	100	782,500	100

estimate because potential ore in many parts of the world, such as Africa, Asia, Australia and South America, is difficult to assess on the basis of available information.

In fact, no total has been given for Australia in the potential ore category.

- (c) While there are very large iron ore resources for each continent (certainly satisfactory supply for the future expansion of steel industries) it should be noted that there are decided irregularities in distribution. Many countries within well endowed continents have no resources, and local scarcities exist even within regions containing vast iron ore deposits. It is obvious that in the future the problem will be to select the best quality of material for economic development and to minimise ore transportation costs for local situations.

Resolving these two factors will frequently point towards the importation of high-grade iron ores rather than the exploitation of indigenous deposits which have physical chemical and mining disadvantages.

- (d) Quantitatively, the greatest resources of iron in the world are found in low-grade deposits, particularly in siliceous iron formations.

It should be noted that in the totals for the United States of America, relatively stringent criteria have been applied in regard to classifying reserves, potential ore being twelve times as great as reserves. This is caused by the fact that reserves in the United States are commonly determined on the sole basis of economic factors.

## 2.1 Classification of Iron Deposits by Type

Iron ore is classified in many different ways to satisfy the needs of engineers, metallurgists, chemists or economists, or the demands of commerce. The system adopted here for classifying iron deposits is to be found in the United Nations survey of world iron ore resources, 1970 (1). In it descriptive geology and empirical data, rather than genetic processes are stressed.

Descriptive data is used and iron deposits are grouped with reference to a few well-known types and examples. The mineralogy, texture, physical features, composition, kinds of associated rocks, mineral alteration and geological setting are described objectively; and familiar examples are chosen to illustrate the nature and type of deposits. In this thesis four types only of the iron deposits classification are presented, and they are given below:

### 2.1.1 Lake Superior type

Characteristically, this is a thin banded cherty rock with iron-rich layers that are found in many sedimentary facies. Granules and oolites composed of both chert and iron minerals have a typical textural feature, and the rocks are practically free of clastic material, except in the transitional border zones or in distinct, well defined members within the formation. Continuous layers of the Lake Superior type of iron formations often extend for hundreds of miles along the margin of a geosynclinal basin. The formations may thicken and thin from a few metres to

several hundred metres and occasionally may increase to over 300 metres. There is a close association of these minerals with dolomite, quartzite, black carbon-bearing shales and slate, chert breccias and volcanic rocks. There are Lake Superior types present in late pre-Cambrian rock groups in nearly all parts of the world. Two major types may be distinguished:

- a - the low-grade ore (quartzite formations with hematite) including Itabirite; Taconite, Metaconite; Jaspilite and Iron-Quartzite.
- b - the high-grade type (almost pure hematite).

Examples:-

- Mesabi Range;
- Brazil - Minas Gerais;
- Venezuela - Cerro Bolivar deposit;
- Krivoi Rog, Ukraine U.S.S.R.

#### 2.1.2 Minette type

The oolitic-texture rocks of this type of iron formation are composed mainly of siderite and iron silicates, such as chamosite or iron chlorides, and of goethite-siderite and chamosite. Many beds containing a high proportion of fine grained clastic material are transitional to sideritic or chamositic mudstones or sandstones. Sand grains may form the nuclei of siderite oolites, as in the Salzgitter and Peace River beds. Occasionally, fossil fragments are present in the oolites. Silica (which is usually more than 20 percent) is present generally in chamosite or iron-silicate minerals or in lesser amounts in clastic grains, rather than chert. The phosphorus content is higher



than that in the cherty Lake Superior types. These iron formations are closely associated with black carbonaceous shale, mudstones and sandy shales, which apparently formed in marine or brackish water in shallow basins. Minette ores are practically important and widespread in Europe, e.g. the sideritic or chamositic ironstones of northern England, the Minette ores of the Lorraine district of France and the Federal Republic of Germany, the Salzgitter ores of lower Saxony, and many other Jurassic beds in northern Europe. This type is also found in the iron formations of the Peace River area in Alberta, and in the enriched Aswan iron ore deposits in Egypt.

### 2.1.3 Bilbao type

This occurs in massive oxide deposits derived from the weathering of underlying iron carbonate, and in iron deposits of irregular shape occurring as iron carbonate below the water-table and as goethite and hematite above the water-table. The principal deposits of this type are the following:

- Bilbao, Spain
- Erzberg, Austria
- Rudabanya, Hungary
- Khenifra, French Morocco
- Ouenza, Boukadra and other deposits in Algeria
- Djerissa, Douaria and Tamera in Tunisia
- Bahariya, Egypt
- Cumberland, England

#### 2.1.4 Kiruna type

This is characterised by massive magnetite intrusions, usually associated with granitoid or syenite type, accompanied by a relatively higher apatite content.

The principal deposits are:

- Dover, New Jersey in the U.S.A.
- Lyon Mountain, New York, in the Adirondacks in the U.S.A.
- Iron Mountain, in Missouri, U.S.A.
- Pilot Knob, Missouri
- Cerro de Mercado (Durango State), Mexico
- Algarrabo, El Tofo, Romeral in Chile

Further details about classification of iron ore deposits can be obtained from references (1) and (3).

### 3.1 The Origin of Marine Phosphorite

The greater part of the phosphorites of the world are of marine origin. There are three principal hypotheses of their formation; biolithic, chemical and volcanic-sedimentary.

#### 3.1.1 Biolithic hypothesis

This is based on the suggestions by Backwalker <sup>(4)</sup> and Bushinskii <sup>(5)</sup> that marine originating phosphate deposits are based upon sudden changes in the marine environment such as major temperature shifts or volcanic submarine and earth movements. It is suggested that these resulted in catastrophic slaughter of the fish population with subsequent decay of the bodies on the sea floor producing phosphate rich deposits.

#### 3.1.2 Chemical hypothesis

About 200 minerals are known that contain one percent or more  $P_2O_5$ . Most of the phosphorus in the earth's crust, however, belongs to the apatite mineral group <sup>(6)</sup>.

The earth's crust contains about 0.27%  $P_2O_5$ . Most phosphorus is carried to the sea as phosphate minerals or adsorbed on iron or aluminium hydroxides or clay, but some is carried in particulate or dissolved organic compounds, and about one-sixth of the total is carried by this method into solution. The phosphorus content of most rivers and lake waters ranges from about 0.01 to 0.5 parts per million <sup>(6)</sup>. The solution of phosphorus in the water may be raised by

local conditions, e.g. high dissolved organic phosphate content, high Ca/Mg ratio, high pH, high temperature and suitable nucleation sites. It has been established that the solubility of apatite in sea water decreases with increasing pH <sup>(7)</sup> and also is precipitated in low oxygen potential environments <sup>(8)</sup>. These conditions are conducive to the precipitation of phosphate on parts of the sea bed forming sedimentary deposits <sup>(7)</sup>.

### 3.1.3 Volcanic sedimentary hypothesis

It is known that only poor phosphorites are found directly in volcanic-sedimentary and volcanic siliceous-schistose deposits. Bushinskii <sup>(5)</sup> expected that the greatest precipitation of phosphates should occur near the point of appearance of submarine thermal springs, in places where the highest concentrations of phosphate solutions are found. With increasing distance from the points of appearance, the phosphates to an ever increasing degree would be mixed with sea water and diluted by it. Accordingly, the possibilities for their chemical precipitation into sediments should decrease sharply.

### 3.2 The Origin of Phosphates in Iron Ores

There are two principal sources of iron at the earth's surface; volcanic activity and continental erosion.

Borchert <sup>(9)</sup> suggested that the iron in the trivalent state is insoluble in the presence of oxygen, when its maximum solubility is of the order of  $1 \text{ mg, m}^{-3}$ . Any

significant solubility of iron in the bivalent state occurs only in acid solutions with a pH value below 7 and then only under reducing conditions and in the absence of free oxygen. In these circumstances its solubility may reach a magnitude of  $5 \times 10^4 \text{ mg, m}^{-3}$ . In the presence of free oxygen iron is chiefly precipitated in trivalent state. He also noticed that corresponding to the normal conditions of sea current the dissolved iron moves predominantly towards the oxygen rich shallow sea where it is deposited as limonitic ooliths. However, a considerable proportion of the dissolved iron is precipitated in the  $\text{CO}_2$  zone to form sideritic clay ironstone. The  $\text{CO}_2$  zone is between the bottom zone where no oxidation occurs and the shallow water zone where there is oxygen (See Fig. 3.1).

Cook and McElhinny <sup>(10)</sup> noticed that most of the phosphorus is associated with the iron in an adsorbed form or perhaps in a poorly crystalline iron phosphate phase. But in some deposits, apatite occurs as discrete laminae and thin beds.

Kaplan and Rittenberg <sup>(11)</sup> pointed out that in reducing environments the phosphate ions tend to stay in solution due to bacterial production of  $\text{H}_2\text{S}$  and  $\text{CO}_2$  which bind  $\text{Fe}^{2+}$  and  $\text{Ca}^{2+}$  respectively as sulphides and carbonates; the removal of these cations from solution would keep the phosphate ion in solution.

Mackereth <sup>(12)</sup> pointed out that the phosphate was released in anoxic pore waters by decomposition of phosphorus

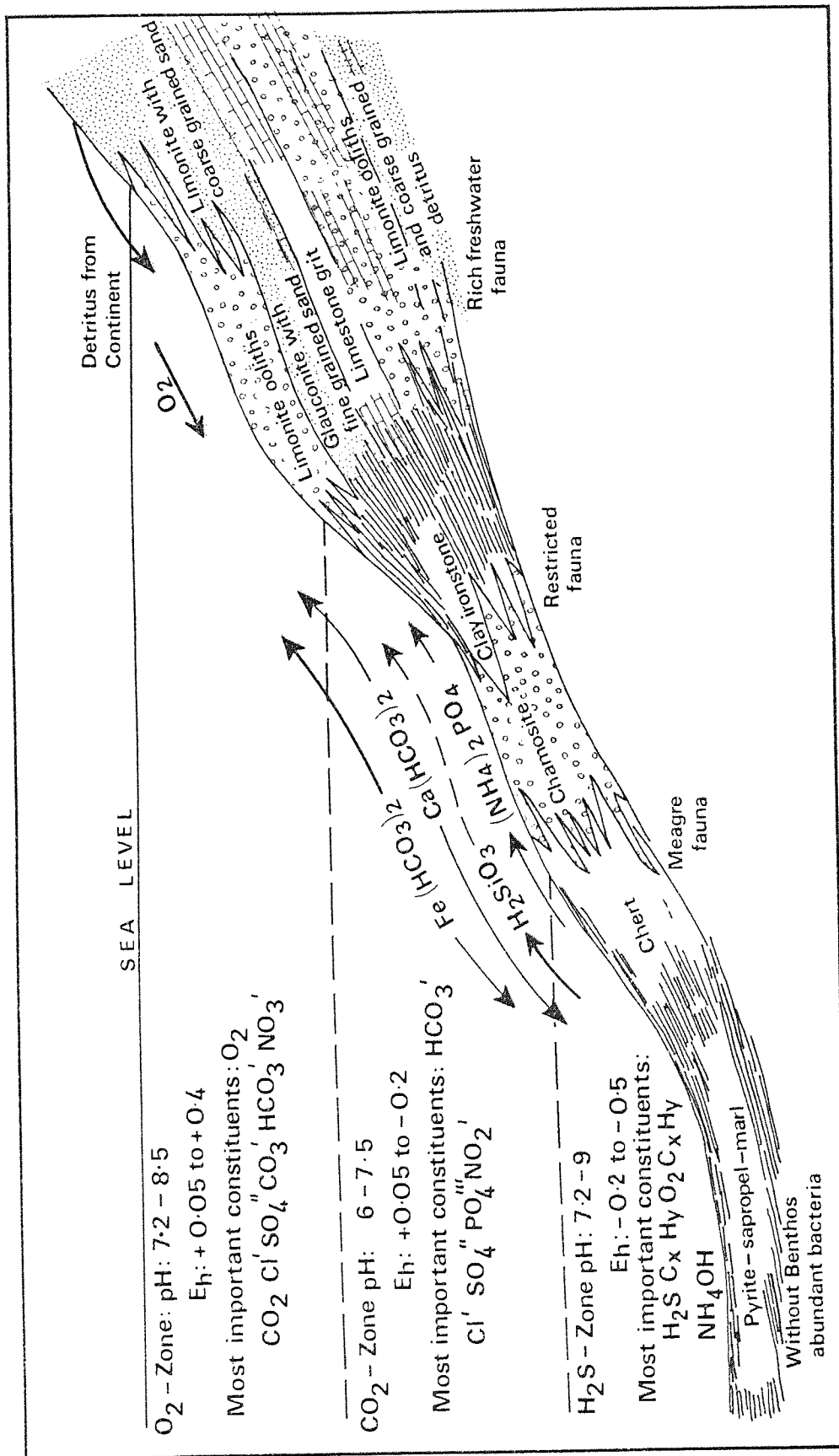
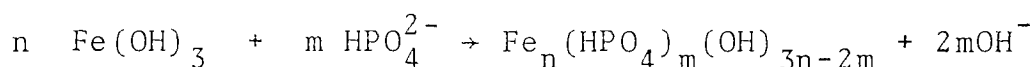


FIG. 3.1 SCHEMATIC SECTION OF IRON ORE FACIES AND PHYSICO-CHEMICAL CONDITIONS (9)

containing organic matter and, by the reduction of hydrated ferric oxides which, under oxidising conditions ( $\text{CO}_2$  zone), bind phosphate onto their surfaces.

Nriagu and Dell (13) suggested that in many instances the ferric oxyhydroxides precipitated from the overlying water was stabilised in the sediments by their subsequent interaction with the phosphorus in the interstitial fluid's as follows:



Ferrosoferric hydroxyphosphates are most stable under oxidising conditions.

Borchert (loc cit.) also noticed that smaller amounts of  $\text{Fe}(\text{HCO}_3)_2$  migrated into zones of increasing reduction potential (phosphorus precipitated) to combine with silica originating in the alkaline  $\text{H}_2\text{S}$  zone so as to form chamosite.

Nriagu (14) suggested that the  $\text{Fe}^{2+}$  can be used as an effective precipitant for removing orthophosphates, particularly from anaerobic sludge digesters where the efficiency of other precipitation mechanisms may be low. They show that the hydrated ferric oxides bind phosphate onto their surfaces under oxidising conditions and thus cause the presence of phosphate in iron ores. It is also clear that Fe occurs in the phosphate deposits as a  $\text{Fe}(\text{HCO}_3)_2$ , chamosite and iron phosphate phases.

## 4. IRON ORE IN EGYPT

### 4.0. Introduction

The Ancient Egyptians occasionally used iron and iron ores. This is proved by the finding of iron beads in some of the tombs and by the well known piece of iron found in the inner joints of the Great Pyramid at Giza (15).

The iron ores in Egypt have thus been known from as early as the Eighteenth Dynasty (about 1350 B.C. to 158 B.C.) but have not received much attention until recently (15). This is probably due to the absence of coal in Egypt and to the occurrence of favourably situated rich iron ores in other countries.

The establishment of an iron and steel plant at the end of the last decade was a national requirement to meet the additional steel capacity necessary for reconstruction and development.

There are two main deposits of iron ore in Egypt:- at Aswan and at Bahariya Oasis (Fig. 4.1), these deposits are briefly described below.

#### Aswan

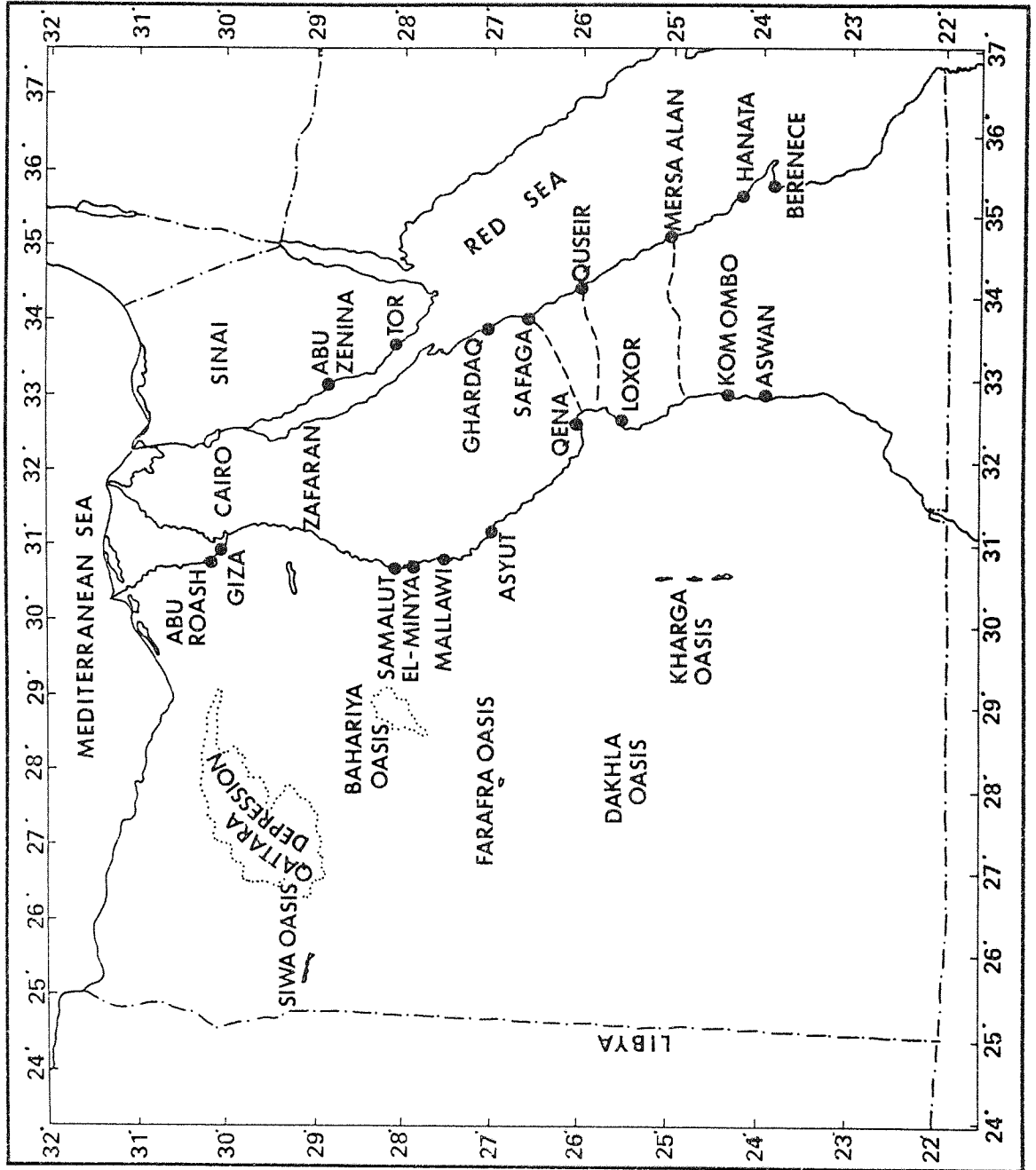
The ore is in oolitic sedimentary deposits (Minette type) occurring as bands in the middle group of the Nubian Series, interbedded with clays and ferruginous sandstones. The beds are horizontal and the ore bands are either at the surface



FIG. 4.1

EGYPT

Scale 1:8000 000,



or close thereto. Hence mining is by the opencast method. Reserve estimates vary from 158 million to 300 million tonnes (16).

The average grade is given by Gheith (16) as 48% Fe and 12% SiO<sub>2</sub> and 1.0% P.

Now that electricity is being produced from the Aswan Dam generators it is possible to mine the iron ores especially those near Aswan.

#### Bahariya

The iron ore deposits of the Bahariya Oasis occur at four localities:

Nasser area; Gebel Ghorabi; El Harra; El Gedida.

The deposits are rather irregular forming a succession of lenticular beds of the lower middle Eocene age. The beds vary in thickness from less than 1 m. to more than 12 m. It is suggested (17) that the ore has been formed by slow but intense metasomatic replacement of the lower Middle Eocene limestone with partial replacement of the uppermost section of the Bahariya formation sandstones and the lower member of the Radwan formation. The overburden is variable. In parts, it forms a thin cover of less than a metre, consisting of alluvium, mainly sands and gravels derived from iron formations and/or quartzite. In other parts, the overburden is formed of thick beds of clastics mainly clays, Quartzites and sandstone. In these parts the overburden may reach a thickness of up to 40 metres.

The ore at Bahariya is of a dark brown to dark red colour and consists mainly of hematite and goethite with pockets of ochre and manganese oxides. The gangue minerals are Halite, Gypsum, Baryte, Quartz and Calcite.

The ore reserves are given as 195 million tonnes with an average grade of 52.5% Fe and 6% SiO<sub>2</sub> and 0.12% P.

The iron ore mines of the Bahariya Oasis in the Eastern desert represent the main potential iron ore resources for the new iron and steelmaking complex because they contain a high percentage of Fe and a low percentage of P.

The present thesis comprises, for the first time, a combined detailed geological, mineralogical and geochemical investigation on the Aswan and the Bahariya (El Gedida) iron ores which represent two different types, the Minette and the Bilbao types.

The aim is to achieve a better understanding of the origin of phosphates and their minerals together with their amount and distribution in the ores. It is believed that the realisation of such can be a help in planning the economic use of the ores and in exploration for similar ores in other areas all over the world.

## 4.1 Bahariya Iron Ore

### 4.1.1 Nasser area (18)

The iron beds of the Nasser area outcrop along a strip of about 5.0 Km in an east-west direction. The northern part of the Nasser area is a Grabenal wadi and the iron bed is covered by different thicknesses of overburden. Topographically the Nasser area is longitudinally divided into eastern and western parts. In the "eastern" section the ore is mainly found in the form of a single bed whose average thickness is approximately 8.2 m. Its colour is dark brown to dark reddish, partly hard to friable, chiefly hematite with pockets and bands of hard goethite especially at the top where there is always a hard cavernous goethite cap.

Occasionally, the ore is black with a low percentage of manganese minerals. In the far western part of the Nasser area there are two beds separated by a clay layer whose thickness varies from 0.5 m to 5.9 m. The ore is generally hard, cavernous, mainly goethite, brown to dark brown at the top, whereas at the lower parts it is dark brown to dark reddish and black. Mostly it is hard, friable hematite but turns to black colour especially when manganiferous. The thickness of the iron ore beds varies from 1.0 to 25.7 m. Halite and gypsum form the main impurities in the ore throughout the Nasser area.

The thickness of overburden varies from a few centimetres to 21.6 m. In the south, the overburden is mainly formed

of unconsolidated sand alluvium and iron gravels with salt pockets. Over the rest of the area there are beds of clay and quartz.

#### 4.1.2 Gebel Ghorabi (18)

Ghorabi is topographically divided into 5 parts, separated by either fault or erosional wadis. (North, East, South, West and Central Ghorabi.)

The ore beds are generally covered by 0.50 m thick of alluvium cap. The upper part of the ore is mainly formed of massive hard, brown, cavernous goethite. The lower part is separated from the upper by a clay bed of an average thickness 0.70 m. This lower part is mainly reddish brown to blue-black, friable to slightly hard manganiferrous hematite ore or mixed hematite and goethite. The average thickness of the iron beds in the Ghorabi area is 8.5 m. Quartz, gypsum, calcite and halite are the main gangue minerals associated with the ore.

#### 4.1.3 El-Harra area (18)

The iron deposit of El-Harra is represented by one bed which splits (in the central part of the area) into a number of clastic intercalations of several bands of iron which may reach 5 in number.

The ore bed is covered by a thin cap of wadi deposits with an average thickness 1.2 m. This cover is mainly formed

of unconsolidated sand and gravels of iron and/or quartzite. Occasionally, remnants of a thin quartzite bed are observed to cover the iron bed. The ore is formed generally of hard, dark brown, goethite with yellow ochrous pockets. The goethite is cellular (especially at the southern parts of the area) generally massive and blocky and sometimes fragmental. Hematite intercalations are observed at the lower parts of the ore bed.

In the central part of the area, the ore is covered by a thick overburden, varying from 0.7 m to 14.8 m with an average thickness of 6.1 m. Clay bands form 47% of the total overburden thickness, the alluvium 20%, the sandstone 15%, the quartzite 12% and the limestone 6%. The hematite ore, in the central part, is mainly reddish brown to dark brown to bluish black, friable and porous. Generally hard fragmental goethite pockets and highly manganiferrous bands interpenetrate the ore body. Bands of yellow clayey ochre, also alternate with the friable hematitic ore. The average thickness of the iron bed at El-Harra area is 6.2 m.

The main gangue minerals associated with the ore are gypsum, calcite and halite. These minerals are irregularly distributed in the ore body. However, gypsum is mainly observed filling cracks and calcite is seen in appreciable amounts in the peripheral parts of the area.

#### 4.1.4 El-Gedida area

##### 4.1.4.1 Topography

El-Gedida, the biggest and richest iron ore deposit of Bahariya, is located on the northern plateau about 15 km

south-east of the northern extremity of the Bahariya Depression. The area is topographically distinguished into three parts.

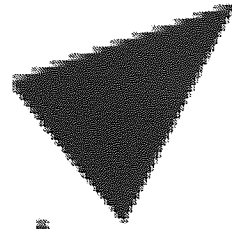
- 1 - the high area in the centre,
- 2 - the low surrounding valleys, and
- 3 - the lower plateau limestone surrounding the whole Gedida area.

The central high area is a levelled plateau intersected by numerous valleys, upon which appear five conspicuous peaks. The highest of these peaks is Lyons Hill which is 255 m above sea level (Fig. 4.2a). The average relief difference between the high hillocks and the plateau level is about 40 m, whereas that between the plateau surface and the surrounding valleys ranges from 20-50 m. The scarp face of this high area displays an irregular shape to form several indentations.

#### 4.1.4.2 Geology

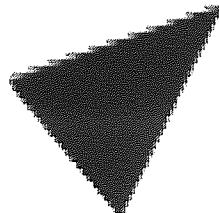
A geological map of El-Gedida area, scale 1:5000 covering an area of 17.4 km<sup>2</sup> (Fig. 4-2b) was prepared by Amer (19). It aimed basically to clarify the relationship between the iron ore deposit and the bounding limestone plateau. The outcrops on the map were measured by a grid survey for the area; the structural features were determined partly from field observations and partly from subsurface data.





Aston University

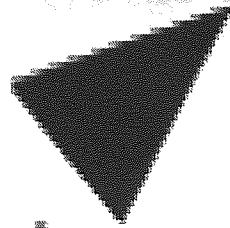
Illustration removed for copyright restrictions



Aston University

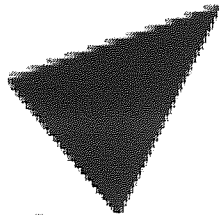
Illustration removed for copyright restrictions





Aston University

Illustration removed for copyright restrictions



Aston University

Illustration removed for copyright restrictions

The geological ages for the outcrops of the different formations recorded in this area are given below (19):

Recent

1. Superficial deposits and sand-dunes

Oligocene

2. The Radwan Formation, sandstone and quartzites.

Eocene

3. Bahr Formation, yellow limestones, thick bedded clays and sandy clays (upper Eocene).
4. Gazzum Formation, white limestone (upper middle Eocene to upper Eocene).
5. Nagb Formation, pink limestone (lower middle Eocene).

Cretaceous

6. Bahariya Formation, sandstone and clays (Cenomanian).

Besides appearing in pits of the surrounding valleys, iron ore beds in El-Gedida form the central high area and take the same stratigraphic position as the limestones. They are underlaid by Bahariya Formation and overlaid by the Radwan Formation.

The maximum thickness recorded for the ore in the area is 27.1 m as a continuous formation without any interbeds. The clay interbeds are generally absent in the central body but are frequently observed at the peripheries of the ore body; the thickness of the interbeds ranges from 0.6 to

7.7 m. On the other hand, the Eocene deposits equivalent to the iron ore beds have a thickness of about 200 m and are followed upwards by the Radwan Formation.

The following section has been measured <sup>(19)</sup> in the central high area, at Lyons Hill, (data is partly from outcrops and partly from subsurface).

Top:	(The Radwan Formation, quartzite and sandstone)	22.5 m
11	- Banded cavernous iron ore (goethite, brown, yellow hematitic and ochrous).	10.5 m
10	- Banded cavernous iron ore (hematite, dark brown with hard pockets of goethite)	10.2 m
9	- Friable iron ore (hematite, blackish or bluish brown) in the lower part conglomeratic	2.8 m
(9, 10, 11 constitute the iron ores; 23.5 m)		
8	- Barite Zone, loose yellow sands with idiomorphic small barite crystals	0.3 m
7	- Sandstone; yellow, medium-grained, indurated, cross-bedded, with thin ferruginous bands	6.0 m
6	- Sandstone, clayey, fine-grained, light-grey with green plastic clay underbeds, yellow ochrous violet or blue shades of colours are observed	3.5 m
5	- Sandstone, light yellow to dark brown, cross-bedded with white quartz grains	10.5 m

- 4 - Sandstone - white to greyish white, friable to indurated, fine to very coarse-grained. Thin clayey interbeds with oblique laminations become common downwards 24.6 m
- 3 - Siltstone, white with bluish shade, clayey and massive in parts, with rare cross bedding planes 18.0 m
- 2 - Sandstone, fine-grained with white quartz grains, yellow with white interbeds at some places, rather compact and ferruginous 6.0 m
- 1 - Clay, grey, sticky, blocky with very thin sand streaks in parts 1.1 m

(1 to 8 constitute the Bahariya Formations; and continue further downwards) 70 m

The following is the subsurface data obtained during drilling of El-Gedida water well No. 1 (Andrawis <sup>(20)</sup>) that lies in the eastern valley 2.5 km east of Lyons Hill.

Top

- 1 - Wadifills and sandy clay 9.3 m
- 2 - Hematite and hydrogoethite, with clay and sandy clay interbeds 32.1 m
- 3 - Clay and sandstone alternating bands: the sandstone is colourless, milky white, pink, ferruginous, fine to coarse-grained mostly medium grained, angular to subrounded, compact, hard, siliceous with traces of pyrite, gypsum,

anhydrite, carbonaceous matter and rare white to whitish yellow limestone. Clays are yellow to yellowish brown, pale grey medium hard, sticky

56 m

- 4 - Sandstone and clay: sandstone is colourless, yellowish, white, medium to coarse-grained, subangular to subrounded, partly calcareous, with traces of pyrite and gypsum. Clay is brownish red to yellowish brown, grey, medium hard and sticky

224 m

(3 and 4 are very poorly fossilised and the alternation of sandstone and clay represents shallow oscillatory sea deposits. Post-Cenomanian age is assigned to it and probably Oligocene)

- 5 - Sandstone with alternating shale interbeds: sandstone is fine to medium grained, angular to subangular, calcareous, partly glauconitic with traces of carbonaceous matter. Shale is dark grey, greenish grey and brownish red, medium to hard, flaky with traces of pyrite. This interval includes microfossils of the Cenomanian age

274 m

- 6 - Sandstone with streaks of shale: sandstone is white to pale yellow and pink, coarse to very coarse-grained, rounded to subrounded, partly glauconitic, loosely cemented. The shale is grey, greenish grey to brownish red, medium hard, flaky with traces of pyrite

Andrawis <sup>(20)</sup> (op. cit.), recorded in sections 3 and 4 only one species of Truncorotaloides rohri Bronnimann and Bermudez which he claimed to indicate Middle Eocene age. Also rare species of Cibicides and Ammodiscus were recorded; but they have no significance for age determination. On lithological basis, he considered this formation to be of Oligocene age "for its resemblance with El-Hamra Formation of Said and Issawi <sup>(21)</sup>". This conclusion was erroneous, since El-Hamra Formation was assigned to upper Eocene by Said and Issawi and not to Oligocene.

#### 4.1.4.3 Classification of El-Gedida iron ores

- 1 - Hard massive ore
- 2 - Banded cavernous ore
- 3 - Friable ore
- 4 - Black manganiferous ore
- 5 - Oolitic-pisolitic ore
- 6 - Ferruginous sandstone

These six ore types differ from each other in mineralogical composition, and in properties of the hand specimen. They also have a fixed field relation with respect to the geological setting of the ore body (Basta and Amer <sup>(17)</sup>).

#### 4.1.4.4 Mineralogy of El-Gedida iron ores

##### 4.1.4.4.1 Hard massive ore

This ore type consists mainly of crystalline hematite or goethite. It is chiefly hematitic, hard, crystalline, with a deep reddish-brown colour and a submetallic lustre. It is usually massive but may be occasionally cavernous, in the latter case crystalline barite is observed filling the

cavities. The grade and density of this type is higher than those of the others. Its density is about 2.72 tonne/m<sup>3</sup> and its iron content averages about 60%. This ore type occurs in the central high area of El-Gedida south of the line F (see geological map, Fig. 4.2b), with a thickness ranging from 0.5 to 8.0 m. Barite which is the chief gangue mineral in this ore type, is mainly present in the lower parts of the ore body in contact with the sandstone of the Bahariya Formation, where it occurs as small euhedral and brecciated crystals.

Halite and gypsum are two other gangue minerals but are much less common than barite, they usually occur in the upper parts of the ore body particularly filling cracks.

#### 4.1.4.4.2 Banded Cavernous ore

This is formed as an intimate association of goethite and hematite and has a brown or yellowish brown colour. It is usually cavernous, and these are filled with red or yellow ochre powder and sometimes with black manganiferous powder. In El-Gedida area, it is found in the central high area in the north of line F (Fig. 4.2b) and partially underlies the previous ore type.

Density varies from 2.60 to 2.67 tonne/m<sup>3</sup>, and the iron content is about 57%. Halite, gypsum, barites are the main gangue minerals in the ore. These occur generally as surface cracks fillings or in the form of a salty crust. They are sometimes found intercalated with the ore or in the form of small limited pockets.



#### 4.1.4.4.3 Friable ore

This is formed mainly from fine crystalline goethite and hematite as well as much amorphous limonite and ochrous clays and has various colours grading from bright yellow to dull dark brown with occasional blue or violet tints. The ore is soft and friable. Its density is approximately 2.0 tonne/m<sup>3</sup> and iron content about 55%. The most common gangue is the clayey material.

#### 4.1.4.4.4. Black manganiferrous ore

This ore type is usually friable. It is constituted from hematite and goethite together with an amount of manganese minerals enough to give it its characteristic black colour.

In El-Gedida, this ore type is present underlying the banded Cavernous ore in the central high area and also at the peripheries of the ore body. Its density is 2.3 tonne/m<sup>3</sup> and average iron content 53% with manganese 3.5%. The common gangue minerals consist of fine dispersed quartz grains which increase towards the peripheries.

#### 4.1.4.4.5 Oolitic-Pisolitic ore

This ore type varies from a purely oolitic ore to an almost pisolitic ore or pisolitic-oolitic ore.

In El-Gedida, the oolitic ore is a brown hematitic ore of moderate to high grade (iron content ranges from 55 to 60%) and density 2.25 tonne/m<sup>3</sup>. The ore is made up of small



oolites (0.5 mm average diameter) with small rhombohedral crystals in the interstices. The main gangue minerals are dispersed quartz grains with halite sometimes filling cavities. This ore type is found in the central high area associating with the banded cavernous ore in the form of pockets or interbeds of small extension.

#### 4.1.4.4.6 Ferruginous sandstone

This low grade ore consists of angular to subangular quartz grains embedded in a matrix of iron oxides and hydroxide (mainly goethite).

#### 4.1.4.5.1 The contact of the iron ore deposit with the underlying Bahariya Formation

1. The contact between the ore body and the underlying sandstone of the Bahariya Formation is sharp but uneven, it shows signs of gradation in places.
2. At the central high area, where the underlying bed is sandstone, a continuous barite zone is always observed just below the iron ore. It consists of small barite crystals and yellow or greenish yellow loose sands. The thickness of this zone varies from 10 to 50 cm in places.
3. A conglomerate band of silicified limestone boulders is sometimes observed either at the base of the ore body or above the base by one or two metres.

4. The last one or two metres of the ore body are always of soft, dark brown ore, except in the case where the conglomerate band or clay marks the actual lower contact. This soft ore has a slightly higher iron content than the main ore that is usually reddish or yellowish brown, much harder and compact. Although the contact between this soft ore and the sandstone is sharp, its irregular nature and the fact that the sandstone below has a similar lithological appearance as the soft ore, may indicate that these few metres of the ore represent the top of the Bahariya Formation that has undergone intense replacement.

4.1.4.5.2 The contact of the iron ore deposit with the overlying Radwan Formation

No clear relationship was observed at this contact but there is an apparent change in facies and the following signs of mineralization.

- 1 - The lower part of the Radwan Formation is yellow and ochrous.
- 2 - Round and flattened oolites were observed at the contact and show a high degree of Ferrugination.
- 3 - In the valleys, the overlying green, glauconitic, gypsum clays show brown stained patches and hematite pockets.

#### 4.1.4.5.3 The contact of the iron ore deposit with the surrounding Eocene deposits

Two types of contacts were observed. The first is inter-fingering contact between the iron ore deposit and the lower middle Eocene deposit, (El-Nagb Formation), and the second is the overlapping contact between it and the other deposits (e.g. Gazzun Formation) with clear unconformity. The first relation is typically represented in the surrounding valleys to the central high area, and is revealed in numerous vertical pits. The second is observed at the northern entrance to the industrial site of El-Gedida mines on both sides of the asphaltic road; here a Ferruginous bed of reworked origin overlaps the white limestone and is separated from it by a flinty conglomerate.

#### 4.1.4.6 Discussion on the origin of the iron ore

The origin of the iron ores of Bahariya has been the subject of discussion by a number of authors. Hum<sup>(22)</sup> and Attia<sup>(15)</sup> considered the ore as a shallow water lacustrine sediment possibly of Oligocene age. El-Shazly<sup>(23)</sup> believed that the iron ores were formed during a lagoonal period (late Eocene-early Oligocene) by slow weathering and leaching of the ferruginous sandstones in the central and southern parts of Bahariya oases. El Akkad and Issawi<sup>(18)</sup> stated that the ore was a result of shallow marine deposition partly with surface replacement of the carbonate rocks. Said and Issawi<sup>(21)</sup> assigned to the iron ores the age of lower middle Eocene and advocated the idea of a diagenetic replacement origin. In contrast to the above mentioned

views Nakhla <sup>(24)</sup> considered the ore as of Eocene age and hydrothermal, replacement origin, and also added the possibility of partial precipitation from colloidal solutions and by cavity filling.

Amer <sup>(19)</sup> suggested iron is most probably derived from volcanic sources. Some of his evidence in favour of such an assumption are:

1. The presence of extensive bodies of volcanic rocks in the Bahariya area and on the same structural lines as the iron ores of El-Gedida, El-Harra and of Ghorabi-Nasser.
2. The intensive replacement of the topmost part of the Bahariya Formation sandstones into a soft iron ore that is richer in iron than the overlying main ore, a fact that indicates the iron solutions came from below, concentrated in the sandstone layer and then migrated upwards into the limestone. In view of this evidence the assumption made by El-Shazly <sup>(23)</sup> that the weathering iron solutions may have infiltrated from above into the underlying Cenomanian rocks cannot be accepted <sup>(19)</sup>.
3. In the main iron ores of Bahariya, the average contents of Ti, Cr, Co, Ni, V, P and Al were all distinctly lower than those of sedimentary iron ores and correspond very well with the values observed in iron ores of volcanic origin.

The average and range of phosphorus contents have frequently been used for the distinction between genetically different iron ores, El-Hinnawi (25). In Figure 4.3 the phosphorus content in the ores of Bahariya and in other famous iron ores from various localities are given. From this Figure it is evident that the average P content in the main iron ores of Bahariya is rather low and shows limited variations. In this respect, the present ores are similar to the ores from Algeria and Tunis related to volcanic processes but are distinctly different from the Aswan, Clinton ores which are subgenetic sedimentary ores derived from weathering solutions.

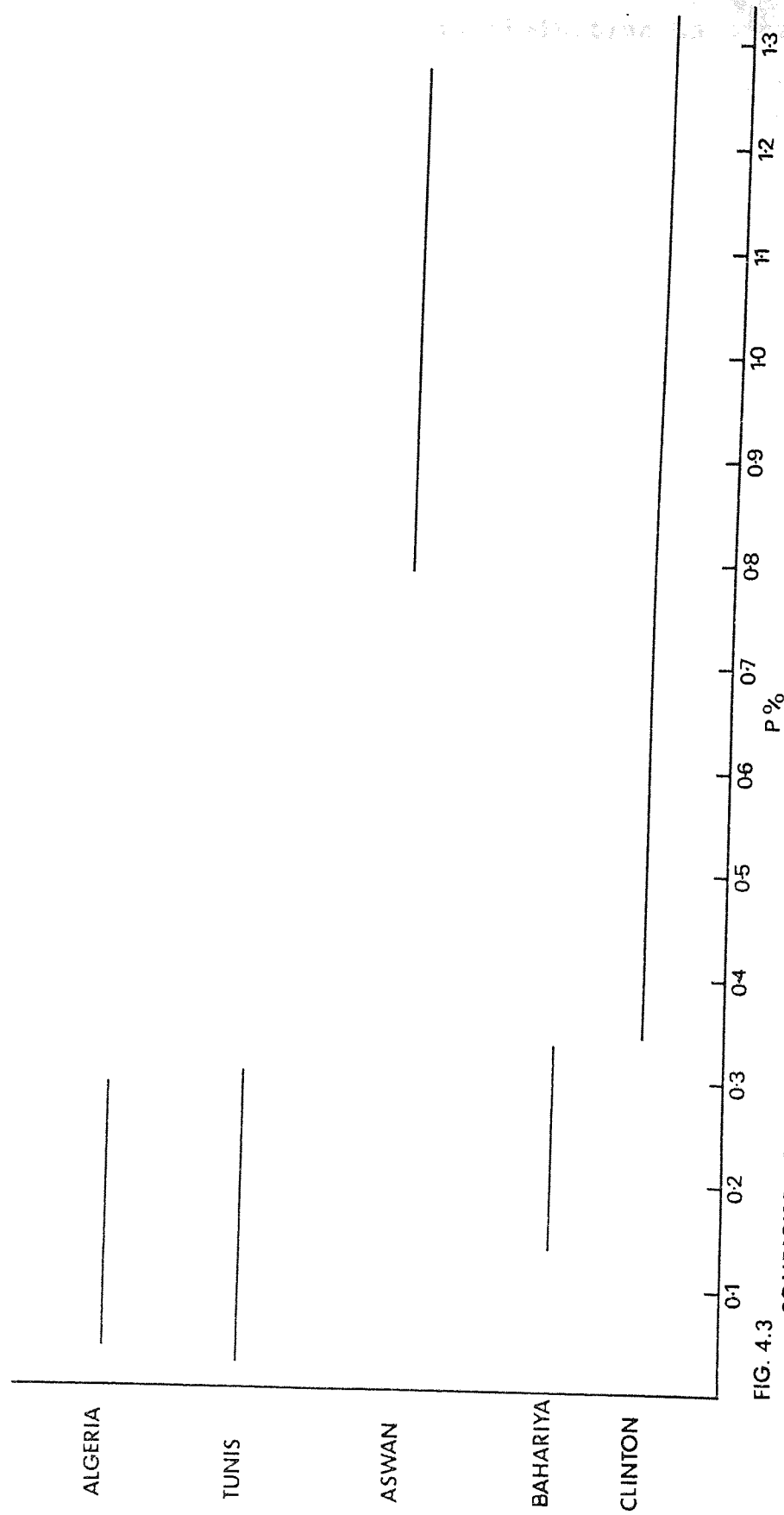


FIG. 4.3 COMPARISON BETWEEN THE PHOSPHORUS CONTENT OF IRON ORE IN DIFFERENT LOCATIONS

#### 4.2 Experimental Work on Bahariya Ore

Even today the mineral content of iron ores is still mainly obtained by chemical analysis. Discrimination is often made only between magnetite and hematite ores, and with less attention paid to the waste associated gangue minerals.

The evaluation of iron ores according to mineral content and in particular, according to the proportion of various gangue minerals, is not often reported on a routine basis from metallurgical plants. However, the gangue minerals occurring in nature could markedly influence the metallurgical reactions, such as softening temperatures, slag formation, and sintering behaviour. Although the above properties would be useful in determining the required additives and preliminary treatment to obtain a useful product, a more detailed knowledge of the mineralogy of the iron ores nevertheless would make it possible to evaluate the ores better.

It is desirable that information about mineralogy, textural relationships, particle sizes, elemental distributions and mineral associations of a deposit should be known as early as possible in mineral exploration. This data helps the exploration geologist to evaluate the deposit. It can often be obtained by microscopic study of the ore, but sometimes this data may be difficult or impossible to obtain. This will be clarified in the following work.

In addition to chemical analyses, the mineralogical investigation of ores was made by microscopic examination, x-ray mineralogy, electron microprobe analysis, and Stereoscan microscopy.



The material used in this study was taken from two cores which were collected from El-Gedida area (see Figure 4.2a).

**In the author's opinion the samples taken were representative of the Bahariya ore in the El-Gedida**

#### 4.2.1 Lithology

This iron ore bed which has a brown or yellowish brown colour consists mainly of an intergrowth of Goethite and Hematite in almost equal proportions.

The cavities and the cracks are filled with black manganese powder. The main gangue minerals are Halite and Barite, and are present as fillings of surface cracks.

The lithology of the iron ore bed has slight variations which is shown in Table 4.1.

#### 4.2.2 Geochemical variation in the vertical section of El-Gedida iron ore deposit (See Table 4.1)

##### Iron

The chemical analyses of samples collected from the core No. 1 show the maximum Fe content is 63.2% with the minimum at 49.8%. The average iron content in all sections is 59.6%. Also Figure 4.4 shows slight variations in the section.

##### Manganese Oxides

The maximum Mn oxide content is 1.61% in the first metre from the top, (the minimum Mn oxide content is 0.16%).

The vertical distribution of Mn oxide is irregular and often exhibits sharp variations.



\*

TABLE 4.1 LITHOLOGY, CHEMICAL ANALYSIS, X-RAY STUDIES  
AND SCANNING ELECTRON MICROSCOPE STUDIES  
FOR BAHARIYA IRON ORE

No	Thick/cm		Fe	CaO	MnO	Al <sub>2</sub> O <sub>3</sub>	MgO	P <sub>2</sub> O <sub>5</sub>	K <sub>2</sub> O	TiO <sub>2</sub>	SiO <sub>2</sub>	NaCl
1	10	Reddish brown manganiferous hematite ores	49.8	0.7	1.17	0.50	0.46	0.57	0.11	0.06	1.7	0.53
2	30	Reddish brown manganiferous hematite ores	54.8	0.4	1.23	0.28	0.23	0.34	0.05	0.03	1.2	0.19
3	20	Reddish brown manganiferous hematite ores, with Barite present as yellowish white, occasional shale partings laterally discontinuous	59.6	0.3	1.20	0.35	0.29	0.36	0.07	0.06	1.7	0.26
4	25	Brown hematite ore with Barite present as yellowish white occasional shale	59.2	0.7	1.49	0.23	0.15	0.37	0.04	0.03	2.0	2.14
5	10		60.8	0.2	1.61	6.20	0.17	0.35	0.03	0.01	1.0	4.44
6	25	Brown hematite and goethite	62.4	0.1	1.36	0.20	0.16	0.33	0.03	0.01	0.8	1.15
7	20	Brown hematite and goethite ores	58.6	0.1	1.44	<0.20	0.15	0.32	0.02	0.01	0.7	6.61
8	20	Reddish brown hematite and goethite with Barite and Calcite filling the cracks	62.6	0.2	0.93	0.20	0.12	0.50	0.03	0.03	1.0	0.41
9	20	Yellowish brown hematite and goethite ores	58.6	0.2	0.16	0.45	0.16	0.77	0.03	0.03	2.1	1.50
10	25	Friable yellowish brown hematite and goethite	61.0	0.1	1.08	0.20	0.08	0.38	0.14	0.01	0.7	6.00
11	30	Friable yellowish brown hematite and goethite	63.2	0.1	0.77	0.25	0.12	0.52	0.05	0.01	1.2	2.86
12	30	Friable yellowish brown hematite and goethite	61.8	0.2	0.67	0.39	0.14	0.47	0.02	0.03	1.2	2.96
13	35	Friable yellowish brown hematite and goethite	62.2	0.4	0.81	0.41	0.16	0.46	0.02	0.03	1.5	Tra
14	25	Friable yellowish brown hematite and goethite	61.4	0.8	0.79	0.51	0.19	0.41	0.02	0.03	1.6	Tra
15	30	Friable yellowish brown hematite and goethite	58.6	0.2	1.18	0.50	0.16	0.57	0.01	0.04	1.3	Tra

PETROGRAPHY STUDIES FOR SAMPLE No. 8 SHOW BANDED PISOLITIC HEMATITE-GOETHITE  
APPROXIMATELY (60/40) AND LITTLE HALITE (SOLUBLE GRAIN).

\* THE CHEMICAL ANALYSIS WAS PERFORMED IN THE DEPT. OF METALLURGY LABS BY THE AUTHOR

X-RAY

SCANNING ELECTRON MICROSCOPE

Hematite and Goethite and little Halite

Hematite and Goethite

Hematite and Goethite and small amount  
of Halite

Hematite and Goethite

The oolites show a concentric banded structure. There are anhedral grains within the concentric layer in some oolites. A few angular grains of Fe (broken oolites) in some areas of the matrix. Fe x-ray distribution map shows a high concentration of Fe in the oolites. The Si x-ray shows a high concentration in two anhedral grains. The Al, P and Ca x-ray distribution are below detection limits. S x-ray distribution shows a high concentration of anhedral grains, some of which are in the oolites and the rest in the matrix. The Cl x-ray distribution shows area of Cl not associated with other elements.

Hematite and Goethite

Hematite and Goethite

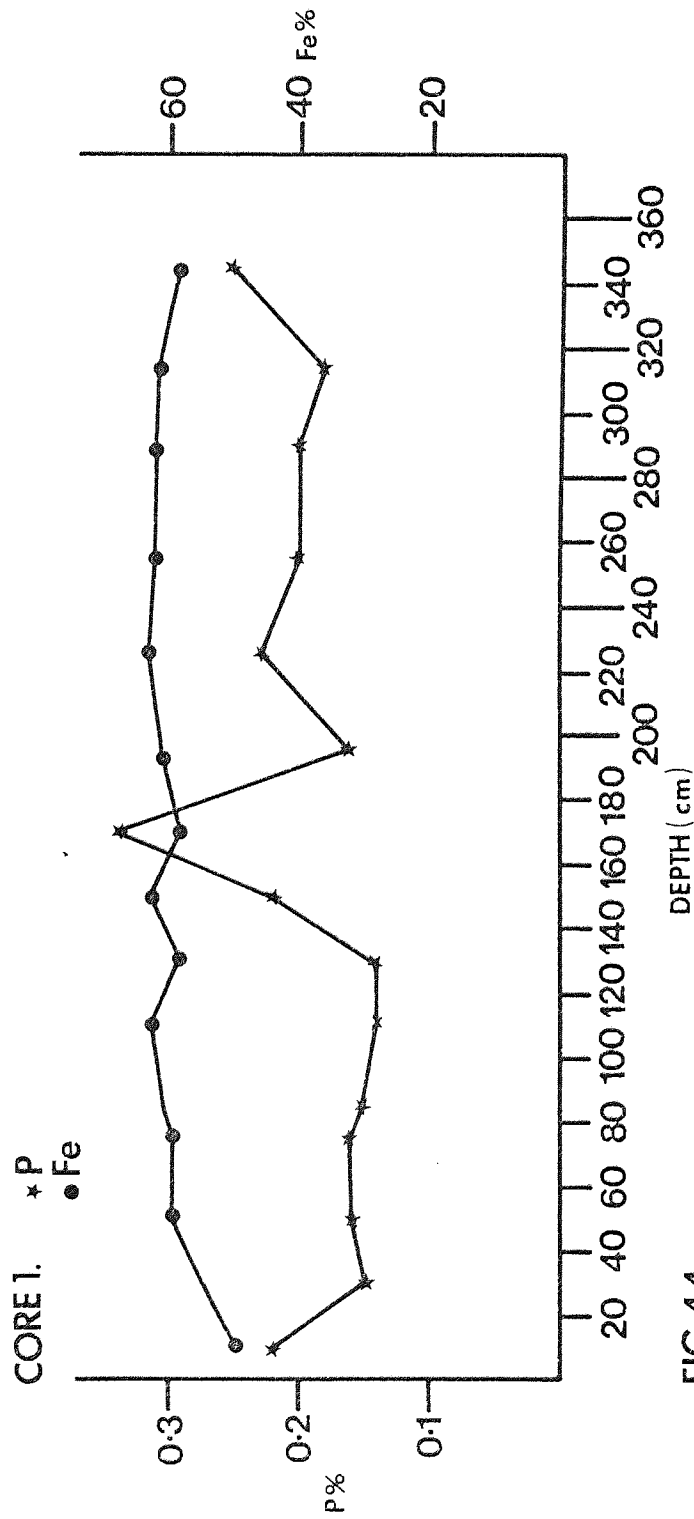


FIG. 4.4  
DISTRIBUTION OF IRON & PHOSPHORUS IN BAHARIYA IRON ORE

### Sodium Chloride

The maximum NaCl content is 6.61%. Its occurrence in the iron ore is due to Halite filling surface cracks.

### Silica

The silica content does not show a remarkable vertical variation in the core, where it is always low. The maximum content is 2.1% and the minimum content is 0.7, and the average content is about 1.3%.

### Phosphorus

This element shows a vertical variation in the ore deposit (Figure 4.4). The maximum phosphorus content is 0.34% and the minimum is 0.14%.

### Minor and trace elements

Other elements were detected in the analyses of the iron ore samples of El-Gedida but were generally present in very minor amounts, e.g. MgO (about 0.18%), CaO (about 0.3%), K<sub>2</sub>O (about 0.04%), TiO<sub>2</sub> (about 0.03%).

#### 4.2.3 Results of Microscopic Examination of Bahariya Ore

The iron ore was studied in polished thin sections. These showed pisolitic Hematite-Goethite (the ratio of Hematite to Goethite was approximately 60:40). Their average diameter was 310 µm. The section consisted of alternating thin concentric bands of Goethite with broad bands of Hematite. There were also a few angular grains of Hematite and Goethite; the length of the major axis varied from 20 µm to 120 µm.

The main gangue minerals seen were Halite which occurred as filling in the cavities.

#### 4.2.4 X-ray Mineralogy

This was achieved by the use of mineralogical analysis on the same samples used for chemical analyses. Dry sample powders were ground using a pestle and mortar. Uniform grinding times and pressures ensured that effects due to variable grain size and surface features would be minimal. Samples were examined on a diffractometer with Fe-filtered Co radiation, or Ni-filtered Cu radiation using operating potentials of 30 kV with a current of 30 mA, and 40 kV with 20 mA respectively. Goniometer traverses from  $3^{\circ}$  to at least  $60^{\circ}$  were run at  $1^{\circ} 2\theta$  per minute.

Diffractograms were studied visually to identify as many mineral phases as possible. All identifications reported are based on the appearance of at least two characteristic peaks of the minerals as given in the ASTM powder diffraction index file.

Results of X-ray diffraction mineralogical analyses of six iron ore samples from El-Gedida are presented in Table 4.1. A typical X-ray diffractogram for two of the iron ore samples is shown in Figures 4.5 and 4.6. Three mineral phases were identified by X-ray techniques within the samples. Typically, two mineral phases were observed within any one sample.

Hematite was the major phase, with varying amounts of Goethite and small quantities of Halite were also identified.

Figure 4.5 Typical X-ray  
Diffractogram of one of Bahariya  
Iron Ore Samples (Sample No. B5)  
(Co K $\alpha$ )

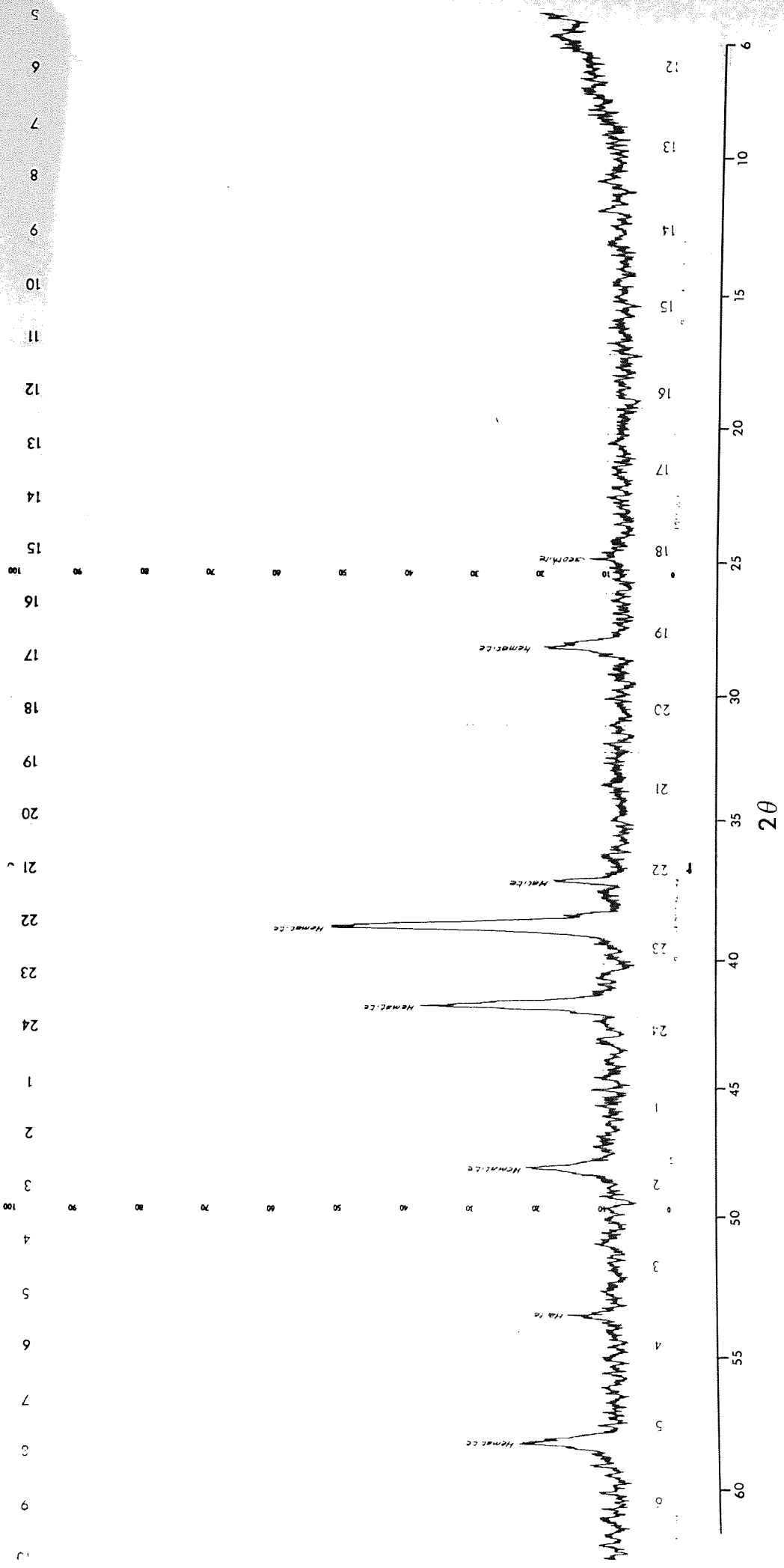
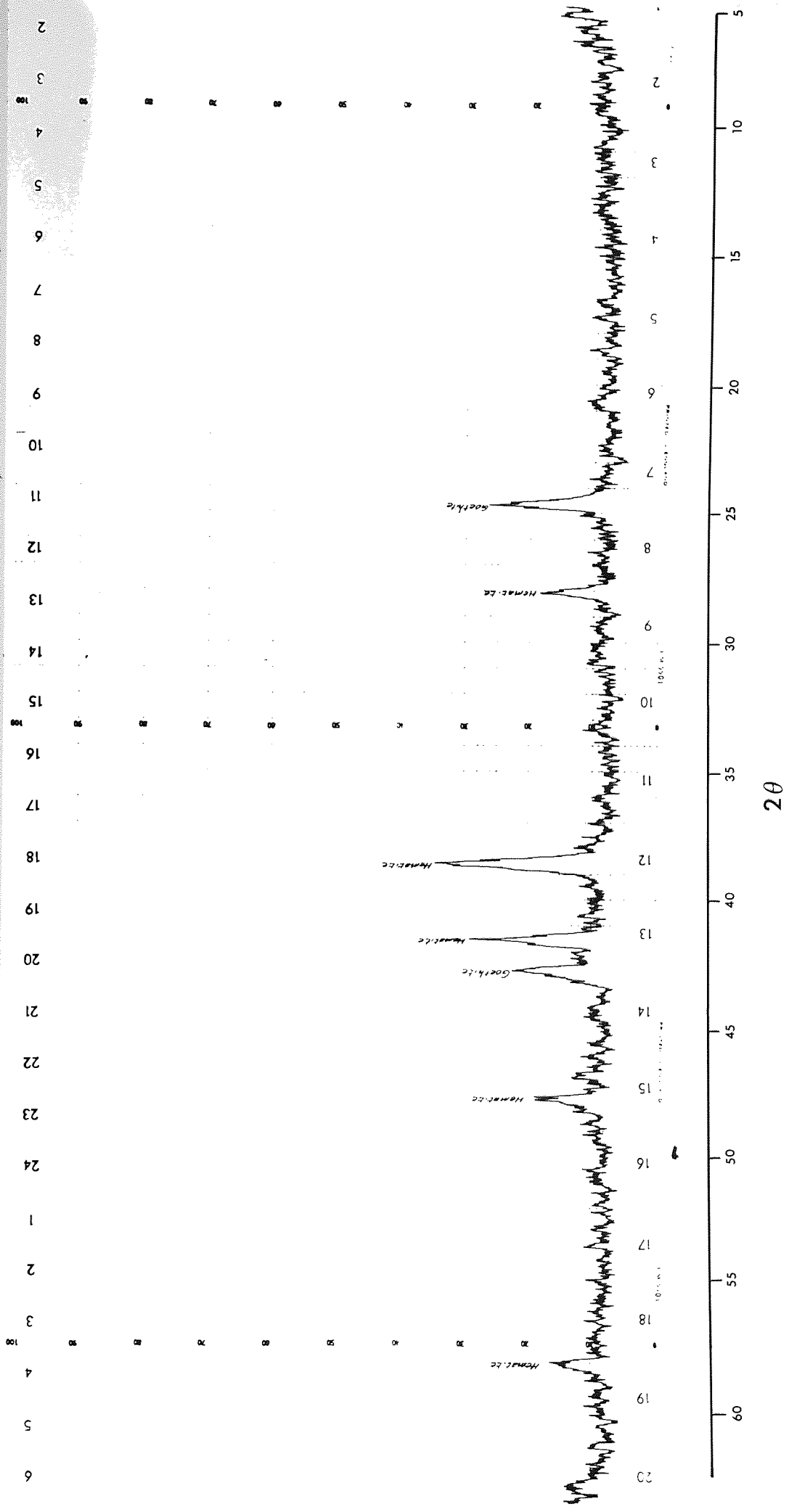


Figure 4.6 Typical X-ray  
Diffractogram of one of Bahariya  
Iron Ore Samples (Sample No. B14)  
(CoK $\alpha$ )





#### 4.2.5 Scanning Electron Microscopy (Operating Conditions p. 204)

Examination of iron ore with an ordinary petrographic microscope does not allow the study of individual apatite crystals because of their extremely fine-grained texture. However, the micron-sized crystals of sedimentary apatite are well within the range of a modern scanning electron microscope.

Burnett (7) reported that apatite crystals were present in a size range from 0.2 to 1 micron. Scanning Electron Microscopy (Stereoscan) makes possible the mapping of elemental distributions by employing electron-beam scan techniques.

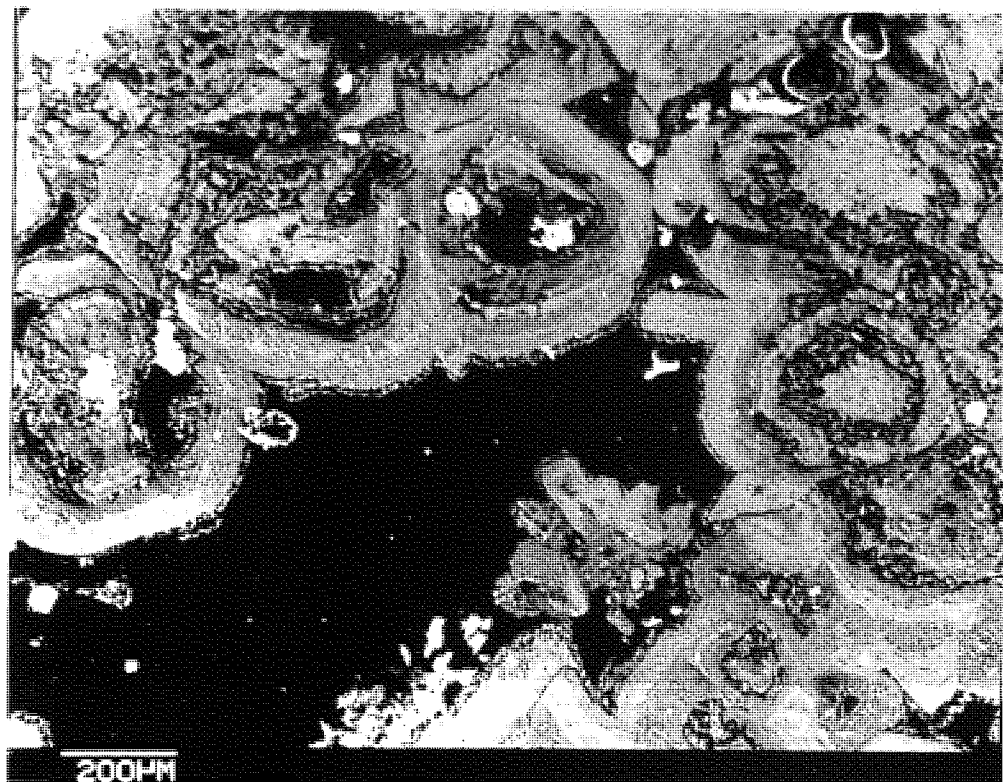
**From the two samples examined, one is presented here**

In the scan photographs (Figure 4.7) the ooliths show a concentric banded structure. In several ooliths there are anhedral grains within the concentric layers. The average length of the major axis for the ooliths is about 310  $\mu\text{m}$ . A few angular grains of Fe (broken ooliths) are seen in some areas of the matrix; the length of the major axis varies from 20  $\mu\text{m}$  to 120  $\mu\text{m}$ . The Fe X-ray distribution map shows a high concentration of Fe in the ooliths.

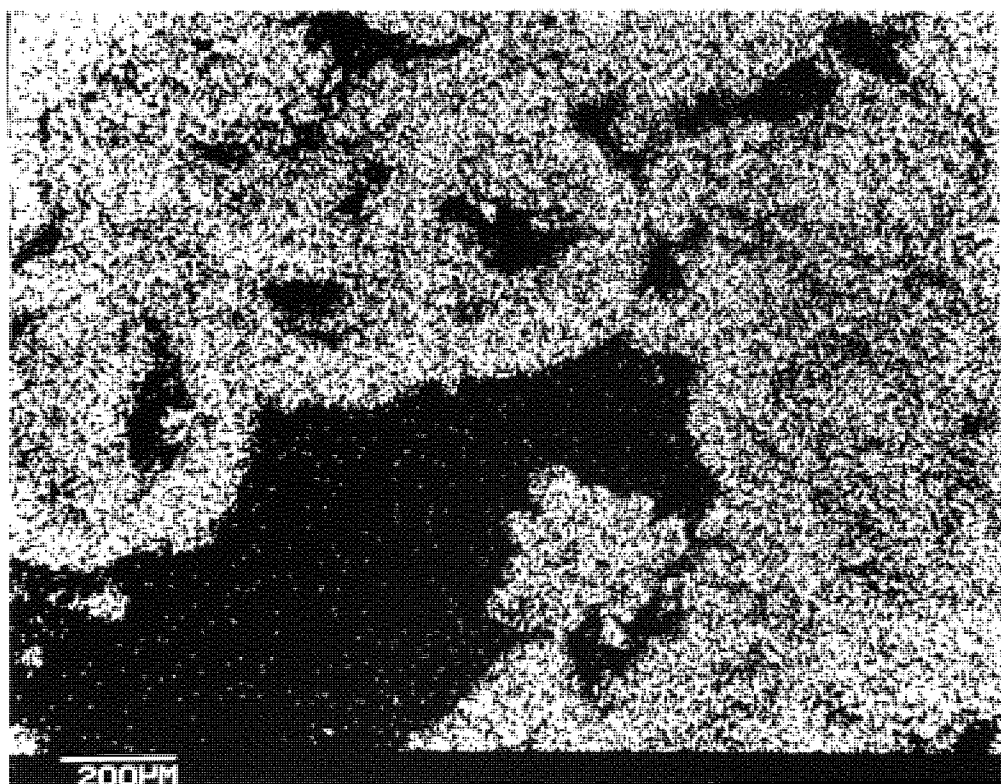
The Si distribution shows a high concentration in two anhedral grains not associated with other elements; the length of the major axis is about 30  $\mu\text{m}$ . Si is also seen disseminated throughout the micrographs in very low concentration. The Al, P and Ca X-ray distribution are below detection limits.

Figure 4.7 Scanning Electron  
Micrograph of Bahariya Iron  
Ore Sample No. 8 and X-ray  
Distribution Maps x100

- a - Scanning electron micrograph
- b - Iron X-ray distribution map
- c - Silicon X-ray distribution map
- d - Aluminium X-ray distribution map
- e - Phosphorus X-ray distribution map
- f - Calcium X-ray distribution map
- g - Sulphur X-ray distribution map
- h - Chlorine X-ray distribution map



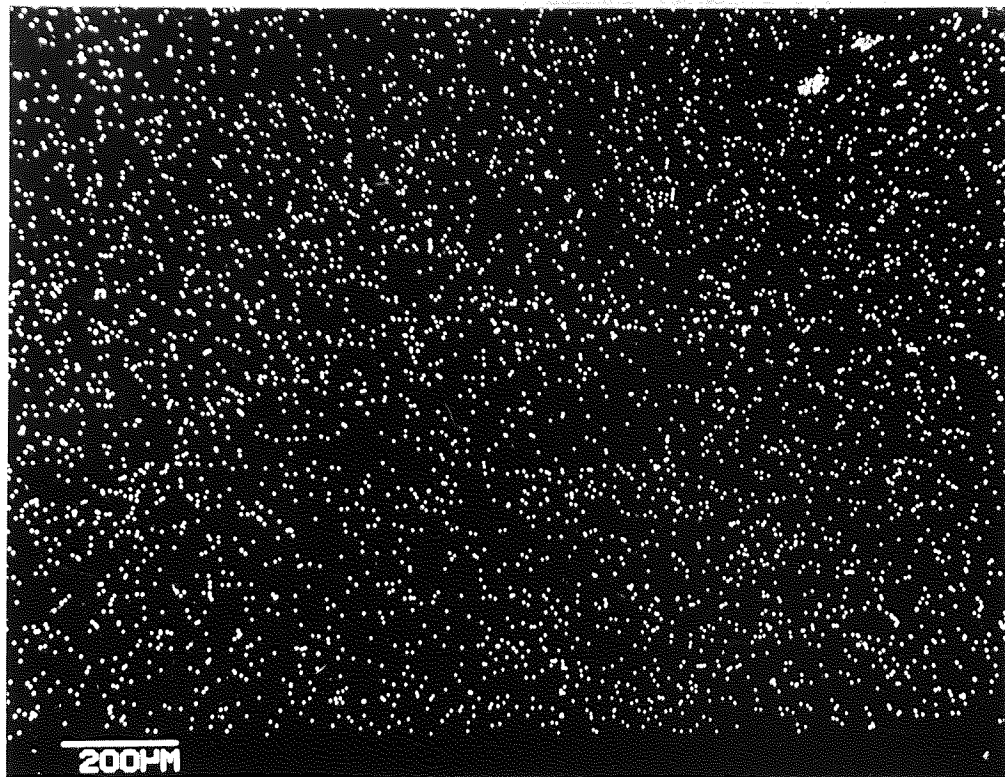
a.



Fe

b.

Fig. 4.7



Si

c.

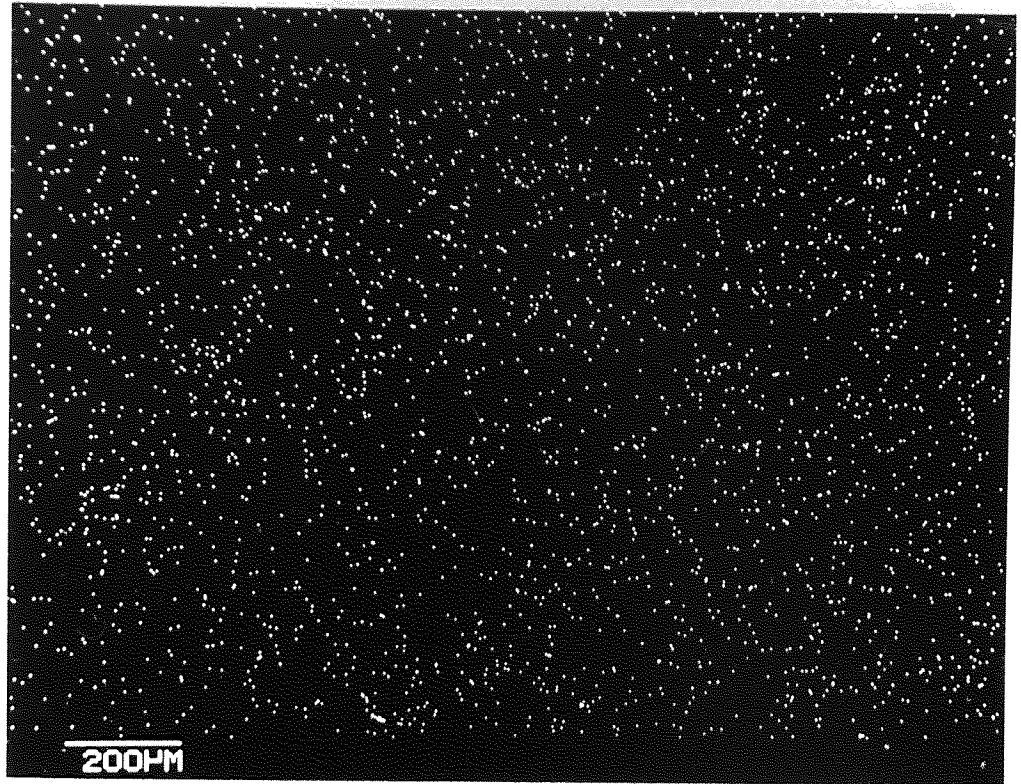


AL

d.

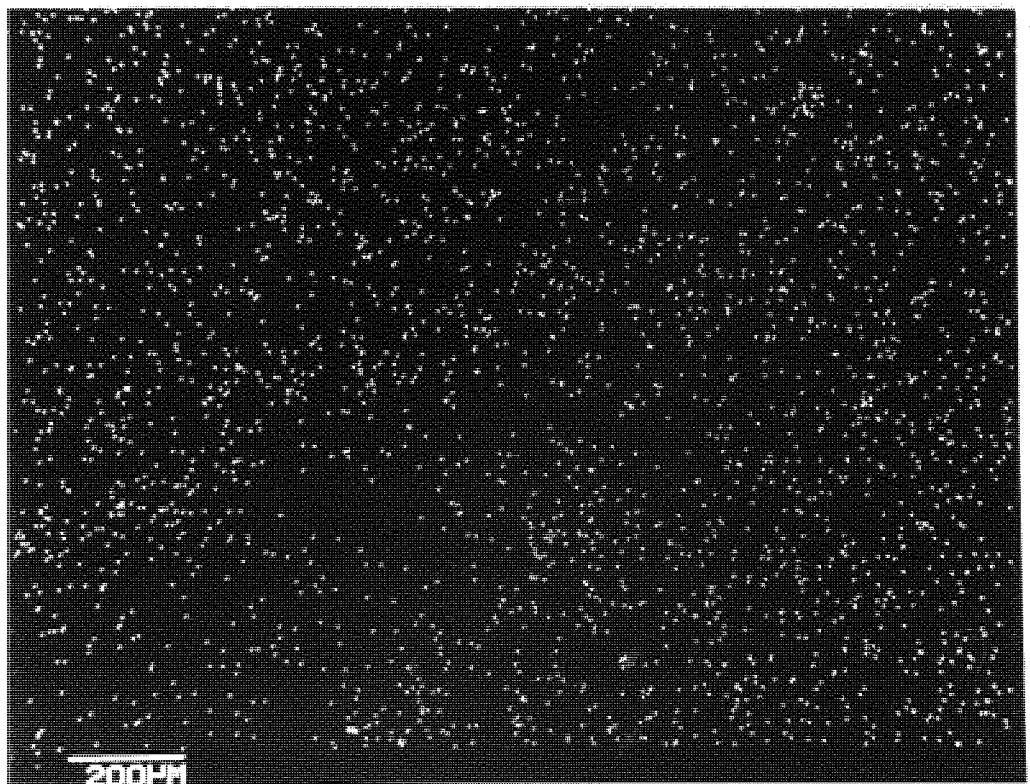
Fig. 4.7





P

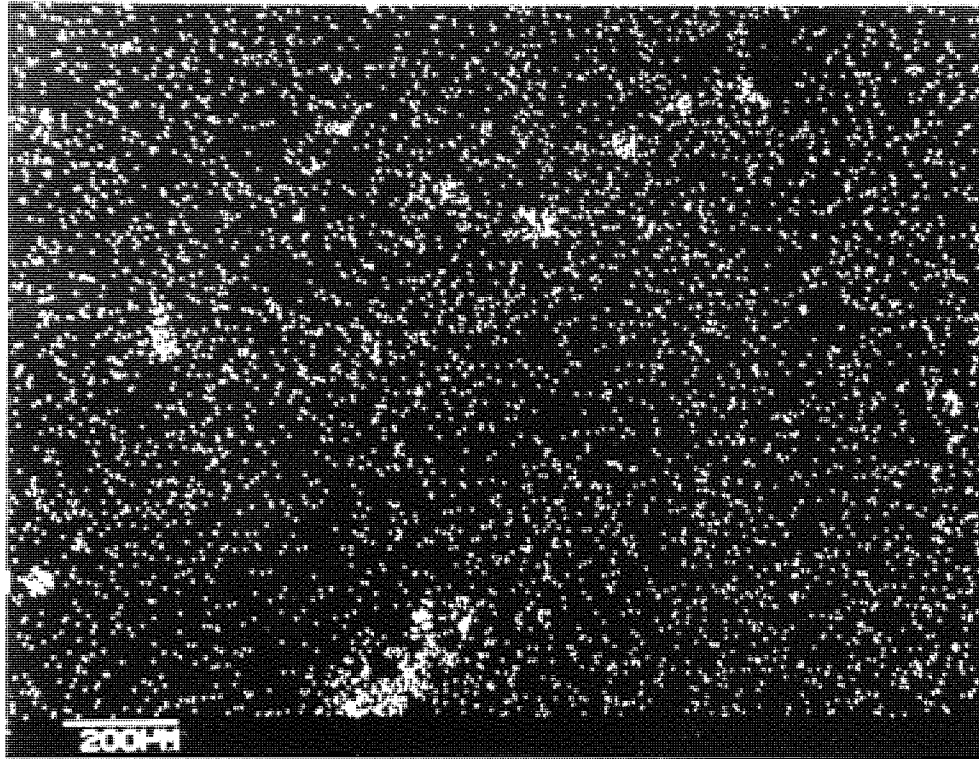
e.



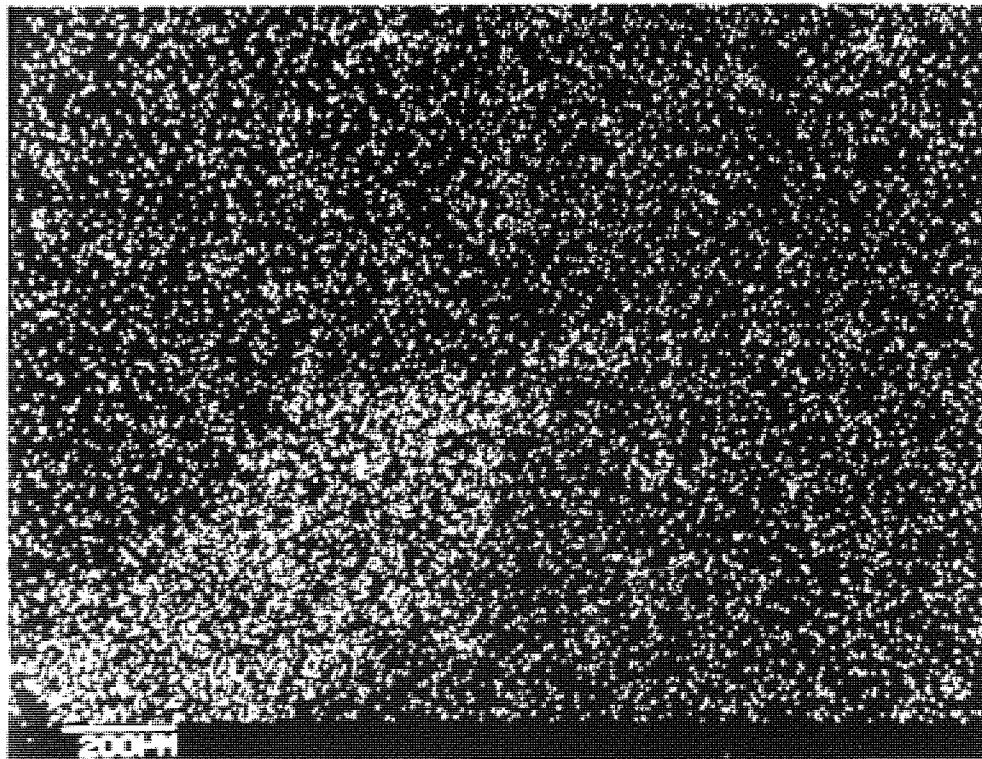
Ca

f.

Fig. 4.7



g.



h.

Fig. 4.7

S distribution shows a high concentration of anhedral grains, some of which are in the ooliths within the concentric layers and the rest in the matrix (see Figure 4.7); the length of the major axis varies from 20  $\mu\text{m}$  to 40  $\mu\text{m}$ .

The Cl distribution shows a moderately high concentration area (bottom left of micrograph) not associated with other elements.

Fe in the ooliths is shown from petrographic studies to be as iron oxides. Si appears in two anhedral grains and is shown from petrographic studies to be quartz.

S is shown as anhedral grains not associated with the other elements it is shown from hand specimen identification to be Barite. Cl occurs as a high concentration area which was shown from X-ray studies and petrographic studies to be dissolved grain of Halite.

#### 4.2.6 Summary of Results

The iron ore deposits considered in this thesis occur at four localities: Nasser area, Gebel Ghorabi, El-Harra and El-Gedida. The ore at Bahariya is dark brown to dark red colour and consists mainly of hematite and goethite with pockets of ochre and manganese oxides. The gangue minerals are Halite, Gypsum, Barite, Quartz and Calcite.

El-Gedida area contains the biggest and richest iron ore deposit of Bahariya. The ore is classified into six types according to the mineralogical composition and the properties of the hand specimen: Hard massive ore, Banded cavernous ore, Friable ore, Black manganiferrous ore, Oolitic-Pisolitic ore



and Ferruginous sandstone. From chemical analysis (Table 4.1) the Fe content is between 49.8-63.2% and P is between 0.14-0.34%. From X-ray examination Hematite was the major phase with varying amounts of Goethite and small quantities of Halite.

Electron microprobe analysis and scanning electron microscope studies proved that there are small apatite fine grains disseminated throughout the ooliths.

### 4.3 Aswan Iron Ore

#### 4.3.1 Topography

The area in which the iron ore deposits occur lies between latitudes  $24^{\circ} 03'$  and  $24^{\circ} 14'$  North and longitudes  $32^{\circ} 52'$  and  $33^{\circ} 22'$  East.

Its western boundary is the Nile Valley; to the north it is bounded partly by Wadi Subeira and partly by Wadi Allawi, to the east by Wadi Allawi; and to the south partly by Wadi Abu Agag. It extends approximately 50 kilometres from east to west and 20 kilometres from north to south; the area is, therefore, roughly 1,000 square kilometres. The iron ore deposits do not cover the entire region but are found scattered within it.

The area is a plateau varying in level from about 150 metres above sea level at the Nile Valley side to about 350 metres above sea level on the eastern side; the highest peak in the area is Gebel Dineisa, in the south-eastern portion, which is 418 metres above sea level. The Nile valley level in the Aswan district is roughly 100 metres above sea level. The depths of the major wadis of the geographical boundaries vary from 50 to 100 metres.

#### 4.3.2 The Nubian sandstone series

The Nubian sandstone covers more than two-thirds of the district. The strata forming this series includes layers of conglomerates, pebble bands, grits, quartzites, sandstones, clayey sandstones, sandy clays, clays or shales and in places valuable beds of oolitic iron ores. These

layers overlie ancient (Precambrian) igneous (granite, etc.) and metamorphic (gneisses but mainly schists) rocks (25).

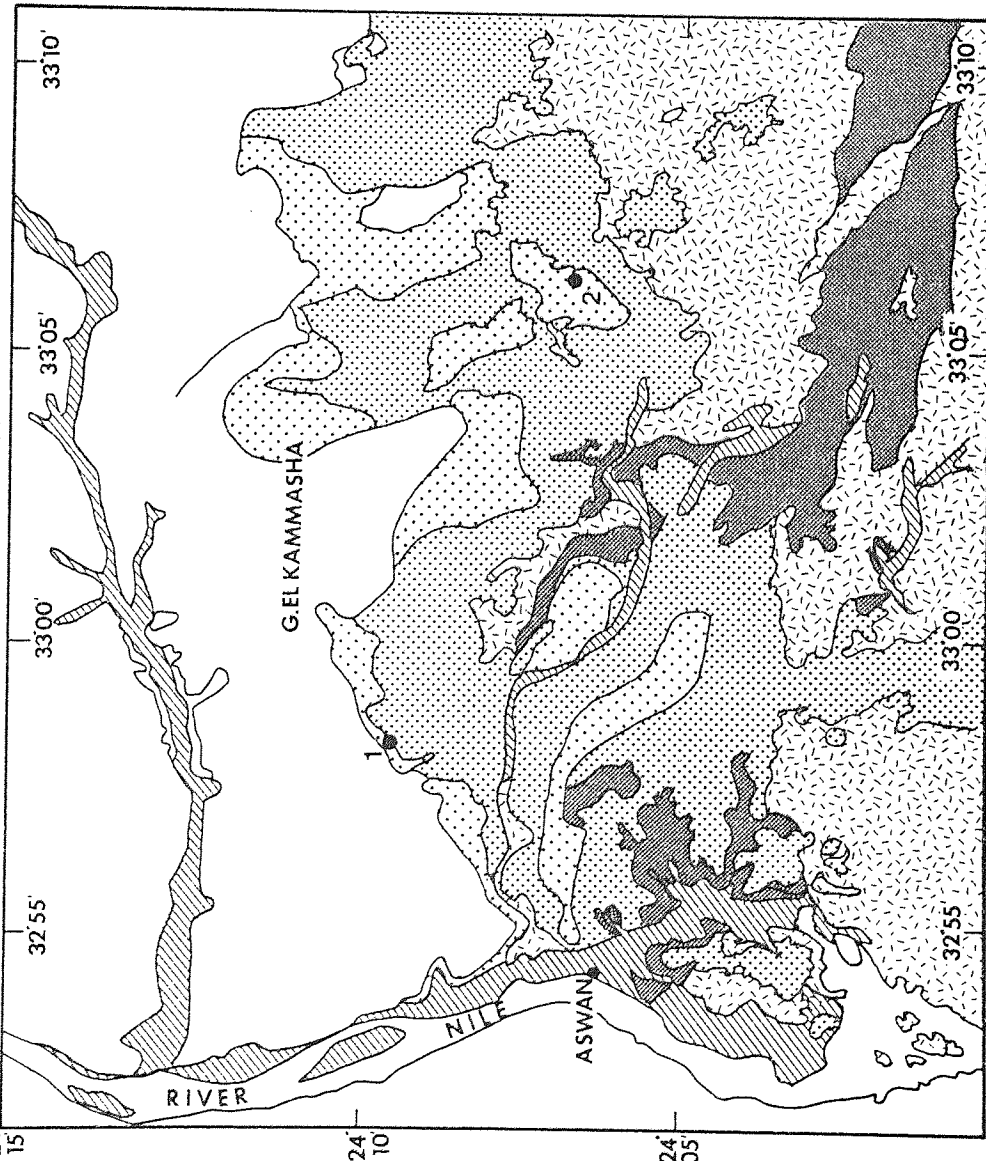
In the district, the total maximum thickness of the groups forming the Nubian sandstone series probably exceeds 150 metres. The complete succession of the strata is to be found in the cliffs bordering the Nile Valley and there it attains a thickness of about 100 metres (see next section).

#### 4.3.2.1 Measured Geological sections of the entire Nubian Sandstone series

Vertical sections have been measured by Attia (27). (His section was taken at a point below the word "Inscription" (see map, Fig. 4.8) on the cliff bordering the Nile Valley). It gave the following succession of strata from top to bottom.

	<u>Top</u>	<u>Thickness in metres</u>
Upper	( 10 Medium to coarse-grained sandstones getting hard and quartzitic near top	35.0
	( 9 Pinkish sandstone	8.0
	( 8 Refractory clays	4.0
	( 7 Ferruginous Sandstone	1.5
Middle	( 6 Red, oolitic iron ore (lower Horizon)	2.5
	( 5 Ferruginous sandstone	6.0
	( 4 Hard, grey sandstone	7.0
	( 3 Variegated, sandy clays	10.5
Lower	( 2 Medium to coarse grained sandstone, clayey towards the middle	13.5
	( 1 Kaolinaceous sandstone, peddly at base	4.0
	( - Kaolinised, pink granite	-
	<u>Bottom</u>	
	Total thickness of Nubian series	92.0

FIG. 4.8  
 24° 15' 24° 10' 24° 05' GEOLOGICAL MAP SHOWING DESERT EAST OF ASWAN



LEGEND.

-  Recent & Pleistocene
-  Upper Group
-  Middle Group (with Oolitic Iron-Ore Bands)
-  Lower Group
-  Granite
-  Metamorphic
-  1 & 2 Cores

The Nubian Sandstone Series

Scale: 1:180 000

### 4.3.3 Geological Classification of iron ore deposits in the District

The different forms of iron ore deposits in the district are as follows:

- 1 - The Ferruginous sandstones
- 2 - The ferruginous concretions
- 3 - The Oolitic iron ore

#### 4.3.3.1 The Ferruginous sandstone

The Ferruginous sandstones are reddish, brownish or dark-grey, fine to medium grained rocks; they may be hard and compact or soft and friable. In some localities, the Ferruginous sandstones are clayey or intercalated by thin bands of Ferruginous clay.

Ferruginous sandstones are associated with the oolitic iron ore; they are generally encountered underlying or overlying the oolitic iron ore but sometimes they are seen intervening two bands of the oolitic ore. In many localities, the Ferruginous sandstones cap the oolitic iron ore and these act as a protective cover and save the iron ore from being eroded.

Ferruginous sandstone may contain a little amorphous or even oolitic hematite and in several occurrences, transitions from Ferruginous sandstones to oolitic iron ore are found.

Several analyses have been made of different samples of these Ferruginous sandstones reported by Attia <sup>(27)</sup>. The range of iron, silica, phosphorus and sulphur is tabulated as follows:

Fe	2.0 - 49.3%
SiO <sub>2</sub>	9.5 - 95.3%
P	0.004 - 2.9%
S	Nil - 0.88%

The table shows the wide range of iron, silica, and phosphorus contents and the presence of sulphur sometimes. As a whole, the iron content of the Ferruginous sandstone is low and the silica content high.

#### 4.3.3.2 The Ferruginous Concretions

Ferruginous concretions are mainly found in sandstones of the Middle Group of the Nubian sandstone series. The concretions are dark-brown or almost black in colour and occur either in the form of spherical nodules ranging from half a centimetre to five centimetres in diameter or as elongated rods or various sizes. They are hard and have a dense usually radiating structure.

Due to the denudation of the sandstone containing these concretions and owing to their resistance to weathering, they are often seen accumulating in places in large quantities, at ground level giving it a black appearance.

Several analyses have been made of different samples of the Ferruginous concretions by Attia <sup>(27)</sup>. The average percent of the iron, silica, phosphorus are given as follows:

Fe <sub>2</sub> O <sub>3</sub>	55%
SiO <sub>2</sub>	32%
P <sub>2</sub> O <sub>5</sub>	0.15%



#### 4.3.3.3 The Oolitic iron ore

The oolitic iron ore is the principal and most valuable ore in the district.

It is a compact, dark red, oolitic hematite. In hand specimens, it is made up of spheroidal or ellipsoidal grains of red hematite. The grains are easily seen by the naked eye, they vary in size in different specimens and even in the same specimen. In some, they range between 0.3 and 1.2 millimetre in diameter but mainly 0.7 millimetre diameter. In others, they range between 0.4 and 1.6 millimetre in diameter but chiefly 1.2 millimetre diameter. The material cementing the oolitic grains is a fine, hematitic substance. Attia's <sup>(27)</sup> work showed that in the Nubian sandstone series, the oolitic iron ore deposits were confined to the Middle Group of the series and that this Group began at the base with the appearance of an oolitic iron ore band of a lower horizon (A) followed by a layer of sandstone with ripple-marks. Then came the strata of refractory clays or their equivalents; these were followed by one or more oolitic iron ore bands of the upper horizon (B) generally separated by Ferruginous sandstone. The band ended with a few layers of various sandstones.

Thickness of the oolitic hematite band (A) varies from 15 to 80 centimetres and the average thickness ranged between 32 and 40 centimetres.

The upper Horizon (B) is the most important one; it usually contains two and sometimes three bands of oolitic hematite separated by sandstone or clay. The oolitic bands are generally accompanied by Ferruginous sandstones.

The extent of the oolitic hematite bands of the Upper Horizon (B) is much more than that of the lower Horizon (A). The total thickness of the oolitic hematite of the Upper Horizon varies from 10 to 350 centimetres; its average thickness in the different areas ranges between 28 and 148 centimetres. Where the oolitic iron ores of both Horizons are present, they are separated from each other by layers, usually of sandstones and clays. In some localities these layers are mainly of sandstones alone with a total thickness varying from 4 to 17 metres (averaging 7.8 metres).

The chemical composition of the ore varies from place to place but the main constituents are  $\text{Fe}_2\text{O}_3$  and  $\text{SiO}_2$ . Analyses of a number of samples from the different localities indicate that the content of iron oxide in the ore varies between 54.8 and 88.1 percent, with an average 71.5 percent (27).

A large number of sections of the oolitic iron ore has been taken at several exposures in various localities of the area. Below is given an example for a section from Gebel Timarch area ( $33^\circ 0'5''$   $24^\circ 1'0''$ ) (27).



	<u>Metre</u>
Overburden - mainly sandstone	0.2 to 8.00
Ferruginous sandstone with oolites	0.70
Oolitic iron ore (B <sub>2</sub> )	1.20
Ferruginous sandstone	0.30
Oolitic iron ore (B <sub>1</sub> )	0.80
Clayey sandstone	0.90
Multi-coloured clays with Ferruginous sandstone band	6.50
Sandstone with ripple-marks	1.50
Whitish sandstone	0.90
Greenish clays	0.40
Ferruginous sandstone with oolites	0.20
Oolitic iron ore (A)	0.50
Overall thickness	14.10 to 21.90

#### 4.3.4 Experimental work

Investigations were carried out on samples collected from two areas in the Aswan Field between longitude 33° 6' and 32° 58' and latitude 24° 6' and 24° 9'. The lithology and chemical analyses throughout the two vertical sections were studied and are presented in Tables 4.2 and 4.3.

**It is the author's opinion that the samples were representative of two types of Aswan ore**

In addition to the chemical analysis and lithology a mineralogical investigation of the ores was made by microscopic examination, X-ray mineralogy, microprobe analysis, and stereoscan microscopy.

\* CHEMICAL ANALYSIS, PETROGRAPHY AND X-RAY STUDIES FOR ASWAN IRON ORE, CORE 1

No.	Depth/cm	Lithology	SiO <sub>2</sub> %	CaO%	Fe%	Al <sub>2</sub> O <sub>3</sub> %	P%	Petrography	X-ray
As 1	300	Overburden clayey sandstone and sandstone	53.30	2.13	1.0	38.83	0.04		Most of the sample is SiO <sub>2</sub> , small siderite, small chamosite and trace hematite.
As 3	25	White coarse grained sandstone	39.66	2.62	20.24	18.65	0.66		Majority is hematite and small SiO <sub>2</sub> , trace of chamosite
As 4			8.40	1.45	52.52	8.87	0.82		
As 5	16	Hard ferruginous sandy clay	4.37	2.09	55.12	16.46	0.42	Hematite oololiths, angular quartz grains are cemented by fine hematite.	Majority is hematite, little SiO <sub>2</sub> and trace chamosite
As 6			6.83	2.11	52.87	6.93	0.67		
As 7			5.23	1.87	54.77	14.77	0.38		
As 8	45	Oolitic iron ore	6.85	4.13	51.88	11.30	1.64	Hematite oololiths, angular quartz grains are set in fine hematite matrix	Majority is hematite, little SiO <sub>2</sub> .
As 9			7.95	3.47	49.11	10.75	1.74		
As 10	16	Red brown ferruginous sandy clay	9.58	6.36	47.01	12.21	2.02	Hematite oololiths, matrix is fine hematite with angular quartz grains	Majority is hematite, small SiO <sub>2</sub> and apatite.
As 11			12.49	3.54	45.33	12.91	1.95		
As 12	20	White sandstone containing CaCO <sub>3</sub>	59.05	4.23	9.77	15.54	1.46	Angular quartz grains set in fine quartz and hematite matrix.	Majority is hematite, small SiO <sub>2</sub> , little apatite.
As 13			65.01	0.77	8.47	14.29	0.05		
As 14	35	Fine - medium sandstone with thin layers rich in white clay mineral	69.16	Tr.	6.57	17.17	0.05	Angular quartz grains cemented by very fine material	Majority SiO <sub>2</sub> , small apatite little hematite, trace chamosite.
As 15			75.90	Tr.	1.10	21.33	0.05		
As 16	45	Oolitic iron ore	61.10	0.98	8.12	19.89	0.14	Angular quartz grains, matrix is fine grains	Majority is SiO <sub>2</sub> , trace of clay.
As 17			8.46	1.78	51.62	5.80	0.52		
As 18	300	Soft clays and sandy clay	2.38	4.11	53.52	18.44	0.95	Hematite oololiths, cemented by fine grains of apatite	Most of the sample is hematite, trace SiO <sub>2</sub> .
As 19			2.91	4.05	50.85	8.75	2.91		
As 20	35	Compact fine oolitic iron ore	5.19	2.53	53.95	8.14	0.94	Oololiths of hematite, angular quartz grains are set in the matrix of very fine hematite grains.	Majority is hematite and trace of apatite.
As 21			14.11	0.24	42.87	12.74	0.96		
As 22	35	CJlay and sandstone	16.28	1.62	44.68	10.24	0.12		Majority is hematite and trace of SiO <sub>2</sub> .
As 23			24.7	0.80	27.77	11.30	0.10		
As 24	35	CJlay and sandstone							Majority is SiO <sub>2</sub> , small hematite.
As 25									

\* THE CHEMICAL ANALYSIS WAS PERFORMED IN THE DEPT. OF METALLURGY LABS BY THE AUTHOR

CONT. TABLE 4.2 SCANNING ELECTRON MICROSCOPE STUDIES AND ELECTRON MICROPROBE ANALYSIS FOR  
ASWAN IRON ORE, CORE 1

No.	Depth/cm	Scanning Electron Microscope	Electron Microprobe Analysis
As 1	1300		Most of the sample is Si associated with Fe, angular and subangular grains of Ca.
As 3			
As 4	25		
As 42			
As 5			
As 6	16	Most of the micrograph is Fe with angular phosphorus grains (17 $\mu$ m), associated with Ca, and anhedral grains of Si associated with Al.	Most of the sample is Fe, angular Si grains, anhedral Si grains, anhedral P grains associated with Ca.
As 7			
As 8		Fe oolites, subangular Si grains in the oolites and anhedral P grains associated with Ca in the oolites and in the matrix. Matrix is fine grains of hematite and agglomerate P grains.	
As 9			
As 10	45	Oolites of Fe, angular Si grains and angular P grains associated with Ca. It also has some patches of P associated with Ca surrounding the oolites	Subangular P grains associated with Ca, and angular Si grains are cemented by fine particles of Fe associated with little Al.
As 11		Oolites and matrix of Fe, subangular Si grains, angular P grains associated with Ca.	
As 12			
As 13	16	Prismatic and subangular Si grains, Fe associated with Al and Si in the matrix. Anhedral P grains associated with Ca in the matrix.	Oolites of Fe, angular Si grains, angular and subangular P grains surrounding the oolites and the Si grains.
As 14			
As 15	20	Most of the sample is subangular Si grains, cemented by Al associated with Si and little Fe, P occurs as very little fine particles.	
As 16			
As 17	15		
As 18			
As 19	45	Fe oolites, matrix is mainly P associated with Ca, anhedral Si grains associated with Al.	Oolites of Fe associated with Al and Si, anhedral grains of P associated with Ca occurs in the oolites.
As 20			
As 21	800		Oolites of Fe associated with Si and Al, matrix is P associated with Ca.
As 22			
As 23			
As 24	35		
As 25		Fe oolites, anhedral P grains associated with Ca in the oolites, subrounded and angular Si grains, matrix is fine Fe associated with Al and Si.	



TABLE 4.3 LITHOLOGY - CHEMICAL ANALYSIS, AND X-RAY STUDIES FOR ASWAN IRON ORE CORE 2

No.	Depth/cm	Lithology	P%	CaO%	Fe%	Al <sub>2</sub> O <sub>3</sub> %	SiO <sub>2</sub> %	X-Ray
AsB1	1500	Overburden - sandstone and clays.						
AsB2	11	Ferruginous sandstone Poor ferruginous sandstone clay, pink mudstone occurs immediately above ironstone, size above 6-1 mm.	3.84 0.60	1.05 2.60	44.16 42.44	8.58 8.91	8.9 9.89	Majority is hematite, small SiO <sub>2</sub> , little apatite, trace of calcite and chamosite
AsB3			1.21	4.59	41.21	20.88	6.69	Majority is hematite, trace of chamosite and little apatite.
AsB4			0.35	1.77	52.78	7.19	6.68	
AsB5	44	Oolitic iron-ore, metallic grey ooliths 0.3-1 mm across in fine red matrix	0.66	1.97	50.92	7.12	6.16	Most of sample is hematite, small SiO <sub>2</sub>
AsB7			1.38	5.16	50.89	9.05	4.93	
AsB8			2.16	3.92	51.63	7.47	5.52	Majority is hematite, little SiO <sub>2</sub> and apatite
AsB9	11	Poorly laminated, reds ferruginous mudrock	0.49	15.88	53.20	5.95	5.20	Majority is hematite, little SiO <sub>2</sub> , trace of chamosite and calcite
AsB10			1.11	2.87	41.83	7.56	12.03	Majority is hematite, small SiO <sub>2</sub> , little apatite and trace of chamosite
AsB11			1.14	3.41	41.11	5.68	15.65	Majority is hematite, small SiO <sub>2</sub> , little apatite, trace of chamosite.
AsB12			1.37	2.87	48.63	6.32	10.59	
AsB13			0.47	3.15	57.34	5.60	4.37	
AsB14			0.90	5.15	56.55	7.15	3.36	Majority is hematite, little SiO <sub>2</sub> , trace of chamosite and calcite
AsB15			1.25	2.57	55.90	8.56	3.76	
AsB16	180		0.97	2.35	56.63	7.64	4.35	
AsB17		Oolitic iron ore, metallic grey ooliths 0.3-1 mm across in fine red matrix	1.09	1.65	56.84	4.60	5.86	
AsB18			2.30	4.79	49.54	14.75	5.24	

\* THE CHEMICAL ANALYSIS WAS PERFORMED IN THE DEPT.  
OF METALLURGY LABS BY THE AUTHOR

Clayey sandstone and clays.

#### 4.3.4.1 Lithology

The oolitic iron ore is a compact- dark-red hematite. In hand specimen it shows spheroidal or ellipsoidal grains of red hematite which are easily seen by the naked eye and whose average diameter is approximately 400  $\mu\text{m}$ . The material cementing the ooliths is a fine hematitic material. The sandstones are reddish, brownish or white, fine to medium grained rocks which are hard and compact. (See Table 4.2).

#### 4.3.4.2 Geochemical variation in the vertical sections of Aswan iron ore deposits (Tables 4.2 and 4.3)

##### Location I

##### In the oolitic iron ore

Iron: Chemical analyses show that the maximum iron content is 55.1% and the minimum is 42%. It is clear that the iron content shows a slight variation within the iron ore bed (Fig. 4.9).

Silica: The maximum silica content is 16.2% and the minimum is 2.3%. The vertical distribution of silica is irregular and often exhibits sharp variations.

Alumina: The maximum alumina is 18.4% and the minimum is 8.1%. The distribution is irregular and occasionally exhibits sharp changes in content.

Phosphorus: This distribution shows a vertical variation throughout the oolitic iron bed with a maximum phosphorus content of 2.9% and a minimum of 0.1% (Fig. 4.9).

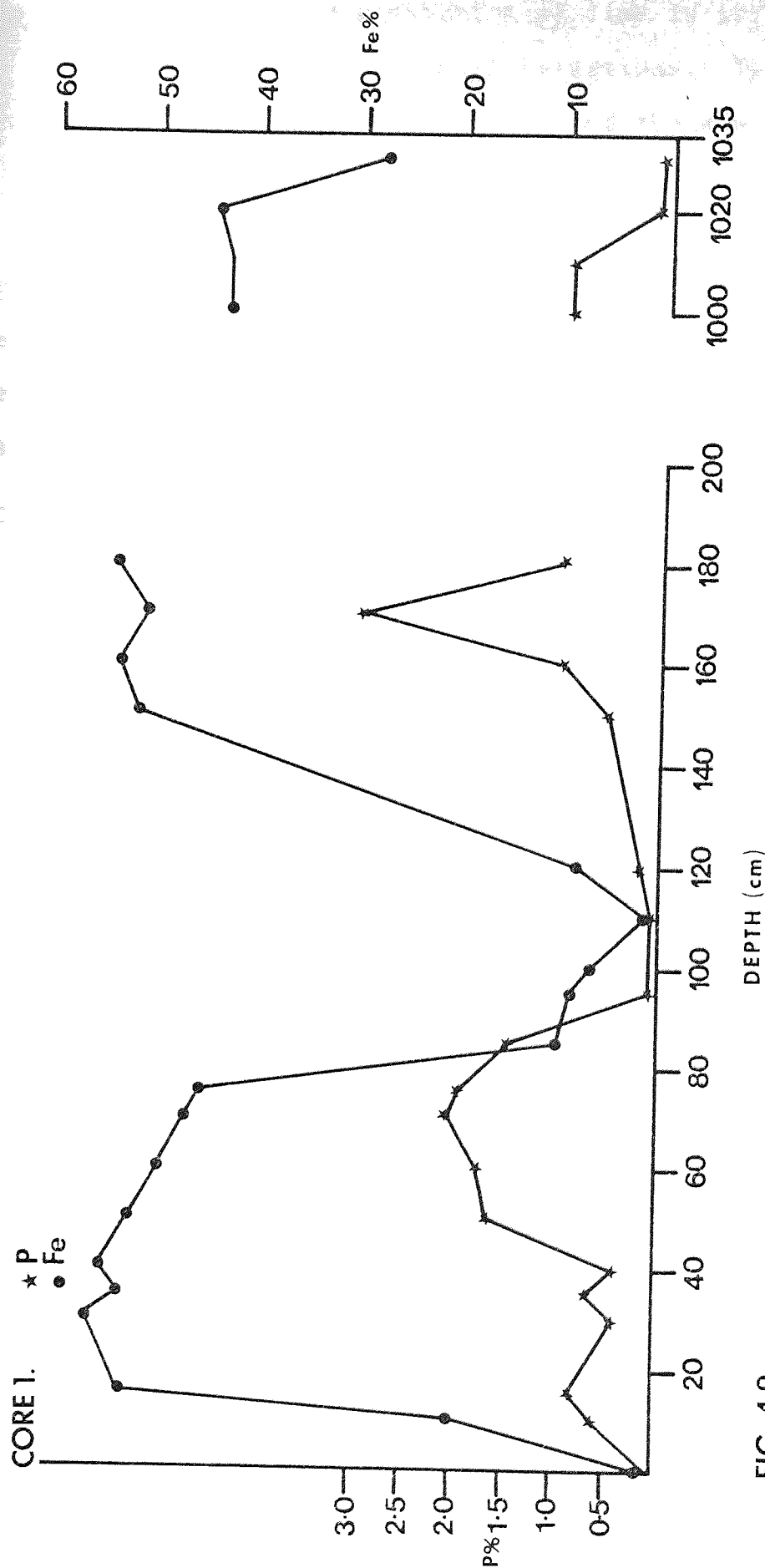


FIG. 4.9  
DISTRIBUTION OF IRON & PHOSPHORUS CONTENT IN ASWAN  
IRON ORE

Lime: The vertical distribution of lime is irregular and often exhibits sharp variations. The maximum CaO content is 6.3% and the minimum is 0.2%.

The sandstone bed

The maximum iron content is 8.1% and the minimum is 1%. The maximum SiO<sub>2</sub> content is 75.9% and the minimum is 53.3%, most of the samples which are high in SiO<sub>2</sub> are also high in Al<sub>2</sub>O<sub>3</sub> content.

Lime varies from 2.3% to a trace; Alumina 38.8-19.8% and P 0.14-0.04%.

In the Ferruginous sandy clays

Iron	20.2 - 6.5%
SiO <sub>2</sub>	69.1 - 39%
Al <sub>2</sub> O <sub>3</sub>	18.6 - 14.2%
P	1.4 - 0.5%
CaO	4.2 - trace

Location II

In the oolitic iron ore

Iron: 57.3 to 41.1%

The distribution of iron is irregular and slightly variable (see Fig. 4.10).

Silica: 15.6 to 3.3%

Its distribution is irregular and often exhibits sharp variations.



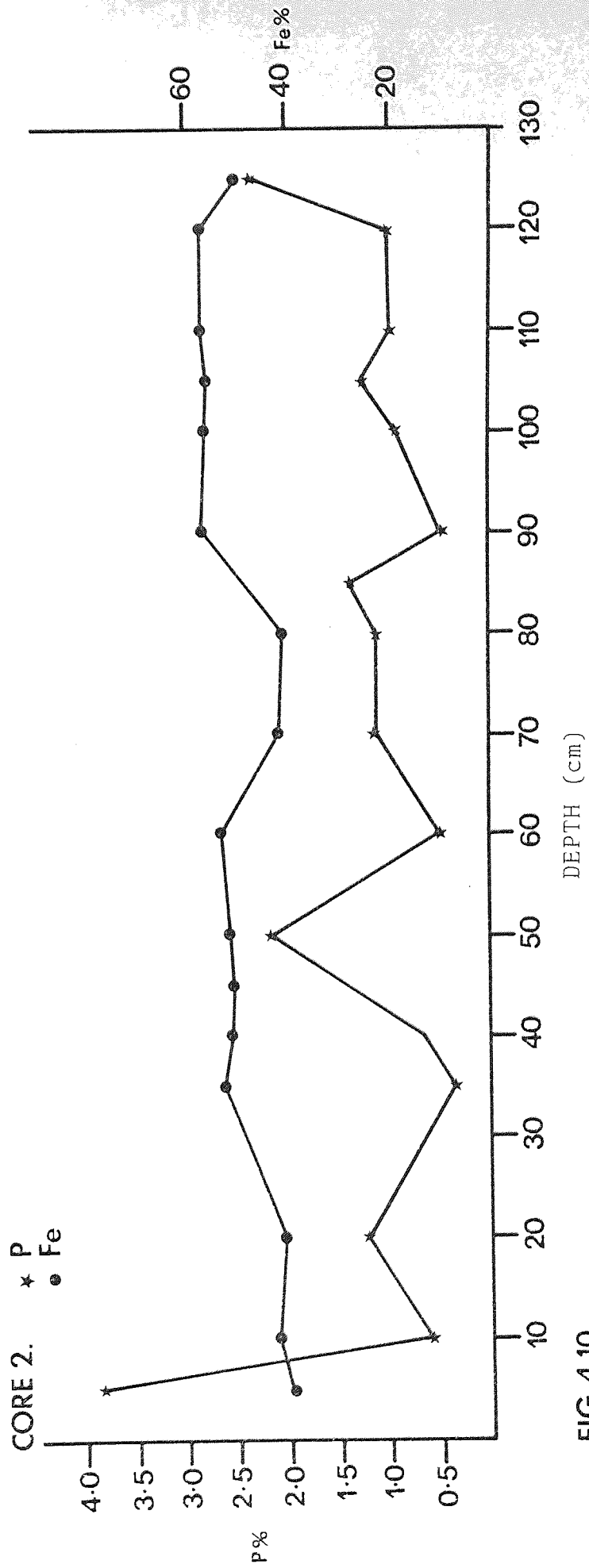


FIG. 4.10 DISTRIBUTION OF IRON & PHOSPHORUS CONTENT IN ASWAN IRON ORE DEPOSIT



Al<sub>2</sub>O<sub>3</sub>: 20.8 to 4.6%

Phosphorus: 2.3 - 0.35%

The distribution of phosphorus is irregular and occasionally exhibits a sharp variation.

CaO: 15.8 - 1.6%

The distribution of CaO is irregular and often shows sharp variation.

In Ferruginous sandstone

Iron content	44.1 - 41.8%
SiO <sub>2</sub> content	12 - 8.9%
Al <sub>2</sub> O <sub>3</sub> content	8.5 - 7.5%
Phosphorus content	3.8 - 1.1%
CaO content	2.8 - 1.0%

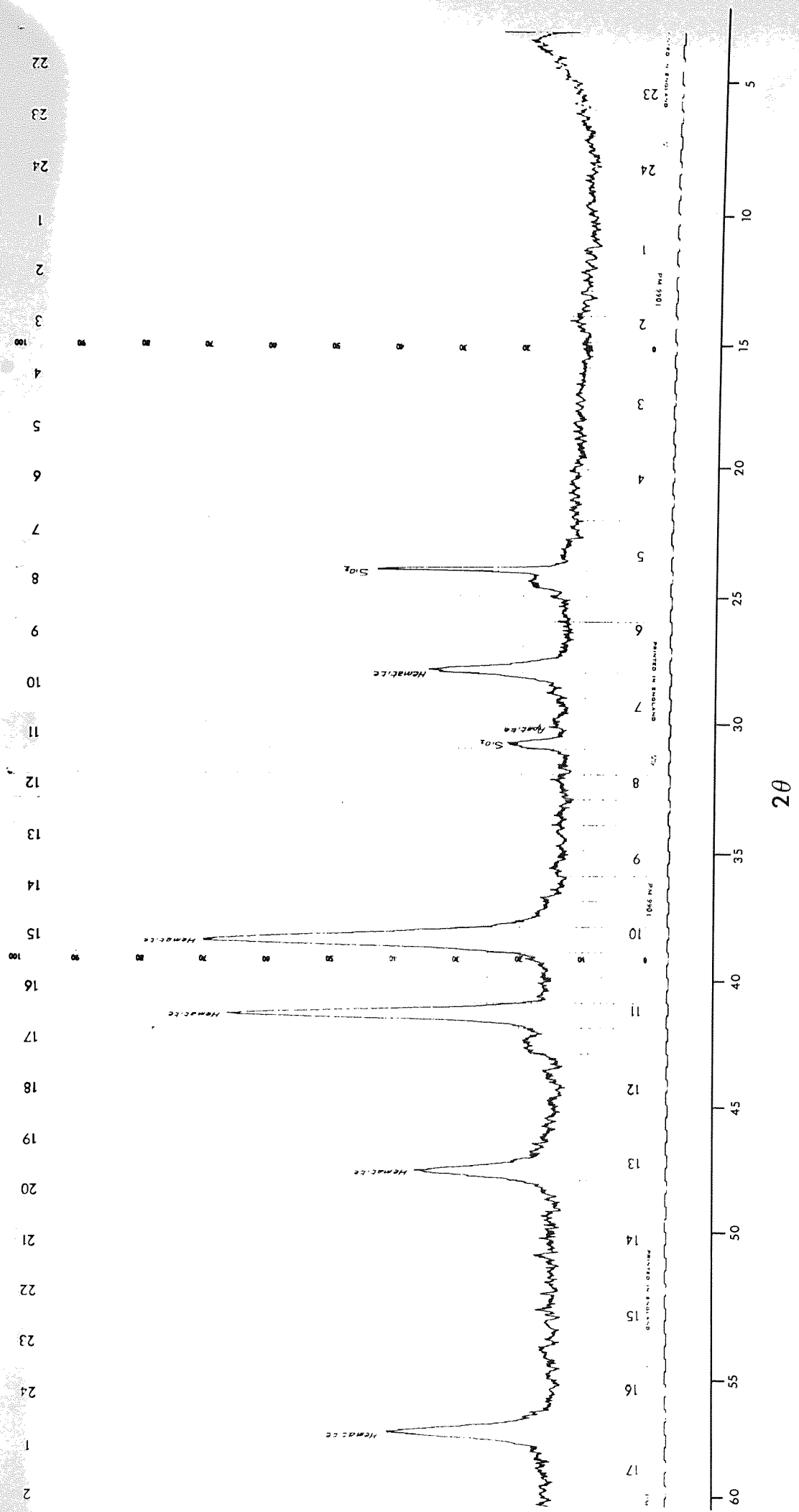
4.3.4.3 Results of X-ray diffraction mineralogical analyses are presented in Table 4.2

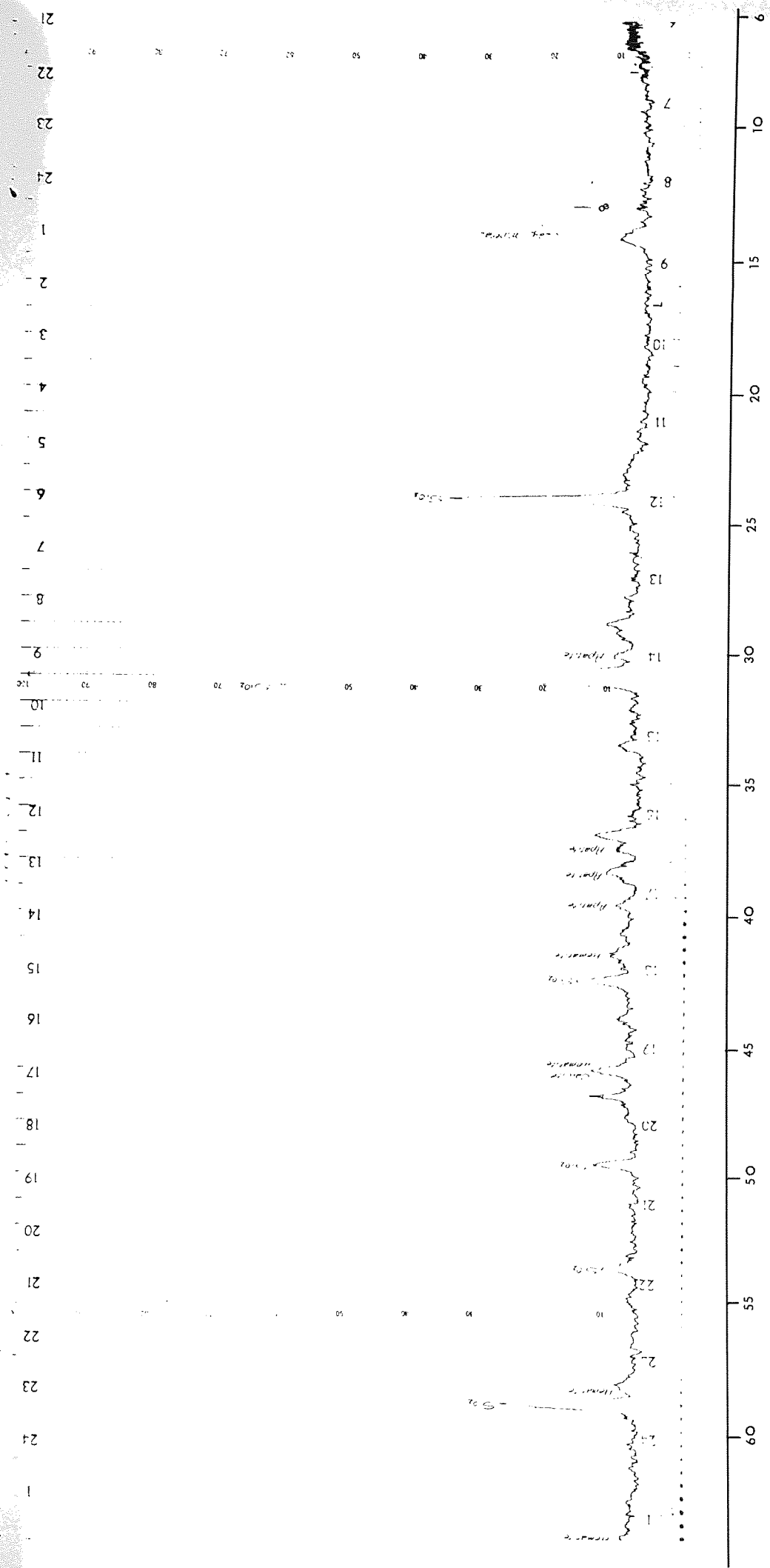
A typical X-ray diffractogram for two of the iron ore samples is shown in figures 4.11 and 4.12. **From 15 samples examined, 4 minerals were** identified within the iron ore samples - hematite, quartz, clay minerals and apatite.

Typically, two mineral phases were observed within any one sample of which hematite was the major phase especially in the oolitic iron ore sample, with varying amounts of quartz.

In the sandstone sample, quartz was the major phase with varying amounts of hematite and apatite.

Figure 4.11 Typical X-ray  
Diffractogram of One of Aswan Iron  
Ore Samples (Sample No. As 7)  
(CoK $\alpha$ )





Small quantities of clay minerals were identified in some samples (characteristic peak at  $7.17 \text{ \AA}$  d space.)

#### 4.3.4.4 Petrography

In oolitic iron ore thin sections <sup>(20 examined)</sup> the ooliths are ellipsoidal in shape, and they display a concentric banding structure mostly, the average length of the major axis is  $400 \mu\text{m}$ . The matrix may be a mixture of fine grains of hematite and clay minerals both of which cement the ooliths and angular quartz grains; or it may consist of fine grain hematite and partially agglomerated apatite crystals, both of which cement the ooliths.

The sandstone thin sections are mainly angular quartz crystals and little of muscovite, and very minor amounts of feldspar. Matrix is a mixture of fine grains of hematite and quartz with a little clay mineral (which is difficult to identify).

#### 4.3.4.5 Scanning Electron Microscopy & EPMA

Examination of Aswan iron ore by stereoscan made possible the mapping of elemental distributions for Fe, Si, P, Ca, Al and S by employing electron beam scan techniques. This was done for fifteen samples from different beds throughout the body of the ore. The technique showed the structure and grain size of the iron oxides and the gangue minerals as may be seen in the data given below.

Figure 4.13 - Scanning electron micrographs of oolitic iron ore sample No. AS10. Fe, Si, Al, P and Ca. X-ray distribution map.

Ooliths are ellipsoidal and circular in shape; the length of the major axis varies from 75  $\mu\text{m}$  to 250  $\mu\text{m}$ . Many ooliths show a concentric banding structure but in a number of cases this cannot be seen. In several ooliths there is the nucleus of another mineral grain which subsequently appears as a subangular grain within the concentric layers. For the angular and anhedral grains, the length of the major axis varied from 25  $\mu\text{m}$  to 80  $\mu\text{m}$ . The matrix cements the ooliths and is Fe rich.

The Fe X-ray distribution map shows high concentrations of Fe in the ooliths and the matrix with the higher contents in the ooliths. It is shown also that Fe concentration is independent of the concentration of Si, Al, Ca or P. The Si occurs primarily as discrete areas of high concentrations and is not associated with the other elements.

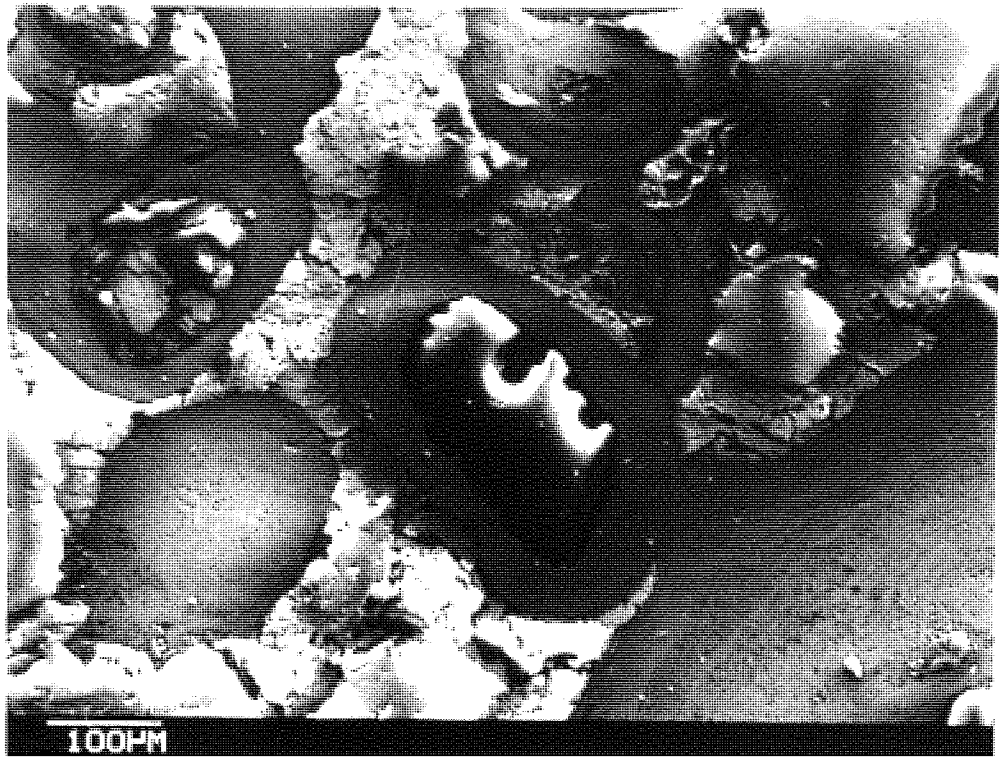
The areas of high Si are associated with the angular detrital fragment seen in the scanning electron micrograph. However, less abundantly rounded areas (75  $\mu\text{m}$ ) of moderately high Si concentration are associated with moderately high Al concentration.

Ca and P are usually associated with each other, the discrete areas ranging in size from 20  $\mu\text{m}$  to 100  $\mu\text{m}$ .

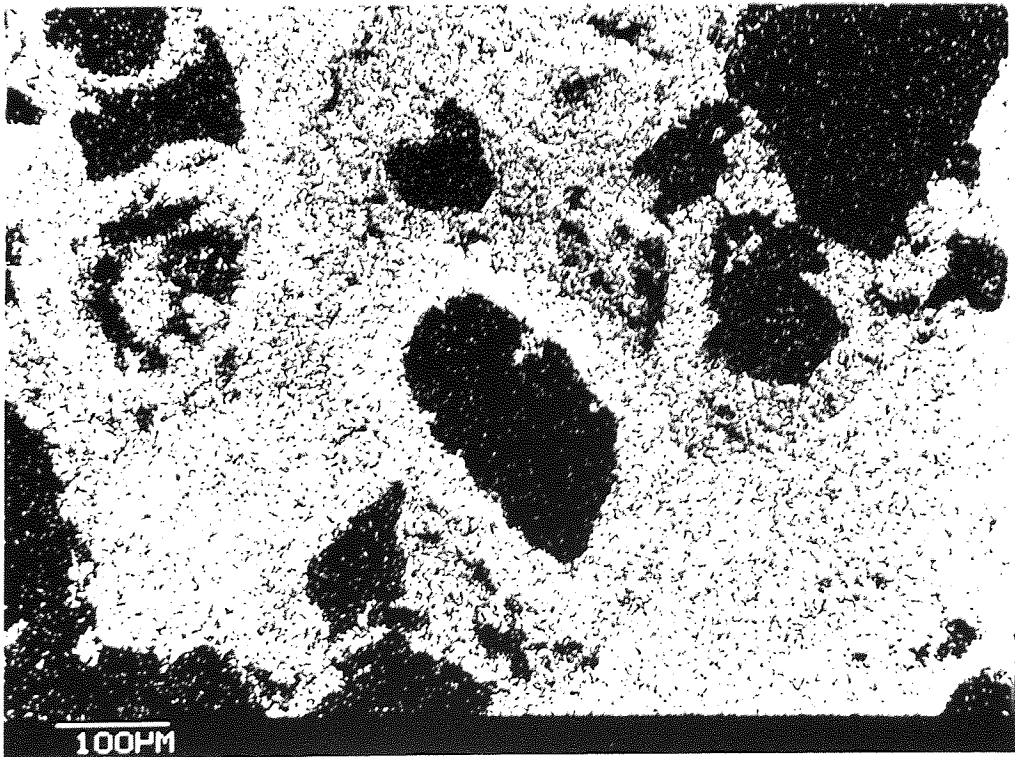
Figure 4.13 Scanning Electron  
Micrographs of Oolitic Iron Ore  
Sample No. As 10 and X-ray  
Distribution Maps x200

- a - Scanning Electron Micrograph
- b - Fe X-ray distribution map
- c - Si X-ray distribution map
- d - Al X-ray distribution map
- e - P X-ray distribution map
- f - Ca X-ray distribution map





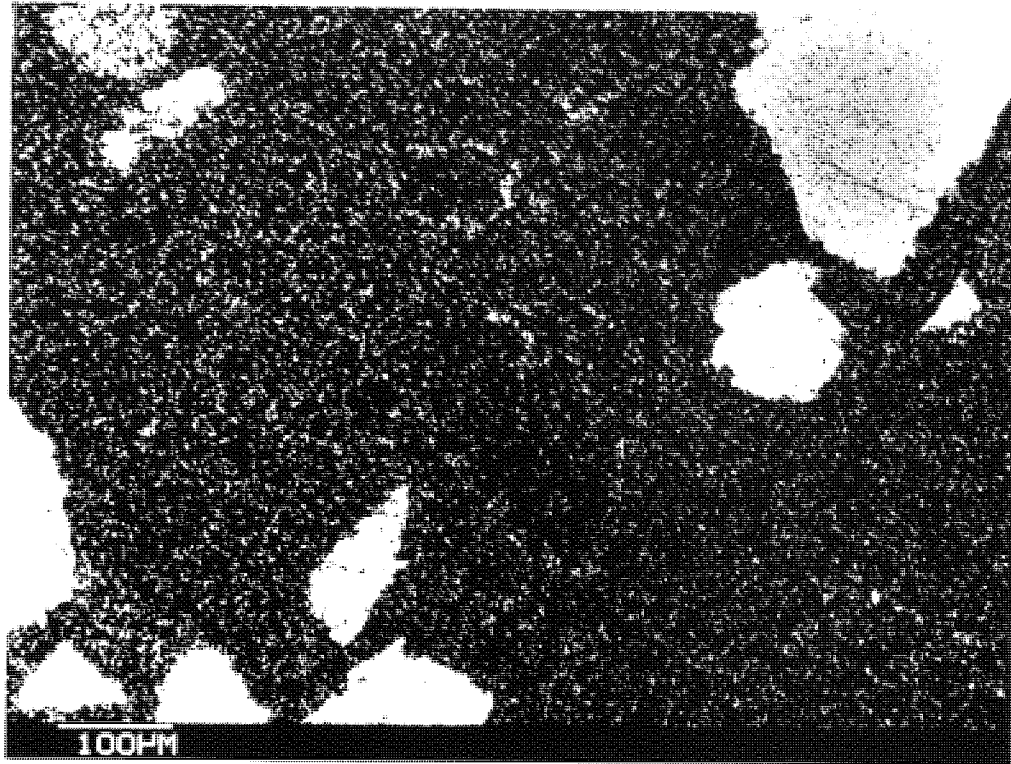
a.



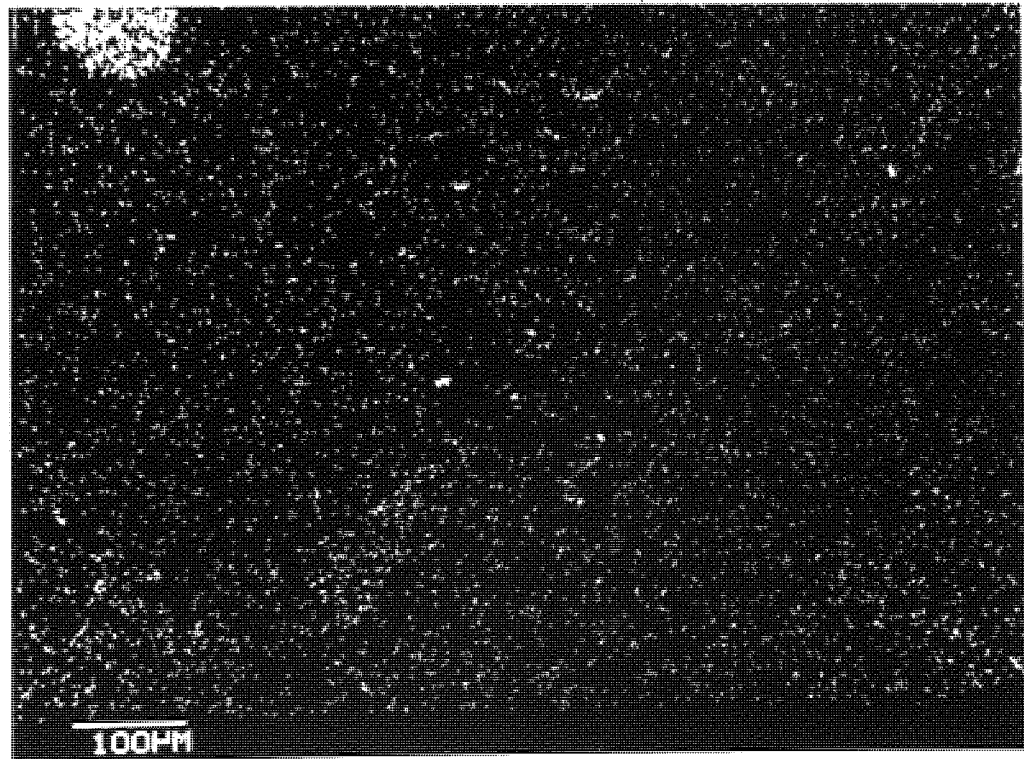
b.

Fig. 4.13





c.



d.

Fig. 4.13

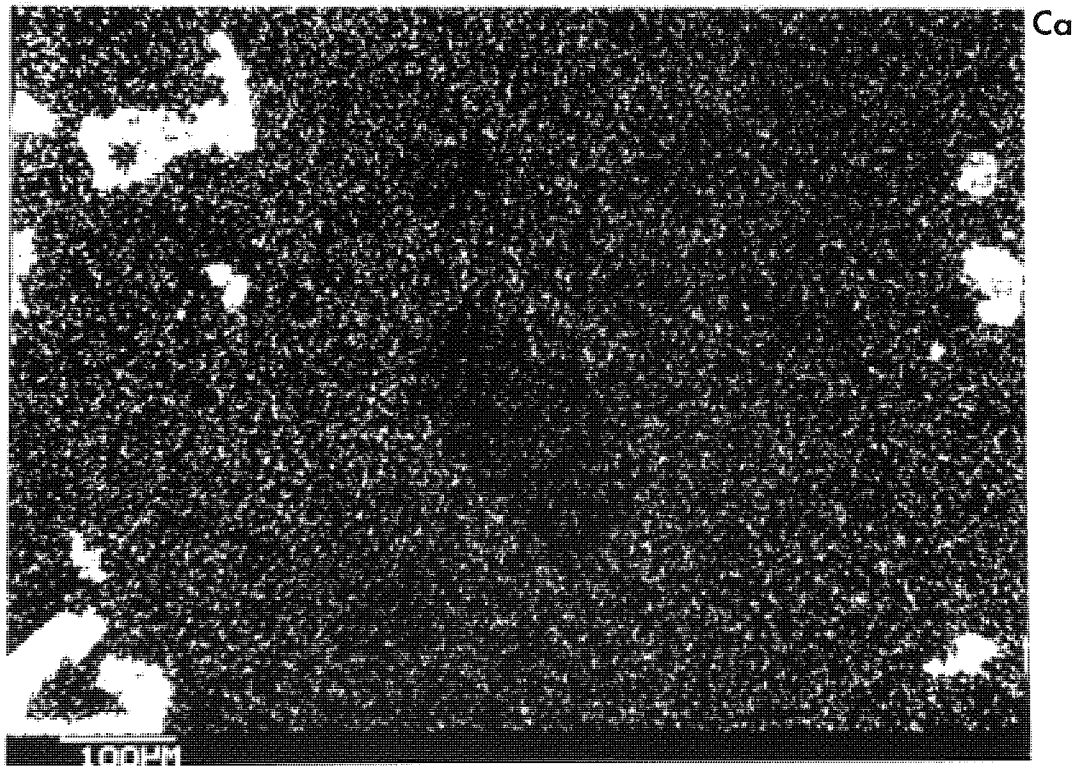
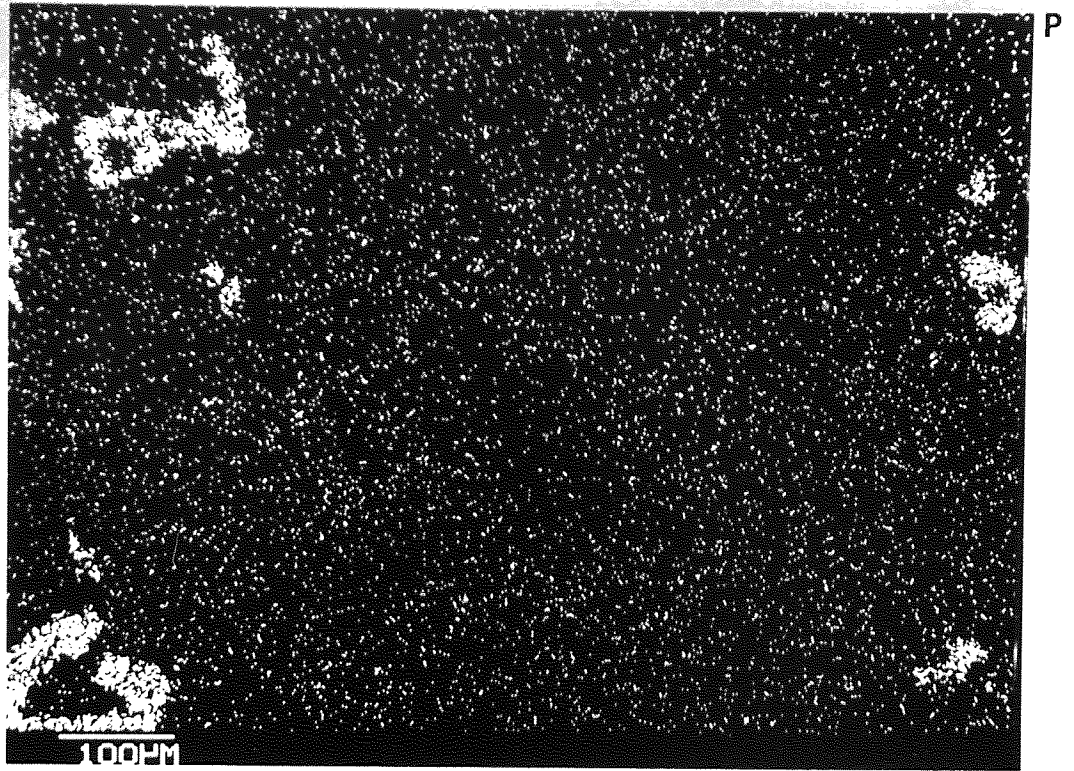


Fig. 4.13

Fe appears in

- a - as the matrix solely Fe rich which is shown from X-ray studies and petrographic studies to be hematite.
- b - oololiths as only Fe, again shown from X-ray studies and petrographic studies as hematite.

Si shows

- a - as discrete angular grains. From X-ray studies and petrographic studies these proved to be quartz.
- b - associated with Al; proved from X-ray studies to be clay minerals.

Ca and P occur as discrete grains in the oololiths and in the matrix, but also locally cementing quartz grains, (bottom left hand corner) from X-ray studies these proved to be apatite.

Figure 4.14 - Scanning electron micrographs of oolitic iron ore sample No. AS9. Fe, Si, Al, P and Ca X-ray distribution maps

Oololiths are ellipsoidal in shape, and display a concentric banded structure, rounded grains are seen within the concentric layers.

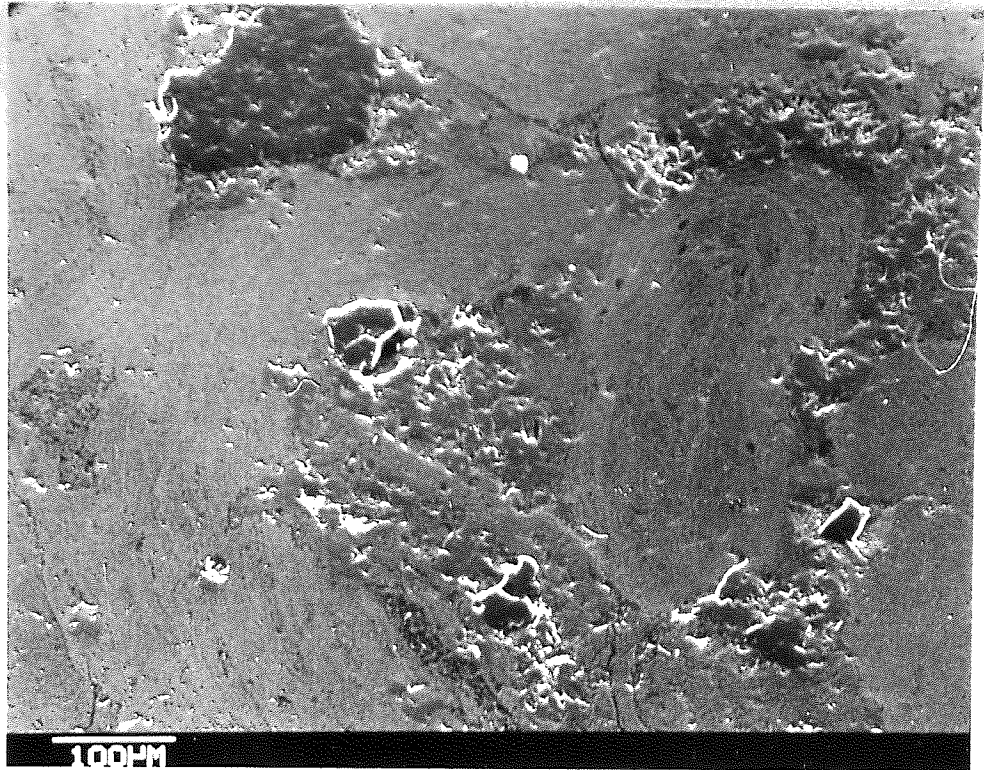
Angular and subrounded grains; the length of the major axis varies from 25  $\mu\text{m}$  to 150  $\mu\text{m}$ .

The matrix cements the oololiths and also the detrital grains. Also there are a few hexagonal grains within the matrix.

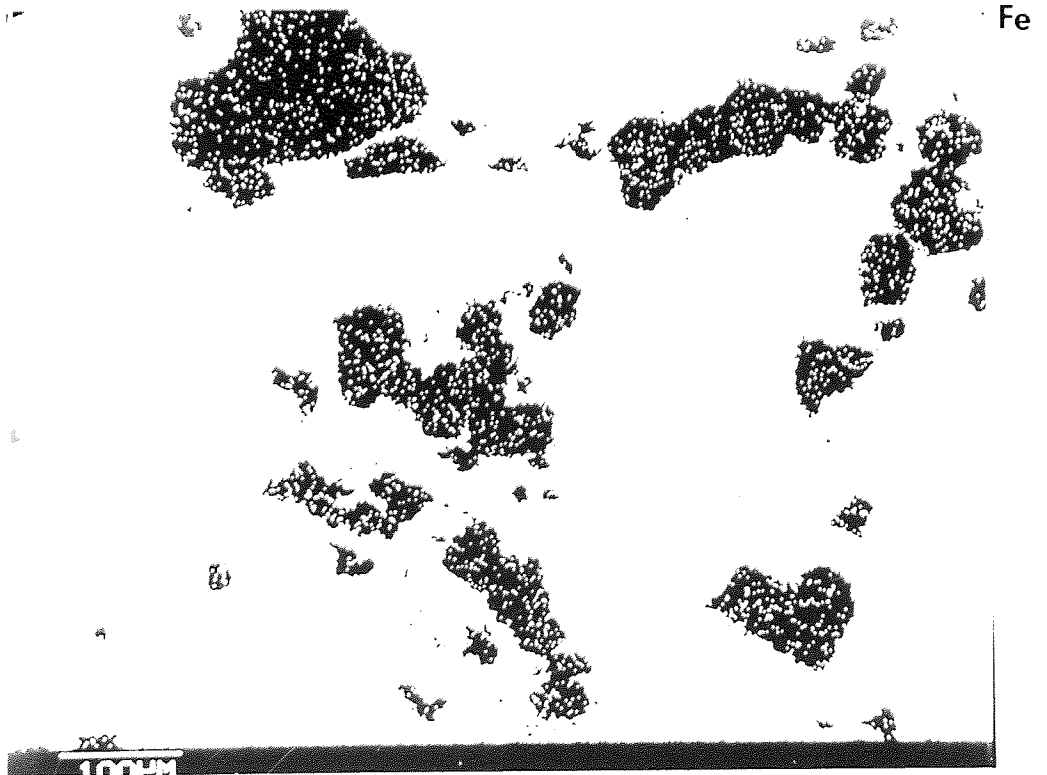
Figure 4.14 Scanning Electron  
Micrographs of Oolitic Iron Ore  
Sample No. As 9 and X-ray  
Distribution Maps x200

- a - Scanning Electron Micrograph
- b - Fe X-ray distribution map
- c - Si X-ray distribution map
- d - Al X-ray distribution map
- e - P X-ray distribution map
- f - Ca X-ray distribution map





a.



b.

Fig 4.14

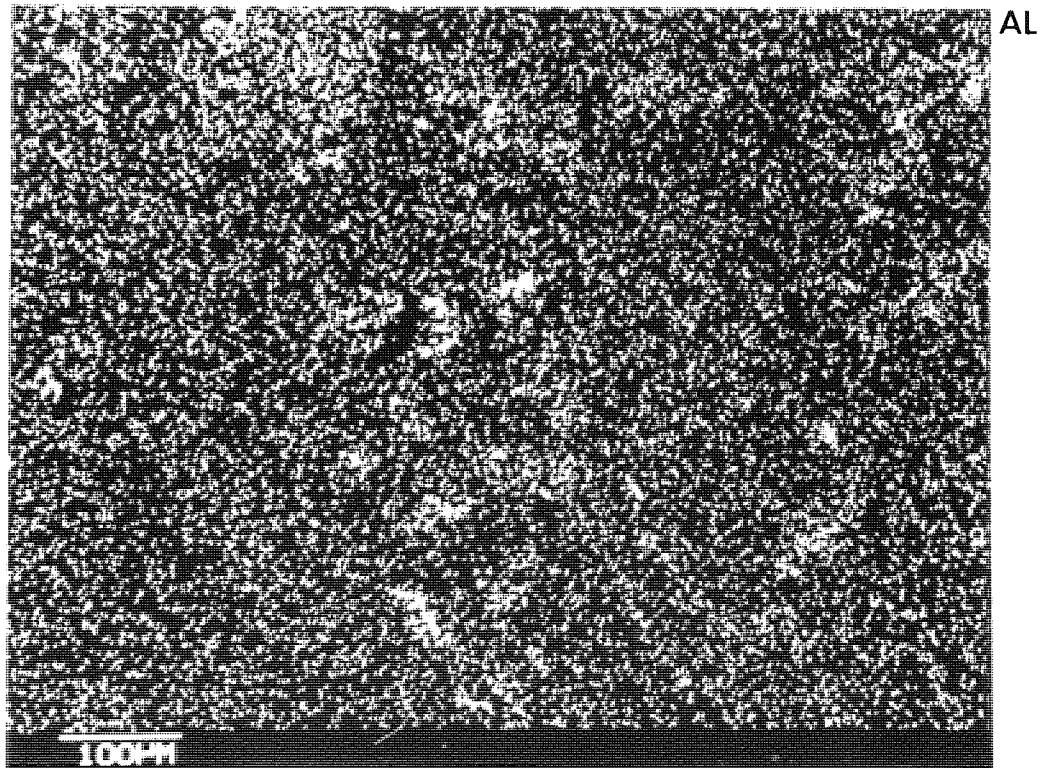
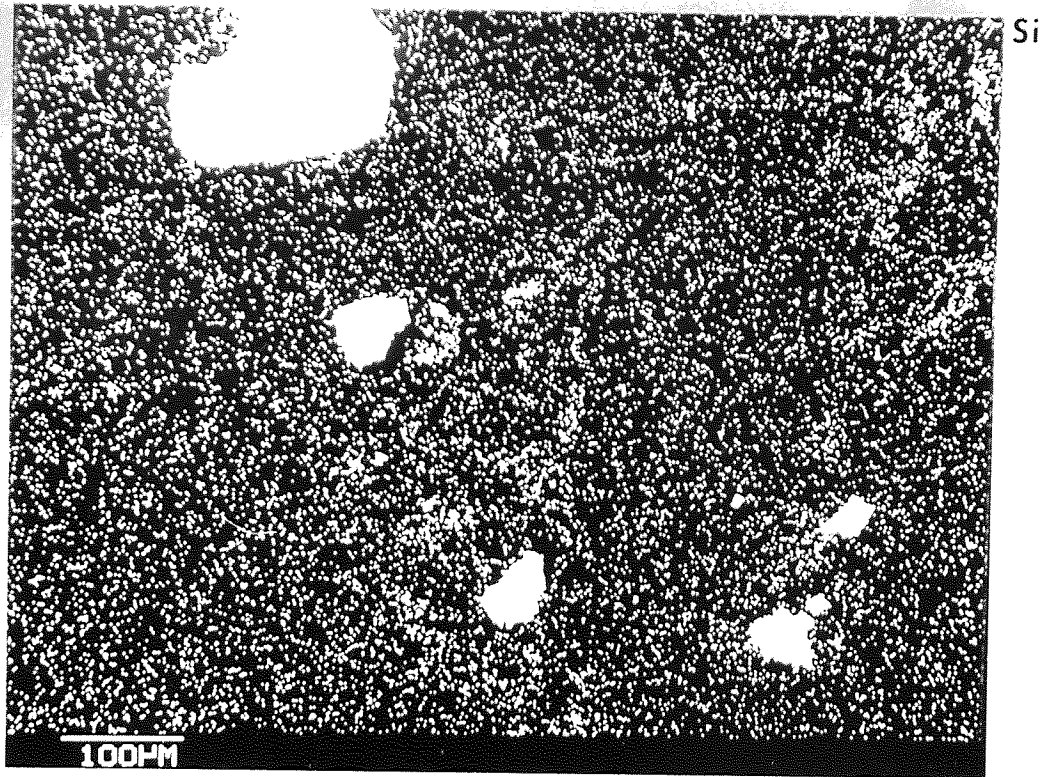
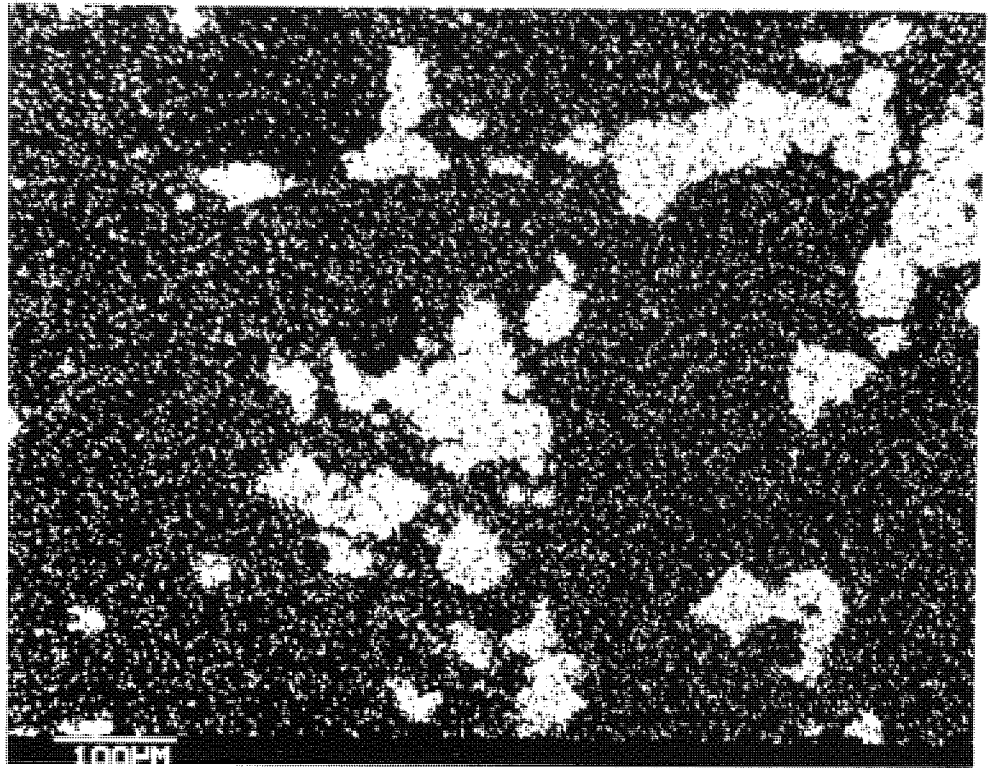
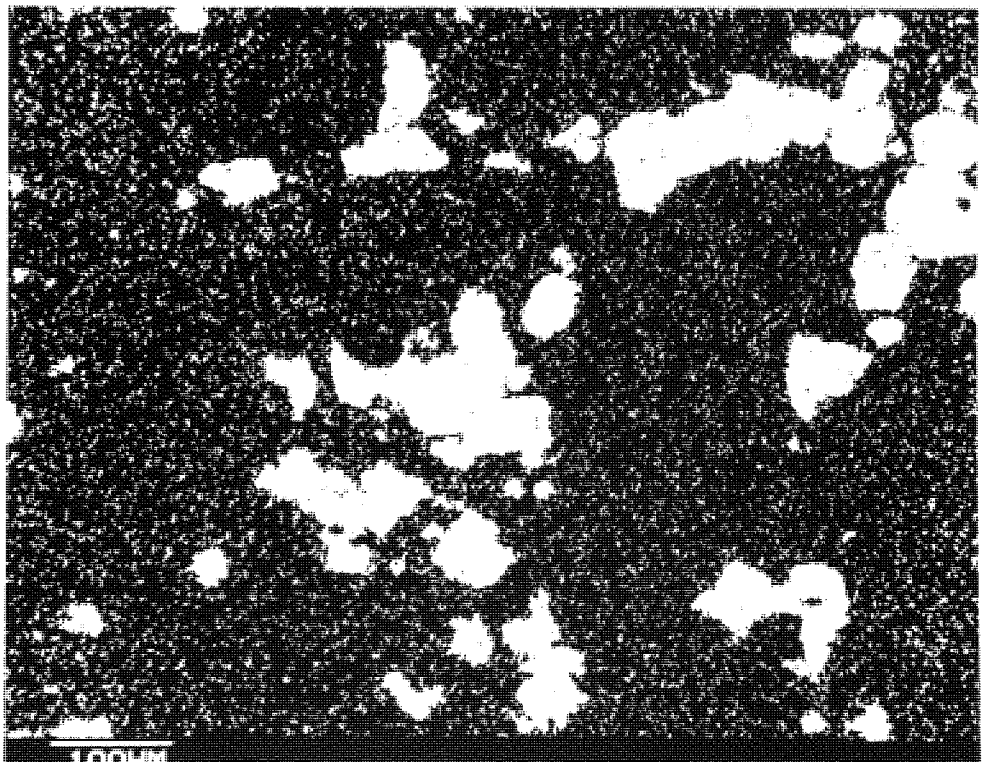


Fig 4.14



P

e.



Ca

f.

Fig. 4.14



The Fe X-ray distribution map shows high concentration of Fe in the ooliths and matrix. It shows that Fe concentration is independent of the concentrations of Si, Al, Ca or P.

The Si occurs primarily as discrete areas of high concentration associated with very small amounts of Al. The areas of high Si concentration are associated with the angular and sub-rounded detrital fragments seen in the scanning electron micrograph. However, less abundantly there exist rounded areas (40  $\mu\text{m}$ ) of low Si concentration associated with low Al concentration.

Both the Ca and P concentration are related to each other, the discrete areas ranging in size from 25  $\mu\text{m}$  to 65  $\mu\text{m}$ .

Fe shows in:

- a - matrix dominantly Fe (oxides)
- b - the ooliths are predominantly Fe (as oxides)

Si shows:

- a - as discrete angular and subrounded grains associated with a little amount of Al (mainly quartz associated with clays).
- b - discrete rounded grains low in concentration associated with low concentration Al (from X-ray studies proved to be clay minerals).

Ca and P occur as apatite which can be seen as discrete round grains in the ooliths, and very anhedral hexagonal grains in the matrix, suggest authogenic growth. Apatite



crystals ranging in size from 20 to 60  $\mu\text{m}$  make up aggregates of 150  $\mu\text{m}$  size.

Figure 4.15 - Scanning electron micrograph of Ferruginous sand clay sample No. As12-2, and the X-ray distribution maps for Fe, Si, Al, P and Ca

Prismatic and subangular grains, the length of the major axis varies from 25  $\mu\text{m}$  to 90  $\mu\text{m}$ .

The matrix cements these grains, but there are two types of matrix materials.

The Fe X-ray distribution map shows high concentrations of Fe in the matrix. It also shows that the concentration of Fe is independent of the concentration of Si, Al, Ca or P.

The Si occurs primarily as discrete areas of high concentration and is not associated with other elements. The areas of high Si concentration are associated with the prismatic and subangular detrital fragments seen in the scanning electron micrograph.

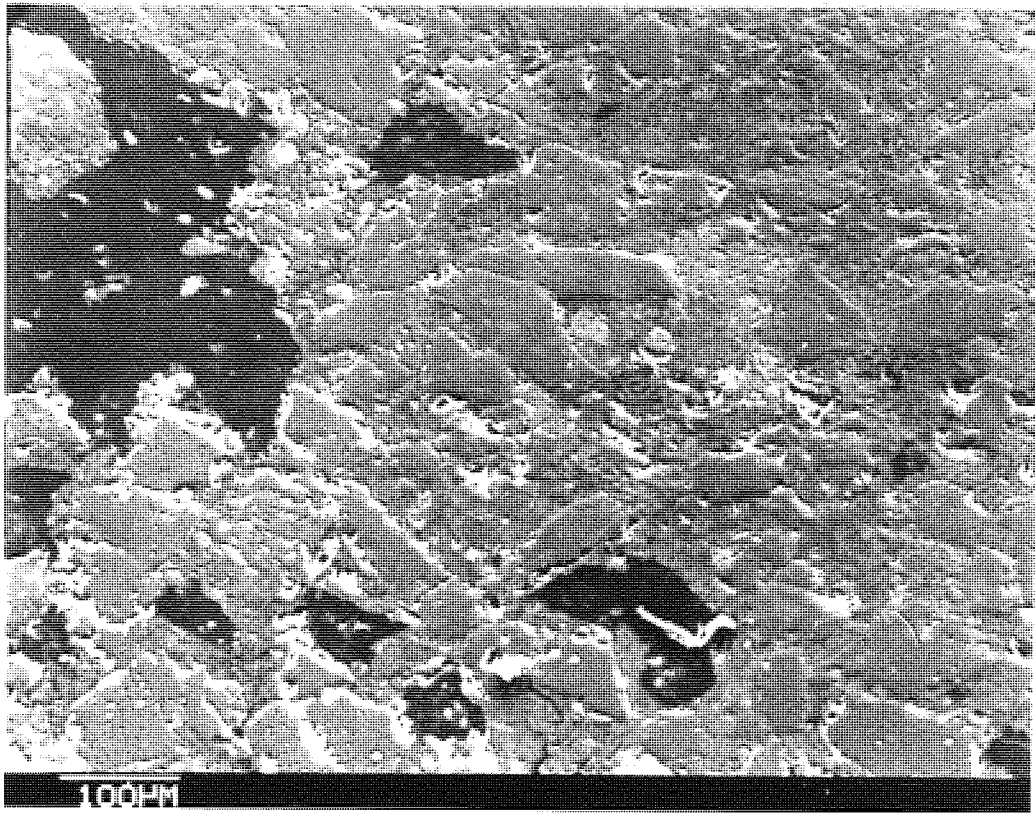
Al in the matrix is associated with Fe and Si.

Ca and P are usually associated with each other, the discrete anhedral grains ranging in size from 5  $\mu\text{m}$  to 50  $\mu\text{m}$ .

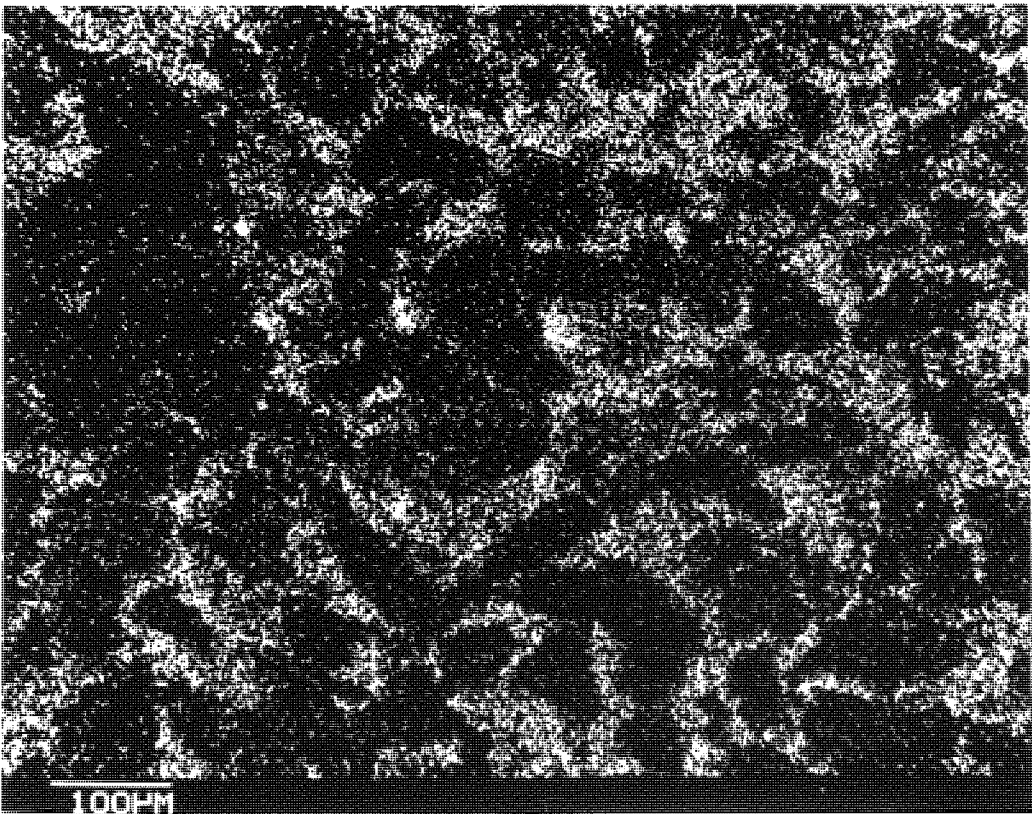
The Fe in the matrix is associated with Al and Si. X-ray studies indicate this to be chamosite.

Figure 4.15 Scanning Electron  
Micrograph of Ferruginous Sand Clay  
Sample No. As 12-2, and X-ray  
Distribution Maps x200

- a - Scanning Electron Micrograph
- b - Iron X-ray distribution map
- c - Silicon X-ray distribution map
- d - Aluminium X-ray distribution map
- e - Phosphorus X-ray distribution map
- f - Calcium X-ray distribution map



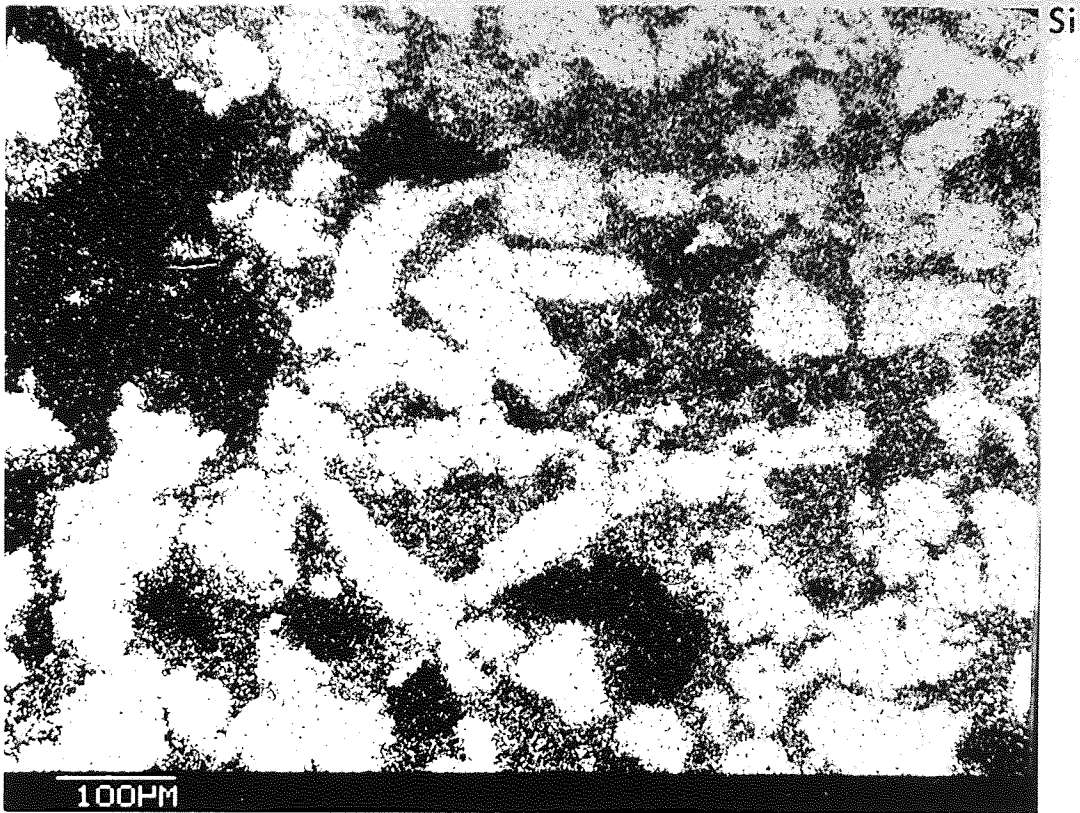
a



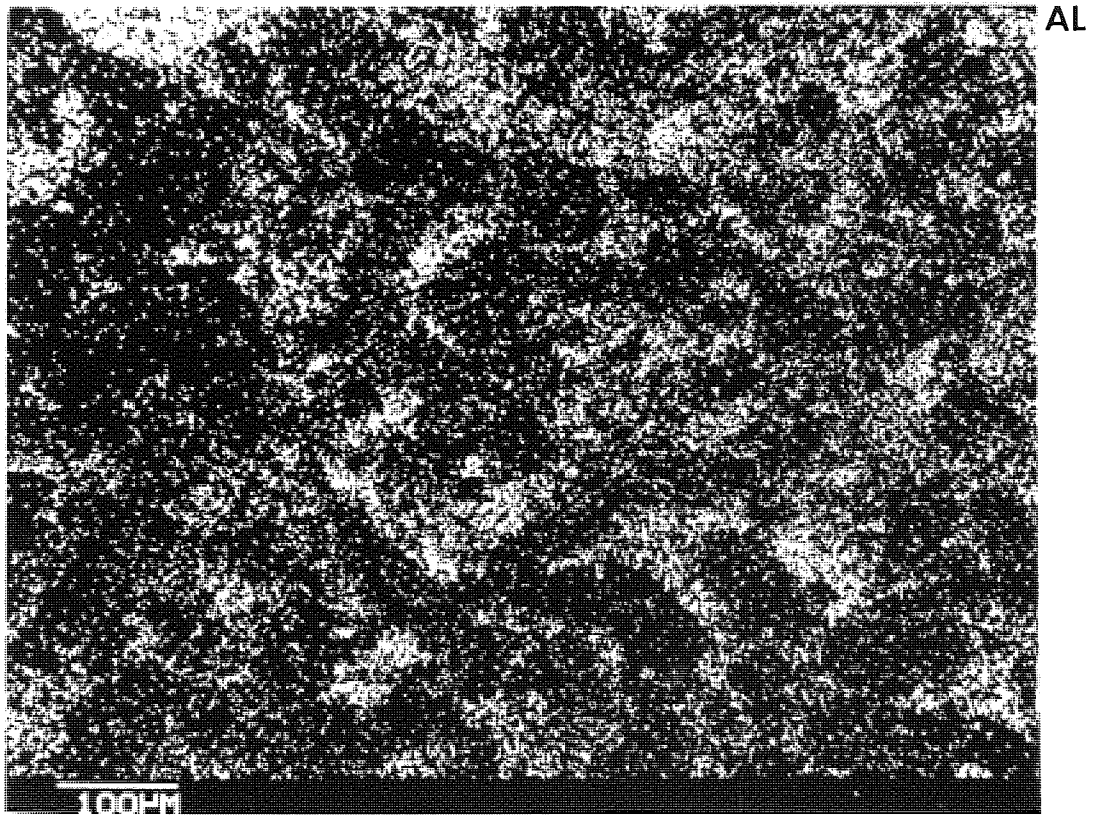
Fe

b.

Fig.4.15



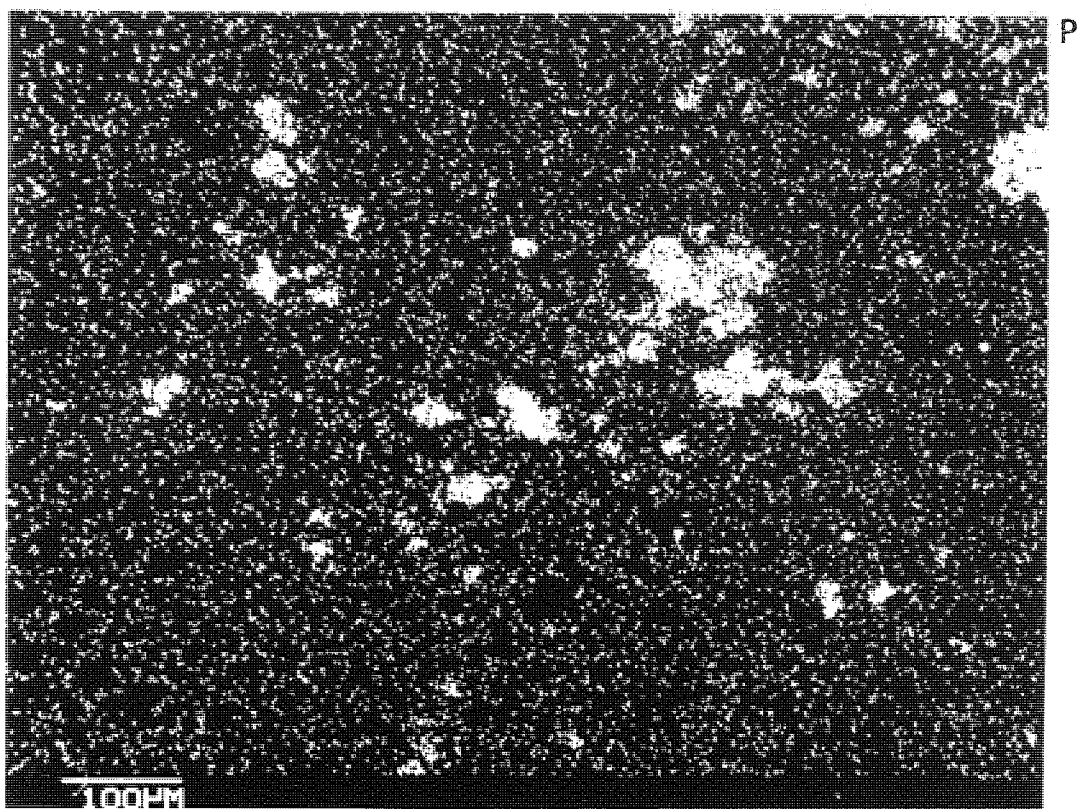
c.



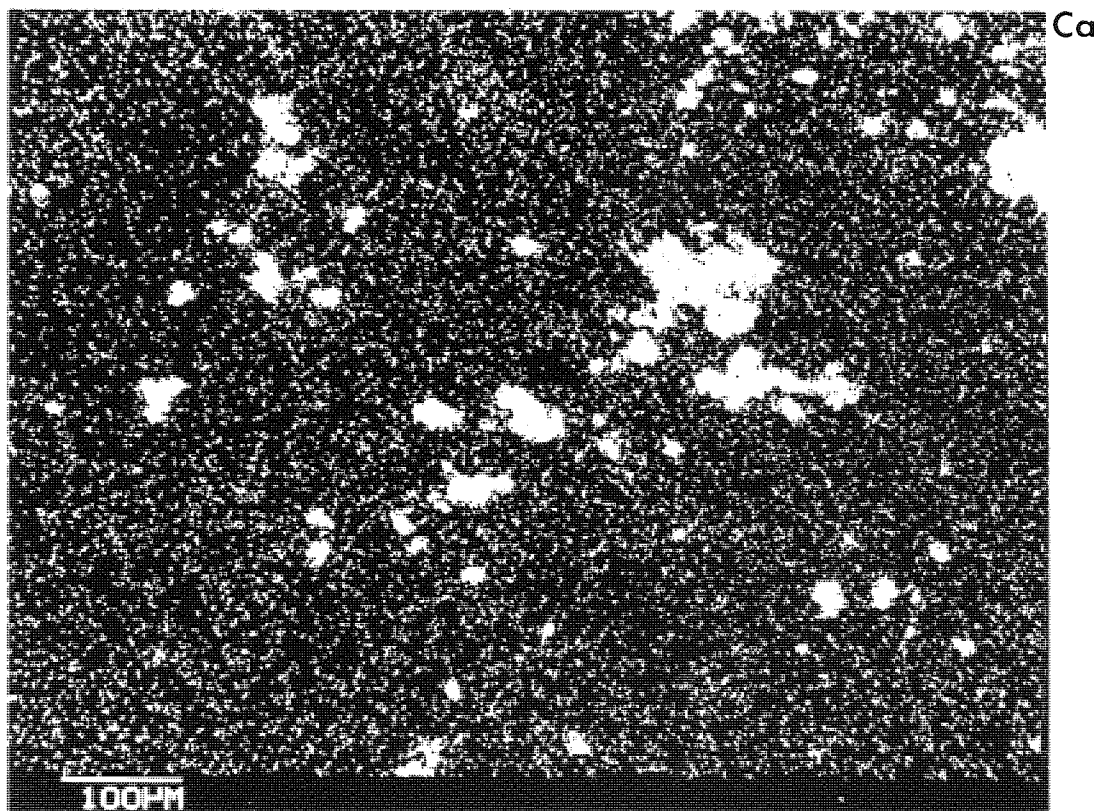
d.

Fig. 4.15





e



f

Fig. 4.15

Si shows:

- a - as discrete prismatic and subangular grains which are shown from X-ray and petrographic studies to be quartz.
- b - associated with Al and Fe; as previously this proved to be chamosite.

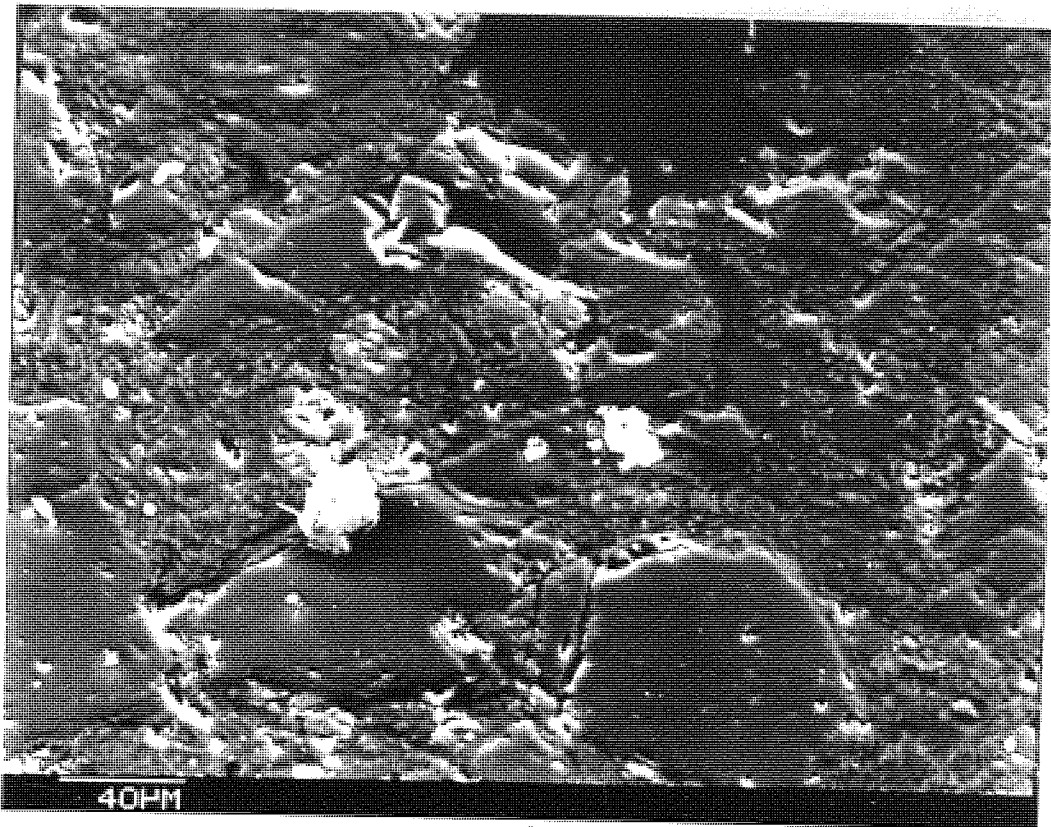
Ca and P occur as discrete anhedral grains in the matrix. They also exist in areas where the anhedral grains agglomerate to form aggregates, the length of the major axis of which is 80  $\mu\text{m}$ .

Figure 4.16 - Scanning electron micrographs of Ferruginous sand clay sample No. AS12, and the X-ray distribution maps for Fe, Si, Al, P and Ca.

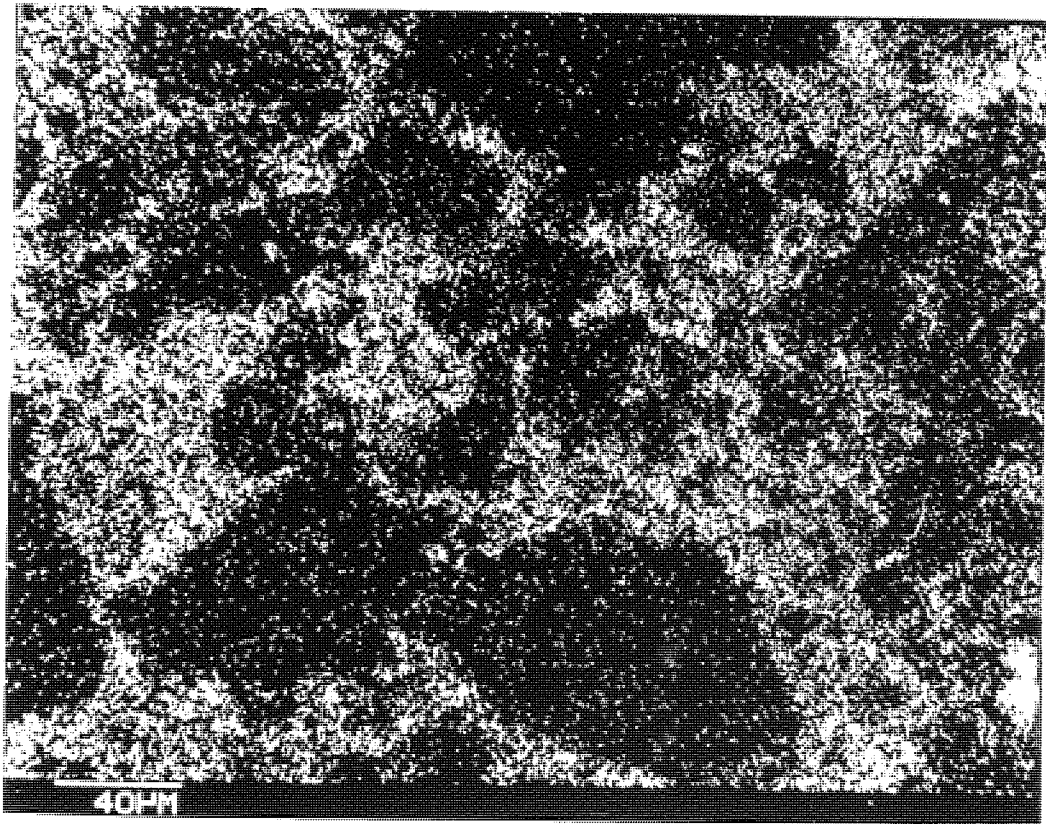
Angular and subangular grains; the length of the major axis varies from 6  $\mu\text{m}$  to 80  $\mu\text{m}$ .

The matrix cements the angular and subangular grains; but there are two types of matrix material, one is lighter coloured than the other.

The Fe X-ray distribution map shows a high concentration of Fe in the matrix. It also shows that the Fe concentration is independent of the concentration of Si, Al, Ca or P, although Si and Al are associated with Fe. The Si occurs primarily as discrete areas of high concentration and is not associated with other elements. The areas of high Si concentration are associated with the subangular and angular detrital fragments seen in the scanning electron micrograph.



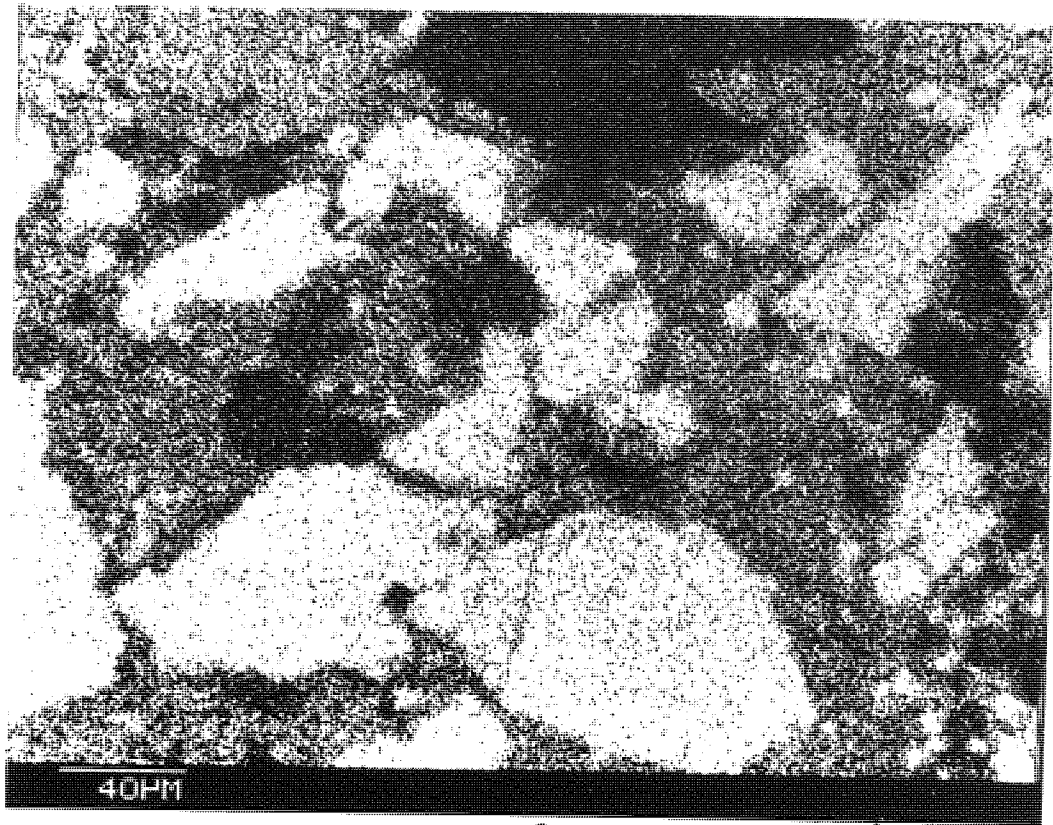
a.



Fe

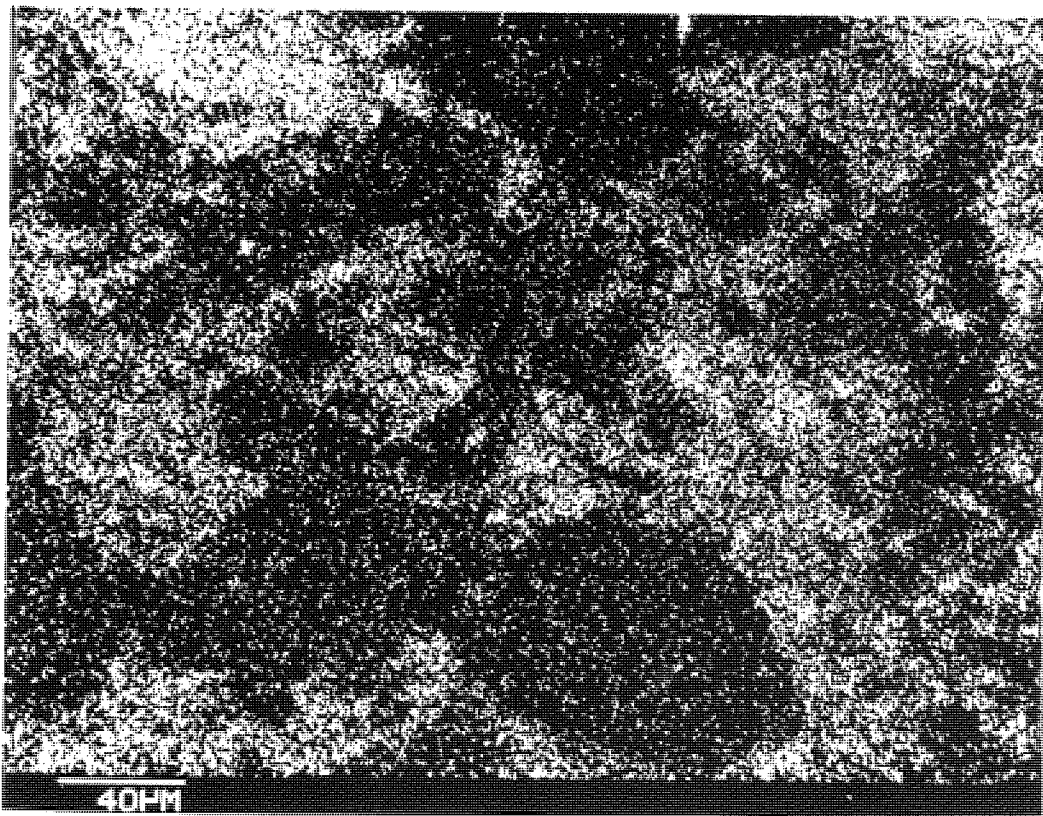
b.

Fig. 4.16



Si

c.

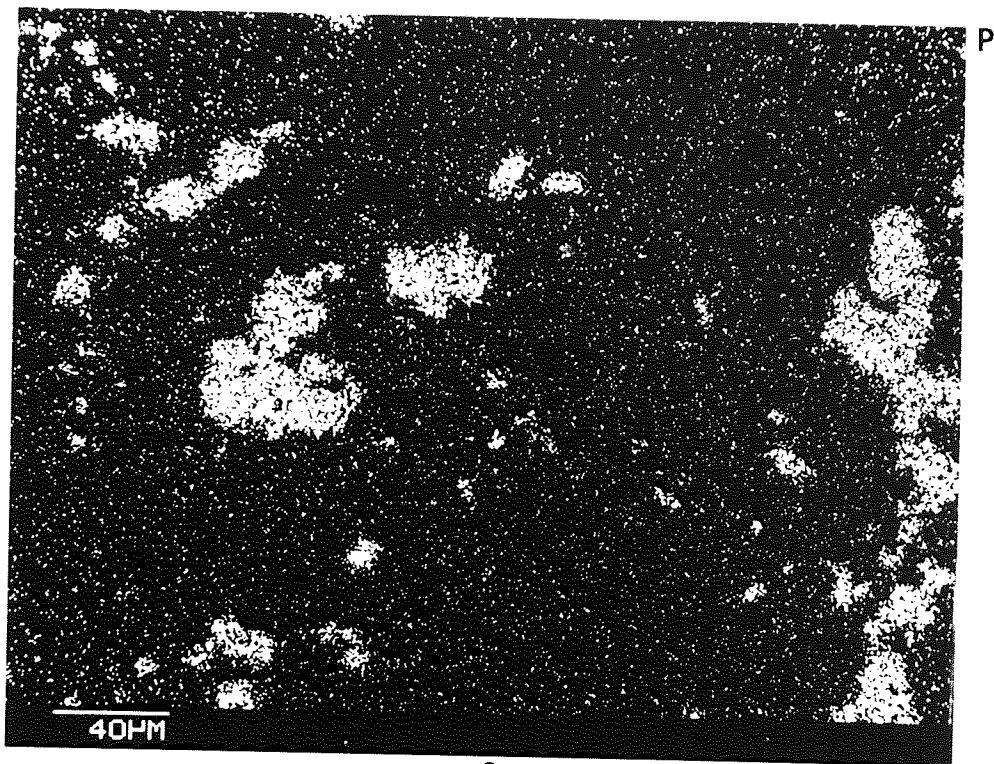


AL

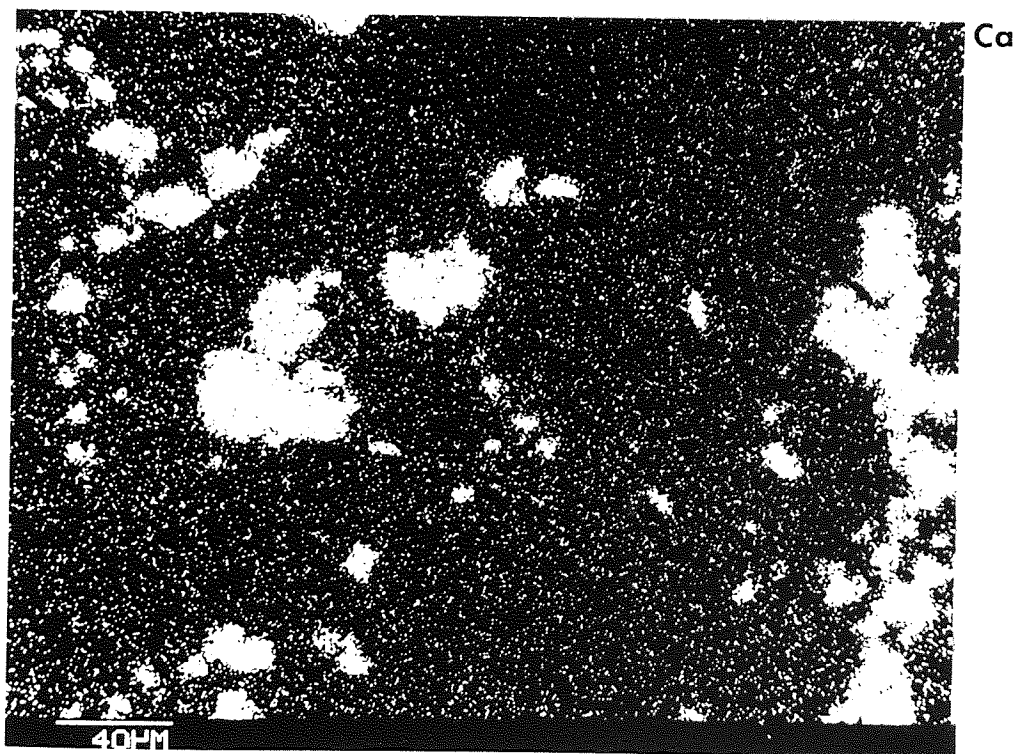
d.

Fig. 4.16





e.



f.

Fig 4.16

Ca and P are usually associated with each other, the discrete subhedral and anhedral grains ranging in size of the major axis from 4  $\mu\text{m}$  to 24  $\mu\text{m}$ . Fe exists in the matrix. It is associated with Al and Si. From X-ray studies this is proved to be chamosite.

Si shows:

- a - as discrete angular and subangular grains which are shown from X-ray studies and petrographic studies to be quartz.
- b - associated with Fe and Al in the matrix, previously proved to be chamosite.

Apatite grains also make up aggregate areas; with the major axis approximately 40  $\mu\text{m}$ .

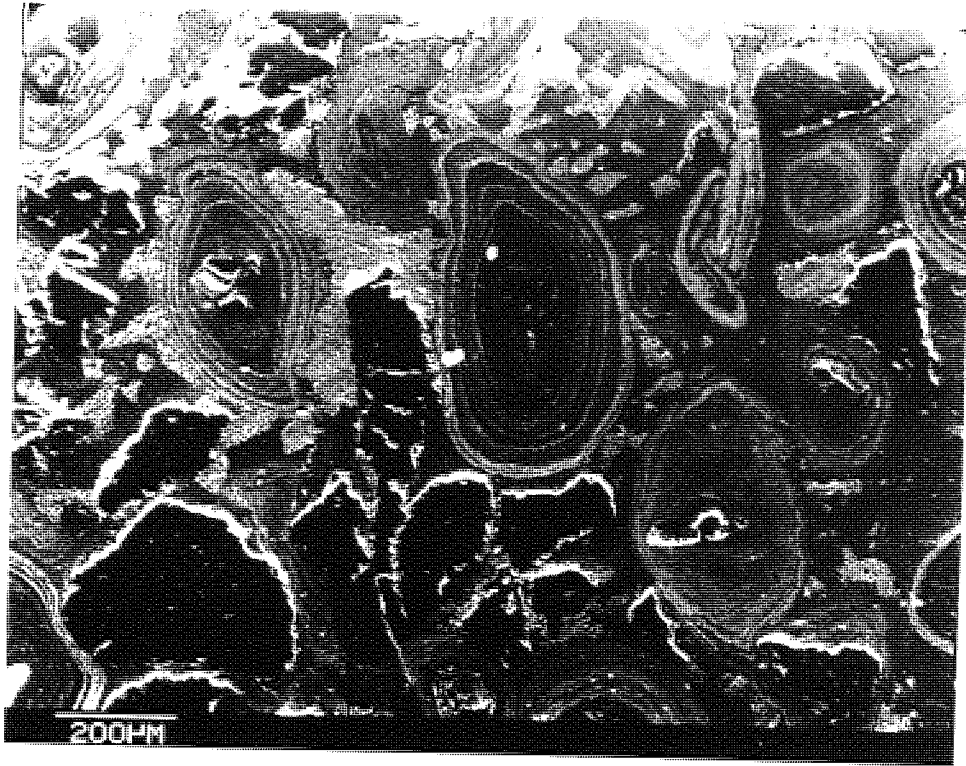
Note: This sample is the same as one in Figure 4.15 showing variations in the ore.

Figure 4.17 - Scanning electron micrograph for oolitic iron ore sample No. AS25, and the X-ray distribution for Fe, Al, Si, P and Ca.

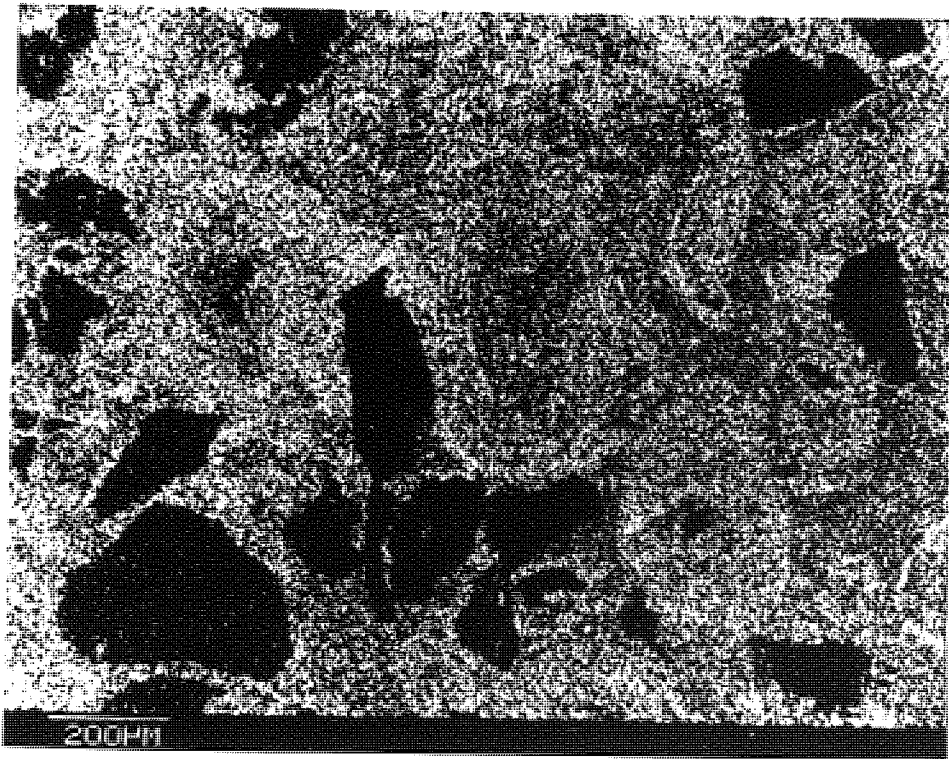
Ooliths are ellipsoidal in shape; the length of the major axis varies from 150  $\mu\text{m}$  to 450  $\mu\text{m}$ . Many ooliths show a concentric banding structure with many bands. In several ooliths there are nuclei of other mineral grains which appear as subangular grains.

Figure 4.17 Scanning Electron  
Micrograph for Oolitic Iron Ore  
Sample No. As 25 and the X-ray  
Distribution Maps x100

- a - Scanning Electron Micrograph
- b - Iron X-ray distribution map
- c - Silicon X-ray distribution map
- d - Aluminium X-ray distribution map
- e - Phosphorus X-ray distribution map
- f - Calcium X-ray distribution map



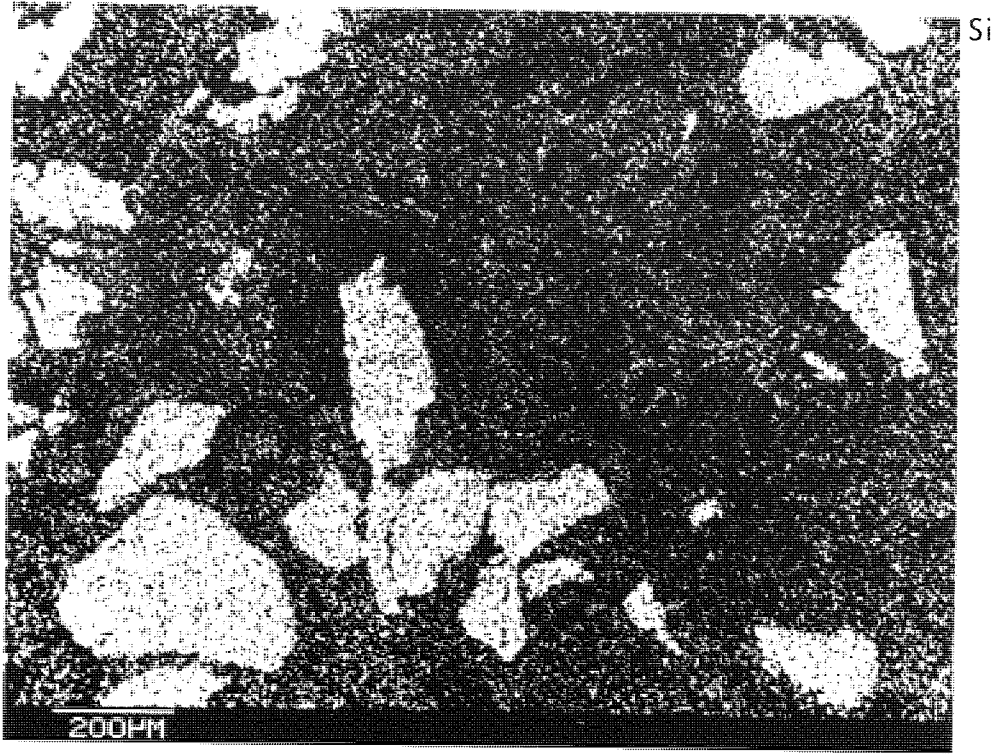
a.



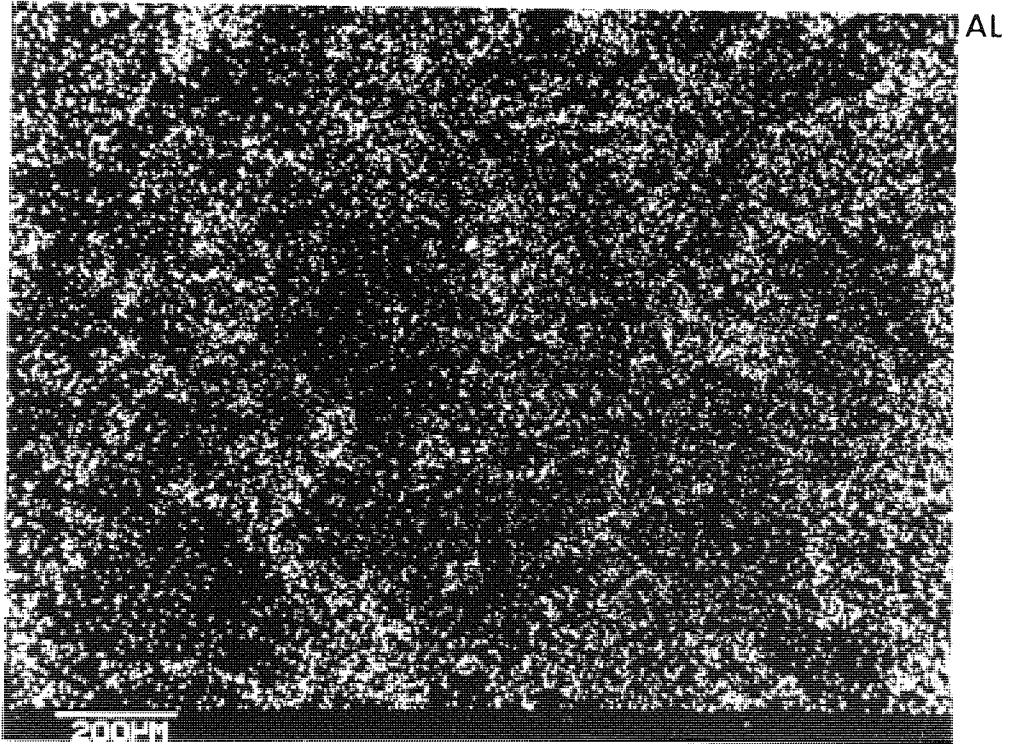
Fe

b.

Fig. 4.17



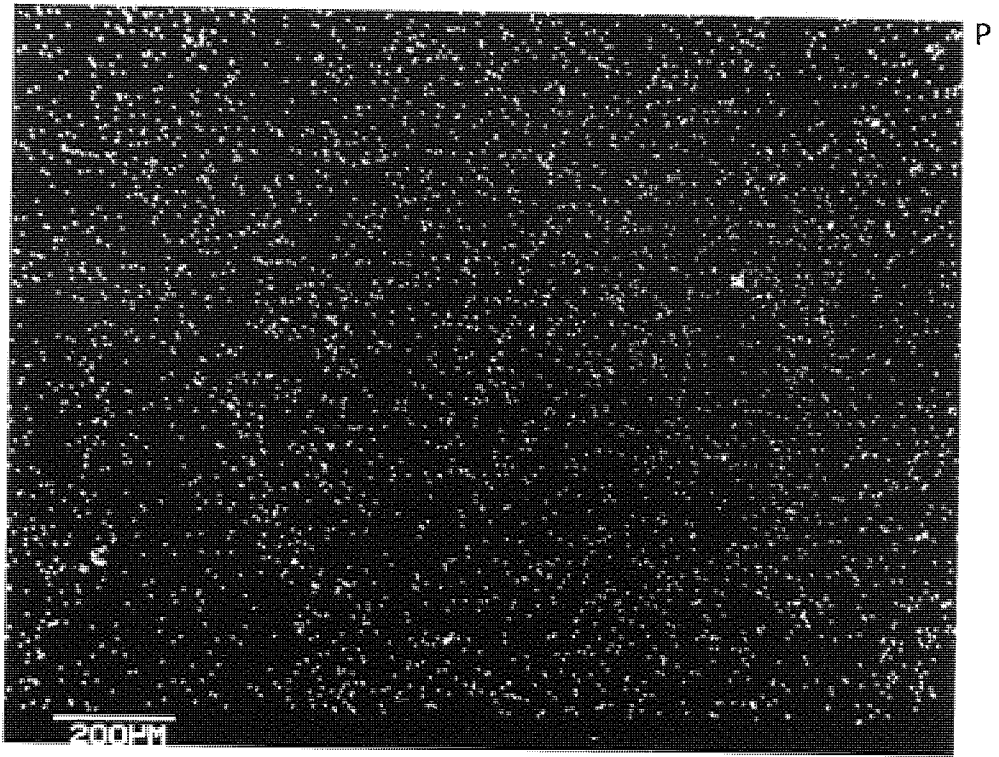
c.



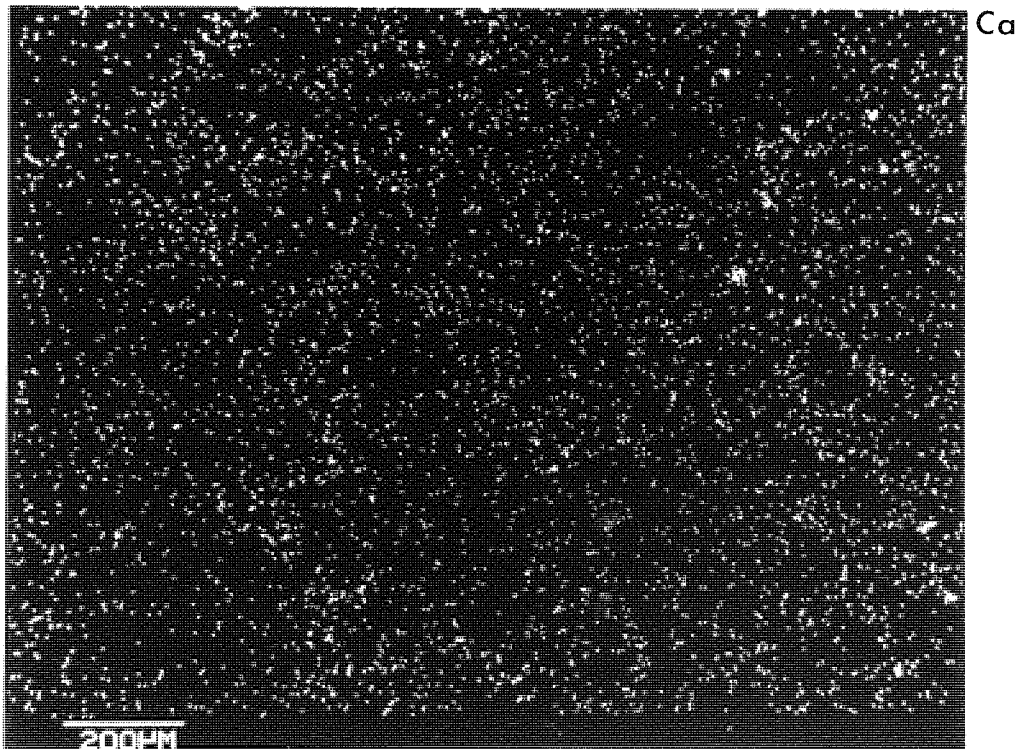
d.

Fig. 4.17





e.



f.

Fig. 4.17

In addition there is a clastic component angular and subangular grains the length of the major axis varies from 80  $\mu\text{m}$  to 300  $\mu\text{m}$ .

The matrix cements the ooliths, but there are two types of matrix material, light and dark, both of which cement the ooliths. The Fe X-ray distribution shows a high concentration of Fe both in the ooliths and in the matrix. There is a slightly higher Fe concentration in the outer area of the ooliths. In some areas of the matrix these are the lighter regions shown in the scanning electron micrograph. It also shows that the iron concentration is independent of Si, Al, Ca or P content. The Si occurs primarily as discrete areas of high concentration not associated with the other elements. The areas of high Si concentration are associated with angular and subangular detrital fragments seen in the scanning electron micrograph. Also there are angular grains of Si in the cores of some ooliths.

Both the Ca and P content are very low and there is one small anhedral grain of P associated with Ca. The length of the major axis of the anhedral grain is about 10  $\mu\text{m}$ .

Fe is shown in:

a - the matrix associated with moderately high Al and low Si. From X-ray studies this is identified as chamosite.

b - the oololiths have a high concentration of Fe in the outer layer, but in the middle of the oololiths the Fe is associated with Al and Si; as previously these proved to be chamosite.

Si shows:

- a - as discrete angular and subangular grains proved from X-ray studies and petrographic studies to be quartz.
- b - associated with Al and Fe in the matrix and in the middle of the oololiths. This, as previously, was proved to be a chamosite.

Ca and P occur as apatite.

Figure 4.18 - Scanning electron micrograph for oolitic iron ore sample No. AS6, and the X-ray distribution maps for Fe, Al, Si, P and Ca

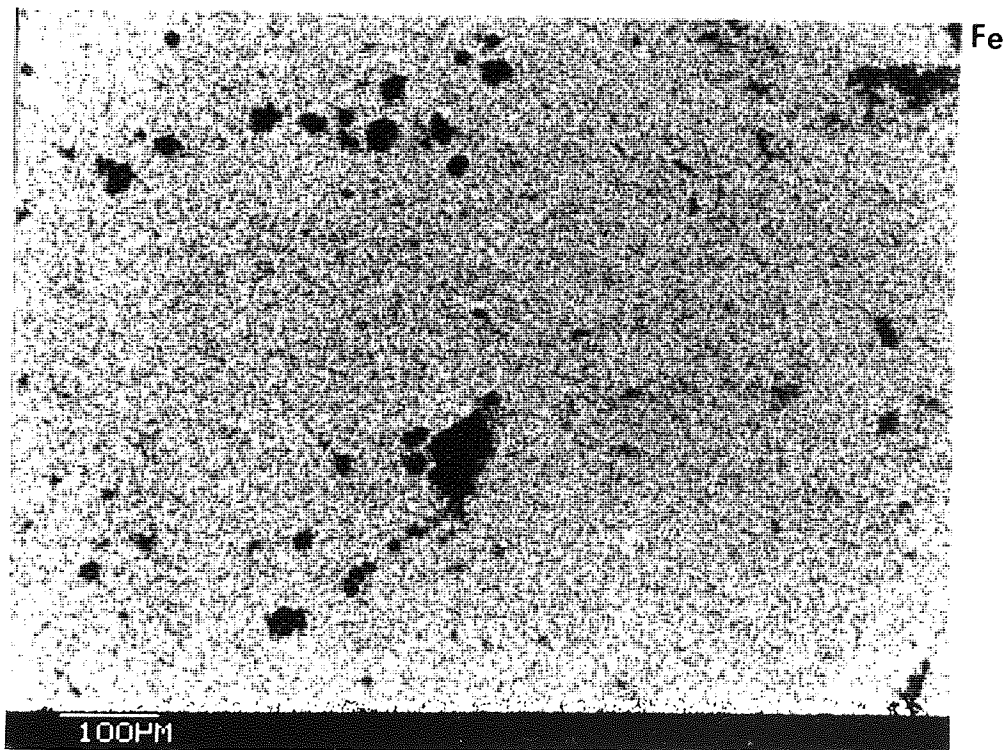
The single oolith is ellipsoidal in shape with a length of the major axis of about 750  $\mu\text{m}$ .

It shows a concentric banded structure with subhedral grains found within the concentric layers; the length of the major axis for these grains varies from 5  $\mu\text{m}$  to 20  $\mu\text{m}$ . Also there is one subangular grain in the centre of the oolith lighter than the others (just below centre of micrograph); the length of the major axis is approximately 60  $\mu\text{m}$ . The Fe X-ray distribution map shows a high concentration of Fe in the oolith. It also shows that the concentration of Fe is independent of the concentration of Si, Al, Ca or P. The





a.



b.

Fig. 4.18

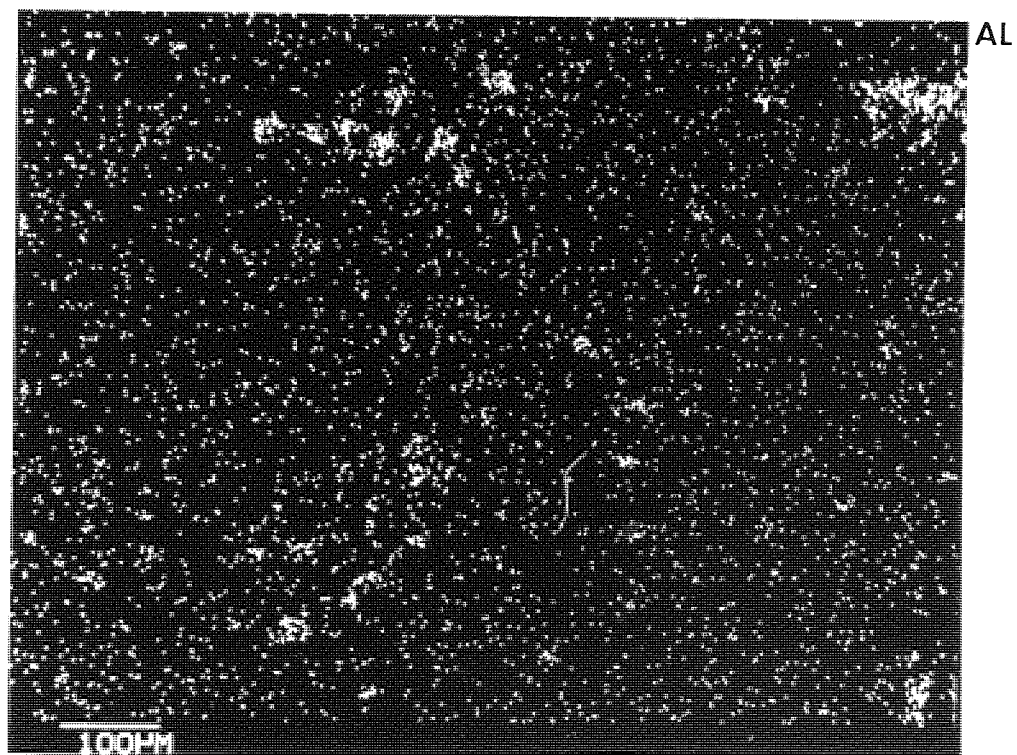
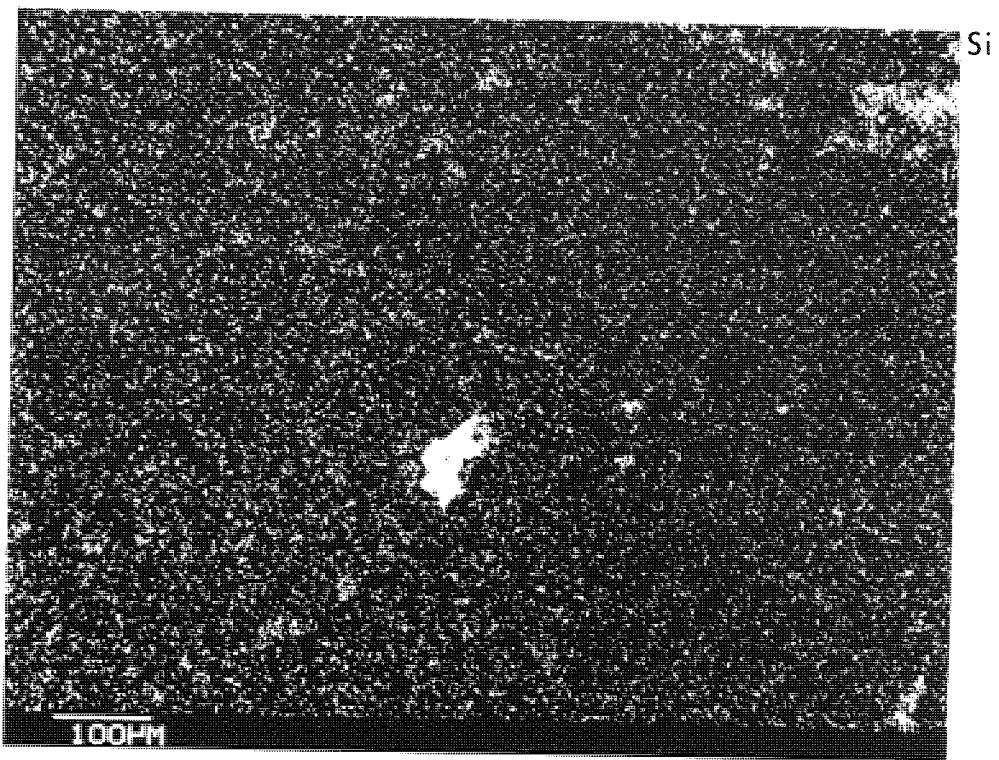
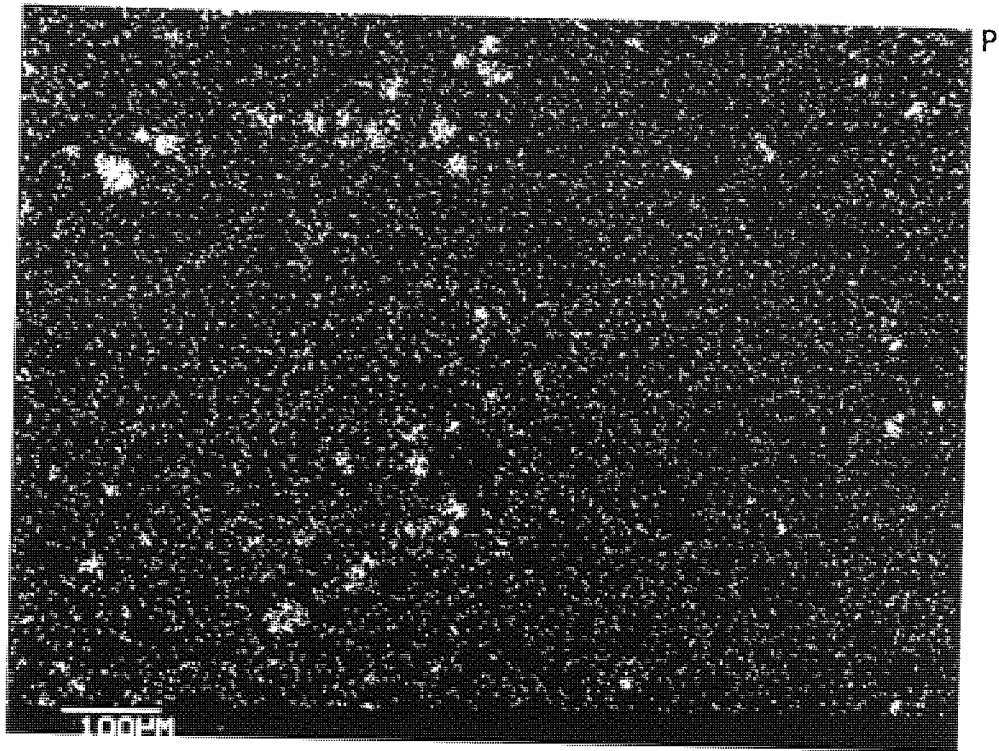
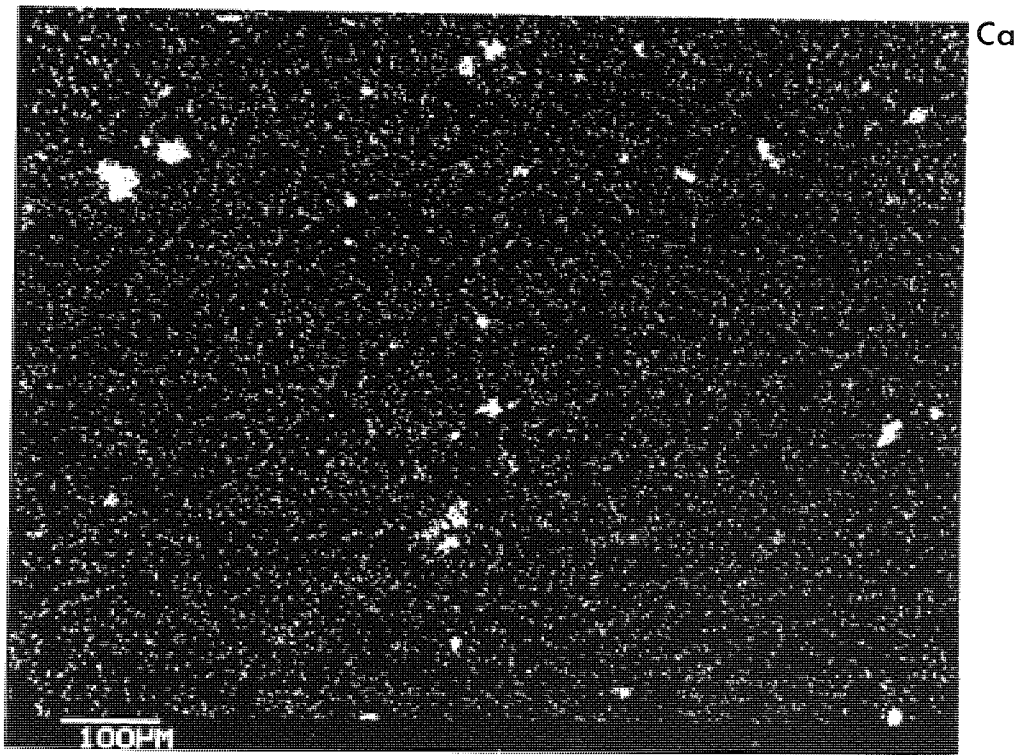


Fig. 4.18



e.



f.

Fig. 4.18

Si occurs primarily as discrete areas of high concentration and is not associated with other elements. The areas of high Si concentration are associated with the subangular detrital fragments seen in the scanning electron micrograph, also shown as areas of moderately high Si concentration in the matrix. (Top right of S.E.M.)

Al is seen as areas of moderately high Al concentration associated with moderately high Si concentration in the matrix and appears as subhedral grains of high Al concentration in the oolith for which the length of the major axis is about 15  $\mu\text{m}$ .

High Ca concentration is always associated with areas of high P concentration in the oolith, the discrete subhedral grains ranging in size from 5  $\mu\text{m}$  to 25  $\mu\text{m}$ .

Fe is shown: in the ooliths which are rich in Fe and from X-ray studies and petrographic studies it was shown to be in the form of hematite.

Si shows:

- a - as discrete subangular grain. X-ray studies proved it to be quartz.
- b - as a, areas in the matrix in which it is associated with Al and proved from X-ray studies to be clay minerals.
- c - as discrete subhedral grains of low Si concentration associated with Al and P (P bearing clay minerals).

Al shows:

- a - as areas in which it is associated with Si; as previously these were proved to be clay minerals.
- b - as discrete subhedral grains associated with Si and P (P bearing clay minerals).

P shows:

- a - a discrete subhedral grain associated with Al and low Si concentration.
- b - associated with Ca. From X-ray studies proved these to be apatite.

Figure 4.19 - Scanning electron micrograph for oolitic iron ore sample No. AS9-2 and the X-ray distribution map for Fe, Si, Al, P and Ca

Ooliths are ellipsoidal in shape; the length of the major axis varies from 70  $\mu\text{m}$  to 500  $\mu\text{m}$ . Many ooliths show a concentric banding structure. In some of the ooliths there are nuclei of certain mineral grains which appear as lighter areas in the core of the ooliths as seen in scanning electron micrograph. The oolith seen in the middle of the scanning electron micrograph is divided into two parts. The outer rim appears lighter in colour and better polished than the adjacent inner layers.

There are subangular grains in the matrix; the length of the major axis varies from 40  $\mu\text{m}$  to 160  $\mu\text{m}$ .

The matrix cements the ooliths and there are two types of matrix material - light and dark.

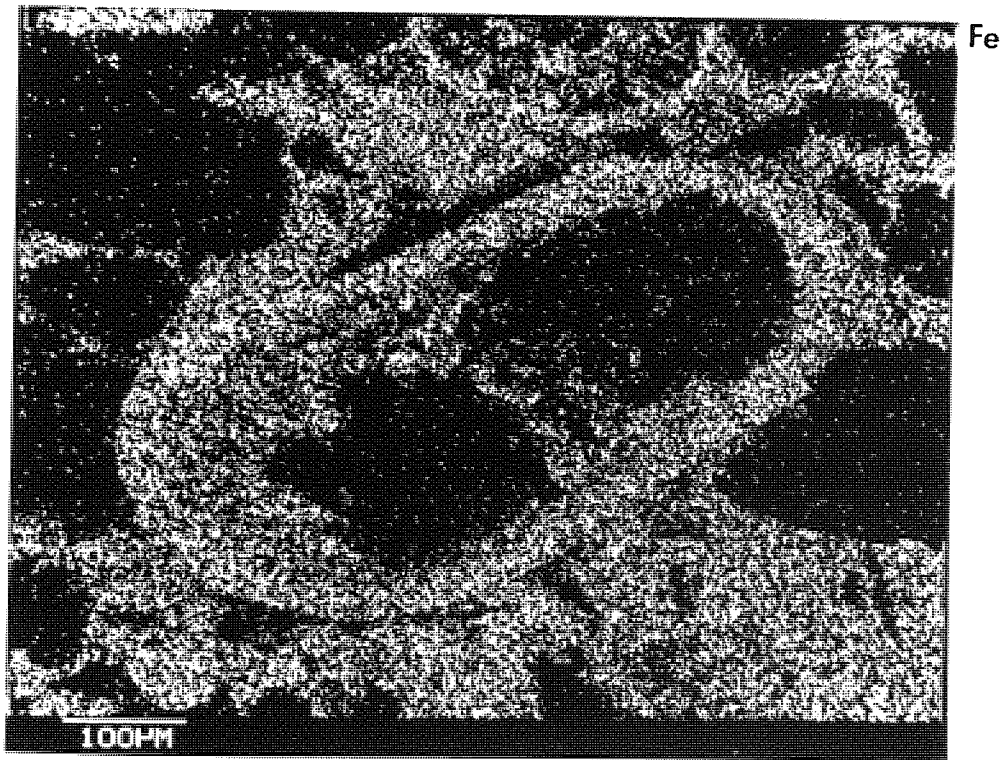
Figure 4.19 Scanning Electron  
Micrograph for Oolitic Iron Ore  
Sample No. As9-2 and X-ray  
Distribution Maps x200

- a - Scanning Electron Micrograph
- b - Iron X-ray distribution map
- c - Silicon X-ray distribution map
- d - Aluminium X-ray distribution map
- e - Phosphorus X-ray distribution map
- f - Calcium X-ray distribution map





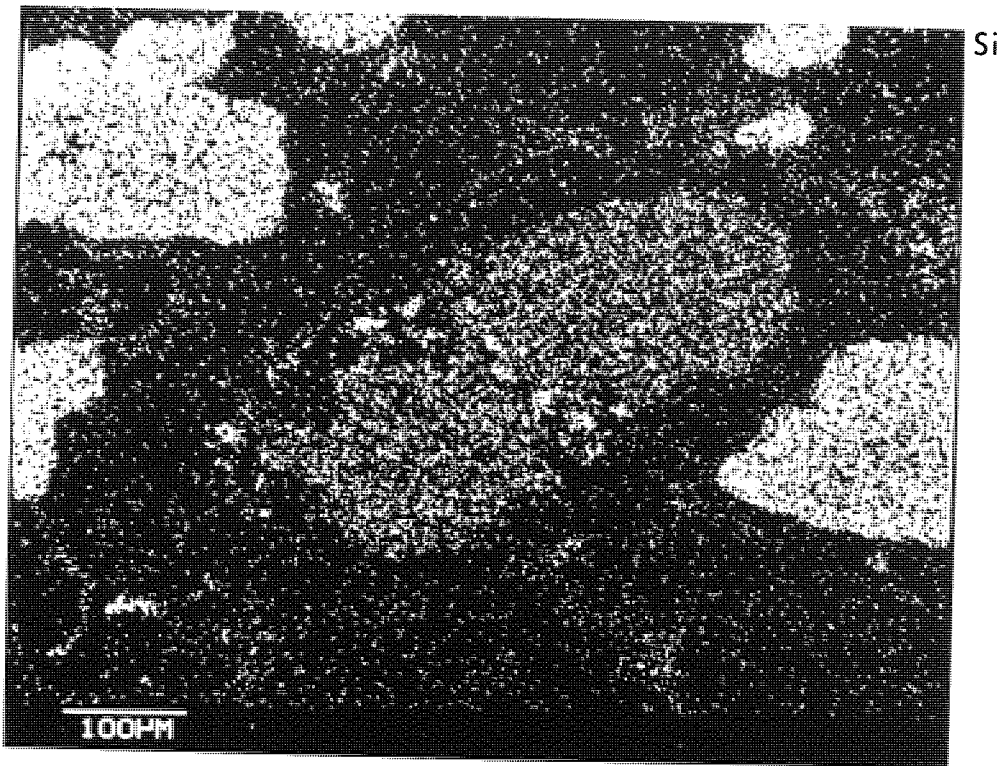
a.



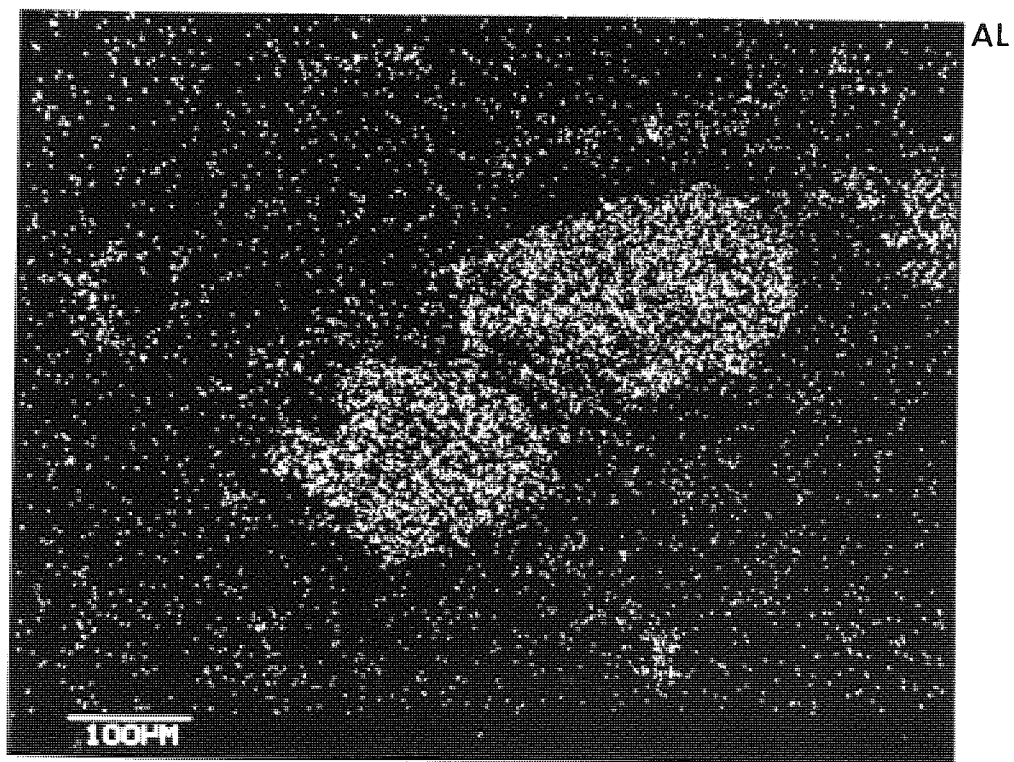
b.

Fig. 4.19





c.



d.

Fig. 4.19

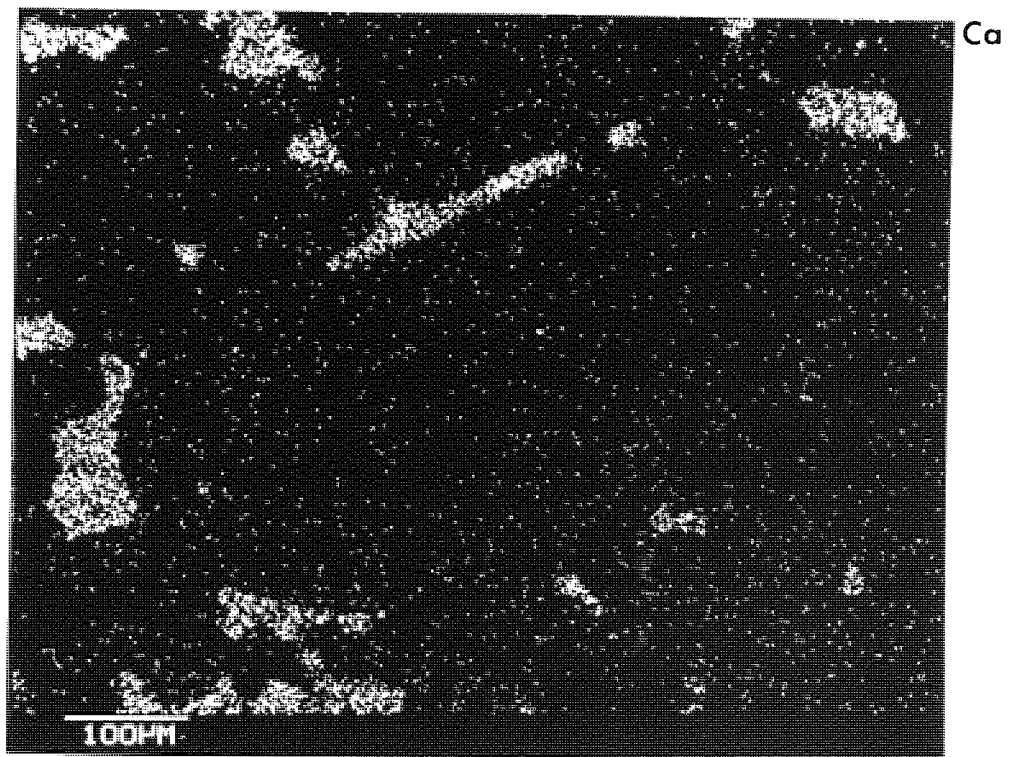
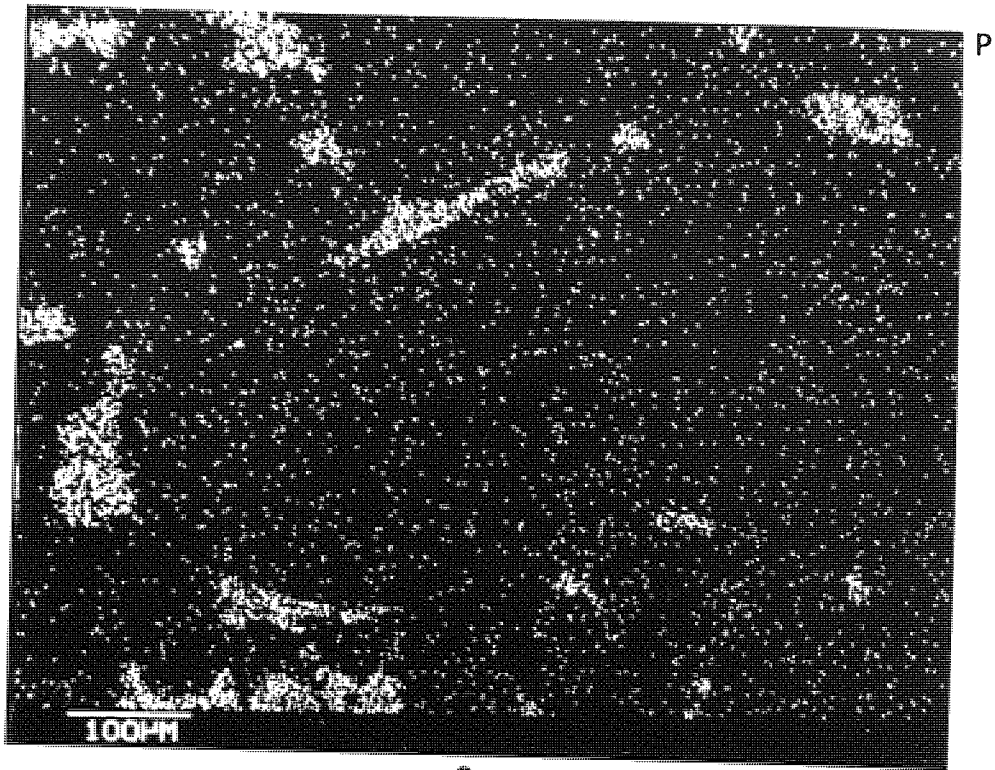


Fig. 4.19

The Fe X-ray distribution map shows a high concentration of Fe in both the matrix and the ooliths. There is a slightly higher Fe concentration in the outer rim of the middle oolith than the inner layers. Some Si occurs as discrete areas of high concentration not associated with the other elements. The areas of high Si concentration are associated with the subangular detrital fragments seen in the scanning electron micrograph.

Also there are anhedral grains high in Si concentration. These divide the oolith into two parts; the length of the major axis is about 10  $\mu\text{m}$ . In each part there is a core of moderately high Si associated with moderately high Al.

Ca and P are associated with each other and are seen as irregular and variable size patches surrounding the oolith. They are also seen surrounding one subrounded high concentration Si grain. There are some anhedral Ca and P grains in the matrix; the length of their major axis is approximately 10  $\mu\text{m}$ .

Fe is shown in:

- a - the matrix which is rich in Fe, shown from X-ray studies and petrographic studies to be hematite.
- b - ooliths as only Fe; again shown to be hematite.

Si shows:

- a - as discrete subangular grains in the matrix and anhedral grains in the ooliths (quartz).

b - associated with Al in the core of the ooliths,  
proved to be clay minerals.

Ca and P show:

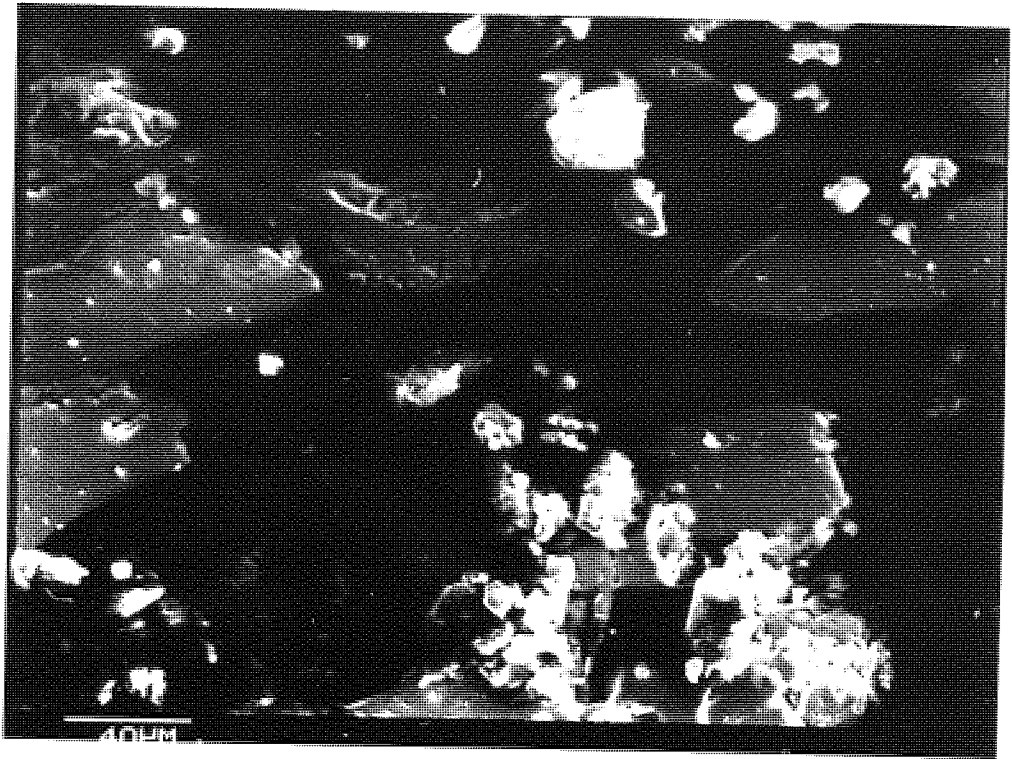
a - associated with each other; (apatite).

Apatite can be seen as irregular patches surrounding the ooliths and as anhedral grains in the matrix.

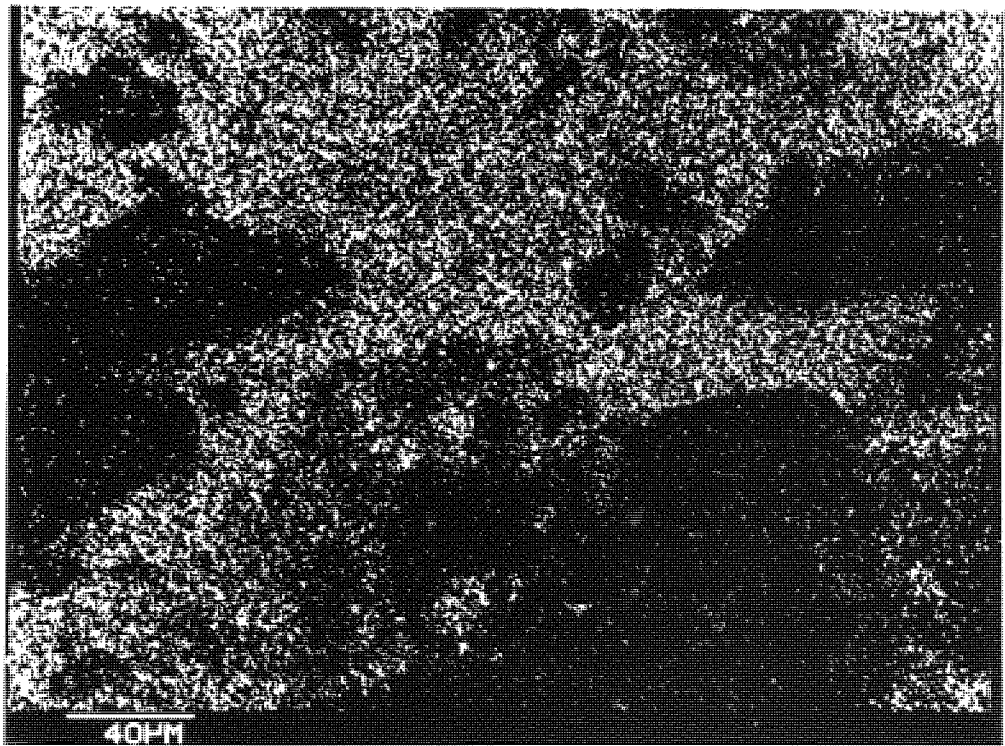
Figure 4.20 - Scanning electron micrograph for oolitic iron with sand sample No. AS11 and the X-ray distribution map for Fe, Si, Al, P and Ca.

Shows long subangular grains in the matrix as well as subrounded white grains for which the length of the major axis is about 10  $\mu\text{m}$ . Also seen are irregular areas variable in size. The size varies from 30  $\mu\text{m}$  to 60  $\mu\text{m}$ . The matrix is uniform except for a small area in the top left of the scanning micrograph.

The Fe X-ray distribution map shows a high concentration of Fe in the matrix. It also shows that the concentration of Fe is lower in the area to the left of the Ca pocket. (In the middle of scanning electron micrograph). The Si occurs as discrete areas of high concentration and is not associated with the other elements. The areas of high Si concentration are associated with the two long subangular grains. The low Si concentration area to the left of the pocket has its Si associated with low Al and Fe concentration. Al is shown to be associated with Fe and Si in the matrix.



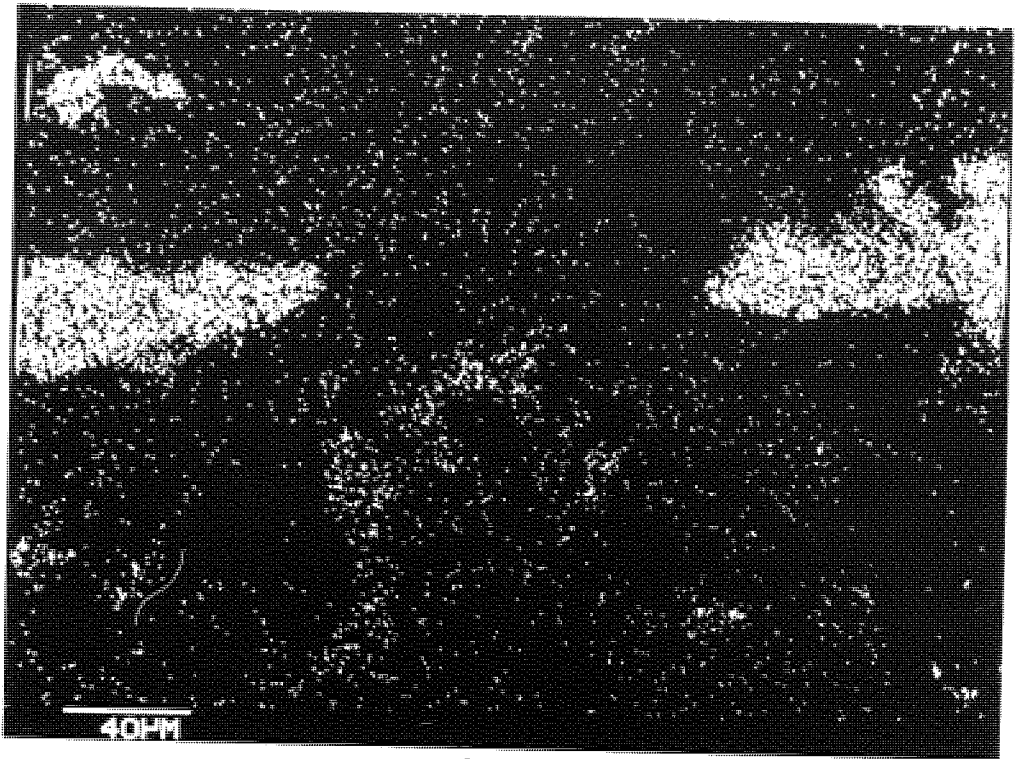
a.



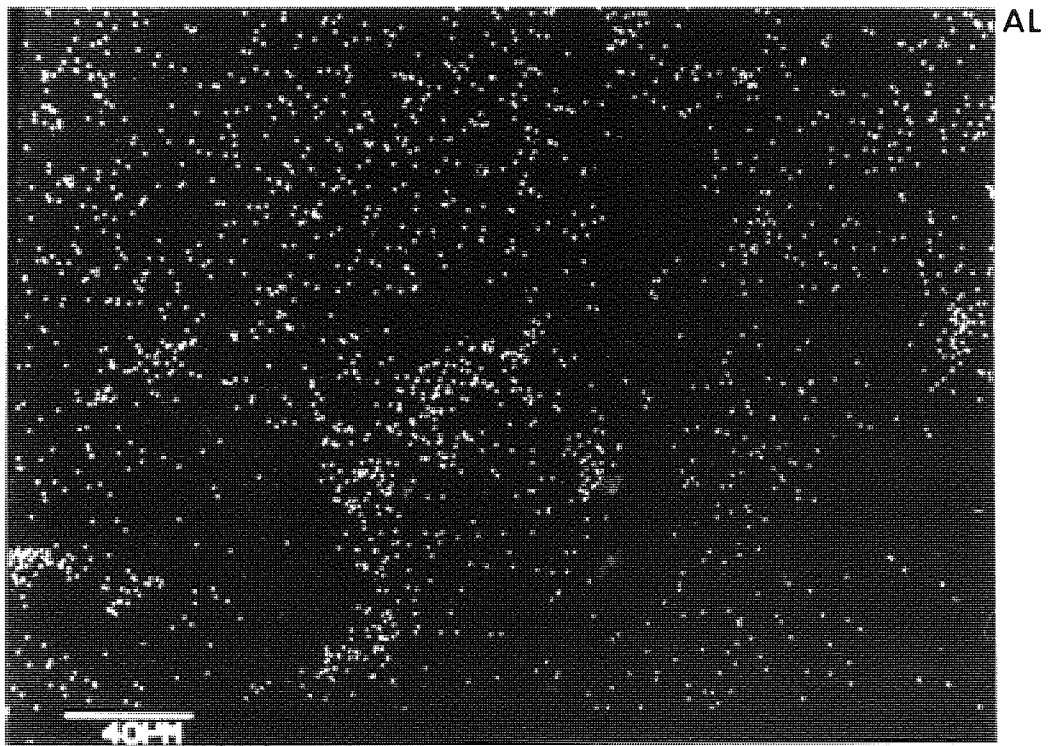
Fe

b.

Fig. 4.20



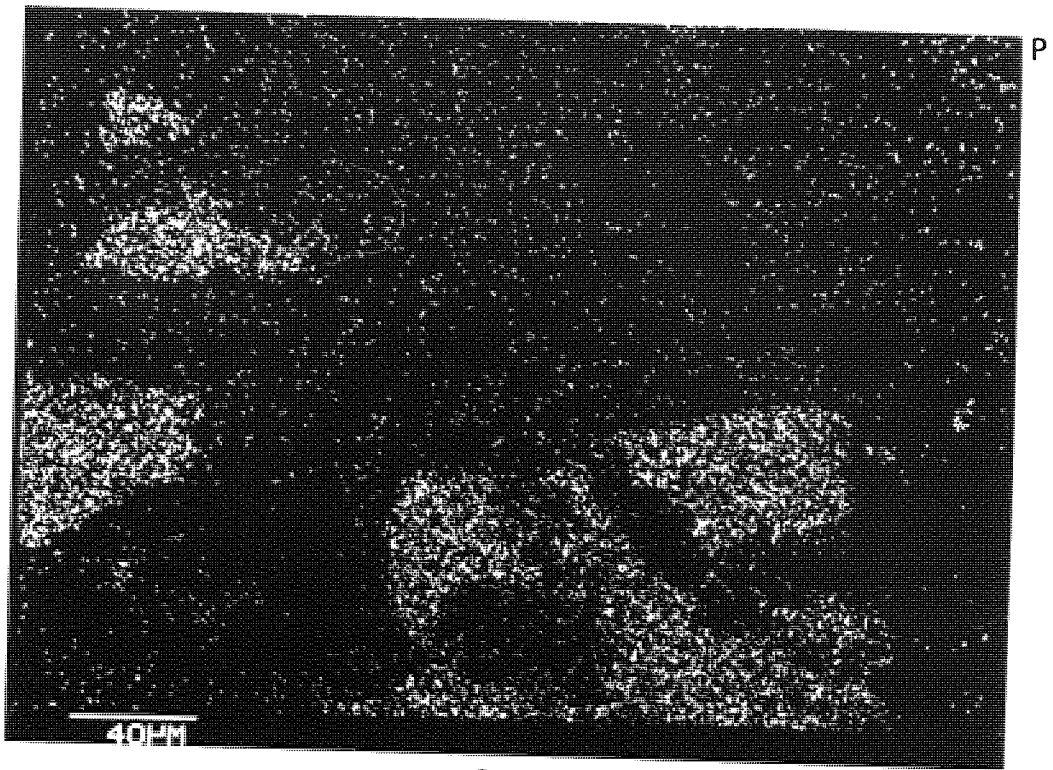
c.



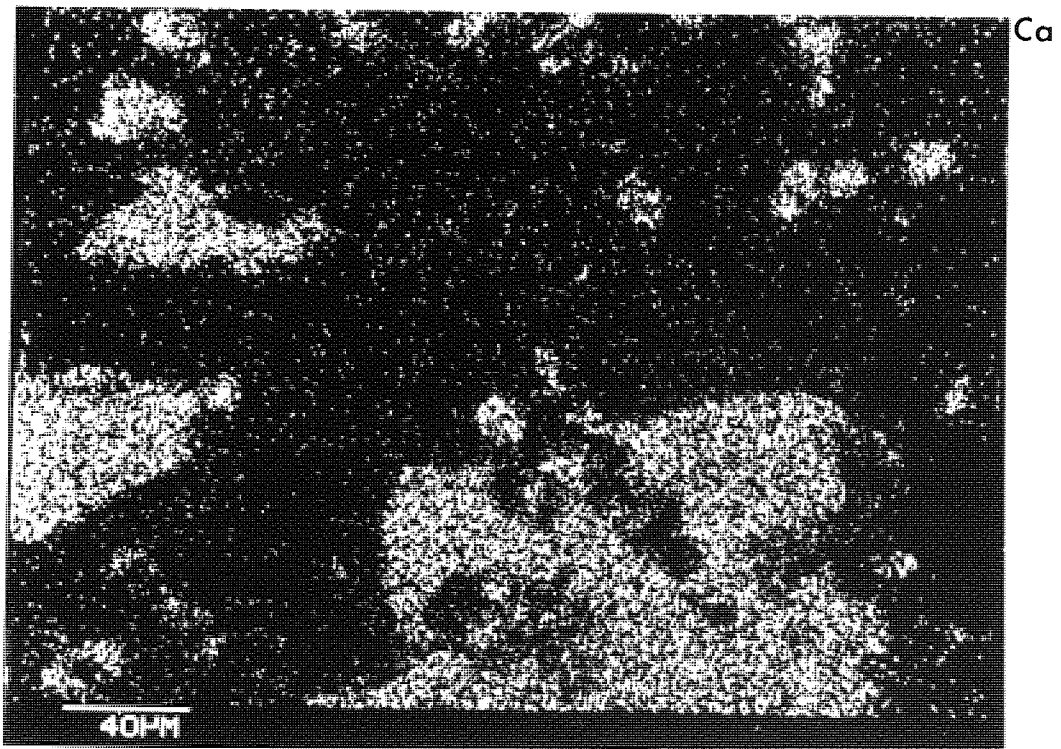
d.

Fig. 4.20





e.



f.

Fig. 4.20



Ca occurs as discrete subrounded grains of high concentration and is not associated with the other elements. It is also seen as irregular pockets in which it is associated with P; the length of the major axis varies from 30  $\mu\text{m}$  to 60  $\mu\text{m}$ .

Also there is a Ca and P grain for which the length of the major axis is about 20  $\mu\text{m}$ .

The Fe is shown to be in the matrix. From X-ray and petrographic studies the Fe was shown to exist as hematite.

Si shows:

- a - as long subangular grains which were shown from X-ray studies to be quartz.
- b - as matrix surrounding the Ca and P grains; proved to be quartz.
- c - associated with Fe and Al; from X-ray studies it was proved to be clay minerals.

Ca shows:

- a - as subrounded grains which are shown from petrographic studies to be calcite.
- b - associated with P. X-ray studies proved these to be apatite.

Figure 4.21 - Scanning electron micrograph for oolitic iron ore sample No. AS20 and the X-ray distribution map for Fe, Al, Si, Ca and P

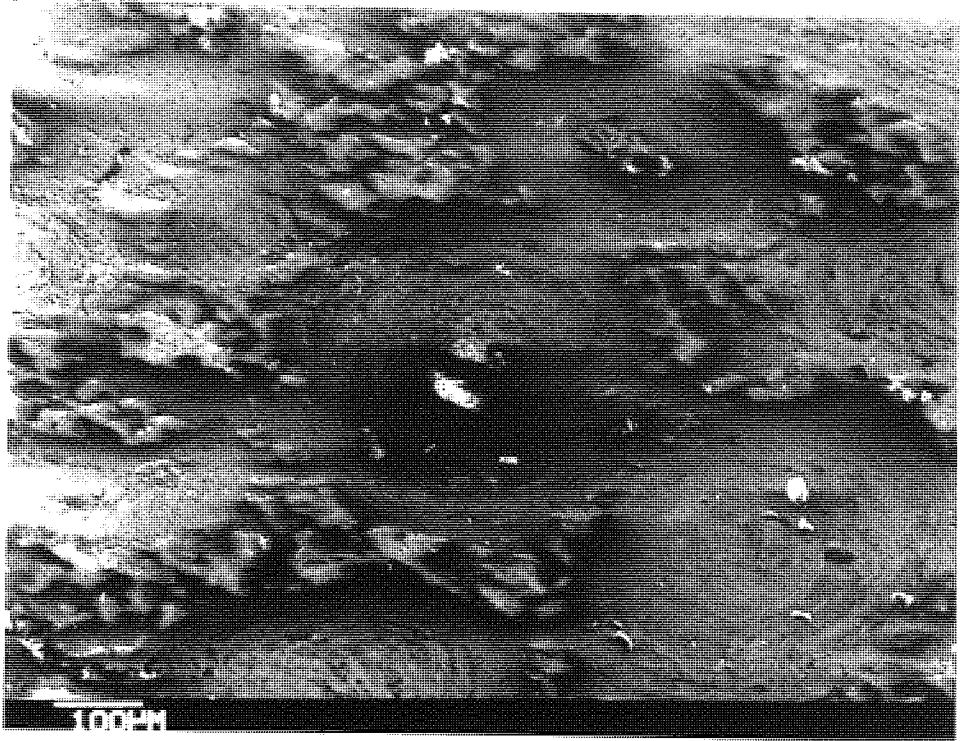
Ooliths are ellipsoidal or circular in shape; the length of the major axis varies from 90  $\mu\text{m}$  to 290  $\mu\text{m}$ . Most of them show a concentric banded structure. In one oolith, in the middle of the scanning electron micrograph, there is the nucleus of another mineral grain which subsequently appears as two subangular grains in the core of the oolith; also there are fine anhedral grains within the concentric layers in the oolith. The matrix cements the ooliths and there are two types of matrix materials. The Fe X-ray distribution map shows a high concentration of Fe in the ooliths. It also shows that there are anhedral grains of Fe which occur in the matrix; the length of the major axis varies from 5  $\mu\text{m}$  to 60  $\mu\text{m}$ .

Si occurs as small anhedral grains of high concentration in the matrix and is not associated with other elements; the length of the major axis is about 10  $\mu\text{m}$ . Also there are subangular grains of moderately high Si concentration associated with moderately high Al concentration in the core of the middle ooliths shown in the electron micrograph. There are fine anhedral grains of Si associated with Al within the concentric layer in the oolith. In addition to this, there are some fine particles of Si dispersed in the ooliths and the matrix.

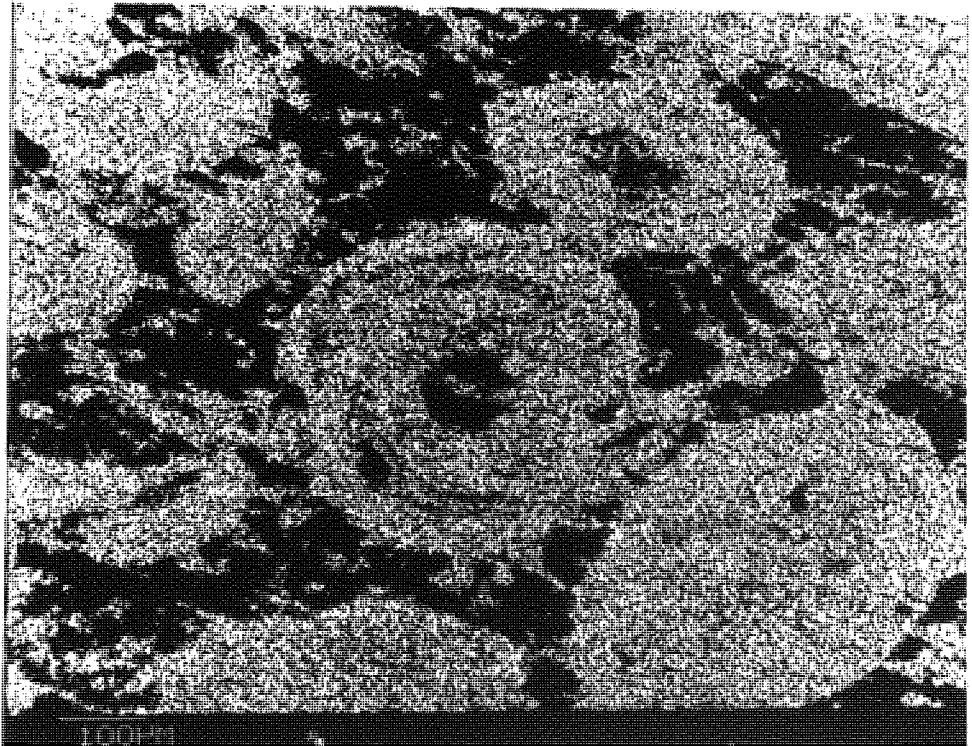
Al occurs within subangular grains in the core of the middle oolith, as anhedral grains within the concentric

Figure 4.21 Scanning Electron  
Micrograph for Oolitic Iron Ore  
Sample No. As 20 and X-ray  
Distribution Maps x200

- a - Scanning Electron Micrograph
- b - Iron X-ray distribution map
- c - Silicon X-ray distribution map
- d - Aluminium X-ray distribution map
- e - Phosphorus X-ray distribution map
- f - Calcium X-ray distribution map



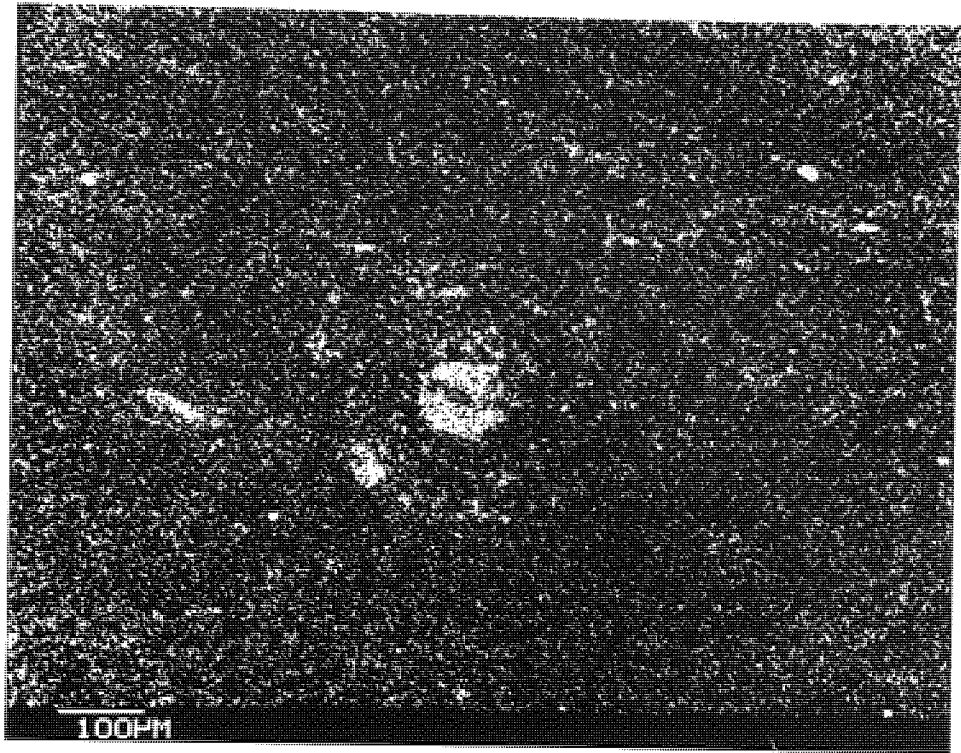
a



Fe

b.

Fig. 4.21



Si

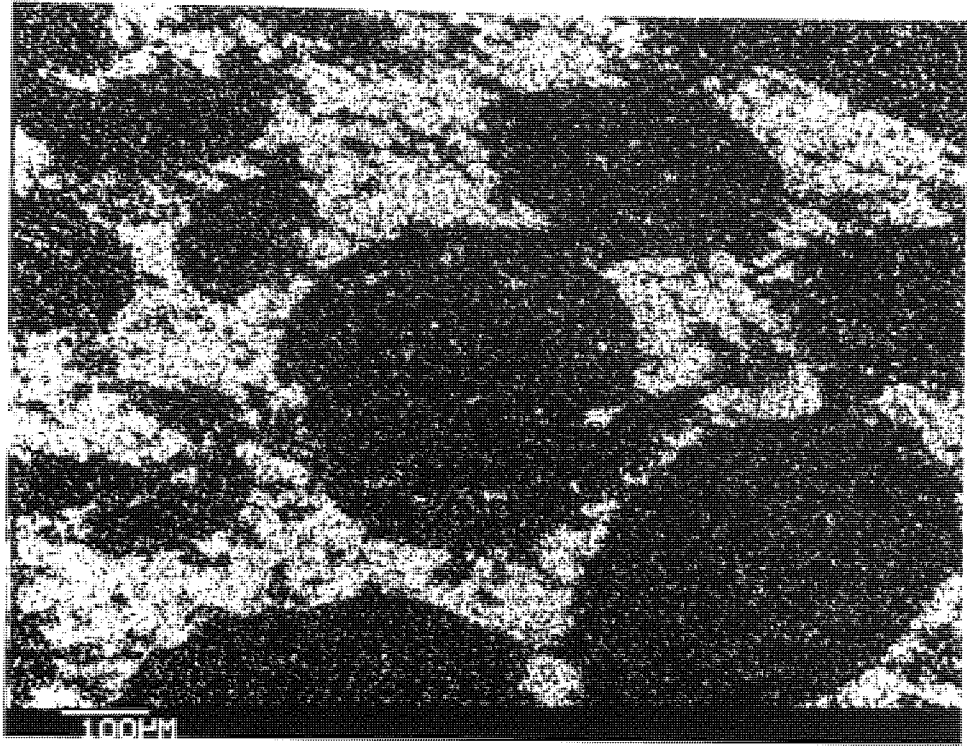
c.



AL

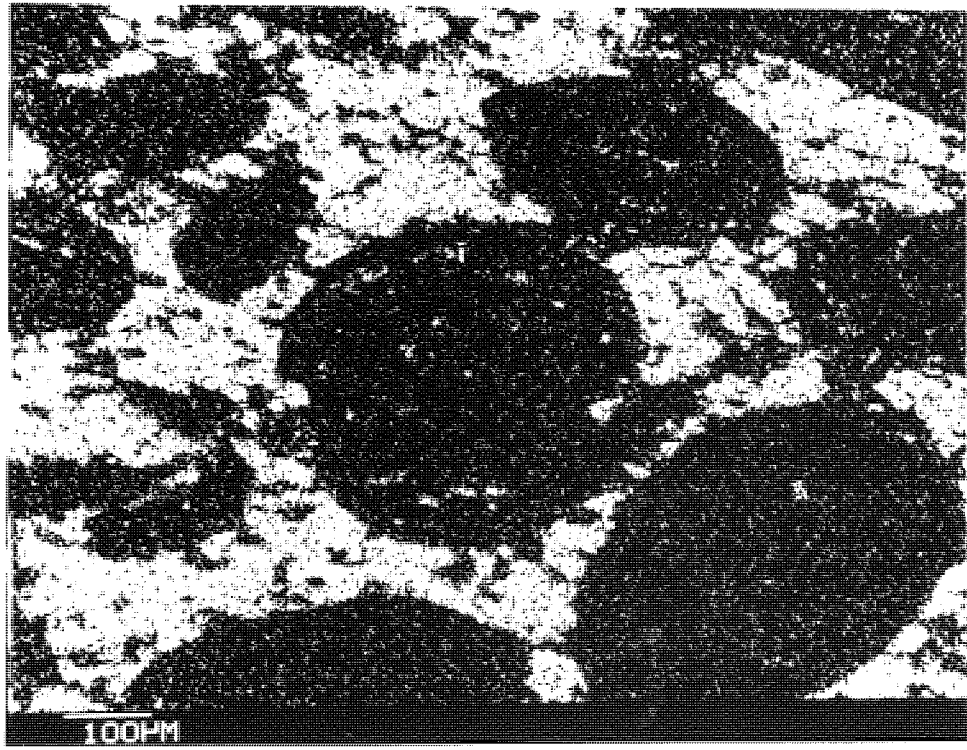
d.

Fig. 4.21



P

e.



Ca

f.

Fig. 4.21



layer and as fine grains dispersed in the ooliths and in the matrix.

Ca and P are associated with each other in the matrix and also seen as fine anhedral grains in the ooliths; the length of the major axis varies from 5  $\mu\text{m}$  to 20  $\mu\text{m}$ .

Fe is shown in:

- a - ooliths rich in Fe (shown to be hematite)
- b - as anhedral grains in the matrix; again shown to be hematite.

Si shows:

- a - as anhedral grains (quartz)
- b - associated with Al. Proved from X-ray studies to be clay minerals.

Ca and P are shown:

- a - in the matrix associated with each other. Shown from X-ray studies to be apatite.
- b - as anhedral grains in the ooliths. These proved to be apatite.

#### 4.3.4.6 Summary of results

It will be recalled that this ore body is an oolitic iron bearing ore of the Minette type, occurring as bands in the middle group of the Nubian series. These horizontal bands are interbedded with clays and Ferruginous sandstones.

Fortunately, the iron ore bands are at the surface or close thereby and the open-cast method of mining is possible. The Aswan iron ore deposits can be classified into three different forms: the Ferruginous sandstones, the Ferruginous concretions and the Oolitic iron ore. From the chemical analysis of Aswan cores it is seen that the oolitic samples from the first core contains 42-55% Fe and 0.1-2.9% P and the second core analysis 41-57% Fe and 0.35-2.3% P. It is also seen that the analysis of the Ferruginous sandy clays in the two cores contained 6.5-20.2% and 44.1-41.8% Fe, with P content between 0.5-1.4% and 1.1-3.8% respectively, while the sandstone bed contained iron between 1-8% and phosphorus between 0.04-0.14%.

From X-ray examination the hematite was shown to be the major iron bearing phase with varying amounts of quartz and apatite, with only a little clay minerals.

## 5. FRODINGHAM IRONSTONE

### 5.0 Introduction

The iron making process as it is known today started in 1709 when Abraham Darby of Coalbrookdale successfully used coke as a fuel in his furnaces in Shropshire (28,29). Many improvements in the making of iron and the perfecting of wrought iron followed during the next hundred years. Up to the middle of the nineteenth century almost the whole of the iron produced in the United Kingdom was smelted from home iron ores. Most of these were sedimentary ores known as ironstones. Since 1875 there has been a swing away from the high phosphorus containing home ores to foreign supplies with their higher iron contents and much lower phosphorus contents. The chief reasons for this movement were decreased unit cost of the iron in the richer ores with increased production and improved quality of the iron product. The proportion of imported to total ore consumed (Figure 5.1) increased from nil before 1860 to about 30% by 1900, and remained constant at that level during the 1939-1945 war, during which imports were restricted. Since the war the proportion of imported ore started to rise again, until it is now about 60% (30).

The tonnage of home ores produced is shown in Figure 5.2 for 5-year periods since 1865 (30). There has been considerable fluctuation, with a record production of nearly 20 Mt in 1942. From 1950 to 1965 output was in the range 15-17 Mt per year, but since that date it has fallen to 12.0 Mt in 1970. Thus the expansion and

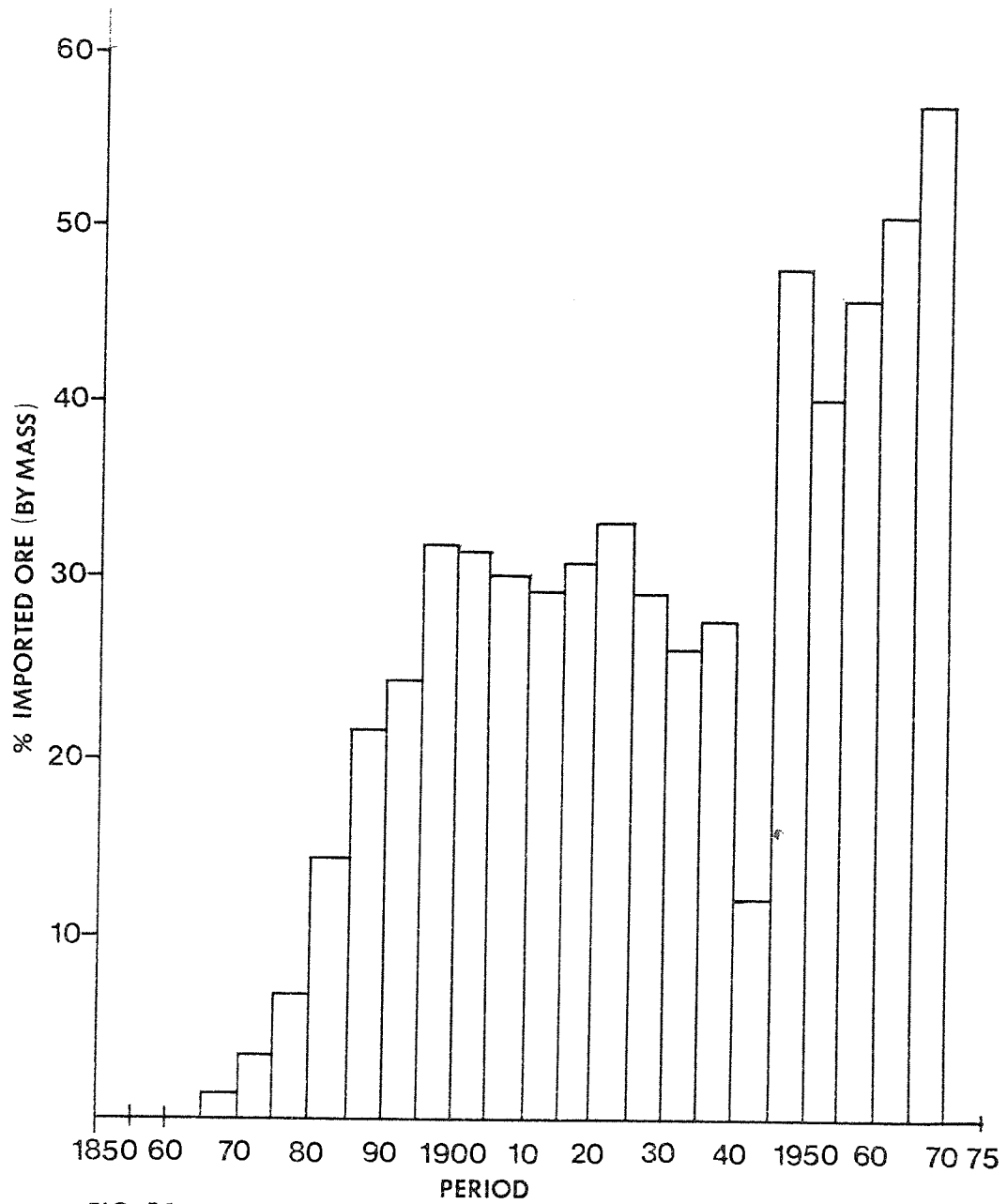


FIG. 5.1

THE PROPORTION OF IMPORTED ORE

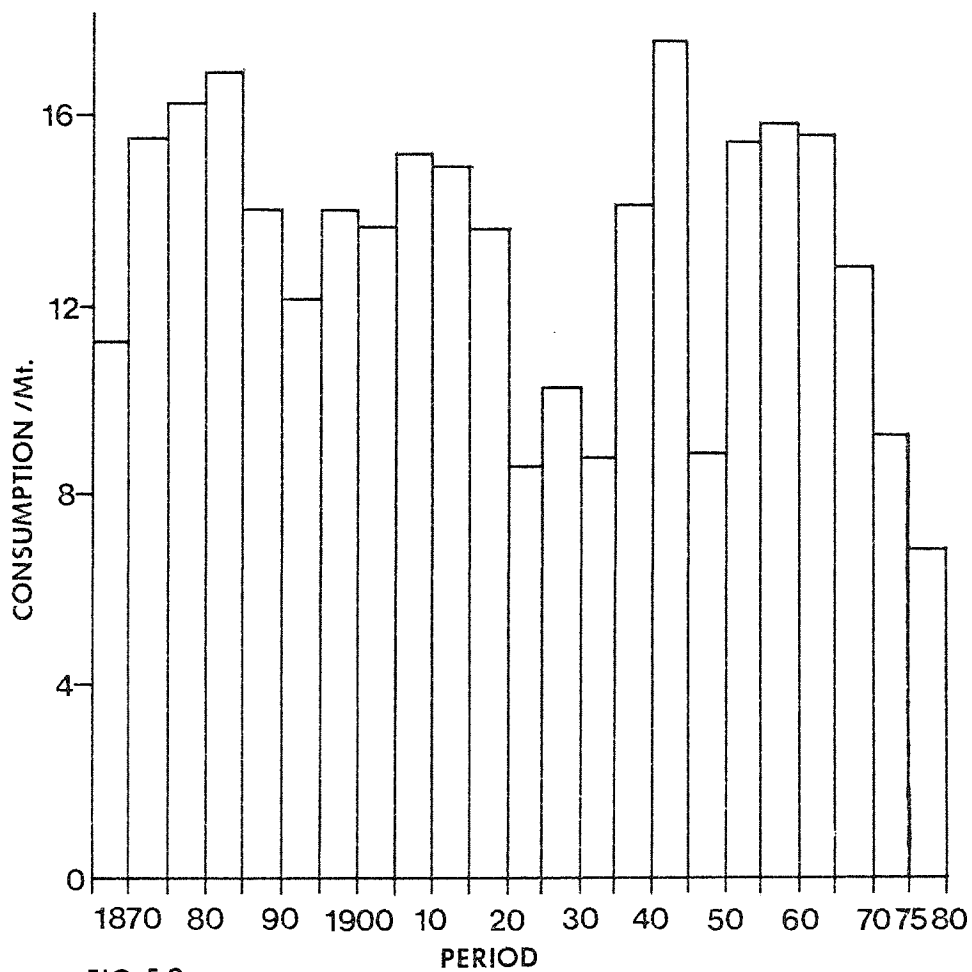


FIG. 5.2  
 AVERAGE CONSUMPTION OF BRITISH HOME IRON ORE IN  
 5 - YEARLY PERIODS

restructuring of the iron and steel industry since 1950 has been largely based on imported ore and it is intended that this trend should continue. The reasons for this are as before resulting in a reduction of iron and steelmaking costs. Although the use of basic oxygen converters is recognised to be the most economical means of large scale steelmaking using molten iron, it is most profitable working with relatively low phosphorus content in the charge (not more than 0.25%).

The United Kingdom's iron ore reserves are approximately 3,000 Mt. Those in Northamptonshire are estimated at 1.050 Mt containing 0.3-1.0% P and 27-34% Fe. The Frodingham deposit in Lincolnshire contains reserves in excess of 1,000 Mt. It is also phosphoric with an average phosphorus content of 0.35% and iron content of 25% <sup>(31)</sup>. Consequently it is clear that there are large iron ore resources with little practical value in the foreseeable future. These considerations have suggested that an investigation into the possibility of eliminating the phosphorus present in the iron ore or reducing its percentage to acceptable levels would be worthwhile. A number of research projects have been undertaken to reduce the concentration of phosphorus in Frodingham ironstone. One <sup>(32)</sup> attempted concentration by flotation and another <sup>(33)</sup> used roasting followed by magnetic separation. In both processes the phosphorus content in the ore and in the concentrated product was nearly the same.



Mineralographic examination of the structure of ironstone is an important part of ore-dressing research. Unfortunately, this technique is not sufficient to elucidate the complex intergrowth of gangue minerals with the valuable iron containing parts of the ore. These can be solved only by the use of advanced modern mineralogical examinations. Most of the analyses and examinations carried out in the earlier work were insufficient to meet the demands for the ore-dressing of Frodingham ores. These analyses do not define carefully enough the mineralogical character of ores showing the amount of impurities and the intergrowth of the useful and gangue components. It is not possible to solve the release size of grains, or, in the case of a complex ore, the combined technology of multi-stage separation.

The mineralogical examination of Frodingham ironstone carried out in this research programme utilised, for the first time, Electron microprobe and Scanning electron microscopy. Their introduction has helped to increase the description of the mineral distribution and sizes throughout the ore samples.

This application of modern electron metallographic techniques to elucidate the mineral particle sizes, quantity and distribution within an ore sample illustrates clearly the use of these techniques to practical problems in the field of mineral dressing for the production of improved mineral concentrates.

## 5.1 Stratigraphy

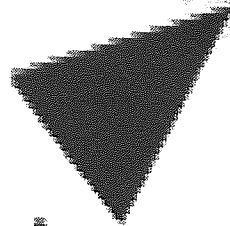
The Frodingham ironstone bed is situated in north Lincolnshire, east of Scunthorpe (Figure 5.3 a and b). It occurs in the lower Jurassic bed of the South Humberside area and the geology of the area is shown in Figure 5.4. The ore contains highly fossilised ferruginous oololiths, with oololiths of chamosite, siderite, and limonite, together with shell fragments, set in a matrix of either chamosite-sideritic mudstone or coarsely crystalline calcite. The beds range in thickness up to a maximum of about 32 feet. The average Fe content is 25% whilst the average  $\text{SiO}_2$  content is 7.5%, CaO 22%, and Phosphorus 0.35%. It has a workable outcrop length of 7 miles north to south (34). The beds extend, under increasing cover, at least for 20 miles to the east.

A generalised section of rocks in this ground with their variation in thickness is as shown in Figure 5.5.

## 5.2 Lithology (35)

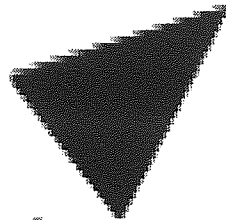
In the southern half of the quarried area the ironstone as a whole is made up of green and brown beds, but in the northern part of the field the general colour is brown with many beds approaching red in colour.

On the whole the ironstone is remarkably free from argillaceous matter. The upper beds near the surface are usually darker and more oxidised than the beds beneath. They are more broken up and carry a considerable amount of natural fines; i.e. the average size of the ore is less



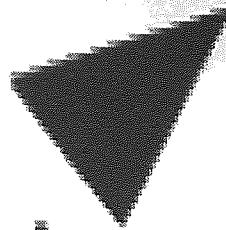
Aston University

Illustration removed for copyright restrictions



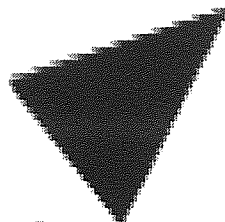
Aston University

Illustration removed for copyright restrictions



Aston University

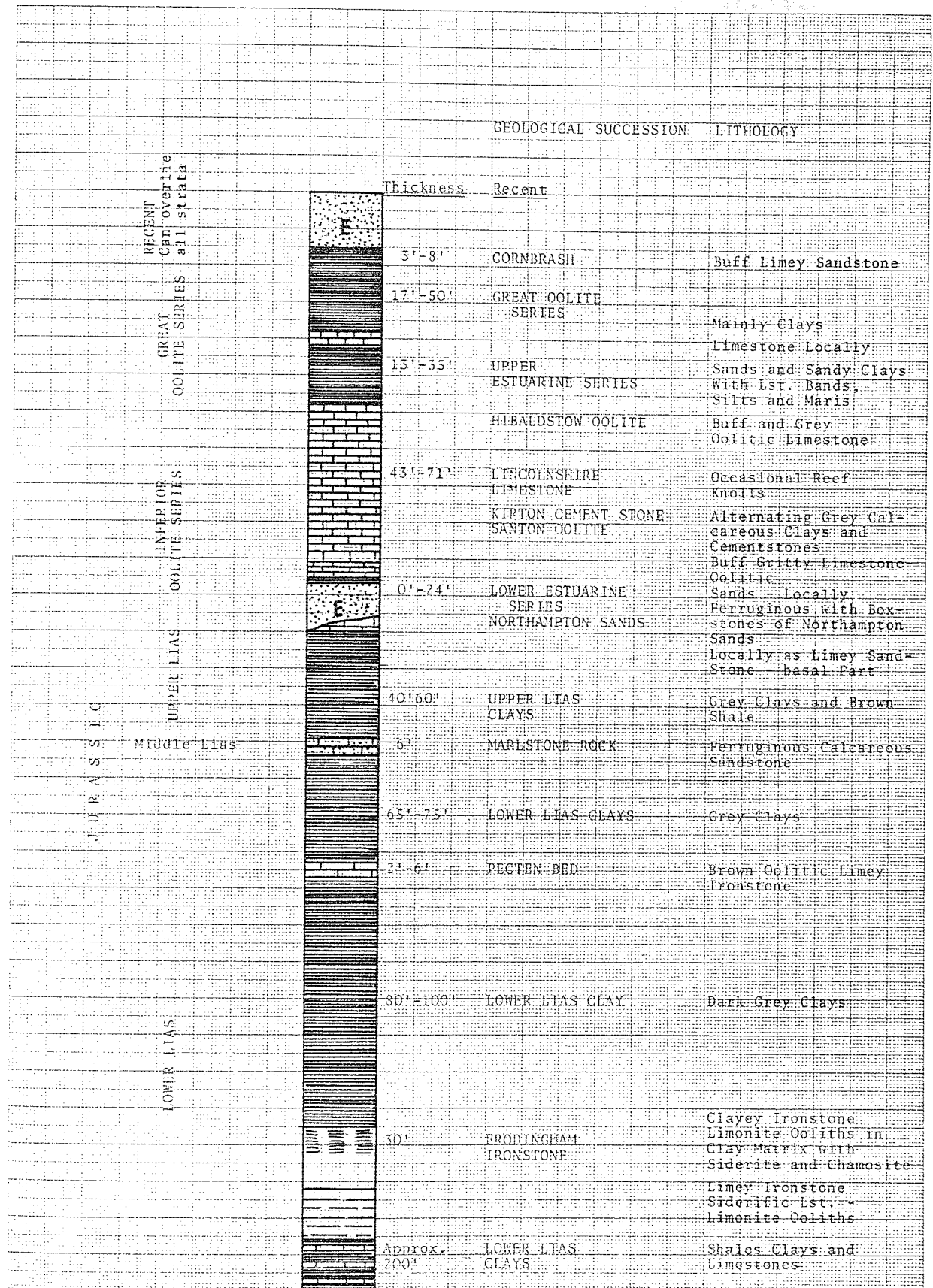
Illustration removed for copyright restrictions



Aston University

Illustration removed for copyright restrictions

Fig 5.5 THE GEOLOGY OF THE SCUNTHORPE AREA



E = Erosion surface

than three quarters of an inch, (20 mm) this is undoubtedly due to the greater effects of weathering in the higher beds. The ore is highly fossilised and contains thick shells, mainly the lamellibranchs *cardinia* and *gryphaea*, which are preserved in crystalline calcite. The excessively calcareous nature of the stone is largely due to the presence of these fossils.

Ooliths of almost pure limonite are found throughout the ironstone, but their distribution is not uniform; they may be patchy in one place, uniform in another and sporadic elsewhere. The individual ooliths also are variable in size and shape; generally they are small with a tendency to be elongated rather than spherical.

The uppermost beds are chamositic mudstones consisting of brown limonitic ooliths with shell fragments and occasional scattered sand grains in a matrix made up of innumerable minute flakes of chamosite roughly parallel with the bedding together with a few flakes of mica and fine quartz plus numerous small rhombs of siderite with dolomite nuclei.

The lower beds are generally more calcareous and their predominately green or greenish-brown colour is due to the fact that the matrix is essentially chamositic mudstone. Parts of individual beds are frequently greyish-blue in colour where the matrix is limestone.

The more limey beds, occurring chiefly in the lower part of the ironstone, are made up of an aggregate of brown

limonitic ooliths, rounded shell fragments and crinoid ossicles cemented with clear crystalline calcite which frequently shows a comby structure indicating the growth of crystals from the walls of the interstitial spaces. Complete lamellibranch shells are often lined with calcite crystals and sometimes wholly or partly filled with a smooth chamositic mud. Some of the shells are worn and riddled with the branching tubules of 'algues perforantes', while others are uninjured or only superficially chloritized.

### 5.3 Mineralogy

The unweathered mineralogical constitution of the Frodingham ironstone, taken from Davies and Dixie <sup>(36)</sup> (1951, p.89), is shown in Table 5.1.

It shows that the ironstone varies according to the nature of the matrix. The ironstone with a calcite matrix is essentially a ferruginous limestone and corresponds to the "limey ore" while that with a chamosite-siderite matrix may be described as clayey ironstone. The shells (principally *Cardinia*) tend to occur in well-defined bands, usually 6 to 12 inches (15-30 cm) thick, the remainder of the ironstone being almost devoid of shells. Consequently, some parts of the clayey ironstone contain little or no calcite.

The nature of ooliths and the shell fragments has been described by Davies and Dixie <sup>(36)</sup>, and the following is summarised from their work. The majority of the ooliths are ellipsoidal, with major axes about 0.30 mm long and twice the length of the minor axis. Locally, thin bands may contain ooliths (or pisoliths) up to 5 mm across. The



TABLE 5.1

THE MINERALOGICAL CONSTITUTION OF  
UNWEATHERED FRODINGHAM IRONSTONE  
(After Davies and Dixie, 1951)

<u>Principal Constituents</u>	<u>Calcite matrix</u>	<u>Chamosite- Siderite matrix</u>
Limonite - mainly as ooliths	30	35
Quartz - as small grains	-	0-10
Calcite - as shells	20	20
as matrix	30	-
Siderite	10	17
Chamosite	0-5	18-23
<u>Minor Constituents</u>		
Sericite	1	3
Collophane	1.5	2.0
Pyrites	0.4	0.5 (locally up to 7.0)
Rutile	-	1

Ooliths in other bands are exceptionally small.

#### 5.4 Mineralogical classification of the ironstone (36,36a)

The ironstone is classified into 4 principal types, viz A, B, C and D (Types A, B and C are 'clayey' ironstones, whilst type D is a limey ironstone). These types are defined as follows:-

##### Type A

In this, calcite shells and limonite-chamosite ooliths, more or less replaced by siderite, all coated with a thin film of chamosite, are closely packed together with the interstices filled with siderite.

The hand specimen, especially when moist, has a distinctive appearance. The siderite has been superficially oxidised to limonite so that the ironstone appears as a sponge-like mass of dark green chamosite, the pores in the sponge being filled by highly polished ooliths of brown limonite and brown aggregates of siderite.

##### Type B

In this type, small rhomb-shaped crystals of siderite are evenly distributed among linearly arranged flakes of chamosite. The hand specimen is a dense, tough, compact, dark bluish-grey rock which breaks with a granular fracture due to the siderite rhombs.

Oololiths and other coarse material are absent. It occurs usually as discontinuous bands, an inch or two thick (2-5 cm), among other types of ironstone and is far less abundant than the others.

#### Type C

This type is characterised by limonite-chamosite oololiths, more or less replaced by siderite, and calcite shells embedded in an extremely fine-grained matrix composed of chamosite and siderite. In the hand specimen, highly polished limonite oololiths are scattered irregularly through a dark bluish-grey matrix. Unlike Type B, this matrix is quite soft when wet, and unlike Type A, chamosite has partly replaced, and not merely coated, the calcite shells. Locally, small subangular quartz grains may be present.

#### Type D

In this type, limonite-chamosite oololiths and calcite shells, more or less replaced by siderite, are set in a matrix composed of coarsely crystalline calcite, some siderite and, less commonly, pale-green chamosite may be present in the matrix. This type is essentially a hard, shelly limestone containing coarse iron bearing particles. The calcite matrix, though often limonite stained, can usually be distinguished in the hand specimen. This ironstone has been formed mainly by the mechanical disintegration of ironstone of the three preceding types, the debris so formed being cemented together with calcite. The occurrence of type D ironstone indicates that, after a period of quiescent conditions on the sea-floor during which ironstones of types A, B and C were deposited, turbulent conditions supervened and churned up the last-formed deposits.

## 5.5 Experimental Work

### 5.5.1 Material

The material used in this study was taken from split cores provided by British Steel Corporation. Cores Y 112, and Y 113 were drilled from the Yarborough pit, (Figure 5.3b). Core drilling was done using 101 mm or 116 mm drilling crows, and core recovery was approximately 100 percent.

Ironstone cores were split longitudinally and one half of the core was boxed in one foot increments. These were collected from Scunthorpe and the following investigations made:

- Descriptive logging
- Photography
- Chemical analyses
- Microscopic examination
- X-ray mineralogical examination
- Microprobe analysis
- Scanning electron microscopy

The other portion of the core was crushed in one foot increments by B.S.C. for chemical analysis and the results are presented in Tables 5.2 and 5.3.

Photographs of Frodingham ironstone cores Y 112 and Y 113 are shown in Figures 5.6 and 5.7, showing the various ironstone types which are readily recognised.

### 5.5.2 Core logs

Detailed logging of the cores (Figs. 5.8 and 5.9) has shown that a variety of different lithologies are present in each.

TABLE 5.2 CHEMICAL ANALYSIS, X-RAY, SCANNING ELECTRON MICROSCOPE STUDIES  
AND ELECTRON MICROPROBE ANALYSIS FOR MOUNDINGHAM IRONSTONE CORE  
Y112

No.	Depth	Iron %	Lime%	Insol %	Sul %	Phos %	X-ray	Scanning Electron Microscope	Electron Microprobe analysis
	76'3"	32.1	4.5	23.0	0.050	0.46			
	77'3"	32.1	4.5	23	0.050	0.46			
-1	78'3"	31.2	6.5	21.6	0.046	0.30	Majority is SiO <sub>2</sub> , trace of chamosite and siderite, and little apatite.		
A7-2							Most of the sample is SiO <sub>2</sub> , small amount of calcite and little of chamosite, apatite hematite and siderite		
A8	79'3"	30.7	11.5	17.0	0.037	0.16	Most of the sample is SiO <sub>2</sub> and calcite, little siderite, chamosite, hematite and apatite.		
	80'3"	26.6	12.1	22.9	0.069	0.18			
	81'3"	22.4	11.4	28.8	0.578	0.23			
	82'3"	23.4	17.8	11.5	0.408	0.10			
	83'3"	27.4	15.5	7.3	2.308	0.07			
	84'3"	27.5	12.8	16.4	0.243	0.23			
	85'3"	30.0	17.4	6.3	0.458	0.16			
	86'3"	24.8	25.0	4.1	0.710	0.20			
	87'3"	23.1	24.1	8.2	0.765	0.12			
	88'3"	21.7	30.0	4.1	0.925	0.21			
	89'3"	37.1	11.3	5.8	0.417	0.33			
	90'3"	29.0	21.0	3.9	0.174	0.37			
	91'3"	36.6	11.2	4.7	0.110	0.38			

Cont. Table 5.2

No.	Depth	Iron %	Lime%	Insol %	Sul %	Phos %	X-ray	Scanning Electron Microscope	Electron Microprobe Analysis
A53							Majority is SiO <sub>2</sub> , small amount of calcite and hematite, trace of apatite.		
	92'3"	43.3	6.0	5.4	0.504	0.49			
	93'3"	21.7	28.6	3.7	0.701	0.32			
	94'3"	25.2	21.8	8.9	1.260	0.20			
A65							Most of the sample is calcite and SiO <sub>2</sub> , little hematite and apatite.	Ooliths of Fe, matrix is mainly Ca associated with little Si and Al.	Ooliths of Fe, one oolith of Fe associated with Ca, Si, Al and P, matrix is mainly Ca with Fe, Si, Al and P.
	95'3"	15.9	36.3	3.5	0.348	1.12			
	96'3"	16.6	35.7	2.8	0.321	0.32		Ooliths of Fe, shell fragment of Ca, matrix is mainly Ca with little Fe, Si, Al and P.	
	97'3"	27.7	19.8	6.0	0.551	0.48			
A82	98'3"	16.0	34.4	4.1	0.078	0.29	Most of sample is SiO <sub>2</sub> and calcite, chamosite, apatite and trace of siderite.		
A85-1									
A85	99'3"	20.2	29.2	5.0	0.047	0.90			
A86							Calcite, and SiO <sub>2</sub> , hematite, apatite and trace of chamosite.	Oolith of Fe associated with Si, Al and Ca. P occurs as fine grains and as anhedral grains (3µm); associated with Ca.	Ooliths of Fe associated with Si and Al, Ca and P; matrix is Ca, in one oolith anhedral grains of P and Ca (15-30µm)
	100'3"	16.6	30.0	4.6	0.047	0.76	Calcite, hematite, SiO <sub>2</sub> , apatite and little chamosite.		
A93	101'3"	18.7	29.9	3.1	0.024	0.14	Majority is calcite, little chamosite, and SiO <sub>2</sub> .		
A85-2									
	102'3"	22.4	26.7	6.3	0.047	0.24	Most of the sample is chamosite and little SiO <sub>2</sub> and siderite		
A99									
	103'3"	27.6	17.4	11.9	0.147	0.58	Hematite, calcite and little chamosite and apatite.	Ooliths of Fe, matrix is mainly Ca with Fe associated with Si, Al and P, plus angular prismatic and shell fragment of Ca, P occurs as very fine grains.	
	104'3"	26.0	21.8	6.3	0.431	0.24			
	105'3"	25.2	24.5	6.1	0.124	0.20			

Cont. Table 5.2

No.	Depth	Iron %	Liue%	Insol %	Sul %	Phos %	X-ray	Scanning Electron Microscope	Electron Microprobe Analysis
A106							Calcite and little siderite, chamosite, SiO <sub>2</sub> and hematite		
107	106'3"	20.5	20.8	17.2	0.302	0.52	Majority is calcite and little SiO <sub>2</sub> , hematite and trace of chlorite and chamosite.	Ooliths of Fe with very little Si and Al. Matrix is mainly Ca. P occurs as very little fine grains in the matrix and in the ooliths	
	107'3"	18.2	32.8	3.3	0.020	0.18			
8							Majority is hematite and little SiO <sub>2</sub> and trace apatite.		
A116	108'3"	21.6	24.6	9.2	0.087	0.24	Majority is calcite		
A117							Majority is calcite and little hematite and apatite		
5							Most of the sample is calcite		

From 76'3" - 108'3"  
 SiO<sub>2</sub> 7.88%  
 Less ignition 24.25%



TABLE 5.3 CHEMICAL ANALYSIS, PETROGRAPHY, SCANNING ELECTRON MICROSCOPE STUDIES AND ELECTROPROBE ANALYSIS  
FOR FRODINGHAM IRONSTONE CORE Y113

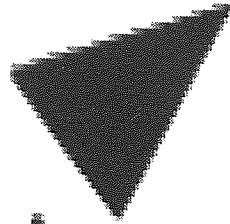
No.	Depth	Iron %	Lime%	Insol %	Sulph %	Phos %	* Petrography	Scanning Electron Microscope	Electron Microprobe Analysis
B2	59	30.9	6.2	21.9	0.082	0.35	Limonite occurs as ooliths and a fine matrix material. Ooliths are generally ellipsoidal, some are circular, some are broken, matrix in general siderite with some ferroan, calcite and shell fragments		
B3	60	30.9	6.2	21.9	0.082	0.35	Limonite ooliths, matrix is limonite and siderite in some area, and ferroan calcite in other areas. Also there are angular fragments of quartz and shell fragments of calcite.		Fe rich ooliths, fine grains of phosphorus associated with fine grains of Ca occur in the ooliths. Matrix is fine grains of Fe, Si, Al and Ca.
B11	61	32.0	6.5	21.6	0.037	0.23	Limonite ooliths, matrix is limonite and siderite in some area, and ferroan calcite in other areas. Also there are angular fragments of quartz and shell fragments of calcite.		
B11	62	27.3	15.8	16.0	0.041	0.20	Limonite ooliths ellipsoidal to circular in shape. Occasionally ooliths have cores of subangular quartz grains or calcite fragment. Variable size patches of Limonite matrix, most of the matrix is ferroan calcite		
B11	63	27.4	9.1	25.7	0.073	0.36	Limonite ooliths ellipsoidal to circular in shape. Occasionally ooliths have cores of subangular quartz grains or calcite fragment. Variable size patches of Limonite matrix, most of the matrix is ferroan calcite		
B19	64	22.2	11.9	23.9	1.379	0.21	Limonite ooliths, matrix is limonite and siderite in some area, and ferroan calcite in other areas. Also there are angular fragments of quartz and shell fragments of calcite.		
B19	65	21.2	21.7	8.3	1.960	0.15	Chamosite ooliths; calcite shell fragments are set in the matrix of fine grained chamosite, siderite, ferroan calcite and siderite		
B23	66	18.4	15.0	29.1	1.910	0.11	Angular and subrounded of quartz grains, matrix is chamosite, shell fragment of calcite, ferroan calcite occurs in some areas in the matrix, Pyrite occurs in the matrix and in the shell fragment.		
B23	67	21.8	23.5	10.7	0.078	0.28	Limonite ooliths set in chamosite matrix, siderite grains and shell fragment in the matrix.		
B23	68	27.0	23.5	5.2	0.622	0.25	Limonite ooliths surrounded by thin rim of chamosite, matrix is siderite and chamosite, in some ooliths limonite is partially replaced by siderite.		
B23	69	31.4	12.5	8.2	0.147	0.17	Limonite ooliths surrounded by thin rim of chamosite, matrix is siderite and chamosite, in some ooliths limonite is partially replaced by siderite.		
B39	70	37.6	7.8	7.2	0.655	0.39	Limonite ooliths set in chamosite matrix, siderite grains and shell fragment in the matrix.		
B39	71	34.0	14.0	6.3	0.073	0.32	Limonite ooliths surrounded by thin rim of chamosite, matrix is siderite and chamosite, in some ooliths limonite is partially replaced by siderite.		Fe rich ooliths with Si; some ooliths replaced partially by Ca; fine grains of P associated with Ca in the ooliths. Matrix is mainly Ca.

Cont. Table 5.3

No.	Depth	Iron %	Lime%	Insol %	Sulph %	Phos %	* Petrography	Scanning Electron Microscope	Electron Microprobe Analysis
	72	30.1	19.6	4.6	0.03	0.35	Limonite oololiths surrounded by thin rim of chamosite, small patches of siderite, shell fragment of calcite occurs in the matrix. Matrix is siderite with variable amount of ferroan calcite.	Oololiths of Fe associated with little of Si, Al, P and Ca, angular grains of Ca; matrix is mainly S with fine particles of Si.	Oololith of Fe associated with Ca. Anhedral grains of P occur in the matrix, matrix is Si associated with Fe, Al and Ca
	73	27.1	23.4	4.0	0.101	0.40			
	74	39.8	8.1	6.5	0.467	0.60			
B54									
B55	75	35.7	13.7	4.4	4.188	0.40			
	76	18.3	31.4	5.7	0.458	0.20			Oololiths of Fe with Si and Al; fine P associated with Ca occur in the oololiths. Matrix is mainly Ca.
B63							Limonite oololiths, shell fragment of calcite set in a matrix of chamosite with ferroan calcite.		
B69	77	22.7	24.8	9.1	0.115	0.50			
	78	15.7	35.9	3.3	0.101	0.20	Limonite oololiths, shell fragment of calcite set in calcite matrix.		
	79	24.7	23.4	5.7	0.033	0.35		Oololiths of Fe associated with fine particles of Si, Al, P and Ca. Matrix is Ca.	
	80	22.2	26.2	6.0	0.092				
B81									
	81	17.9	29.4	6.0	0.033	0.18			Fe oololiths associated with Si and Al. Matrix is mainly Ca. Small particles of P are associated with Ca.
B98							Limonite oololiths, shell fragment of calcite set in the matrix of ferroan calcite and siderite; fine grained chamosite occurs as matrix in small areas, limonite oololiths occasionally replaced partially by chamosite		
	82	16.8	30.9	6.0	0.033	0.15			Oololiths rich Fe with little fine grains of Si, P and Ca. Matrix is Ca.
B100									
	84	24.1	25.8	6.0	0.042	1.11	Limonite oololiths, quartz grains, shell fragments of calcite set in the matrix of ferroan calcite with patches of chamosite		
B105									
	85	23.5	18.4	14.6	0.096	0.56		Oololiths of Fe associated with Si, Al, P and Ca. Matrix is mainly Ca.	

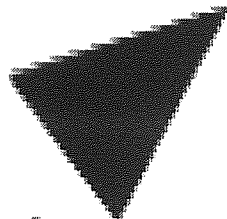


Figure 5.6 Typical Reference  
Photograph of Split Core Y 112  
(Frodingham Ironstone)



Aston University

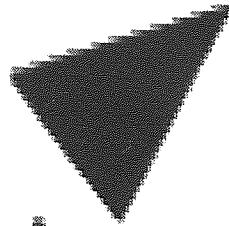
Illustration removed for copyright restrictions



Aston University

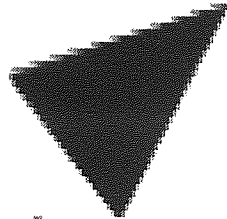
Illustration removed for copyright restrictions

Figure 5.7 Typical Reference  
Photograph of Split Core Y 113  
(Frodingham Ironstone)



Aston University

Illustration removed for copyright restrictions



Aston University

Illustration removed for copyright restrictions



LITHOLOGY OF APPLEBY FRODINGHAM CORES

A Geologist (S. James) was working on the structure of oolites in ironstones. Consequently he was very interested in the two cores from Yarborough which are the subject of a part of the present work. Consequently he prepared a complete lithology of the two cores and these are included here in order to locate the samples described in section 5.5.2.

FIGURE 5.8 shows the descriptive lithology of core Y 112 from 76' 3" - 109' depth

76'

Commence  
Core

TYPE

76' 3"



Chamosite lenses  
Black/dark grey  
material forms  
thin lenses.

Rust brown limonite oolites are  
ellipsoidal, 0.2mm across, with  
polished surfaces. These are set in  
a limonite matrix. Black to dark  
grey fine grained material forms  
thin, splitting and coalescing  
lenses. Occasional irregular lcm  
greenish grey chamosite lenses  
are present at the base. Shell  
fragments occur throughout.

C



Grey material  
forms thicker  
lenses in place  
of black.



Bivalve shells  
infilled with  
fine grey  
material.

77'

Light grey  
material disappears.  
fine dark red  
brown material  
forms thin, short  
lenses.

Black/dark grey  
material returns.

Black/dark grey material forms  
thicker lenses than before and  
contains a number of limonite  
oolites.

C

78'



Burrow infilled  
with fine grey  
material.

Black material decreases in frequency,  
the rock has a more reddish tinge.  
Oolites become discoidal, 0.5mm across.  
The limonite matrix becomes reddish  
brown and between black lenses is dark  
brown. Black lenses in frequency and  
are 3/4cm thick.

C



Lense of grey fine  
grained material.

Black lenses increase in frequency, but  
are considerably thinner, shorter and  
often curved.

79'



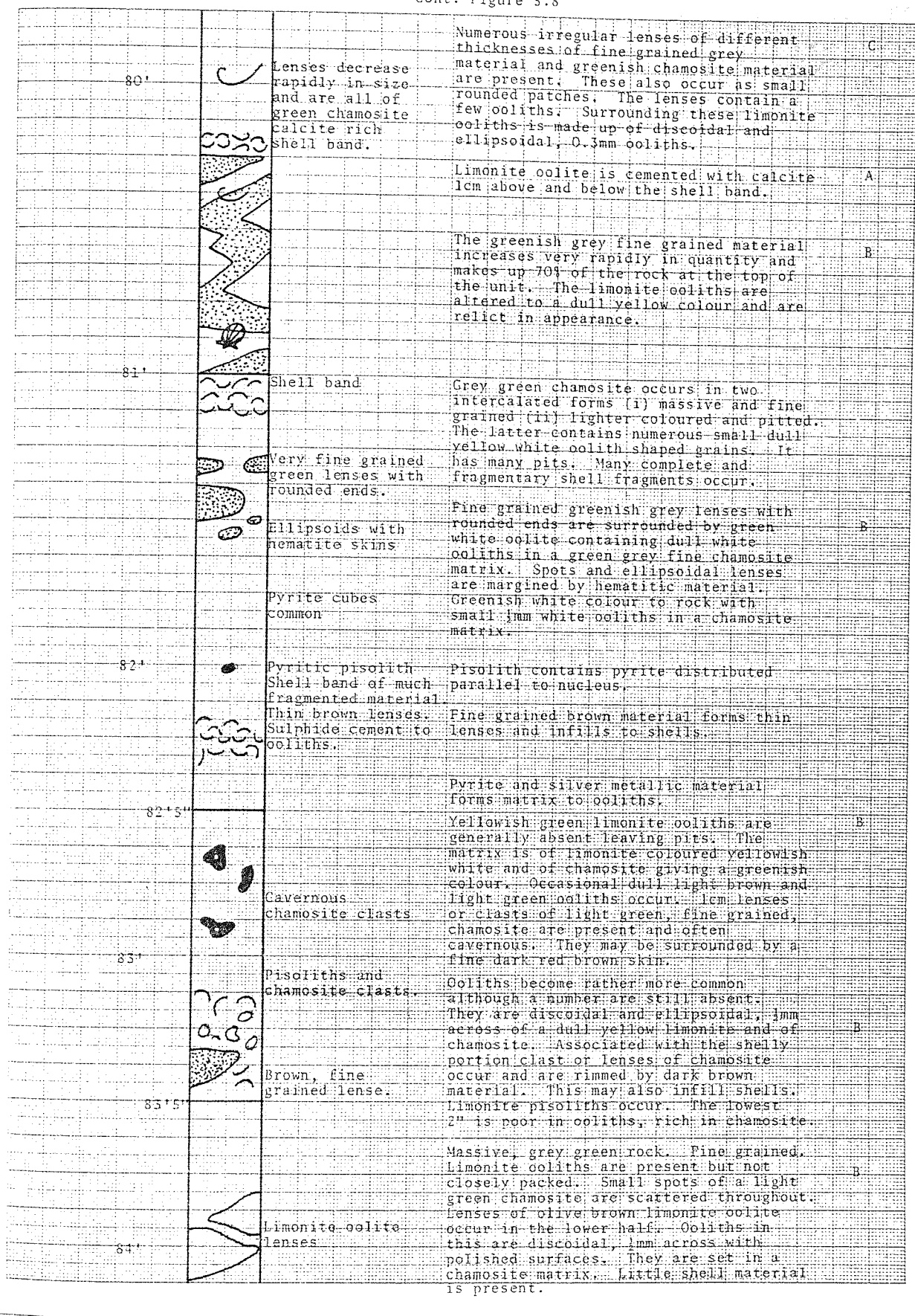
Black/dark grey  
material disappears,  
red takes over as  
thin lenses.

Lense of grey, fine  
grained material.

Red material  
disappears, grey  
and grey green  
takes over.

Red fine grained material appears  
forming short and long thin lenses  
in all orientations and a matrix to  
the oolites. The lenses contain a  
few oolites. Small patches of fine  
grey material occur.

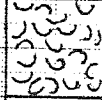
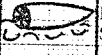
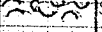
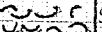

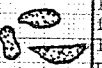
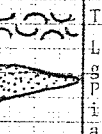
Cont. Figure 5.8



Cont. Figure 5.8

84'5 1/2"		Shell band with limonite oolite clast	Greenish grey shell rich material. The matrix is of fine grained greenish grey chamosite. Occasional limonite ooliths occur. Limonite oolite clasts, with	
84'5 1/2"		Grey green fine grained lense.	limonite matrix. Ochre coloured oolite. Ooliths are ellipsoidal, 0.3mm across, with slightly tarnished surfaces. These are set in a matrix of limonite, chamosite and calcite.	C
		Pisoliths 3/4cm across with limonite rims and a chamosite core.	Limonite and chamosite pisoliths occur. Lenses of dark grey green chamosite and a fine red brown material occur. Chamosite post dates this as it is often molded around it.	
85'		Inclined shell band of complete and fragmentary bivalves.	Rock is altered. Large areas of a fine, dull limonite occur and contain 'relict' ooliths. Chamosite rich areas are dark grey green. Calcite matrix areas are pitted, the ooliths being generally altered.	
		Small, fine grained, grey patches.	Yellowish olive brown limonite oolite. Ooliths are ellipsoidal and discoidal with polished surfaces, 1mm across. The upper portion has limonite matrix, the lower portion a dominantly calcite cement. Chamosite is occasionally a matrix mineral. Small fine grained grey patches occur.	A
85'10 1/2"		Clast of calcite matrix oolite with pisoliths but lacking ooliths.	Lower 3" olive brown limonite oolite. Ooliths are ellipsoidal, 1mm across, with polished surfaces. Chamosite ooliths also occur. They are set in a chamosite matrix.	
86'		Shell band	Brownish grey limonite oolite. Ooliths are discoidal, 1mm across, with polished surfaces. The matrix is generally of calcite but in places near the top is of chamosite. Three bands of fragmentary shell material occur with coarsely crystalline interstitial calcite. Occasional limonite ooliths are present in this.	D
86'4 1/2"		Shell band		
86'10 1/2"		Lense of dark black/brown material with areas of chamosite and few ooliths.	Olive green limonite. Ooliths are ellipsoidal, 0.3mm across, and dull yellow brown in colour. They are set in a chamosite matrix. Irregular patches of black, fine grained, reflective material - perhaps hematite - occur.	C
87'			Olive brown limonite ooliths are discoidal and ellipsoidal, 1mm across and dull yellow brown in colour. These are in a chamosite matrix. Small 1cm patches of chamosite only occur.	C
87'1 1/2"		Shell rich band.	Brownish grey limestone of shell material and coarse calcite. Polished 0.3mm ooliths.	
87'3 1/2"		Black/dark grey, thin irregular, markings approximately parallel to bedding and as small lenses finish.	Olive brown limonite oolite. Ooliths are ellipsoidal and discoidal, 0.3-0.5mm across, with a dull brown colour. In places the ooliths have a relict appearance. They are set in a matrix of chamosite and limonite. Immediately above the shell rich band at the base the ooliths are set in a calcite matrix. Fine grey green material often occurs within bivalve shells. Thin, black to dark grey, fine grained markings parallel to bedding and forming small lenses are restricted to the upper portion. Shell material is distributed throughout the unit, but is concentrated in a band at the base.	D
88'				

Cont. Figure 5.8

89'		Shell rich band	
		Black markings commence	Olive green limonite oolite. Ooliths are discoidal and ellipsoidal, 0.3mm across, and are dull yellowish brown. In places the ooliths are relict. They are set in a matrix of dark green chamosite. Thin lenses of a black fine grained material mark the rock. It also forms short, 0.75cm thick, lenses. Shell fragments are the only indication of fauna.
90'		Belemnite Shell band	Olive brown limonite oolite. Ooliths are ellipsoidal and discoidal, 0.3-0.5mm across and may be either dull or polished. The matrix is generally of chamosite but where shell bands occur calcite also becomes a matrix mineral. Complete shells and fragmentary shell material occur throughout the unit and in addition are concentrated as shell bands. Coarse calcite is interstitial to these bands, has a greenish colour and contains a few ooliths. Thin lenses of fine grey material occur.
		Shell band	
		Shell band	
		Shell band	
90'9"			
91'		Thin, black, fine grained lenses, parallel to bedding containing few ooliths. Some pyrite.	Olive green limonite oolite. Ooliths are 0.3mm and 0.5mm across in different areas generally a dull yellow brown in colour (relict) but occasionally brown and polished. They are set in a matrix of chamosite and limonite. Black to dark brown fine grained material is present in the upper portion of the unit and may also act as a matrix material. It may also form long, thin, lenses, lenses thicker than 0.5cm and as irregular patches. The material contains a few ooliths. Where several dark lenses occur together interstitial oolite is of relict limonite ooliths in a limonite matrix. Little shell material occurs.
92'			
92'10"		Thin shell band Lense of fine grey material Polished limonite ooliths in a calcite matrix	
93'			


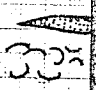



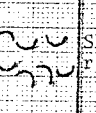
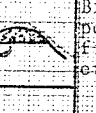
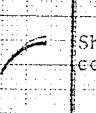




Cont. Figure 5.8

97'1"		Chamosite matrix. Shell fragments	Brownish grey limonite oolite. Oolites are discoidal, 0.3mm across, with polished surfaces. In the upper portion they are occasionally ellipsoidal. The upper portion has an entirely chamosite matrix, the lower calcite. The upper portion contains numerous patches of dull yellow limonite, and a number of polished, black, rounded clasts also occur. Shell fragments are generally coated in chamosite. In the lower portion contains numerous complete bivalves. Shell rich areas often contain coarse calcite between shells with few oolites. Patches of chamosite are also associated.	C
98'98'0 1/2		Calcite matrix. Shelly matrix. Fine grey material forming lense. Shell material. Fine grey material forming lense.		
98'5"		Irregular chamosite lenses. Chamosite lense	Brownish olive green limonite oolite. Oolites are ellipsoidal, 0.2mm, polished but often dull. Chamosite matrix. Fine, grey, irregular lenses.	C
98'10"		Lense of fine grey material.	Light brown limonite oolite. Oolites are ellipsoidal, 0.2mm across, with polished surfaces. They are set in a grey green chamosite matrix. A number of bivalves occur, and are large, together with fragments. Where these occur a calcite matrix is often present. Some areas of calcite have few oolites and are grey.	C
99'		Lense of fine grey material. Shell rich band. Lense of fine grey material. Lense of fine grey material.	Greenish grey limonite oolite. Oolites are ellipsoidal, 0.2mm across, and are dull brown in colour. They are often relict and in places of a fine black to dark grey material. The oolites are set in a grey green chamosite and limonite matrix in the upper portion which gives way to calcite matrix at 99'3". Here the oolites become 1mm across. Where shell rich bands occur coarse calcite and chamosite spots also occur.	C
99'6"		Shell rich base. Lense of fine grey material.		
99'10"		Clast of limonite oolite. Fine grey lense.	Olive brown coarse grained material. Poorly rounded 1.3mm grains are coated with a red brown material and set in a chamosite and limonite matrix. Ochrous patches of limonite occur. Shelly. Top 1" has ellipsoidal 1-1.5mm oolites, dull. Chamosite, limonite matrix.	D
100'		Lense of fine grey material. Lense of fine grey material. Lense of fine grey material. Lense of fine grey material.	Olive brown limonite oolite. Oolites are ellipsoidal, 0.15mm across, dull brown or relict. They are set in a grey green chamosite matrix.	C
		Lense of fine grey material	Olive green limonite oolite with rust brown markings. Oolites are ellipsoidal, 0.2-0.3mm across and are dull brown; frequently relict. They are set in a greyish green matrix. The matrix is limonitic with a dull yellow ochre colour in places. Patches in the upper portion contain polished oolites. Rust brown markings occur throughout. These are irregular in shape and due to the presence of polished red brown oolites and red brown shell fragments. The matrix to these is commonly limonite and occasionally chamosite. Shell fragments are scattered throughout and form two distinct inclined bands at the base. Between and immediately above these small patches of hematite and a black fine grained material occur. Micropisolites of limonite 2.3mm across and polished oolites also occur.	C
		Inclined shell band	Where shell fragments are close together coarse interstitial calcite occurs.	D
		Inclined shell band		

Cont. Figure 5.8

101'6"		Lense of fine grey material. Shell band. Chamosite rich bands. Chamosite rich bands.	Olive grey green limonite oolite. Oolites are discoidal and ellipsoidal 0.3mm across, with polished surfaces. The matrix is grey green chamosite except in the shell rich bands where calcite is also a matrix mineral. Chamosite forms lamellae where few oolites occur. These are 1-2mm thick and occur between the two grey lenses. Shell fragments are present throughout and form two shell rich bands. An overturned bivalve has trapped fine grey material below it.	C
102'		Lense of fine grey material. Shell rich band with occasional bivalves in life position.		
102'3"		Numerous burrow, generally infilled with red brown material occasionally with fine grey.	Olive green, reddish tinged, limonite oolite. Oolites are ellipsoidal, 0.2-0.3mm across, with polished surfaces. They are set in a matrix of greenish grey chamosite. Numerous burrows are present, infilled with either fine grey material or more commonly with a reddish brown material. This is composed of a red fine grained matrix containing many oolites. Two thirds of the way down, dark markings with a black/dark grey fine material making them up, occur subparallel to bedding but are discontinuous. The lowest 1" contains much dark green chamosite with sparse oolites. No fauna.	C
103'		Black markings commence. Black markings finish.		
103'3"		Chamosite rich base.	Olive brown limonite oolite. Oolites are ellipsoidal, 0.2-0.3mm across dull brown and often yellow ochre in colour. The latter have a relict appearance. They are set in a dull grey green chamosite matrix which is limonitic in places. Dark red brown hematitic markings occur in the central portion. The lower 2" is more coarse grained oolites being 1mm across and occasionally polished. Pyrite is present in trace quantities throughout. Shell fragments are not uncommon, and a shell fragment rich band occurs.	C
104'		Shell fragment rich band.		
104'5"		Coarse lower 2". Bivalve in life position with fine grey material within it.	Olive brown limonite oolite. Oolites are 0.1-0.2mm across, discoidal and polished. They are set in a dominantly calcite matrix, with some chamosite.	A
104'7"			Red brown limonite oolite. Oolites are difficult to distinguish from the matrix. They are 0.1-0.2mm across; some are brown or red brown and polished; others dull brown. The matrix is of limonite, chamosite and a fine red brown material. The limonite and red brown material forms small areas with very few oolites. Occasional small patches of a fine grey material occur. Fauna is present but not common.	C
105'		Shell fragment coated red.		
105'3"				



Cont. Figure 5.8

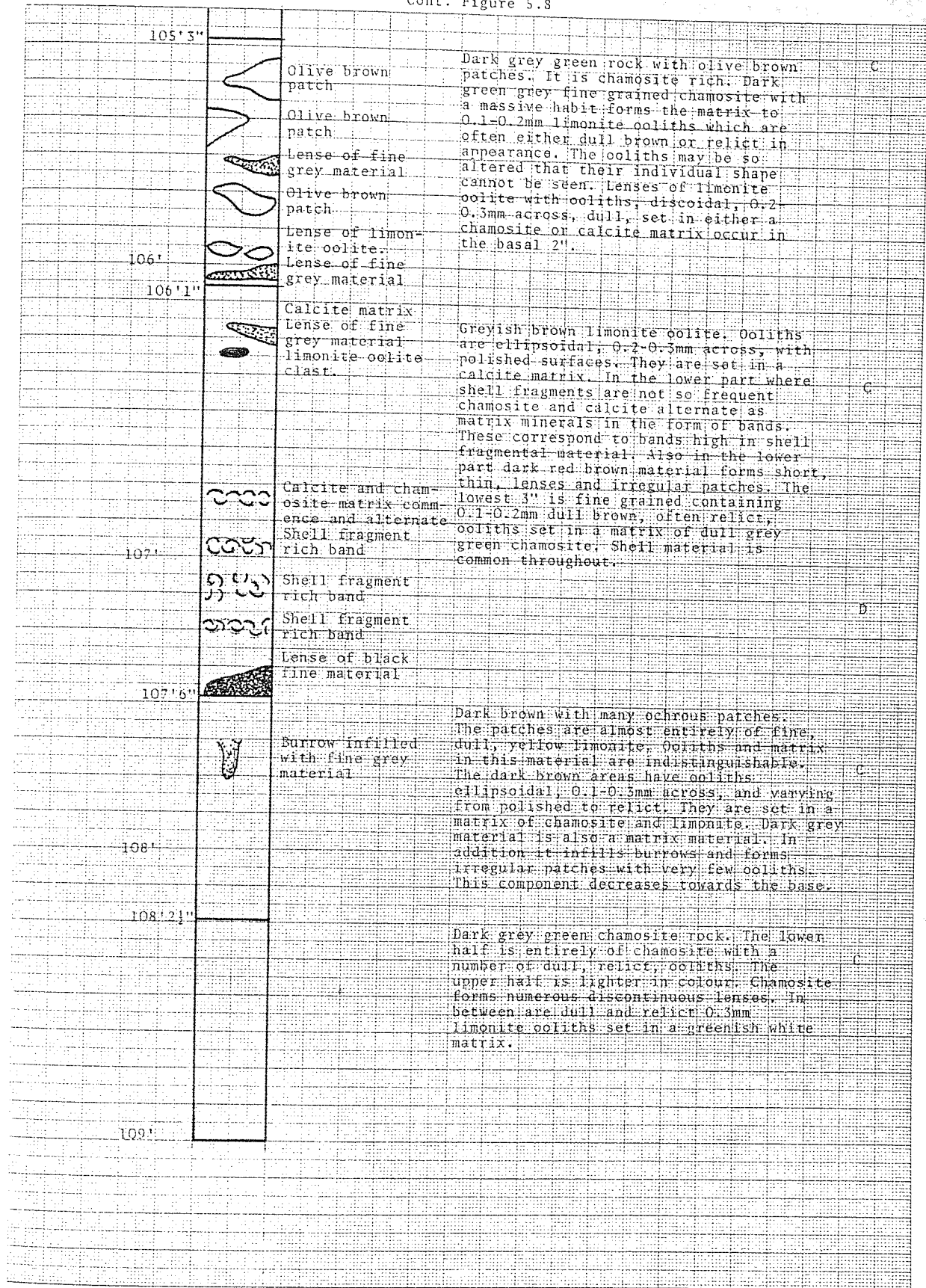
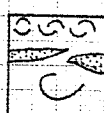
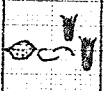

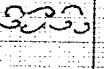
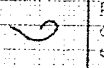
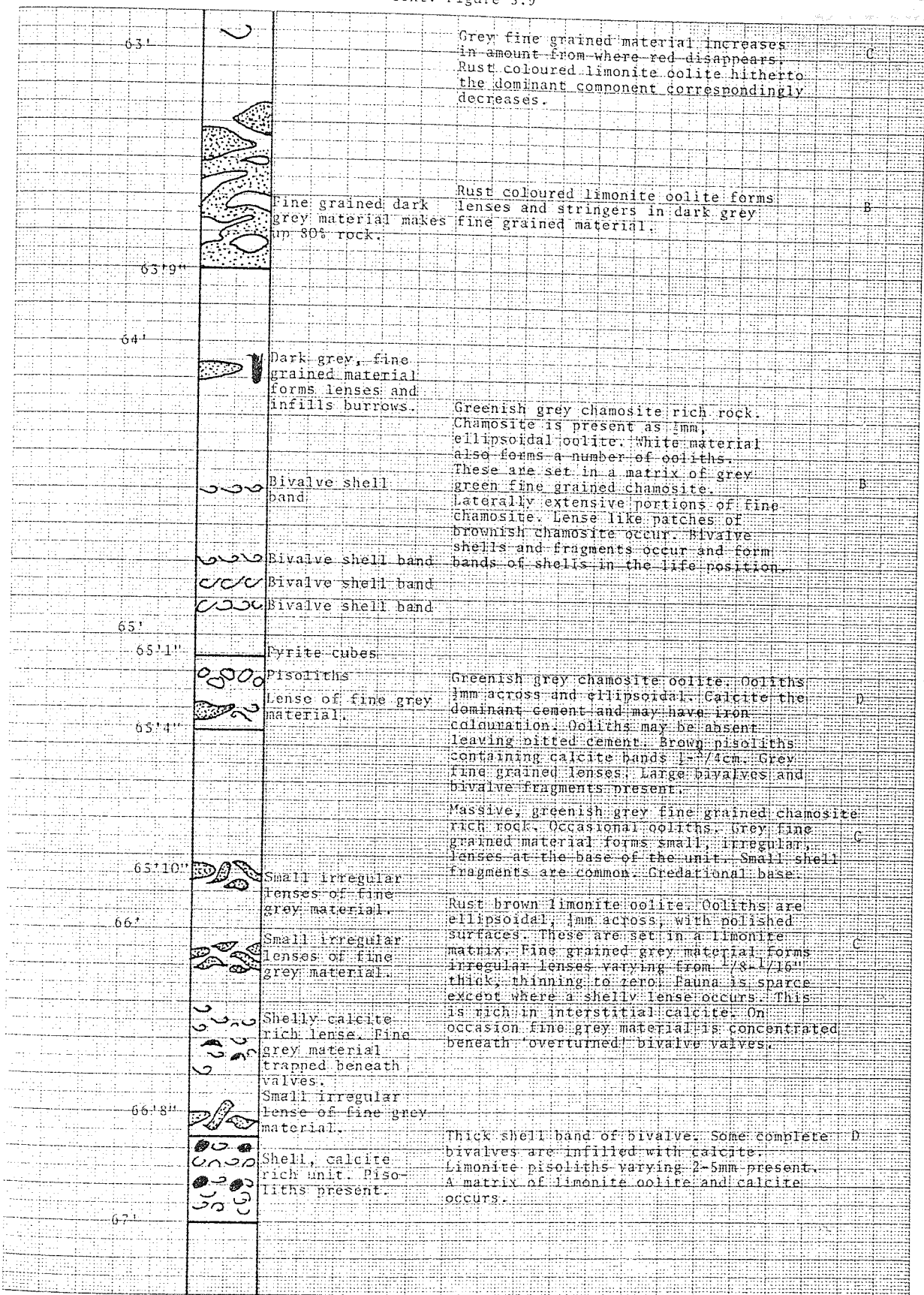


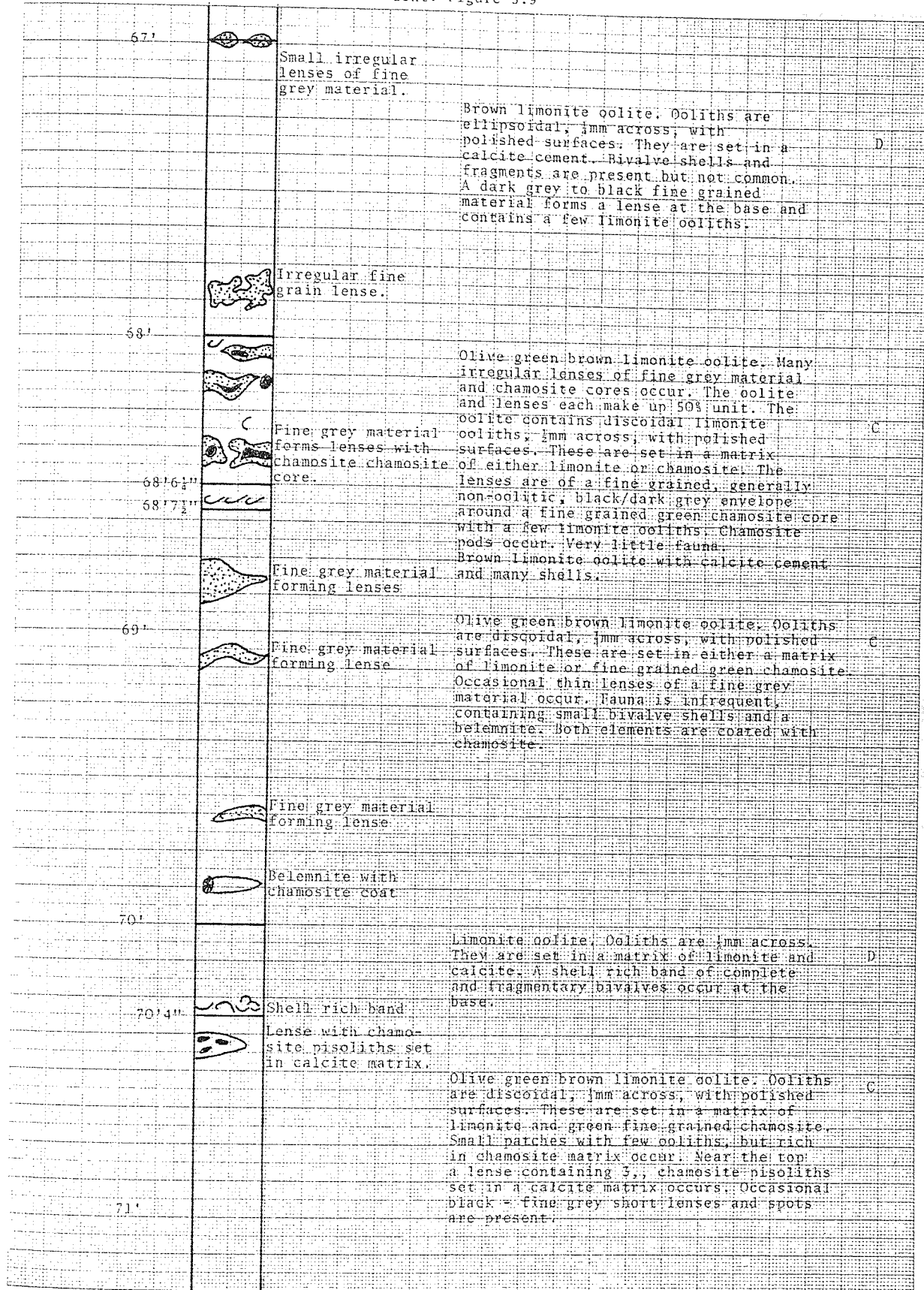
FIGURE 5.9 LITHOLOGY OF FRODINGHAM IRONSTONE CORE Y 113

				TYPE
50'		Shell band Lenses of fine grey material	Rust brown limonite oolite. Oolites ellipsoidal, 1mm across, polished surfaces. Closely packed in limonite cement. Grey fine grained material forms lenses of variable size and shape. Fragments thin bivalve shells common.	
		Black markings become prominent.	Black to dark grey markings appear with branching and coalescing form. Oolite texture in places. Colour perhaps due to oolites being of hematite.	
60'		Burrows infilled with fine grey material. Thin band of small bivalve and rhynchonellid valves	Bivalve shells and fragments become infrequent. Dark markings become fine grained, hardly any oolites present. Material infills burrows. Occasional black oolite patches.	C
		Black markings disappear, replaced by red.	Very small (1") lenses of grey fine grained material occur. Bivalve fragments more common.	
61'		Small lense of black oolites, 1"	Red markings replace black. Red material fine grained, polished. Tends to have sheet form - but not flat - with branching and coalescing form. Variable thickness. Coats shell fragments and where occurs forms matrix to oolites instead of limonite. Markings irregularly distributed.	
		Shell band, broken bivalves, 1"		
			Occasional complete bivalves, not apparently in life position, with which are associated small patches of black oolites (hematite). More common bivalve fragments.	C
62'		Red markings disappear, replaced by grey fine material.	Red material disappears and is replaced by grey, fine grained, material. Has branching and coalescing form, but may also form discreet lenses. Occasional large bivalves.	C

Cont. Figure 5.9

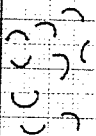

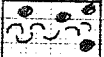


Cont. Figure 5.9





Cont. Figure 5.9

71'			
71'7"			Limestone. Calcite is present as broken shell fragments and coarsely crystalline calcite. Interstitially, limonite oolite occurs. Oolites are discoidal, 1mm across and set in a calcite matrix. D
71'11" 72'			Olive brown limonite oolite. Oolites are discoidal, 1mm across, with polished surfaces. The matrix is generally limonite but a chamosite matrix is not uncommon. A calcite rich lense occurs at the base, rich in shell fragments with limonite oolites in a calcite matrix. Occasional black, fine grained, markings are present. C
72'7"		Calcite lense rich in shell fragments	
72'11" 73'		Red brown clasts Shell rich band	Limonite oolite. Oolites are discoidal, 1mm across, with polished surfaces. They are set in a calcite matrix. The upper third is rich in calcite, as shells and coarse calcite. Hematite streak. Clasts 1-1cm across with red brown colour in this position also. D
74'			Olive brown, massive, limonite rich rock. Oolite texture is poorly developed. Oolites are poorly formed, varying from discoidal to ellipsoidal to relict. The majority are of limonite, but some are of chamosite. Chamosite forms thin, irregular, veinlets within the rock. Occasional reddish brown clasts 2-3mm across occur. The matrix is generally limonite but some chamosite occurs. Bivalve fragments occur throughout but are not frequent. C
74'10" 75'		Bivalve shell band	

Cont. Figure 5.9

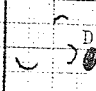


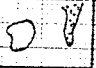
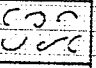
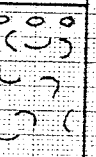

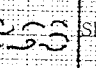
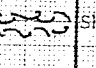
75'			Calcite rich rock. Calcite occurs as coarsely crystalline material around numerous shell fragments. This tends to form three bands between which limonite oolite occur. The oolites are ellipsoidal, 0.3mm across and set in a limonite and calcite matrix.	D
		Bivalve shell band		D
75'9"		Bivalve shell band		D
76'			Overall vertical colour change from olive brown at top to greyish green at base as chamosite content of matrix increases.	C
			Limonite oolite. Oolites are ellipsoidal and discoidal, 0.3-0.5mm across, with polished surfaces. They are set in a matrix of chamosite and limonite.	C
77'		Limonite oolite clasts		
		Thin lense of fine grey material	Matrix becomes entirely chamosite, oolites decrease in quantity. Clasts of fine greyish green chamosite with a few limonite oolites occur and are of a variety of sizes, maximum being 4cm.	C
77'31"		Shell band	The base is shell and calcite rich with bivalves in a variety of orientations. In between are a few limonite oolites in a chamosite matrix. Chamosite occurs as occasional clasts, matrix material, infill and shell coatings.	D
77'71"		Shell band	Limestone. Large, small and fragmentary bivalves occur in a variety of orientations. A fine grained grey green material acts as matrix and contains a few ellipsoidal, 1mm oolites.	
		Shell fragment band, rich in calcite	Bioclastic rich limonite oolite. Oolites are discoidal, varying from 1-1mm across with polished surfaces. These are set in a dominantly limonite matrix, although chamosite is the dominant matrix mineral in places. Greenish grey fine grained chamosite forms small irregular lenses and coats shells. Bivalves, complete and fragmentary are scattered throughout the rock and at the base there is a shell rich band which coarsely crystalline calcite is associated.	D
78'		Irregular chamosite lense	Olive brown limonite oolite. Oolites vary in size from 0.3-0.5mm and are ellipsoidal and discoidal in shape. These are set in a chamosite and limonite matrix. Occasional dark green, irregular, lenses of chamosite occur. These contain very few oolites.	C
78'71"		Thin lense of fine grey material	Limestone. Many shells and shell fragments are set in a matrix of coarsely crystalline calcite.	D
78'91"		Limonite coats to shells	Discoidal, 1mm. limonite oolites.	
79'				

Cont. Figure 5.9

79'		Burrows infilled with fine grey material.	Brownish grey limonite oolite. Oolites are discoidal, varying in size from 0.2-0.6mm with polished surfaces. These are set in a matrix of chamosite and calcite in approximately equal amounts. A shell band with interstitial grey green chamosite occurs at the base.	C
79' 2 1/2"		Shell fragment band	Olive brown limonite oolite. Oolites are discoidal, 0.2-0.5mm across, with polished surfaces. These are set in a fine grey green chamosite and limonite matrix. Small, thin, irregular lenses of a fine grey material occur. Shell fragments are scattered throughout.	C
79' 8"			Greyish brown limonite oolite. Oolites are brown, discoidal, 0.2-0.5mm across. They are set in a greenish grey chamosite matrix. Numerous fragmentary bivalve shells occur.	C
80'			Grey, shelly limestone. Coarsely crystalline calcite occurs in the interstices. Occasional limonite oolites and patches of light greyish green chamosite occur.	D
80' 7"		Gastropod. Limonite oolite clast.	Olive brown coarse grained limonite oolite. Roughly spherical to ovate limonite oolites 1-1.5mm across. These are set in a chamosite, calcite and limonite matrix. Fine grained grey material also acts as a matrix.	C
80' 10"		Dark grey/black fine grained material forming thin lenses.	Olive green limonite oolite. Oolites are ellipsoidal, 0.2-0.4mm across. They are set in a generally chamosite matrix, with patches of limonite matrix. Thin lenses of a black dark grey material run sub-parallel to bedding and containing a little white mica. They are laterally discontinuous.	C
81'				
81' 3"		Limonite oolite clasts.	Brownish grey limonite oolite. Oolites are discoidal, 0.5mm across, with polished surfaces. In the upper half these are set in a calcite matrix. Patches of limonite matrix occur throughout. Occasional clasts of limonite oolite or limonite oolites in a limonite matrix occur in the upper portion. Numerous complete and fragments of bivalves are present throughout.	D
82'		A Chamosite and calcite in equal amounts as matrix minerals		
		B Belemnite. Small red-brown clasts		
		C Chamosite clasts		
		Complete, large bivalve, infilled with calcite. Overturned	CD coloured red	
83'				



Cont. Figure 5.9

83'		Matrix entirely chamosite	Calcite disappears as a matrix mineral, chamosite the dominant matrix mineral.	C
83' 3"		Patches of red oolites	Shell material is rare in the lower 3".	
		Clasts or lenses of chamosite. Burrow infilled with fine grey material	Greyish green limonite oolite. Oolites are ellipsoidal, 1mm across and have polished surfaces. They are set in a fine grained greyish green chamosite matrix. Near the top 1-2cm lenses or clasts of a fine grey green chamosite occur. There are occasional, thin, fine grained grey lenses. The same material infills a burrow. Shell fragments occur spasmodically.	C
84'		Burrows infilled with either fine grey material or limonite	Olive brown limonite oolite. Oolites are ellipsoidal; 0.5-0.5mm across with polished surfaces. They are set in a limonite matrix; chamosite may also occur as a matrix mineral. Burrows are infilled with either fine grey material containing a few oolites or limonite with rather more. Thin lenses of a fine grained grey material occur.	C
84' 5 1/2"		Bivalve	Limestone. Many shells or shell fragments in a matrix of coarse calcite in places limonite oolite occurs with oolites set in a calcite and chamosite.	D
84' 7 1/2"		Thick stringers of fine chamosite	Chamosite rich limonite oolite. The chamosite is green and fine grained occurring as splitting and coalescing lenses, 1cm thick at maximum. In between limonite oolite of oolites set in chamosite occurs. Oolites 1mm. There is no fauna.	C
85'		Limonite pisoliths	Greyish brown, bioclastic rich, limonite oolite. Oolites are ellipsoidal, 0.5mm across. They are often altered to a dull yellow coloured material. These are set in a chamosite and calcite matrix. The chamosite component decreases towards the base. Occasional limonite pisoliths occur near the top. Occasional limonite clasts 2cm across occur in the lower portion.	D
85' 8"		Limonite clast	shells and fragments are very common, coarse calcite common between these.	
85' 9"			Olive brown limonite oolite. Oolites ellipsoidal, 1mm. Chamosite matrix and veinlets	
86'		Shell rich band	Brownish grey limonite oolite. Oolites are ellipsoidal, 0.5-0.5mm across, with polished surfaces. A number are altered to a dull yellow material. They are set in a matrix dominantly of chamosite but with subordinate calcite. The rock is rich in bioclastic material throughout and has two layers particularly rich in shells and shell fragments.	
86' 5"		Shell rich band		
		Band rich in chamosite cement	Red brown limonite oolite. Oolites are ellipsoidal, 0.3mm across, with polished surfaces. These are set in a limonite cement. A band rich in chamosite as a matrix occurs. There are abundant thin red marks. These are irregular branching and coalescing bands of a fine red material. It may also act as matrix.	C
86' 11"				
87'				

Cont. Figure 5.9

87'		Large bivalves in life position with chamosite banked up in them	Olive brown limonite oolite. Oolites are ellipsoidal; 0.3-0.5mm across, with polished surfaces. Shell material of the same grade is coated in limonite. The matrix is dominantly of chamosite with subordinate occasional limonite. Fine grained, dark green, chamosite containing very few oolites infills burrows and is banked up against, and in, bivalve shells in their 'life' position.	C
87'7"		Burrows infilled with fine chamosite		
		Shell concentration with chamosite in a bivalve 'cup'		
88'		Lense of fine grey material	Brownish grey limonite oolite. Oolites are ellipsoidal; 1mm across with polished surfaces. These are set in a matrix dominantly composed of calcite with patches in which the matrix is chamosite. The rock is high in bioclastic components; complete and fragments of shell material occurring throughout. There are four bands where shell material is concentrated. Occasional shells in the 'life' position contain chamosite.	C
		Shell concentration		
		Shell concentration		
		Shell concentration		
88'8"		Lense of fine grey material	Olive brown limonite oolite. Oolites are ellipsoidal; 0.3mm across. They are often altered to a dull yellow material. The matrix is of a greenish grey chamosite and occasional limonite. Patches of a fine red brown material occur as blebs and stringers. Little shell material.	C
89'		Chamosite in bivalve 'cup'	Brownish grey limonite oolite. Oolites are discoidal; 0.3mm across. They are set in a calcite matrix. Chamosite occurs in 'life' position bivalve shells. Small red brown lenses occur.	D
89'5"		Lense of fine grey material with irregular top, flat base	Yellowish brown limonite oolite. Oolites are ellipsoidal; 0.5mm across with polished surfaces. The matrix is of chamosite. Very thin red brown lines mark the rock. A fine grey lense with a flat base and irregular top occurs.	C
89'6 1/2"		Fine grey material forming rounded lense	Brownish grey limonite oolite. Oolites are 0.3mm across; ellipsoidal, with polished surfaces. The matrix is of calcite and chamosite. Fragmentary shell material occurs.	
89'9 1/2"		Limonite pisoliths	Olive brown limonite oolite. Oolites are ellipsoidal; 0.2mm across and often altered to a dull yellow brown. Set in a limonite and chamosite matrix. Lenses of chamosite poor in oolites occur. A shell band occurs centrally. Large limonite pisoliths with chamosite cores and oolites tangential to the nuclei occur above this.	C
90'		Shell band		
90'2 1/4"		Lense of fine grey material		
90'2"		TERMINATE CORE	Massive, fine greenish grey chamosite. This has an irregular top. The rock contains oolites which are widely separated, and often altered to a dull yellow material.	
91'				

The overall mineral assemblage remains constant, comprising calcite, siderite, limonite, chamosite. Calcite forms the dominant matrix mineral in a number of instances, and is also present as numerous shell fragments. Siderite occurs in dark grey lenses of siderite mudstone. Limonite forms ooliths and may be common in the matrix. Chamosite occurs in a massive form as chamosite mudstone, and as a dominant matrix mineral.

The detailed logs have been simplified into four lithologies as shown below:

- A - limonite oolite with a dominantly calcite matrix,
- B - chamosite mudstone,
- C - limonite oolite having a dominantly chamosite matrix,
- D - Bioclastic limestone.

The petrography of lithological types A, B, C and D is described below:

#### Lithological type A

Limonite ooliths, pisoliths of limonite, chamosite and siderite, several different intraclast types, and shell fragments are set more or less randomly in a cement of low-iron ferroan calcite. All coated with a thin film of chamosite.

Examination of the arrangement of the component allochemical grains shows that the larger shell fragments are oriented with their long axes parallel to bedding. Where ooliths are

in contact with such fragments they lie with their major axis parallel to the shell.

#### Lithological type B

This lithological type is a chamositic mudstone. Siderite, limonite and calcite also occur but are very subordinate. The overall colour of the lithological type is a dull greyish green. Allochemical grains are rather less common than in the lithological types A, but comprise ooliths, pisoliths and complete and fragmentary bivalve shells.

Two oolith types have been recognised:

- 1 - Limonite ooliths. These are characterised by a dull yellow colour.
- 2 - Chamosite ooliths. These ooliths are coloured greyish green.

The limonite ooliths are far more abundant than the chamosite ooliths. The shell material present is represented by barids consisting of shell fragments and complete, but disarticulated, shells. The dominant matrix mineral is fine grained chamosite. In addition to this, siderite - a dull white mineral - and pyrite also participate in the matrix. Where siderite acts as a matrix mineral, the rock is coloured a greyer shade of green and is much harder. In addition, to its matrix occurrence, siderite also forms dark grey lenses.

#### Lithological type C

Limonite ooliths, three different interclast types, shell fragments, diagenetic siderite grains, and detrital quartz

grains are set in a fine grained matrix of chamosite and limonite. Low iron ferroan calcite forms small patches of matrix. Oolites may be oriented with their major axis parallel to bedding, but more commonly are not oriented with any preferred direction. Large shell fragments are oriented with their long axis parallel to bedding. Chamosite mud often forms thin discontinuous lenses in which quartz and siderite detrital grains may be common, but all other allochemical grains are absent. In other areas this distribution is reversed; quartz and siderite are uncommon whilst the other allochems are common.

#### Lithological type D

This is a bioclastic limestone, composed predominantly of complete and fragmentary bivalve shells set in a coarsely crystalline calcite matrix. The colour of this lithology varies from grey-brown to grey. A small proportion of the component allochems are limonite oolites. These are discoidal in shape with polished surfaces and a grain size variation of 300 to 500  $\mu\text{m}$ . In some instances the surfaces of the shell material may be coated with limonite. Lenses of dark grey siderite mudstone are occasionally present.

The most important points for Davies and Dixie (36) classification of the Frodingham ironstone and the present classification are described below in Table 5.4.

TABLE 5.4

Principal  
Types  
According  
to Davies  
and Dixie

	<u>Detritus</u>	<u>Matrix</u>
A	Limonite-chamosite ooliths (closely packed), calcite shells - all coated with a thin film of chamosite.	Dominantly granular siderite
B	-	Rhomb-shaped crystals of siderite distributed between linearly arranged flats of chamosite.
C	Limonite-chamosite ooliths, and calcite shells partly replaced by chamosite	Very fine-grained, of chamosite and siderite some quartz grains at times
D	Calcite shells, limonite-chamosite ooliths	Coarse crystalline calcite (some siderite and chamosite)
<u>Present Classification</u>		
A	Limonite ooliths, pisoliths of limonite, chamosite and siderite. Calcite shell fragments. All coated with a thin film of chamosite	Low-iron ferroan calcite
B	Chamosite and limonite ooliths. Calcite shells	Fine grained of chamosite, siderite and pyrite occur also in the matrix. Siderite lenses
C	Chamosite limonite ooliths, calcite shell	Fine grained chamosite and limonite and low iron ferroan calcite forms small patches of matrix. Thin discontinuous lenses mainly quartz. Siderite grains occasionally present.
D	Calcite shells, limonite ooliths. Shell material coated by limonite	Coarsely crystalline calcite. Lense of siderite mudstone are occasionally present.

### 5.5.3 The Chemistry of the Ironstone

Since 1958 many boreholes have been drilled close to and to the east of the B.S.C. steel plants in Scunthorpe. The opencast and underground working ironstone core recovery from these boreholes is frequently between 95 and 100 percent.

As for the B.S.C. operations in South Lincolnshire, each foot (30 cm) of the ironstone cores, after drying was analysed for total iron, lime, silica, and sulphur; silica was determined as a perchloric acid insoluble. In this work the chemical analysis for phosphorus was completed and added to the above list (see Tables 5.2 and 5.3).

An average chemical analysis for the total thickness of the ironstone is as follows:

	Core: Y 112	Y 133
Fe	25.6%	24.6%
Lime	20.5%	21.2%
SiO <sub>2</sub>	7.88%	8.58%
Sulphur	0.38%	0.43%
Phosphorus	0.33%	0.32%
Loss on ignition	24.2%	24.1%

#### 5.5.3.1 Vertical chemical variation within the ironstones

In Tables 5.2 and 5.3 the chemical analyses are shown for two cores Y 112 and Y 113, the analyses being done for each foot (30 cm) from the top of the ironstone.

Vertical variation in chemistry, principally in terms of variation in Fe content and phosphorus content, are shown in Figures 5.10 and 5.11.



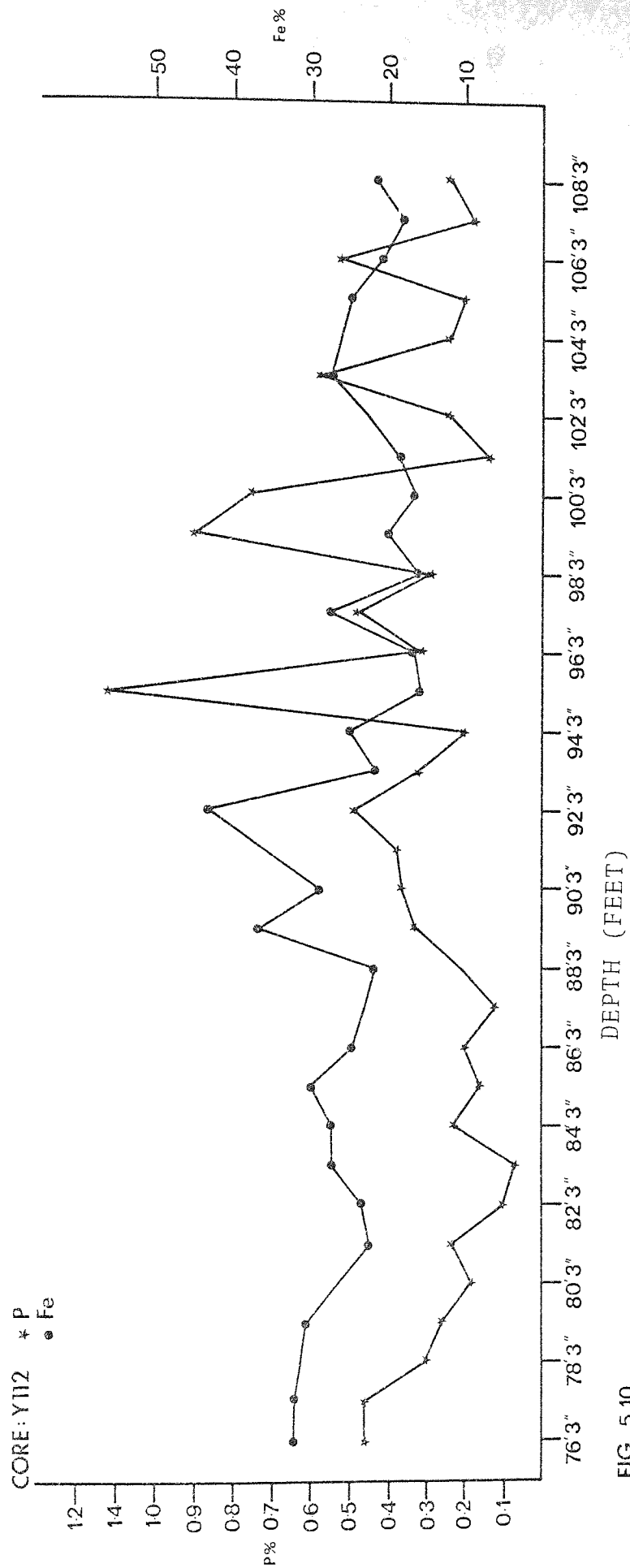


FIG. 5.10  
DISTRIBUTION OF IRON & PHOSPHORUS CONTENT IN FRODINGHAM IRONSTONE

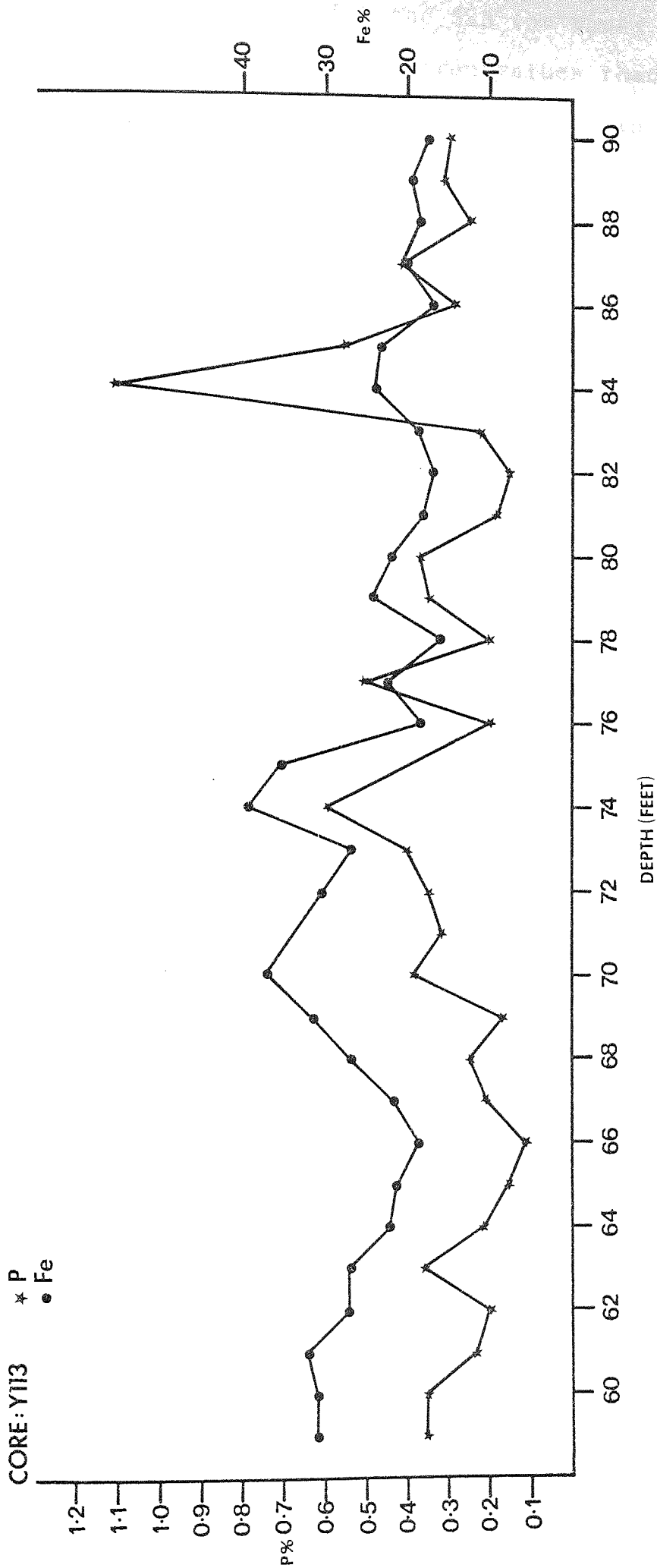


FIG. 5.11 DISTRIBUTION OF IRON & PHOSPHORUS CONTENT IN FRODINGHAM IRONSTONE

From the data shown in Tables 5.2 and 5.3 the upper type C is seen to contain generally higher iron values than the type D, and generally higher silica values occur in the upper part of the cores compared with the lower bed except where transition beds are found. Phosphorus shows a vertical variation in the two cores. It is irregular and often exhibits sharp variations.

From Table 5.2 the maximum iron content is 43.3% and the minimum 15.9%, lime content is between 36.3% and 6%, sulphur content is between 2.3% and 0.037%, phosphorus between 1.12% and 0.05%. From Table 5.3 the iron content is between 39.8% and 15.7%, lime between 35.9% and 6.2%, sulphur between 4.1% and 0.019% and phosphorus content is between 1.1% and 0.11%.

#### 5.5.4 Result of X-ray diffraction mineralogical analyses

18 Frodingham ironstone samples and two concentrated ironstone samples were analysed by X-ray diffraction methods, but the two concentrated ironstone samples were subjected to the following treatment before X-ray analysis.

- 1 - Dry sample No. B100 was ground using pestle and mortar (uniform grinding times)
- 2 - Samples were analysed for their phosphorus content
- 3 - Dry sample powdered dissolved in 20% Acetic Acid to dissolve the calcite (37). After the reaction stopped, the filtered, dried powdered samples were concentrated by

4 - high intensity magnetic separation, followed by the determination of the phosphorus content in the magnetic and non-magnetic product.

The magnetic sample product contained 4.55% P and the non-magnetic sample product contained 3.48% P. Both were analysed by X-ray diffraction.

#### X-ray analyses

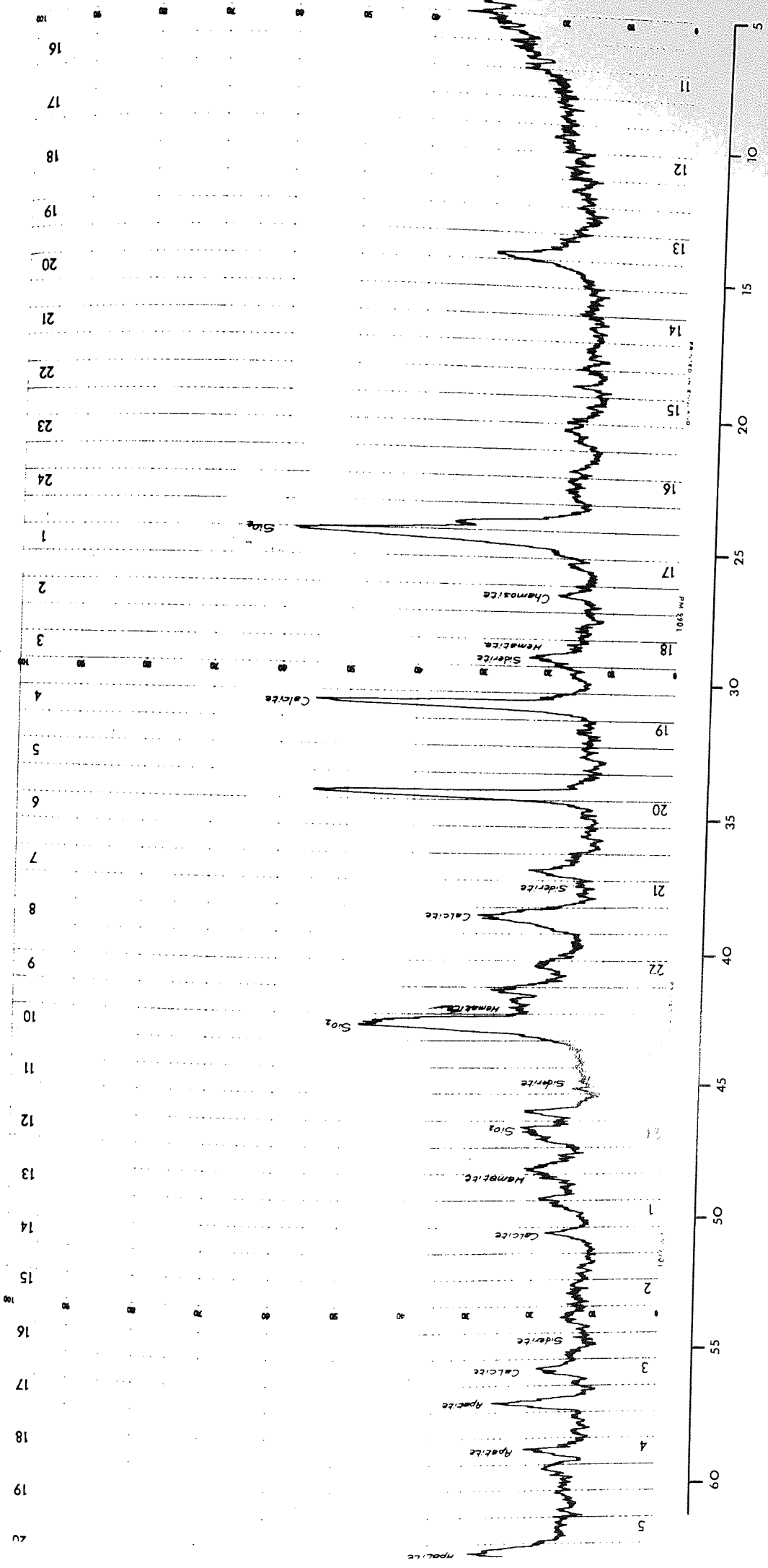
Samples were examined on a diffractometer with Fe filtered, Co radiation, and Ni filtered, Cu radiation using operating potentials of 30 Kv with a current of 30 mA, and 40 Kv with 20 mA respectively. Goniometer scans from  $3^{\circ}$  to at least  $60^{\circ}$  were run at  $1^{\circ} 2\theta$  per minute. Diffractograms were studied visually to identify as many mineral phases as possible.

Four mineral phases were identified within the two samples, Hematite, Apatite, Quartz and Clay mineral. Apatite was the major phase.

A typical X-ray diffractogram for one of the ironstone samples is shown in Figure 5.12. Seven mineral phases were identified by X-ray techniques within the ironstone.

The percentage of the phases in descending order were as follows: calcite, quartz, chamosite, hematite, siderite, apatite and chlorite.

Figure 5.12 Typical X-ray  
Diffractogram of One of  
Frodingham Ironstone Samples  
(Sample No. A 8)  
(Co K $\alpha$ )



### 5.5.5 Scanning Electron Microscopy

Examination of Frodingham ironstone by Stereoscan enables the mapping of elemental distributions for Fe, Si, P, Ca and Al by employing electron beam scan techniques. This was done for <sup>40</sup> samples from different beds throughout the body of the ore. This technique showed the structure and the grain size of the iron oxides and the gangue minerals as may be seen in the example given below.

Figure 5.13 Scanning electron micrographs of Frodingham ironstone Sample No. B 100-2 Fe, Si, Al, P and Ca, X-ray distribution map. This figure shows that the ooliths were ellipsoidal in shape; the length of the major axis varied from 100  $\mu\text{m}$  to 250  $\mu\text{m}$ . Some of the ooliths were broken. They showed a concentric banding structure but in a number of cases this could not be seen. The matrix cemented the ooliths, and there were two types of matrix material - light, poorly polished and a smaller amount of darker, better polished material.

The Fe X-ray distribution shows a high concentration of Fe in the ooliths. Fe is also shown as very fine grains dispersed throughout the matrix.

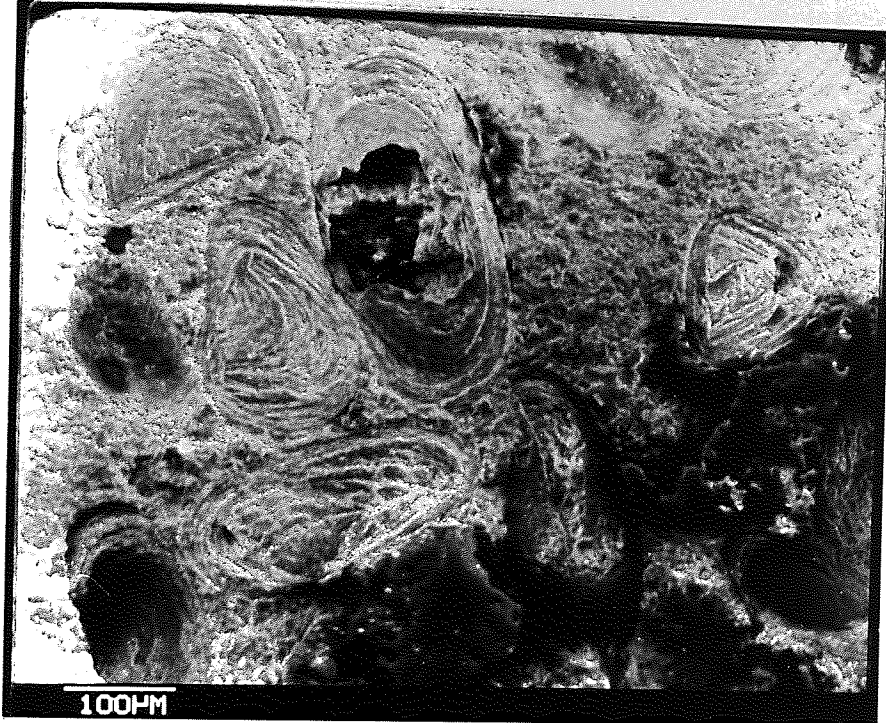
The Si occurs finely disseminated in the matrix associated with moderately high concentration of Ca and P and low concentration of Fe and Al.

Al occurs within the matrix in low concentrations associated with Si, Fe, Ca and P.

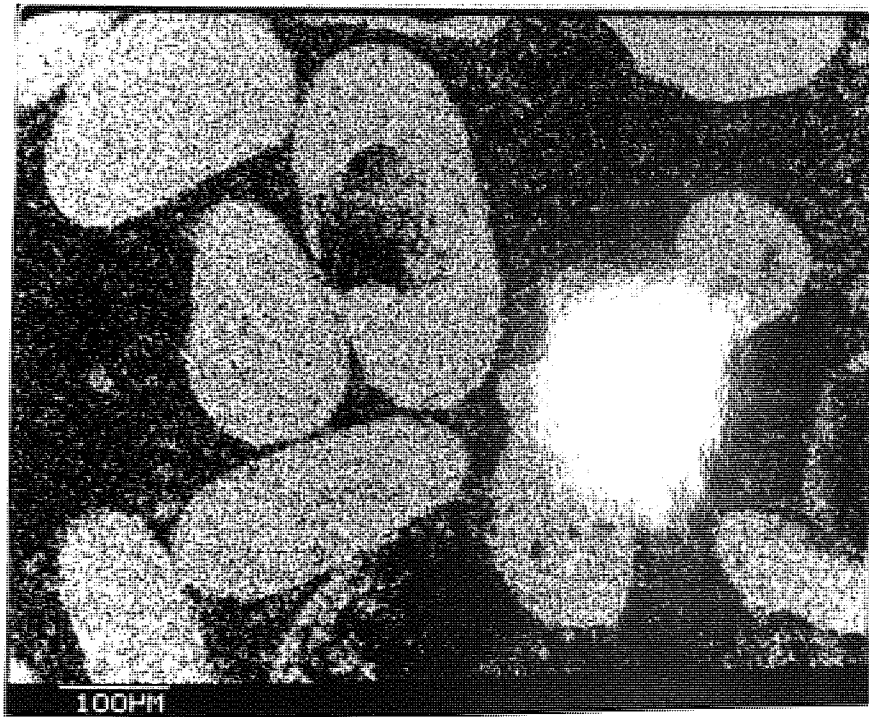


Figure 5.13 Scanning Electron  
Micrograph of Frodingham Ironstone  
Sample No. B 100-2 and X-ray  
Distribution Maps x200

- a - Scanning Electron Micrograph
- b - Iron X-ray distribution map
- c - Silicon X-ray distribution map
- d - Aluminium X-ray distribution map
- e - Phosphorus X-ray distribution map
- f - Calcium X-ray distribution map



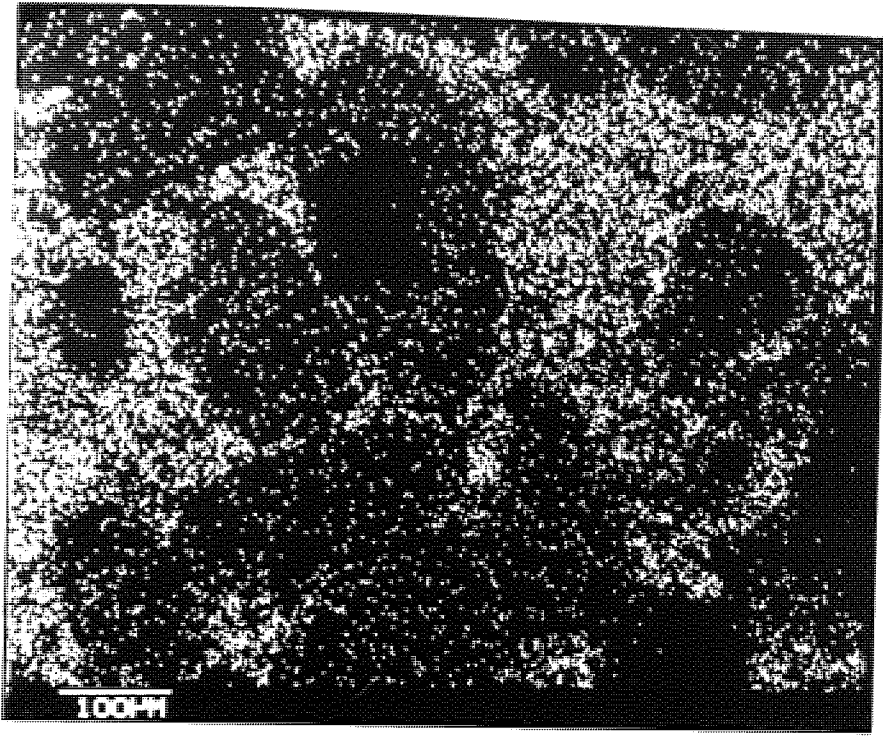
a.



Fe

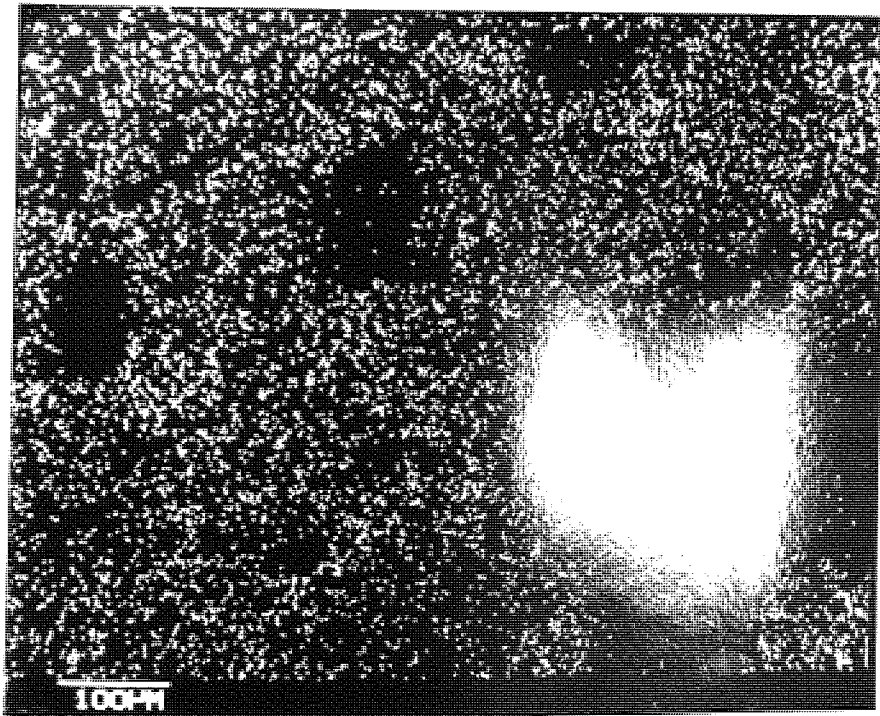
b.

Fig. 5.13



Si

c.



AL

d.

Fig. 5.13



e.



f.

Fig. 5.13



The matrix contains high concentrations of Ca associated with P and low concentration of Si, Al and Fe. In addition, there are anhedral Ca grains in some ooliths not associated with P.

P occurs in the matrix in high concentrations associated with Ca, and smaller amounts of Al, Si and Fe.

Fe is shown:-

- a - as high concentration in the ooliths. X-ray studies proved these to be hematite.
- b - as low concentration associated with Ca, P, Al and Si in the matrix. From X-ray studies this was likely to be chamosite.

Si was associated with Al, Fe, Ca and P in the matrix.

Proved from X-ray studies to be chamosite.

Ca is shown in:-

- a - large calcite crystals and also as anhedral grains in some ooliths. X-ray studies proved these to be calcite.
- b - associated with P, Al, Si and Fe in the matrix. From X-ray studies this was shown to be calcite with apatite.

P is shown in the matrix associated with Ca, Fe, Si and Al and, as previously, proved to be apatite. Matrix is apatite, chamosite and calcite intimately intergrown.

Figure 5.14: Scanning electron micrographs of Frodingham ironstone sample No. B 55, Fe, Si, Al, P, Ca and S.

Ooliths are ellipsoidal in shape; the length of the major axis varies from 225  $\mu\text{m}$  to 350  $\mu\text{m}$ . The ooliths show a concentric banding structure. The matrix cements the ooliths but there are two types of matrix materials, light and dark both well polished.

The Fe X-ray distribution map shows a high concentration of Fe in the ooliths and in most of the light coloured matrix. It also demonstrated that the concentration of Fe was independent of the concentration of Si, Al, Ca or P. The Si occurred as discrete areas of high concentration in which it was associated with Al. The areas of high Si concentration are present in the outer rim surrounding the Fe rich ooliths. There are also very low concentrations of Si dispersed in the ooliths and the matrix.

Al is shown to be associated with Si in the outer rim of the ooliths, and as very low concentrations dispersed in the ooliths and the matrix.

Ca is shown in the matrix in high concentration as rims surrounding the ooliths and as discrete large areas. It is also shown as anhedral grains in the matrix associated with P; the length of the major axis is about 20  $\mu\text{m}$  (top right).

P is shown to be associated with Ca in the matrix.

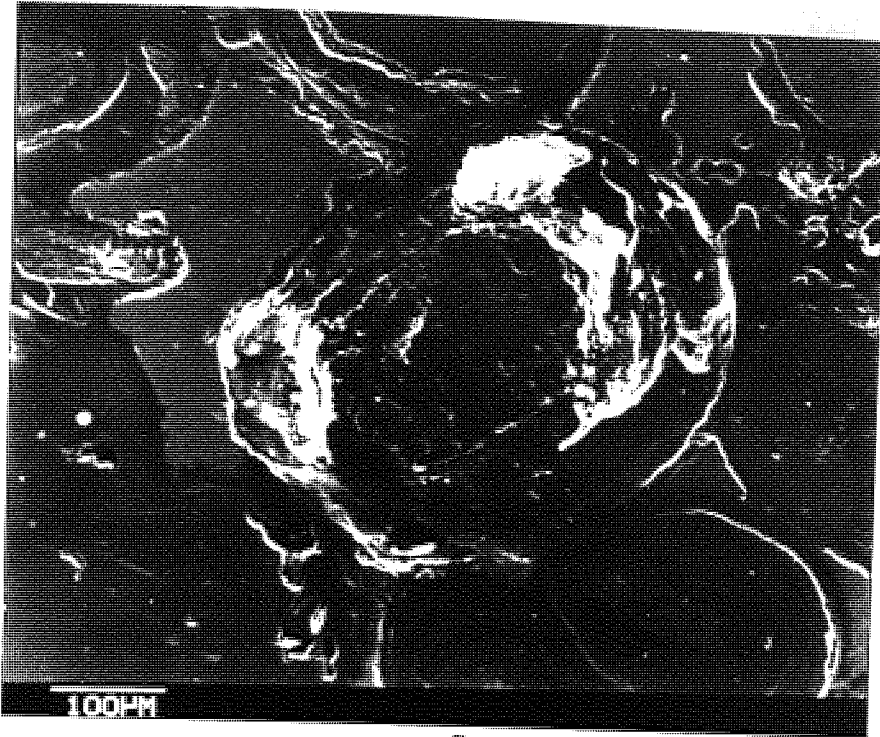
Figure 5.14 Scanning Electron  
Micrograph of Frodingham Ironstone

Sample No. B 55 and X-ray

Distribution maps x200

- a - Scanning Electron Micrograph
- b - Iron X-ray distribution map
- c - Silicon X-ray distribution map
- d - Aluminium X-ray distribution map
- e - Phosphorus X-ray distribution map
- f - Calcium X-ray distribution map
- g - Sulphur X-ray distribution map





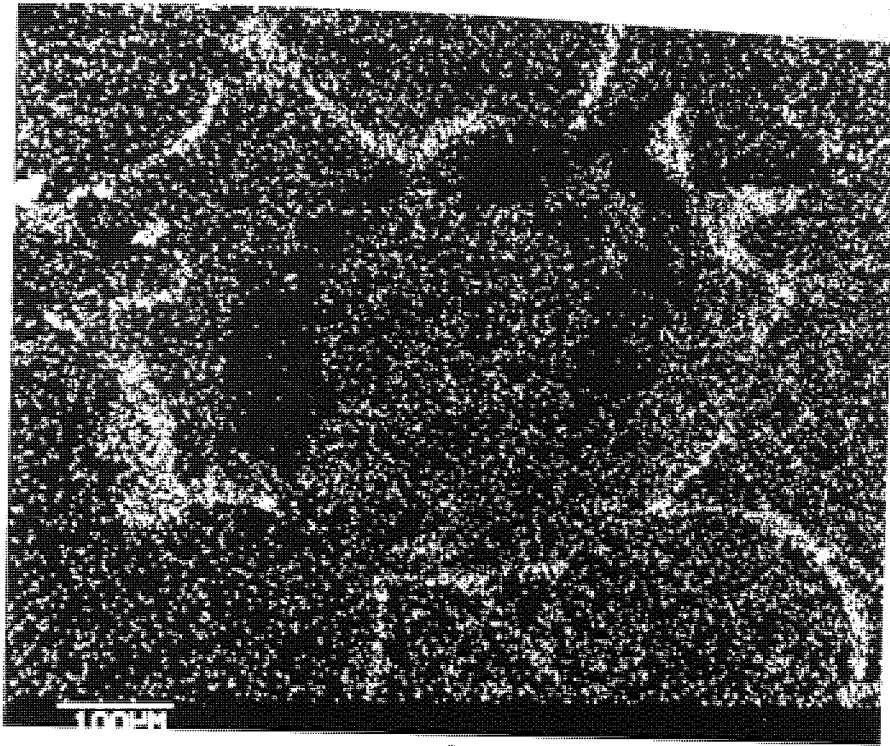
a.



Fe

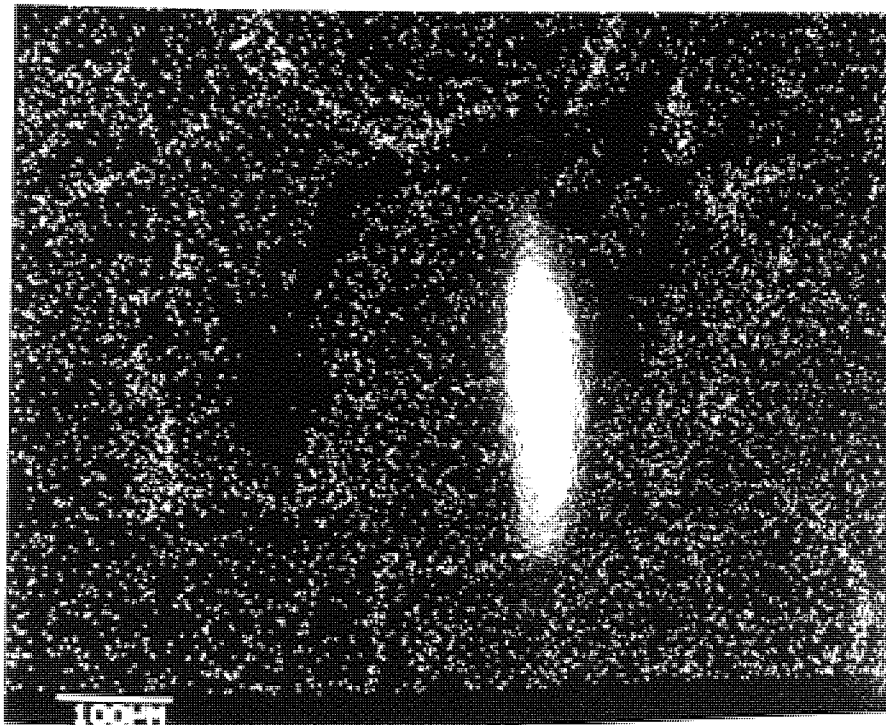
b.

Fig. 5.14



Si

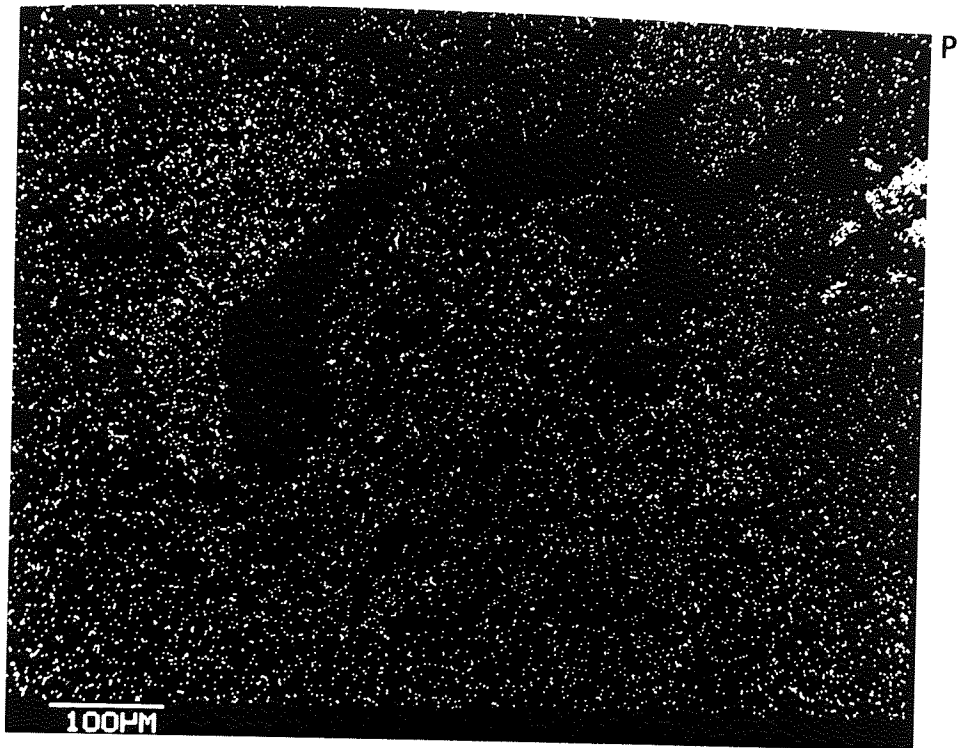
c.



AL

d.

Fig. 5.14

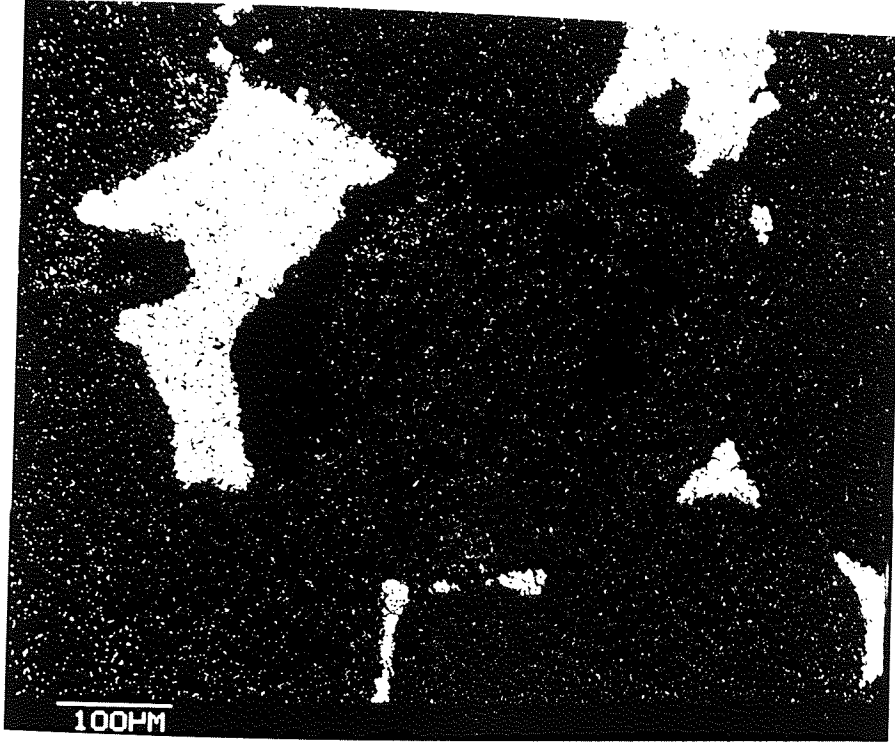


e.



f.

Fig. 5.14



g.  
Fig.5.14



S, in high concentration, is found in some parts of the matrix associated with Fe.

The Fe is shown to be in:-

- a - the matrix associated with S. Petrographic studies showed this Fe to exist as pyrite.
- b - the ooliths are rich in Fe (shown to be hematite).

Si shows in the outer rim of the ooliths associated with Al. Proved from X-ray studies to be clay minerals.

Ca shows:

- a - in the matrix - shown to be calcite
- b - as anhedral grains in the matrix associated with P. These proved to be apatite.

P is shown in the matrix as anhedral grains associated with Ca (apatite).

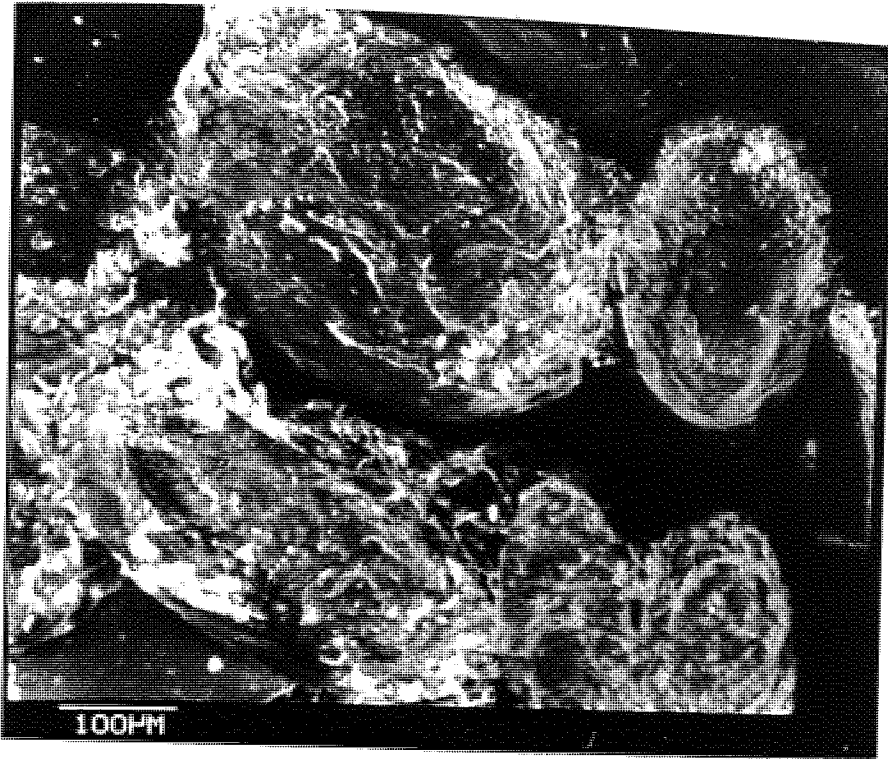
S is shown in the matrix associated with Fe (shown to be pyrite).

Figure 5.15: Scanning electron micrographs of Frodingham ironstone sample No. A.85, Fe, Si, Al, P and Ca, X-ray distribution map. The ooliths are ellipsoidal in shape; the length of the major axis varies from 180  $\mu\text{m}$  to 340  $\mu\text{m}$ . The matrix cements the ooliths. The Fe X-ray distribution map shows high concentration of Fe in the ooliths. The Fe in the matrix is seen in the right hand side of the photo-

Figure 5.15 Scanning Electron  
Micrograph of Frodingham Ironstone  
Sample No. A 85, and X-ray  
Distribution maps, x200

- a - Scanning Electron Micrograph
- b - Iron X-ray distribution map
- c - Silicon X-ray distribution map
- d - Aluminium X-ray distribution map
- e - Phosphorus X-ray distribution map
- f - Calcium X-ray distribution map



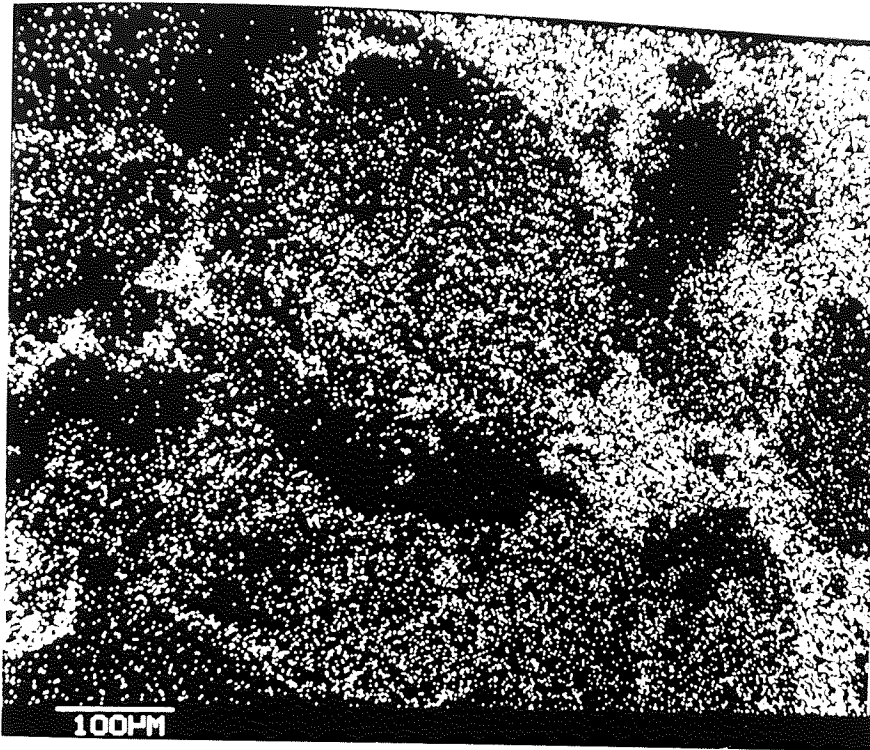


a.



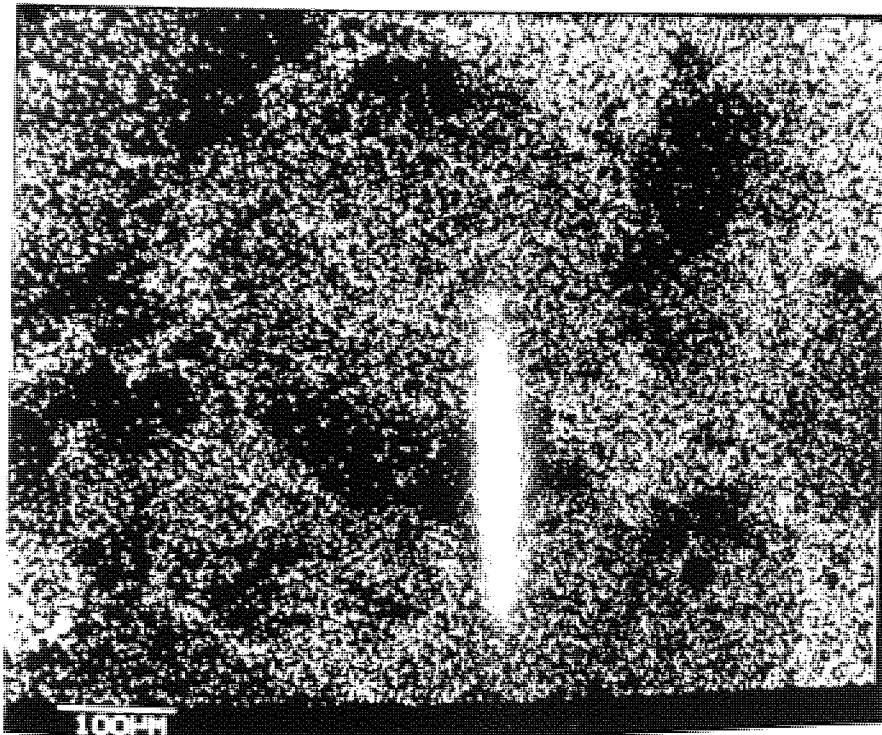
b.

Fig 5.15



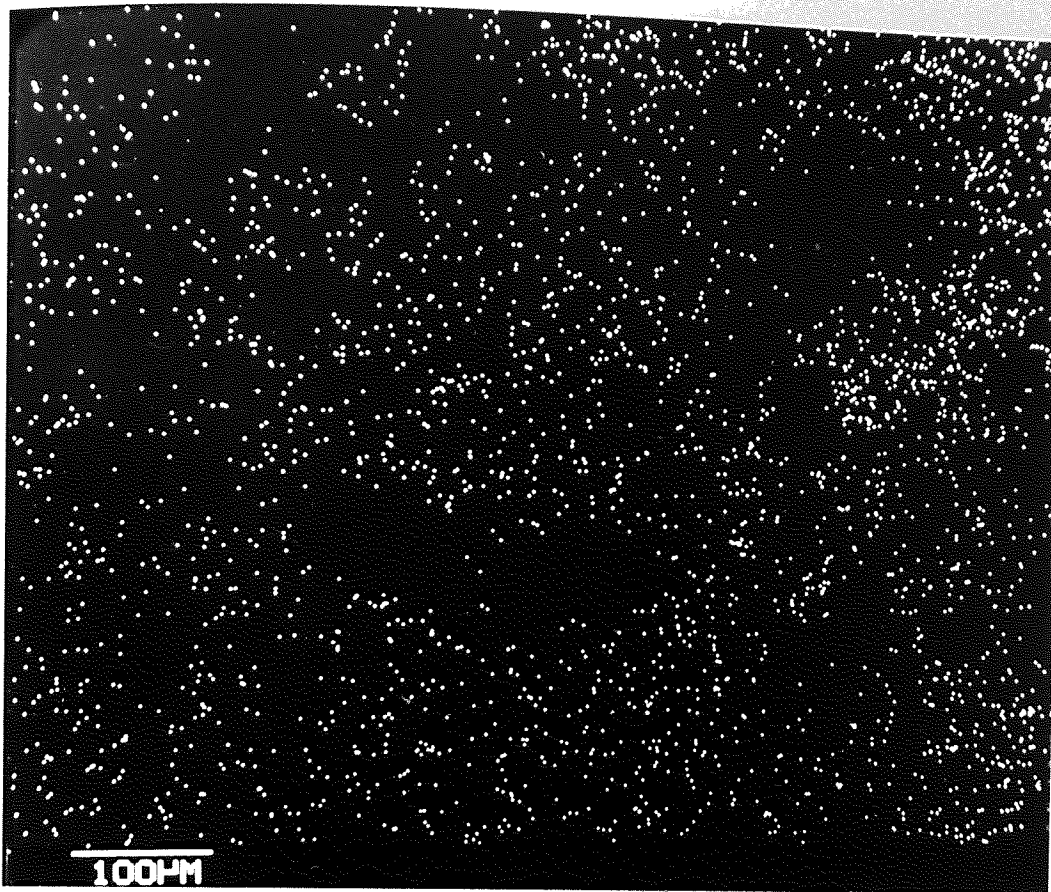
Si

c.



AL

d.  
Fig 5.15



e.



f.

Fig. 5.15

micrograph in low concentrations associated with Si, Al, Ca and very little P.

The Si occurs in the matrix and the ooliths, the higher concentration being at the right hand side of the map.

In the ooliths the Si is associated with Al and Fe. In the matrix it is associated with Al, Fe, Ca and very little P.

Al occurs in low concentration in the ooliths and the matrix.

In both cases it is associated with Si and Fe. In the matrix, the left hand side of the map shows a higher concentration of Ca than the right hand side. Ca is also associated with Fe, Si, Al and a little P in the right hand part of the matrix.

P is shown as very low concentration mainly within the matrix.

Fe is shown in:

- a - the right hand side of the matrix associated with Si, Al, Ca and little P. Shown from X-ray studies to be a mixture of siderite and chamosite.
- b - ooliths associated with Si and Al (chamosite).

Si shown in:

- a - the matrix associated with Al, Fe, Ca and little P. (chamosite).
- b - ooliths associated with Fe and Al (chamosite).



Ca is shown in:

- a - the left hand side of the matrix in high concentration (calcite).
- b - the right hand side of the matrix associated with Fe, Si, Al, and a little P (shown to be calcite)

P is shown as low concentrations dispersed in the matrix which is mainly Ca (apatite).

#### 5.5.6 Microprobe examination (Operating Conditions p. 204)

Microprobe analysis studies for the Frodingham ironstone made it possible to characterise the amount of impurities and the intergrowing of the useful and gangue components. In this work interest was in the phosphorus distribution and the study of the elements associated with the phosphorus and occurring with it in the ironstone. **The number of samples investigated using this method was 40 samples**

By comparing the result from electroprobe analyses and X-ray examination it was possible to deduce the kind of phosphate minerals present and the minerals intergrowing or associated with it.

Using Microprobe analysis techniques, the above was done for samples from different beds throughout the core and this technique showed the structure and the grain size of iron oxides and the gangue minerals and the intergrowth between them may be seen in the examples given below.

Figure 5.16: Microprobe electron micrographs of Frodingham ironstone sample No. B.100-1, Fe, Si, Al, P and Ca X-ray distribution map.

The X-ray distribution shows that the ooliths are ellipsoidal in shape; the length of the major axis varies from 224  $\mu\text{m}$  to 384  $\mu\text{m}$ . The matrix is of Ca rich material. The Fe X-ray distribution map shows a high concentration of Fe in the ooliths and is associated with small amounts of low concentration Si, Al, P and Ca except for the grain in the bottom left of the map where its concentration is much higher. In addition, there is a rim of high Fe concentration associated with Al and Si surrounding a shell fragment in the matrix (see extreme top centre and right of map).

The Si X-ray distribution shows a low concentration of Si in the ooliths associated with low concentrations of Al, P, Ca and Fe. It is also seen associated with Fe in the rim of the shell fragment in the matrix.

The Al X-ray distribution shows the same distribution as Si.

The matrix is of Ca rich materials which cement the ooliths and are not associated with the other elements.

Ca occurs as a subangular grain in an oolith (top of the micrograph). It has partially replaced the Fe in this oolith. Ca is also dispersed in low concentration in the ooliths.

In addition there is a shell fragment of high concentration of Ca in the matrix.



Figure 5.16 Microprobe Electron  
Micrographs of Frodingham Ironstone

Sample No. B 100-1, x125

- a - X-ray distribution map for Iron
- b - X-ray distribution map for Silicon
- c - X-ray distribution map for Aluminium
- d - X-ray distribution map for Phosphorus
- e - X-ray distribution map for Calcium

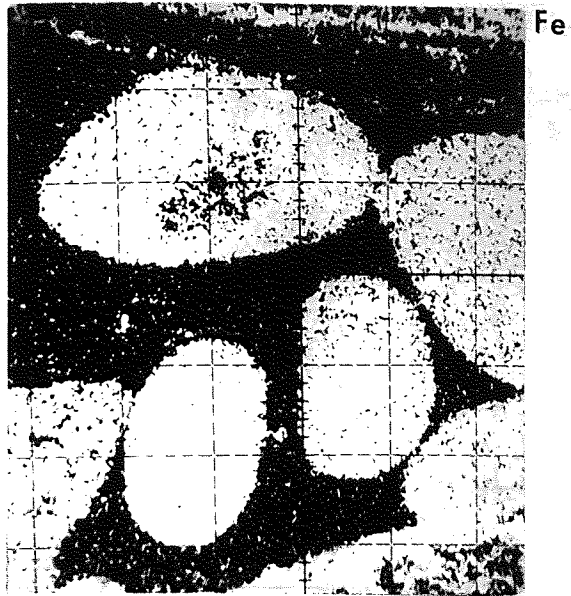
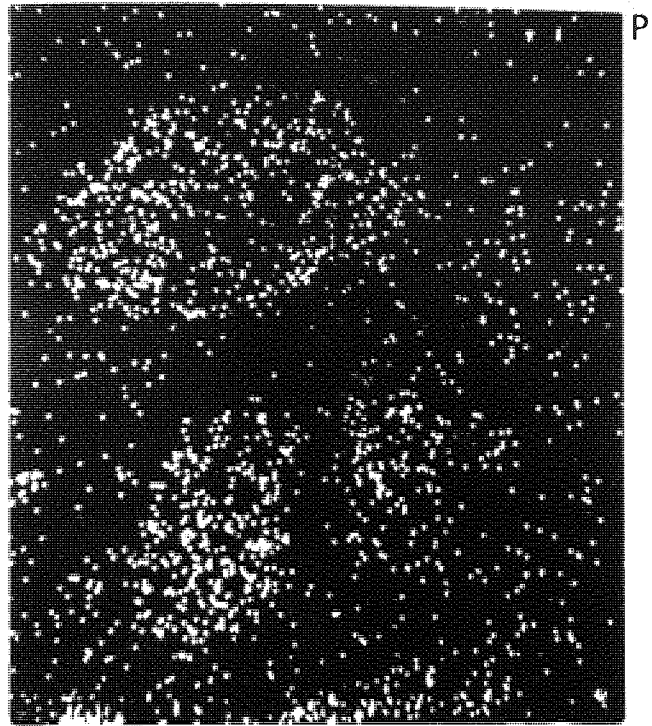
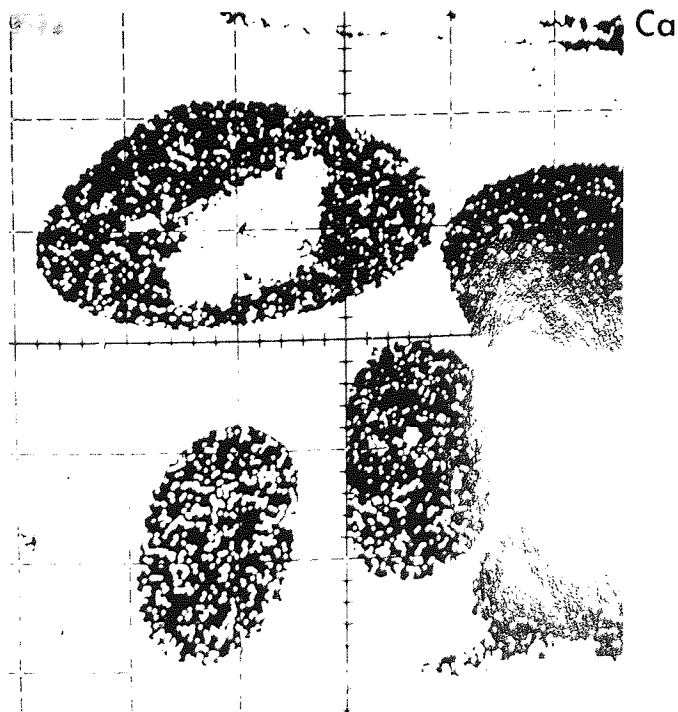


Fig. 5.16



d.



e.

Fig. 5.16

p is dispersed in the ooliths in low concentration and is associated with Al, Si, Fe and Ca.

Fe is shown in:

- a - ooliths associated with Si, Al, P and Ca. This was shown from X-ray studies to be chamosite.
- b - as a rim surrounding the shell fragment, associated with Si and Al, again shown to be chamosite.

Si shows:

- a - dispersed in the ooliths associated with Fe, Al, P and Ca, and as previously proved to be chamosite.
- b - in the matrix as fine particles and as a rim surrounding the shell fragment; in both cases associated with Al and Fe. Proved to be chamosite.

Al shows in:

- a - ooliths associated with Si, Fe, Ca and P (chamosite)
- b - the matrix associated with Si and Fe (chamosite)

Ca shows as matrix rich in Ca, and as shell fragment and also a partial replacement for Fe in an oolith; proved from X-ray studies to be calcite.

P is shown disseminated in the ooliths and associated with Fe, Si, Al and Ca. X-ray studies proved these to be apatite.

Figure 5.17: Microprobe electron micrographs of Frodingham ironstone sample No. B.9, Fe, Si, Al, P and Ca. X-ray distribution map.

In the upper part of the figure there are Fe ooliths which are ellipsoidal in shape; the length of the major axis varies from 150  $\mu\text{m}$  to 350  $\mu\text{m}$ .

Also there are two subrounded grains of Si for which the length of the major axis varies from 50  $\mu\text{m}$  to 100  $\mu\text{m}$ . In addition, there is a small amount of low concentration Si within the ooliths.

The matrix is mainly Ca in the upper part and a mixture of Fe, Si, Al and Ca in the lower part where the Fe and Si concentration appears to be higher than that of Al and Ca.

The Fe X-ray distribution shows a high concentration of Fe in the ooliths and in the lower part of the matrix, with a higher concentration in the oolith than in the matrix of the bottom half.

The Si occurs as subrounded grains in the upper part of the micrograph. Within the matrix, it occurs in high concentration in the lower parts. In addition it is seen within one oolith in low concentration (middle left hand of the micrograph).

Al is shown within the matrix in low concentration and is associated with Si, Fe and Ca. It is also shown within the ooliths in small amounts of low concentration associated with Fe and a small amount of low concentration Si.

In the upper part of the micrograph the matrix contains a high concentration of Ca which is not associated with the

Figure 5.17 Microprobe Electron  
Micrographs of Frodingham Ironstone

Sample No. B 9, x100

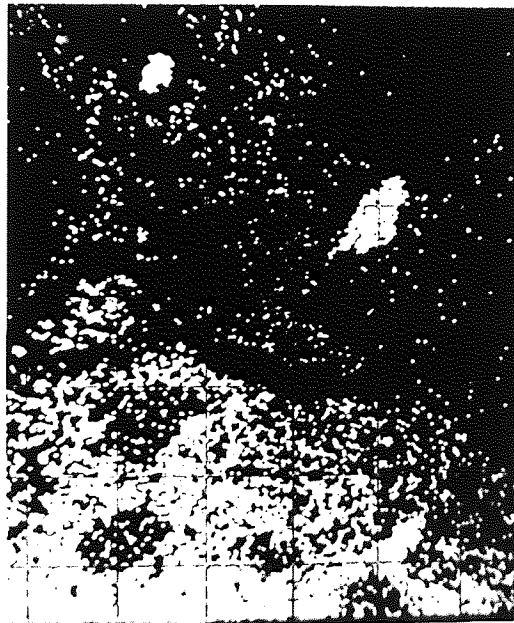
- a - X-ray distribution map for Iron
- b - X-ray distribution map for Silicon
- c - X-ray distribution map for Aluminium
- d - X-ray distribution map for Phosphorus
- e - X-ray distribution map for Calcium





Fe

a.



Si

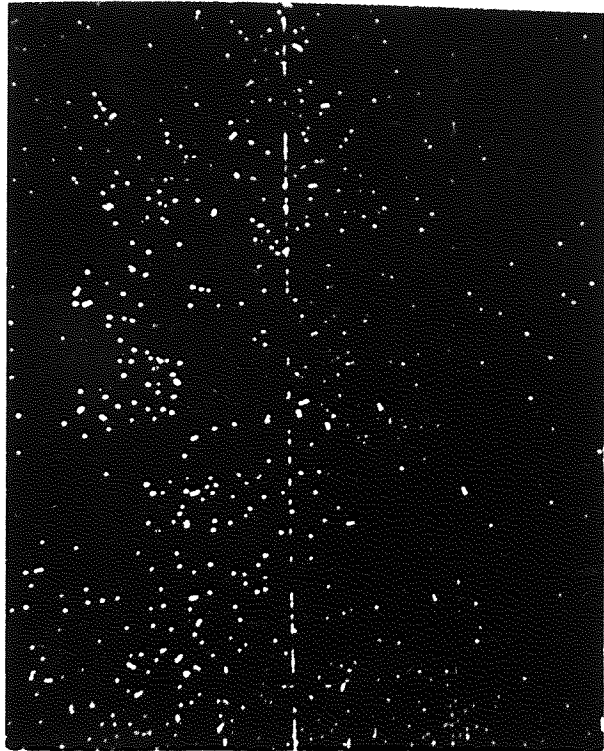
b.



Al

c.

Fig. 5.17



P

d.



Ca

e.

Fig. 5.17

other elements. In the lower part the matrix contains less Ca which is associated with Fe, Si and Al.

P occurs in the ooliths and within the matrix in very small amounts of low concentration.

Fe is shown:

- a - in high concentration within the ooliths associated with small amounts of low concentration of Si, Al, P and Ca. From X-ray and petrographic studies these proved to be hematite.
- b - in high concentration associated with Si, Al and Ca in the matrix. From X-ray studies this was likely to be chamosite.

Si shows:

- a - as subrounded grains of high concentration not associated with other elements. Proved from X-ray studies to be quartz.
- b - as small amounts of low concentration in the ooliths associated with Al and Fe. From X-ray studies this was shown to be clay minerals.
- c - as high concentration in the lower part associated with Al, Fe and Ca (chamosite) and other clay minerals.

Al is shown:

- a - as small amount of low concentration in the ooliths associated with Fe and Si; as previously proved to be clay minerals.

- b - in the lower part within the matrix associated with Si, Fe and Ca; as previously proved to be chamosite and other clay minerals.

Ca is shown:

- a - in high concentration in the matrix. From X-ray studies proved to be calcite.
- b - within the matrix associated with Si, Al and Fe. Proved to be calcite.

P is shown as a very little amount of low concentration in the ooliths associated with small amounts of low concentration Ca, Al and Si, and high concentrations of Fe. From X-ray studies this was likely to be apatite.

In the upper part the matrix is mainly Ca in high concentration and in the lower part it is a mixture of high concentrations of Fe and Si with low concentration of Al and Ca. From X-ray studies this was proved to be calcite in the upper part and a mixture of chamosite, calcite and clay minerals in the lower parts.

Figure 5.18: Microprobe electron micrographs of Frodingham ironstone sample No. B.49, Fe, Si, P and Ca, X-ray distribution map.

Ooliths are ellipsoidal in shape; the length of the major axis varies from 250  $\mu\text{m}$  to 450  $\mu\text{m}$ . In several ooliths the

nuclei are of an element different than the surroundings. These subsequently appear as subrounded grains in the cores of the ooliths.

The matrix is Ca rich. The Fe X-ray distribution map shows high concentration of Fe in the ooliths. It also shows that Fe concentration is independent of the concentration of Si, Ca or P.

The Si X-ray distribution shows high concentrations of Si associated with Fe in the rim surrounding the ooliths. The Si is also seen in high concentration in the matrix associated with Fe in the right hand side of the micrograph.

P occurs as high concentration of anhedral grains associated with Ca in the ooliths; the length of the major axis varies from 10  $\mu\text{m}$  to 70  $\mu\text{m}$ . It is also seen disseminated in the ooliths in low concentration.

Ca occurs as a matrix of high concentration and is not associated with the other elements. Also there are anhedral Ca grains associated with P in the ooliths.

Fe is shown:

- a - in high concentration within the ooliths associated with small amounts of Si, P and Ca. From X-ray studies proved these to be hematite.
- b - in some areas of the matrix associated with Si. From X-ray studies this was shown to be composed of clay minerals.

Figure 5.18 Microprobe Electron  
Micrographs of Frodingham Ironstone

Sample No. B 49, x100

- a - X-ray distribution map for Iron
- b - X-ray distribution map for Silicon
- c - X-ray distribution map for Phosphorus
- d - X-ray distribution map for Calcium





Fe

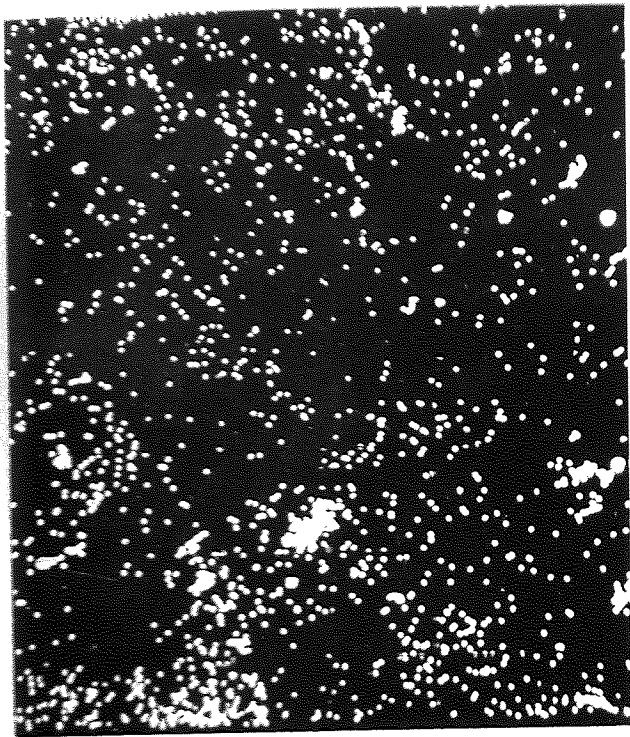
a.



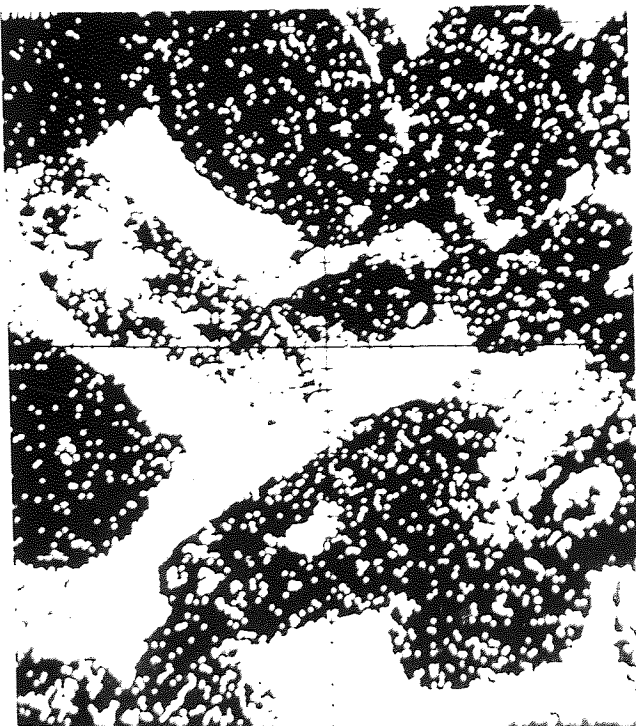
Si

b.

Fig. 5.18



c.



d.

Fig. 5.18

Si is shown in:

- a - a rim of high concentration surrounding the ooliths and associated with Fe. These were proved to be clay minerals.
- b - in some areas of the matrix associated with Fe (clay minerals).

P is shown in one of the ooliths as a subrounded grain in the centre and also as anhedral grains in other ooliths. In all cases it was associated with Ca. X-ray studies proved these to be apatite.

Ca is shown in:

- a - the matrix not associated with the other elements. From X-ray studies proved this to be calcite.
- b - the ooliths associated with P (apatite)
- c - the ooliths as anhedral grains not associated with other element (calcite).

#### Figure 5.19

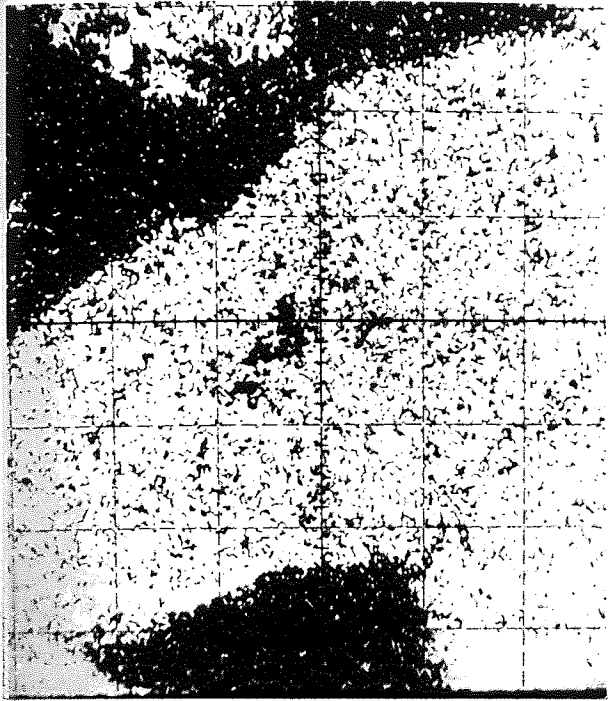
This figure illustrates part of the same area shown in Figure 5.18 but at a magnification of x250 compared with x100 in Figure 5.18. The main feature which has been highlighted is the elliptical oolith sited bottom centre in the previous figure.

The matrix is of Ca rich material and is not associated with the other elements. Fe X-ray distribution shows high concentration of Fe in the oolith associated with small amount of Si, P and Ca.

Figure 5.19 Microprobe Electron  
Micrographs of Frodingham Ironstone

Sample No. 49, x250

- a - X-ray distribution map for Iron
- b - X-ray distribution map for Silicon
- c - X-ray distribution map for Phosphorus
- d - X-ray distribution map for Calcium



Fe

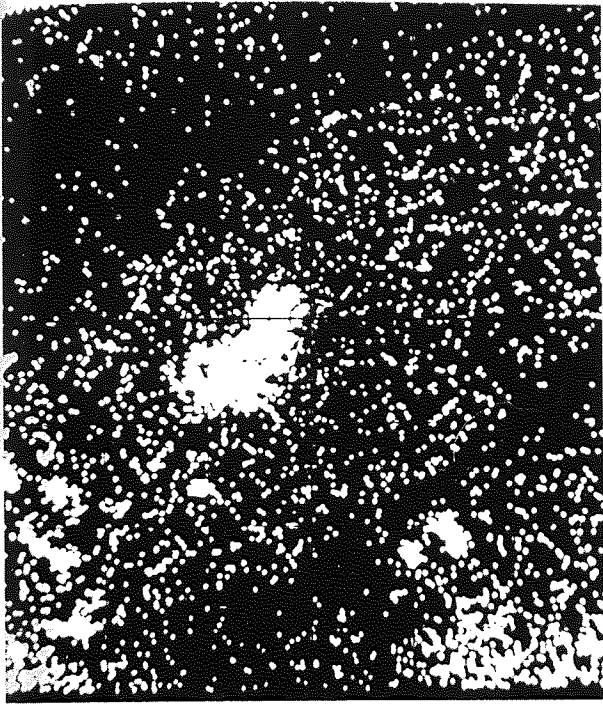
a.



Si

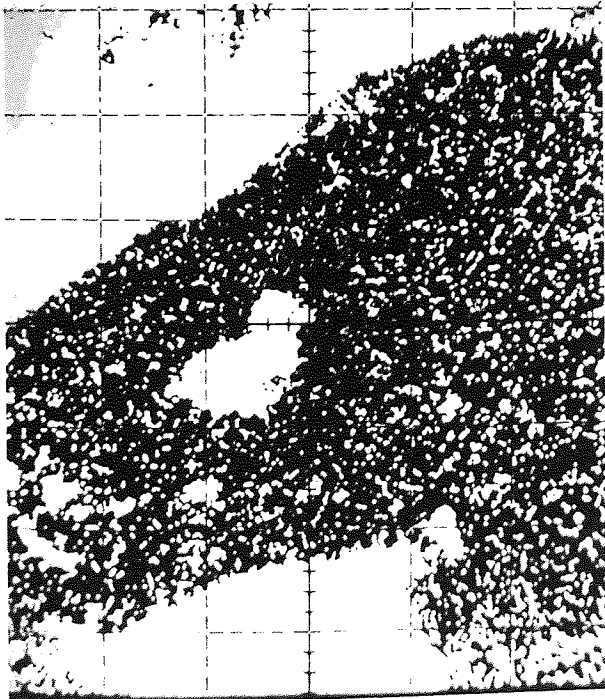
b.

Fig. 5.19



P

c.



Ca

d.

Fig. 5.19



The Si X-ray distribution shows a relatively higher concentration of Si associated with Fe in a rim surrounding the oolith. The Si is also seen disseminated in the oolith in lower concentration. In the core of the oolith is a subrounded grain containing moderately high concentration of P and Ca associated with each other; the length of the major axis is about 72  $\mu\text{m}$ . Also there are anhedral grains of high concentration of P and Ca associated with each other in the oolith; the length of their major axes varies from 8  $\mu\text{m}$  to 28  $\mu\text{m}$ .

Fe shows in the Fe rich oolith associated with Si, P and Ca (shown to be hematite).

Si shows:

- a - as a rim surrounding the oolith associated with Fe.  
Proved from X-ray studies to be clay minerals.
- b - in the oolith associated with Fe, P and Ca (clay minerals).

P as indicated above appears as anhedral grains in the oolith (apatite).

Ca shows in:

- a - the matrix not associated with other elements (calcite).
- b - in the oolith associated with P (apatite).

### 5.5.7 Summary of Results

The Frodingham ironstone bed is situated in North Lincolnshire - east of Scunthorpe. It occurs in the lower Jurassic bed of the South Humberside area.

From the logging of the cores in Figures 5.8 and 5.9 it is clear that calcite forms the dominant matrix mineral in most of the samples, and is also present as numerous shell fragments. Siderite occurs in dark grey lenses of Siderite mudstone. Limonite forms ooliths and may be common in the matrix. Chamosite occurs in a massive form as chamosite mudstone, and as a dominant matrix mineral. The detailed logs have been simplified into four lithologies as shown below:

- A. Limonite ooliths with a calcite-dominant matrix,
- B. chamosite mudstone,
- C. limonite ooliths having a matrix dominated by chamosite,
- D. limonite ooliths and calcite shells, more or less replaced by siderite, are set in calcite matrix.

The lithology shows that most of the cores are made up of type C and type D.

The average chemical analyses for the total thickness of the ironstone are as follows:

	<u>Core Y112</u>	<u>Y113</u>
Fe	25.6%	24.6%
Lime	20.5%	21.2%
SiO <sub>2</sub>	7.88%	8.58%
Sulphur	0.38%	0.43%
Phosphorus	0.33%	0.32%
Loss on ignition	24.25%	24.15%

Vertical chemical variation within the ironstone

	<u>Core Y112</u>	<u>Y113</u>
Fe	15.9-43.3%	15.7-39.8%
Lime	6-36.3%	6.2-35.9%
Sulphur	0.037-2.3%	0.019-4.1%
Phosphorus	0.05-1.11%	0.11-1.1%

X-ray analyses\* revealed the presence of calcite, chamosite, apatite, quartz, hematite, siderite, chlorite and clay minerals. Wedd (55), Whitehead et al (35), and Davies and Dixie (36) mentioned that the phosphate mineral in Frodingham ironstone was collophane, Hallimond et al (56) suggested it was titanophosphate. But this study proved for the first time that it is apatite, by using new techniques (X-ray diffraction and scanning electron microscope) for the examination of this ore.

\* The total number of X-ray samples examined were 18 in number & Co K $\alpha$  & Cu K $\alpha$  radiation were used on each sample (Section 5.54 & fig. 5.12)

## 6.0 Dephosphorisation of Iron Ores

Modern high speed basic oxygen steelmaking plants are inconvenienced by the presence of phosphorus in the hot metal to be refined. Although lime blowing and double slag techniques can overcome the chemical problems of phosphorus removal it would be advantageous if this impurity was removed from the ore before it was charged to the blast furnace. In fact, the Japanese ore buyers in Australia have put a maximum of 0.07% P in the specification for ore supplies in order to eliminate the double slag processing of hot metal. Many methods have been suggested for this elimination including: Chemical processing (38,39,40,41,42,43), Roasting followed by leaching with dilute acid or alkali (44,45), Flotation (46) and Oil agglomeration methods (47,48,49).

### 6.1 Chemical Processing

#### 6.1.1 Nitric Acid

Lucia and Losada (43) treated an oolitic magnetite ore concentrate containing 0.3 to 0.5% P with (35-75 g/litre) nitric acid using a 25% pulp density. They found that up to 95% of the phosphorus present as apatite was dissolved at ambient temperatures with only 1.5% iron loss in solution. They presented the process from a purely technical point of view, but it seems that the major cost is the acid supply and maintenance because this acid can cause severe corrosion to the steel structure.

#### 6.1.2 Sodium Carbonate

This process of Mueller et al (40) consisted of washing an iron oxide concentrate with a 10% sodium carbonate solution

at slightly elevated temperatures (up to 70°C) followed by washing the solids with water. Using a Brazilian hematite, the phosphorus content was reduced from 0.16 to 0.05% and sulphur from 0.052 to 0.015%. It would seem that the high temperature of operation would cause too large an energy and water input to make this process economic, although for a high value metal such as copper it is an economic proposition.

### 6.1.3 Flox Process

Reeve (39) studied the possibility of concentrating the low grade ores used at Appleby-Frodingham to raise their iron content and reject as much as possible of their gangue content. He described a cyclic chemical process for treating these ores, using hydrochloric acid and volatilising the iron as ferric chloride at 300-350°C. All other major constituents, including sulphur and phosphorus, remained in the solids. The ferric chloride so produced was hydrolysed and converted at 550°C to pure ferric oxide, with the regeneration of HCl gas for recycling. The process described was most conveniently carried out on finely crushed ore, fluidized in a stream of reactant gases. The process only just failed to be economic due to the high cost of the make up hydrochloric acid and high temperature of reaction although producing very pure oxide.

**SEE ADDENDUM (p.205)**

### 6.2 Roasting and Leaching with Dilute Acid or Alkali (Amdephos)

There are in the Pilbara region in the north west of Western Australia large tonnages of iron ore with a phosphorus concentration of about 0.15%.

For the ores studied by the Amdel Iron Ore Mining Company, optical and microchemical methods failed to detect phosphate minerals in polished sections of the ore, which consisted of grains of martite ( $\text{Fe}_2\text{O}_3$ ) scattered through very fine-grained goethite, with some cavities containing clay. By electronprobe microanalysis, however, one grain of calcium phosphate mineral less than 10  $\mu\text{m}$  surrounded by clay was detected in one specimen, and examination of another specimen revealed that some patches of goethite contained small amounts of phosphorus estimated to be between 0.1% and 0.5% and rarely up to 1%. This was not concentrated in definite mineral grains but was dispersed throughout the goethite, and was probably adsorbed by hydrated iron oxide from phosphate bearing solutions. It was not uniformly distributed and much of the goethite showed no phosphorus above background interference. Phosphorus was not detected in any grains of martite or hematite.

In the process developed on a laboratory scale known as "Amdephos", heat treatment (1200-1250 $^{\circ}\text{C}$ ) caused the P to segregate without the use of any additives and it was then extracted by leaching with dilute acid (0.5 N  $\text{H}_2\text{SO}_4$ ) or alkali (0.5 N NaOH) at 90 $^{\circ}\text{C}$ . The phosphorus content was reduced from 0.15% P to 0.035% P.

A cost study was made for a plant treating  $1 \times 10^6$  tonne/a pellets and it indicated that the major cost was for acid supply. Hence, with acid regeneration total treatment cost became 50 C (20p) per tonne of product. This cost for



Amdephos process was most likely to be economic without the inclusion of costs for the roasting process. They suggested that this process could be partially or wholly debited to another operation, e.g. the firing of pellets which is necessary for their induration, as well as for phosphorus solubilisation. In the case of a goethitic lump ore for which heating results in a considerable concentration of the iron content, the cost of firing could be shared between upgrading and dephosphorisation.

A more detailed discussion of the Amdephos process has been given by Gooden et al (44).

### 6.3 Flotation

Bahr (46) studied the dephosphorisation of the Mancorvo iron ore deposit in Portugal by flotation. Tests were carried out with a sample of hematite ore ground to 95% below 80  $\mu\text{m}$ . The contents of a sample which was deslimed in a hydrocyclone at approximately 10  $\mu\text{m}$ , were 45.7% Fe and 0.46% P. A two stage flotation process was used and the yield from the first was phosphate mineral and from the second hematite. The P yield was 73% and Fe yield in the P concentrate of 11%. The phosphorus content in the Fe concentrate was 0.2% P. It was noticed that the incomplete flotation of the phosphate minerals could have been due to extremely fine intergrowths of the phosphate minerals with hematite. This process did not produce a sufficiently low phosphorus content in the final product to be feasible.

#### 6.4 Beneficiation of Phosphoric Iron Ore by Oil Phase Agglomeration Methods (47, 48)

The Snake River iron ore deposit, in the northern Yukon, Canada, was estimated to contain some 30,000 million tonnes of ore; with chemical analysis as follows:

	Fe	SiO <sub>2</sub>	P	CaO	Al <sub>2</sub> O <sub>3</sub>	TiO <sub>2</sub>	S
wt%	44	30	0.34	3.0	1.4	0.10	0.02

The ore body consisted mainly of microcrystalline hematite, and chalcedonic quartz in several varieties of aggregation. The hematite was most commonly in the form of irregularly bonded interlocking crystals ranging in size from 5 to 200  $\mu\text{m}$  and averaging 30  $\mu\text{m}$ . The phosphorus-containing minerals were apatite and colophonane. The gangue minerals were finely disseminated and occurred in particle size down to 4  $\mu\text{m}$ . Selective agglomeration of the phosphorus minerals was carried out in the ball mill by the addition of fatty acids, such as oleic and linoleic, during the initial wet fine grinding to -400 mesh (-38  $\mu\text{m}$ ) at a pulp density of 70%. The ground ore was then further treated to selectively agglomerate the iron minerals which were separated from the remaining gangue minerals. Successful beneficiation was achieved on both the crude iron ore and jig concentrate (54.6% Fe and 0.39% P) with some concentrates assaying 65.9% Fe and less than 0.02% P.

## 7.0 Possible Application of Dephosphorisation Techniques to Bahariya, Aswan and Frodingham Ores

### 7.1 Bahariya Ore

This ore consists mainly of hematite and goethite with pockets of ochre and manganese oxides. The gangue minerals are halite, gypsum, barytes, quartz and calcite, with the following chemical analysis:

Fe content is between	49.8 to 63.2%
Manganese oxides	0.16 - 1.61%
Sodium Chloride	Trace - 6.61%
Silica	0.7 - 2.1%
Phosphorus	0.14 - 0.34%

The chemical and reduction processing of this ore is complicated by the presence of halite which causes more difficulties in the smelting than does the phosphorus content which is in the lower medium range.

From the microprobe and scanning electron microscopic examination the phosphorus is below detection concentrations mainly because of the very fine particle sizes (range  $-5 \mu\text{m}$ ) and the even distribution throughout the ore. Removal of such material requires very fine grinding similar to or finer than the Yukon ore to expose one of the facets of the gangue mineral to enable it to be contacted by a solvent during a leaching operation. There could be an advantage to be gained from the presence of chloride ions in a leaching process if they are in sufficient quantity to reduce the pH

of the water solvent to act as a hydrochloric acid solution. Such a process as acid process could then be considered but leaching with alkalies, e.g. sodium carbonate, would be too expensive due to the loss of alkali with the chloride present, but the presence of chloride suggests acid process as the possible beneficiation technique. However, for the main ores of this type another leaching solvent may be more appropriate than water, e.g. acid or alkali dependent upon the gangue content.

The great advantage of the processes in the case of Bahariya iron ore would be the simultaneous removal of sodium chloride from the ore.

It should be noted that the Bahariya iron ore is a Bilbao type <sup>(1)</sup>, i.e. it is similar to:

- Cumberland in Great Britain;
- Bilbao in Spain;
- Erzberg, Austria;
- Ouenza, Bou kadra and other deposits in Algeria;
- Djerissa, Douaria and Tamera in Tunisia.

The Bahariya iron ore is presented in this thesis as an example of Bilbao type.

## 7.2 Aswan Iron Ore

From the chemical analyses of the Aswan Cores it is seen that the first core contained 42-55% Fe and 0.1-2.9% P, and the second analyses 41-57% Fe and 0.35-2.3% P. X-ray

examination showed the iron present as hematite with variable quantities of quartz and apatite but only a small amount of clay minerals. Scanning electron micrographs (Figs. 4.13, 4.14 and 4.17-4.21) showed the iron bearing ooliths measuring 75-750  $\mu\text{m}$  in length with quartz crystals of sizes in range 40 to 220  $\mu\text{m}$  although the majority are less than 100  $\mu\text{m}$ . The apatite crystals were much smaller, all  $<80$   $\mu\text{m}$  and mostly  $<60$   $\mu\text{m}$ . From the micrographs in Figs. 4.13-4.15, 4.18, 4.19 and 4.21 it can be deduced that apatite occurs in the oolitic iron ore

- (i) in the hematite matrix
- (ii) in the hematite matrix surrounding the ooliths and the quartz grains
- (iii) filling in the pores in the oolithic surfaces
- (iv) as matrix cementing the ooliths with the hematite grains.

In the sandstone and clay beds the chemical analysis showed only 1-8% Fe and P 0.04-0.14%. The Microscan showed that quartz crystals up to 90  $\mu\text{m}$  size were found in a chamositic matrix with small apatite crystals  $<25$   $\mu\text{m}$  in the chamosite cementing the quartz grains.

It would be seen that iron oxides and chamosite adsorb apatite crystals. Cook and McElhinny <sup>(10)</sup> suggested that most of the phosphorus is associated with the iron in an adsorbed form. Barbour <sup>(50)</sup> studied the distribution of phosphorus in the iron ore deposits of Itabira, Minas Gerais, Brazil. This study indicated that iron hydroxides were able to fix phosphorus.

Stout (51), Toth (52) and Colman (53) suggested that the fixation of phosphorus by hydrated oxides of iron and aluminium was a simple replacement or change of phosphate by hydroxyl ions. The results of Emerson and Widmer (54) from electron microprobe investigations for a sample collected from sedimentary core taken in Greifensee, Switzerland, showed a strong correlation between iron and phosphorus. These results are further evidence to support the idea that phosphorus is associated with the iron in an adsorbed form.

Figures 4.13, 4.14 and 4.17-4.21 show that most of the apatite occurs in the matrix or as matrix (Fig. 4.21). The amount of apatite which occurs in the ooliths is very small (about 5%).

Table 7.1 shows the size distribution of quartz, apatite and clay mineral grains in the ooliths and in the matrix for oolitic iron ore samples which were taken to represent the two cores in the Aswan area. It also shows that the liberation size for the apatite grains is about 20  $\mu\text{m}$  but in many cases apatite grains make up aggregates up to 150  $\mu\text{m}$  (Fig. 4.14) or 80  $\mu\text{m}$  (Fig. 4.15). In this case it is suggested that the size liberation be  $\sim 80 \mu\text{m}$ . It was mentioned earlier that Bahr (46) had used flotation to separate the phosphate mineral from the very finely ground Portuguese Moncorvo iron ore (95%  $< 80 \mu\text{m}$ ). A 73% P yield was achieved. Poor results were due to the extremely fine intergrowth of the phosphate with hematite.



TABLE 7.1 THE SIZE DISTRIBUTION OF QUARTZ, APATITE AND CLAY MINERAL GRAINS IN THE OOLITHS AND IN THE MATRIX

Sample No.	OOLITH				MATRIX			
	Quartz	Clay Minerals	Apatite	Oolith size	Quartz	Apatite	Hematitic	Clay Minerals
As10			30	75-250	60-220	20-60	Fine	
As9			20		25-150	25-65 aggre- gate to 150	H.Mat.	
As25	50-100		Very fine	150-450	80-300	10	Chamosite Mat.	
As6	60		5-25	750			H.Mat.	
As9-2	10	120-160		70-500	40-160	Irregular patches	H.Mat.	
As11			5-20	90-290	80	20-60	H.Mat.	Little
As20		30-50				As matrix	5-60	

From the Aswan ore results it can be seen that there are no very small grains of apatite intergrown with the hematite and only in one case, Fig. 4.21, are there hematite grains (4-60  $\mu\text{m}$ ) small enough to interfere with the apatite. Thus, it would seem that flotation concentration could be applied to the removal of apatite from Aswan ore crushed and ground to <80  $\mu\text{m}$ , with an expectation of 90% P removal.

In the earlier classification of iron ores it was indicated that the Aswan ore was similar to ores from Lung-yen (Chahar Province) in China and Sierra Grande (Rio Negro, Patagonia in Argentina).

### 7.3 Frodingham Ironstone

The results of the electron microprobe and scanning electron microscope investigation for the distribution of phosphorus in the Frodingham ironstone are shown below:

1. Apatite occurs as very fine grains (<5  $\mu\text{m}$ ) and intergrown with the hematite grains in the hematite oololiths (100-450  $\mu\text{m}$ ).
2. It is also found as very fine grains (again <5  $\mu\text{m}$ ) intergrown with chamosite grains in the chamosite oololiths (Figure 5.15 and 5.16).

3. Apatite occurs as matrix of fine grains (as above) intergrown with chamosite and calcite grains (Figure 5.13), and in the lower part of Figure 5.17. It is also seen intergrown with chamosite grains only.
4. Occurring as anhedral and subrounded grains in the ooliths (8-28  $\mu\text{m}$ ).

It would seem from this study that the apatite is associated with the hematite and chamosite in an adsorbed form, and the apatite occurs in fine grains which are located in the pores in the ooliths. It was also found that the apatite was in the chamosite and hematite ooliths or in the chamosite matrix more than it occurred in calcite matrix, as shown in Figures 5.17, 5.18 and 5.19.

Berner (57) and Serruya (58) noticed that the concentration of dissolved reactive phosphate was significantly lower in sediments containing high weight percentages of calcium carbonate than in those of lower calcium carbonate percentages. The present results confirmed that the phosphorus was more likely to be present in a chamosite matrix than in a calcite matrix.

Electron microprobe results on phosphorus by Emerson and Widmer (54) for a sample collected from sedimentary cores in Greifensee, Switzerland, of P-rich particle showed a strong correlation between iron and phosphorus. They showed superimposed iron and phosphorus electron microprobe line diagrams for the same sediment particle.

Emerson and Widmer (54) results were identical to the results of our investigation on Frodingham ironstone for one oolith by electron microprobe analysis. The present investigation which was carried out on ooliths from different samples showed superimposed phosphorus and iron electron microprobe line diagrams (Figure 7.1). This result would appear to support the theory that phosphorus or apatite is associated with iron oxides in an adsorbed form. It was also confirmed that the major phosphorus mineral in the Frodingham ironstone was apatite.

In an attempt to remove phosphorus from Frodingham ironstone some preliminary investigations have been carried out previously on wet washing methods but the results were not sufficiently promising (33).

Tests were made on Frodingham ironstone by kiln roasting followed by magnetic separation. Reeve (33) found that iron recoveries as high as 93% were attained with percentage iron in the tailings below 6% and the iron percentage in the concentrate was 37% on average. No phosphorus analysis was given in Reeves (33) results but it seemed that the phosphorus percentage was increasing in the concentrate because the phosphorus was intermeshed in fine grains by hematite or chamosite which was removed in the concentrate, while the amount of phosphorus which occurred in the calcite matrix was negligible as in Figure 5.19 and the non-magnetic phase was mainly calcite. The liberation size he used for the feed for magnetic separation was  $\sim 800 \mu\text{m}$  which was much too large to achieve the liberation of the phosphorus bearing grains (5-72  $\mu\text{m}$ ).

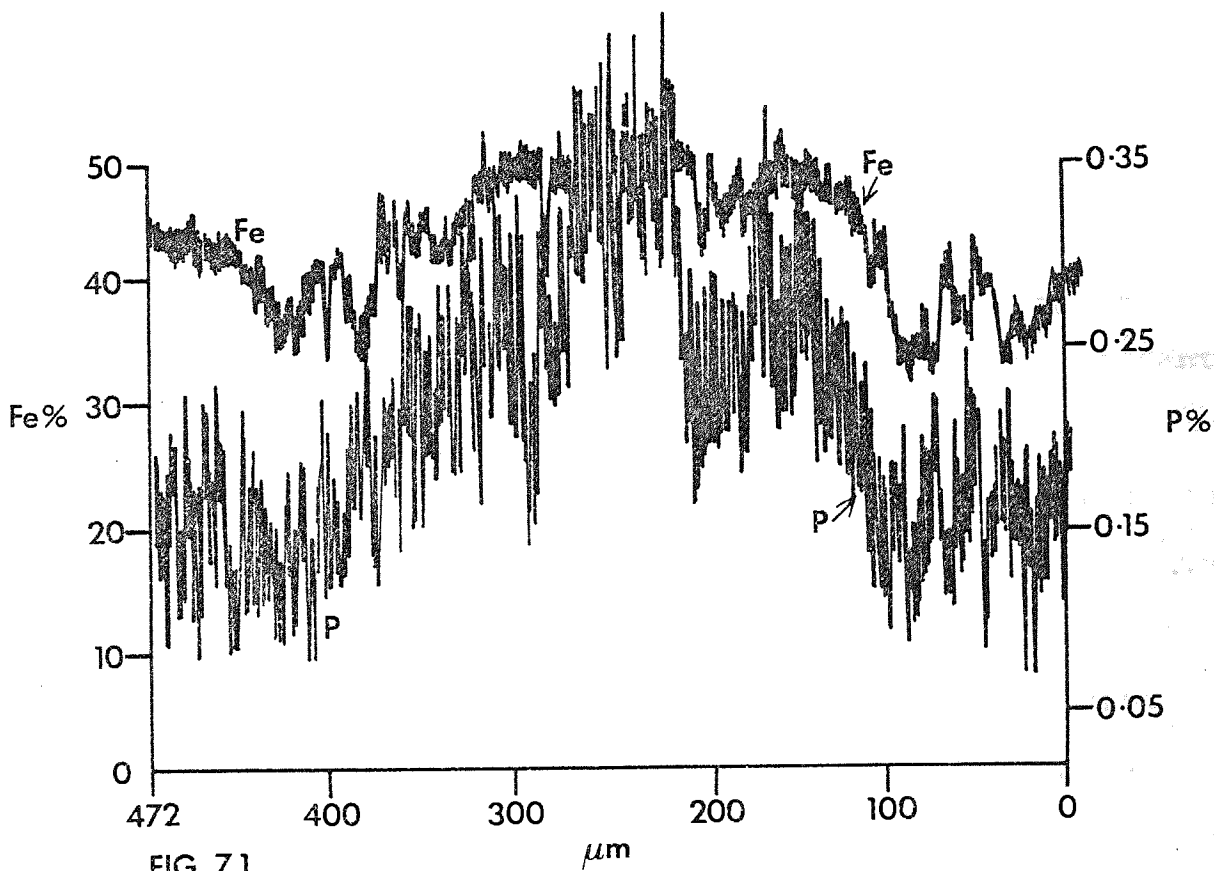


FIG. 7.1

SUPERIMPOSED IRON & PHOSPHORUS ELECTRON MICRO-  
PROBE LINE DIAGRAMS FOR THE SAME OOLITH

As mentioned before in the section 6.1.3, Reeve (39) treated Frodingham ironstone using hydrochloric acid and volatilisation of the iron as ferric chloride at 300-350°C, while all other gangue minerals including phosphorus minerals remained in the solids. The ferric chloride so produced was hydrolysed and converted at 550°C to produce pure ferric oxide.

Dephosphorisation studies on the calcareous iron ores of the Big Seam from the Birmingham district of Alabama (45) included a reduction roasting operation followed by magnetic separation. The iron ore analysis was 36% Fe, 13% CaO and 0.33% P. From the data given neither reduction roasting nor magnetic separation of the reduced ore ground to minus 38  $\mu\text{m}$  effectively achieved liberation of the phosphorus and subsequent rejection from the iron concentrate. An additional test was made to determine the effect of grinding much finer than 38  $\mu\text{m}$ . In this case the reduced ore was ground to a product containing less than 13 percent by weight of material coarser than 20 microns. Magnetic separation of this material yielded a concentrate with improved phosphorus rejection but recovery of iron was significantly reduced. This magnetic concentrate analysed 61.1% Fe, 3% CaO, 0.19% P and 8.3% insoluble. The authors suggested that some additional treatment such as acid leaching would be required for more effective reduction of the phosphorus content. The additional treatment (acid leaching) showed that the acid requirements for effective reduction of the phosphorus content were more than the



stoichiometric requirement for the CaO reaction. It also showed that essentially all of the CaO must be made soluble before the acids reacted with the phosphorus bearing compound. Test results showed that the reduction roasting followed by fine grinding, magnetic separation, acid leaching, filtration and washing processes yield iron concentrates containing 62% Fe and 0.04% phosphorus, with iron recoveries of 82 to 90% and phosphorus extraction of 90 to 93%. However, acid requirements were high.

It is suggested that two processes are possible for the dephosphorization Frodingham ironstone:

1. Flox process (Section 6.1.3)
2. Reduction Roasting followed by fine grinding, magnetic separation, acid leaching, filtration and washing.

A detailed economic analysis is required for both processes to assess the feasibility of these processes but it would seem that they must both be uneconomic under present day iron ore costs.

Frodingham ironstone is a Minette, marine sedimentary type of ore and is similar to the following ores:

Lorraine Basin, France,  
Luxembourg,  
Salzgitter type Sidiments,  
Federal Republic of Germany,

and hence it would be reasonable to assume the results presented may be applicable to the dephosphorisation of these and similar ores.

## 8.0 CONCLUSIONS

The techniques developed in this research were used to investigate the physical state of phosphorus found in Bahariya, Aswan and Frodingham iron ores. These are similar to many iron ore deposits throughout the world, and because of this, the benefits to be derived from ore dephosphorisation are self evident. The techniques used in this study were mainly geological:- Lithology, Mineralogy, Microscopy, X-ray analysis, Electron microprobe analysis and Scanning electron microscope.

### 8.1 Bahariya Ore

It was shown that this ore:

1. is brown or yellowish brown in colour and consists mainly of hematite and goethite. The gangue minerals are halite, gypsum, barytes, quartz and calcite; with an iron content between 49.8 to 63.2% and phosphorus 0.14 to 0.34%.
2. The phosphorus occurs as very fine particles of apatite ( $-5 \mu\text{m}$ ) and is distributed throughout the ore.
3. Removal of the phosphorus would require fine grinding ( $-40 \mu\text{m}$ ) to expose the phosphate mineral so that it can be attacked by a solvent as for acid leaching.

### 8.2 Aswan Iron Ore

1. This is an oolitic iron ore of enriched Minette type, occurring as bands in the middle group of the Nubian series. The iron ore bands are at the surface or close thereby with iron contents between 41-57% and

phosphorus 0.1-2.9%. X-ray examination showed hematite with variable quantities of quartz, apatite and small amount of clay minerals. Scanning electron micrographs show hematite ooliths (75-750  $\mu\text{m}$ ), quartz crystals (40-220  $\mu\text{m}$ ), and the apatite crystals were -80  $\mu\text{m}$ .

2. In the oolithic iron ore beds apatite occurs in many phases but usually concentrated in one or two of them never throughout the ore cross sections examined. Thus, it appeared in the hematite matrix; in the hematite matrix surrounding the ooliths and the quartz grains; filling in the pores in the oolithic surfaces; and as matrix cementing the ooliths with the hematite grains.
3. In the sandstone and clay beds, the chemical analysis showed 1-8% Fe and 0.04-0.14% P; quartz crystals up to 90  $\mu\text{m}$  size were found in a chamositic matrix with apatite crystals <25  $\mu\text{m}$ .
4. The distribution of the apatite was mainly in the matrix or as matrix; while the amount of apatite distribution in the ooliths is very small (about 5%).
5. The liberation size for the apatite grains is about 20  $\mu\text{m}$  but in many cases apatite grains made up aggregates of 150  $\mu\text{m}$  or 80  $\mu\text{m}$ . From this study, it is suggested that the liberation size would be -80  $\mu\text{m}$ .
6. Flotation concentration could be applied to the removal of apatite from Aswan ore crushed and ground to -80  $\mu\text{m}$ .

### 8.3 Frodingham Ironstone

1. Occurs in the lower Jurassic bed of South Humberside.
2. Detailed logs have been simplified into four lithologies A, B, C and D. The lithology shows that most of the cores are made up of type C and type D.
3. The average iron content is 25.1% and the phosphorus 0.32%. X-ray analysis showed the presence of calcite, chamosite, apatite, quartz, hematite, siderite, chlorite and clay minerals.
4. Apatite is found associated with several minerals but only as very fine particles ( $<5 \mu\text{m}$ ) intergrown with the hematite grains in the hematite ooliths; as very fine grains intergrown with chamosite in chamosite ooliths; as the matrix of fine grains intergrown with chamosite and calcite; intergrown with chamosite grains only in the matrix; as anhedral and subrounded particles ( $8-28 \mu\text{m}$ ) in the ooliths.
5. Apatite is associated with the hematite and chamosite in an adsorbed form. It is found in the chamosite and hematite ooliths or in the chamosite matrix more than it occurs in the calcite matrix.
6. Based on the findings from this research, it is suggested that dephosphorisation of Frodingham ironstone by the Flox process or Reduction roasting followed by fine grinding, magnetic separation, acid leaching should be feasible.

## 9.0 SUGGESTIONS FOR FUTURE WORK

The specialised techniques used in this work have been shown to be useful in the examination of phosphorus bearing minerals in iron ores. These could be involved in studying other classes of iron ores to discover their phosphorus content and distribution.

The suggested methods of dephosphorisation for the three ores investigated need to be proven by mineral dressing and leaching tests. In this way it should be possible to make an economic assessment of dephosphorisation for the Aswan, Bahariya and Frodingham ores.

### 9.1 Economics

It is possible that in the work described above dephosphorisation processes were said to be uneconomic on very limited data. However, the economics of an ore dephosphorisation method need to be worked out for the whole iron and steel production route. For example, on the ore beneficiation costs it is unlikely that any suggested process could be economic from the increased value of the ore product. If, however, the extra costs at the B.F. (increased coke rate) and increased slag forming additions and process time extension in the steelplant were used in the accounting system, then a much more favourable economic picture would emerge. Thus, an important extension to the dephosphorisation work would be this overall process evaluation.



## 10. ACKNOWLEDGEMENTS

The author wishes to express his gratitude to individuals and organisations that are mentioned below.

To Dr. J.C. Billington for his continuous guidance and supervision throughout the whole project, also to Dr. R.A. Ixer of the Geology Department for his advice and help.

To B.S.C. geologists in Scunthorpe for their help and co-operation also to the Egyptian Iron and Steel Company for providing some specimens and information.

Gratitude is also due to the Egyptian Government for providing financial support during this doctoral programme.

## 11. REFERENCES

1. Survey of World Iron Ore Resources, United Nations, New York, 1970.
2. Miller, J.R., The Inevitable Magnitudes of Metallized Iron Ore, *Iron and Steel Engineer*, 49, (12), 41-51, 1972.
3. Bolodel, F., The Types of Iron Ore Deposits, *Chronique des Mines Coloniales (Paris)*, 23, (231), 1955.
4. Blackwelder, E., The Geologic Role of Phosphorus, *American Journal of Science*, 4th series, 42, 285-298, 1916.
5. Buchinsky, G.I., The Origin of Marine Phosphorites, *Lithology Mineral Deposits*, 292-311, 1966.
6. McKelvey, V.E., Phosphate Deposits, U.S. Geological Survey Bulletin 1252-D, D1-D21, 1967.
7. Burnet, W.C., Phosphorite Deposits from the Sea Floor of Peru and Chile, National Technical Information Service, U.S. Department of Commerce, AD-782587, 1-164, 1974.
8. Bonatti, E., Fisher, D.E., Joensuu, O., and Rydell, H.S., Post-depositional mobility of some transition elements, phosphorus, uranium and thorium in sea sediments. *Geochimica et Cosmo-Chimica Acta*, 35, 189-201, 1971.
9. Borchert, H., Genesis of Marine Sedimentary Iron Ores. *Bulletin Institute Mining and Metallurgy*, (640), 261-279, 1960.

10. Cook, P.J. and McElhinny, M.W., A re-evaluation of the Spatial and Temporal Distribution of Sedimentary Phosphate Deposits in the Light of Plate Tectonics, *Economic Geology*, 74, 315-330, 1979.
11. Kaplan, I.R. and Rittenberg, S.C., Basin Sedimentation and Diagenesis, (editor M.N. Hill), *In the Sea*, Interscience, Vol. 3, 583-619, 1963 (from ref. 8).
12. MacKereth, F.J.H., Some Chemical Observations on Post-glacial Lake Sediments, *Phil. Trans. Roy. Soc., Sect. B*, No. 250, 165-220, 1966.
13. Nriagu, J.O. and Dell, C.I., Diagenetic Formation of Iron Phosphates in Recent Lake Sediments, *American Mineralogist*, 59, 934-946, 1974.
14. Nriagu, J.O., Stability of Vivianite and Iron-pair Formation in the System  $\text{Fe}_3(\text{PO}_4)_2\text{-H}_3\text{PO}_4\text{-H}_2\text{O}$ . *Geochimica et Cosmo-chimica Acta*, 36, 459-470, 1972.
15. Attia, M.I., *Geology of Iron Ore Deposits of Egypt*, Government Press, Cairo, 1950.
16. Gheith, M.A., Classification and Review of Egyptian Iron Ore Deposits, *SYMP. Applied Geology*, 106-113, 1955.
17. Basta, E.Z. and Amer, H.I., El-Gedida Iron Ores and their Origin, Bahariya Oases, Western Desert, U.A.R. *Economic Geology*, 64, 424-444, 1969.
18. El-Akkad, S and Issawi, B., *Geology and Iron Ore Deposits of the Bahariya Oasis*, *Geol. Surv. Egypt*, Cairo, Paper 18, 1963.

19. Amer, H.I., Geology and Mineralogy Studies on Bahariya Oasis, Ph.D. Thesis, Faculty of Science, Cairo University, 1973.
20. Andrawis, S., Paleontological report on El-Gedida Water Well, Gen. Pet. Co., Intern. Rep. No. 849, 1-7, 1970 (From ref. 19).
21. Said, R. and Issawi, B., Geology of Northern Plateau, Bahariya Oases, Geol. Surv., Cairo, Report 29, 1964 (From ref. 19).
22. Hume, W.F., The Distribution of Iron Ores in Egypt, Survey Department Paper, N.20, Cairo, 1909.
23. El Shazly, E.M., The Results of Drilling in the Iron Ore Deposit of Gebel Ghorabi, Bahariya Oasis, and Report on the Mineralogy of the low grade iron ores of El-Heiz Area, Geological Survey, Cairo, Government printing, 1962.
24. Nakhla, F.M., The Iron Ore Deposits of El-Bahariya Oasis, Egypt, Economic Geology, 56, 1103-1111, 1961.
- 24a.** (see below)
25. El-Hinnawi, E., Contributions to the Study of Egyptian Iron Ores, Economic Geology, 60, 1497-1509, 1965.
26. United Nations, Survey of World Iron Ore Resources, 1955.
27. Attia, M.I., Topography, Geology and Iron Ore Deposits of the District East of Aswan, Geological Survey, Cairo, 1955.
- 24 a.** TOSSON & SAAD. EL-BAHARIYA IRON ORE DEPOSITS. N. Jb. MINER Abh. 121,3, 293 -317, 1974

28. Iron Ore Industry of Great Britain, National Council of Associated Iron Ore Producers, 1-16, 1960.
29. Robert, M., British Ironstone Mining, The Mining Engineer, 51-61, 1970.
30. Goldring, D.C., British Iron Ores: their future use, Proc. R. Soc. Lond., A.339, 313-328, 1974.
31. Elford, D.G., Iron Ores in the U.K., Internal report, British Steel Corporation, Scunthorpe Division, 1975.
32. Carpenter, J.E., Flotation of Iron Ore from Appleby-Frodingham Internal Report, Steel Co. Ltd., Scunthorpe District, England, 1949.
33. Reeve, L., Magnetic Concentration Experiments upon Iron Ores used in North Lincolnshire Practice, Journal of the Iron and Steel Institute, 275-280, 1948.
34. Internal report, Opencast working of Frodingham Ironstone, British Steel Corporation, Scunthorpe Division, 1977.
35. Whitehead, T.H., Anderson, W., Wilson, V. and Wray, D.A., The Frodingham (lower Lias) Ironstone of Lincolnshire. Memoirs of The Geological Survey of Great Britain, 68-93, 1952.
36. Davies, W. and Dixie, J.M., Recent work on the Frodingham Ironstone, Yorkshire Geological Society, 28, (2), 85-96, 1951.
- 36a. TAYLOR, DAVIES, DIXIE 19th INT. GEOL. CONGR. pp. 453- 466 1952

37. D'Anglejan, B.F., Origin of Marine Phosphorites of Baja California, Mexico. *Marine Geology*, 5, 15-44, 1967,
38. Australian Mineral Development Laboratories, Process for the reduction of the Phosphorus content of iron ores, Patent Specification No. 1367102, 1974.
39. Reeve, L., Development of chemical treatment of low-grade iron ores at Appleby-Frodingham. *Journal of The Iron and Steel Institute*, 26-40, 1955.
- 39a. (see below)
40. Mueller, D.E. and Segura, M.A., Ore Pretreatment Process, United States Patent 3, 928, 024, Dec. 1975.
41. Maletskii, N.A. et al., Development of the Technology for producing high-grade phosphorus and low-arsenic concentrates from Kerch ores. Translated from the Russian *Obogashch. Polez, Iskop*, (6), 10-14, 1970. (BHP Central Research Laboratories).
42. Del-Brio, R., Dephosphorisation of Iron Ores, BISI 10586, *Boletin Geologico Y Minero*, 79, (1), 17-20, 1968.
43. Lucia, J.M. and Losada, C., Chemical Dephosphorisation of Iron Ore, British Industrial and Scientific International-Trans. No.10265, From Spain, *Revista Metallurgiz. Cenim*, 2, (1), 42-55, 1966.
44. Gooden, J.E.A., Waker, W.M. and Allen, R.J., 'Amdephos' A Chemical Process for Dephosphorisation of Iron Ore. Chemical Engineer Conference "Process Industries in Australia, Queensland, July 1974.
- 39a. REEVE L. & BLAKEY B.C. J OF IRON & STEEL I. 1966 204 No 11 pp.1087 - 1092



45. United States, Department of the Interior, Bureau of Mines Report of Investigations, Phosphorus Removal from Birmingham, Ala. Calcareous Iron Ores, R.I. 7728, 1973.
46. Bahr, A., Investigation into Dephosphorisation of Iron Ore by means of Flotation. Translation No. CRL/T.4995, From German, Erzmetall 24, (1), 12-18, 1971, The Broken Hill Company Limited, Australia.
47. Sirianni, A.F., Colman, R.D., Goodhue, E.C. and Puddington, I.E., Separation Studies of Iron Ore Bodies Containing Apatite by Spherical Agglomeration Methods. International Journal of Mineral Processing, 1, 231-241, 1974.
48. Sparks, B.D. and Sirianni, A.F., Beneficiation of a Phosphoriferrous Iron Ore by Agglomeration Methods, International Journal of Mineral Processing, 1, 231-241, 1974.
49. Sirianni, A.F. and Sparks, B.D., Oil-Phase Agglomeration of Peace River Iron Ore, C.I.M. Bulletin, 137-140, 1977.
50. Barbour, A.P., Distribution of Phosphorus in the Iron Ore Deposits of Itabira, Minas Gerais, Brazil, Economic Geology, 68, 52-64, 1973.
51. Stout, P.R., Alteration in the crystal structure of clay minerals as a result of Phosphate fixation. Proceedings Soil Science Society of America, 4, 177-182, 1939.

52. Toth, S.J., Anion adsorption by soil colloids in relation to changes in Free Iron Oxides. *Soil Science*, 44, 299-314, 1937.
53. Coleman, R., The mechanism of phosphate fixation by Montmorillonitic and Kaolinitic clays. *Proceedings Soil Science Society of America*, 9, 72-78, 1944.
54. Emerson, S. and Widmer, G., Early diagenesis in Anaerobic Lake Sediments - II. Thermodynamic and Kinetic Factors Controlling the Formation of Iron Phosphate. *Geochimica et Cosmo-chimica Acta*, 42, 1307-1316, 1978.
55. Wedd, C.B., Frodingham District (Lower Lias). *Memoirs of the Geological Survey*, 12, 71-105, 1920.
56. Hallimond, A.F., Ennos, F.R. and Sutcliffe, R., Limonite Oolites, *Memoirs of the Geological Survey*, 19, 76-84, 1925.
57. Berner, R.A., Kinetic Models for the early diagenesis of Nitrogen, Sulphur, Phosphorus, and Silicon in anoxic marine sediments, *The Sea*, Edited by Goldberg, E.D. A. Wiley-Interscience Publication, 5, 427-450, 1974.
58. Serruya, C., Lak Kinneret: The Nutrient Chemistry of the Sediments. *Limnology and Oceanography*, 16, 510-521, 1971.